UNIVERSITY OF LEEDS

Quantification of Placental Dysfunction in Pregnancy Complications

Mohamed Saad Elsayed ElMoursi

MBChB, MSc

Section of Obstetrics and Gynaecology

School of Medicine, Faculty of Medicine and Health

University of Leeds

Submitted in accordance with the requirements for the Degree of Doctor of Philosophy (PhD)

February 2017

Declaration

All placental tissues were collected from Leeds Teaching Hospitals Trust (LTHT), Leeds, UK. Case selection and collection was undertaken by myself and my supervisors. Clinical data was retrieved and analysed by myself. All stereological data collection, analysis, histological and immunohistochemical preparation was carried out by myself in the Section of Pathology and Tumour Biology, Leeds Institutes of Molecular Medicine (LIMM), St James' University hospital. Molecular analysis was carried out by myself in the Leeds Institute of Genetics and Health (LIGHT).

Statement 1

This copy has been supplied on the understanding that it is copyright material and that no quotation from the thesis may be published without proper acknowledgement.

Statement 2

This thesis is the result of my own investigations, except where otherwise stated. Where correction services have been used the extent and nature of the correction is clearly marked in a footnote(s). Other sources are acknowledged by footnotes giving explicit references. A bibliography is appended.

Statement 3

The right of **Mohamed Saad Elsayed ElMoursi** to be identified as Author of this work has been asserted by him in accordance with the Copyright, Designs and Patents Act 1988, © (2016). "The University of Leeds and Mohamed Saad Elsayed Elmoursi".

Print Name: Mohamed Saad Elsayed ElMoursi

Signed:  (candidate)

Date: 03/02/2017

Dedication

To my beautiful wife Sara and my kids;

Hadi and Mariam

To my father, mother, brother and sister

To Science

Acknowledgements

Supervision

I would like to express my gratitude to my supervisors Nigel AB Simpson, Valerie Speirs, Jens Stahlschmidt, Karen Forbes, Darren Treanor and Derek Magee for their expertise, support and guidance throughout my PhD. I would like to thank Dr Nigel Simpson for being a perfect and exceptional supervisor; he is very approachable and easy to talk to. His extremely fast responses to review my data are a big encouragement and motivation while doing this work. His attention to details always made me feel that I was his only PhD student.

Very special thanks go out to Valerie Speirs and Karen Forbes, whose consistent support and seemingly infinite patience both in and out of the lab was vital for me getting where I am today. I would also like to thank both for their advice and help in shaping my PhD project.

I would like to thank Jens Stahlschmidt (Histopathology department, Bexley wing, St James's University Hospital) for his expert histopathological examination and teaching, continuous support and guidance, validation of my results and helping me with sample retrieval from the archive.

Lab work

I would like to thank members of the section of Obstetrics & Gynaecology, department of Pathology and Tumour Biology as well as the division of Reproduction and Early Development. Special thanks goes to Filomena Esteves for her expert help in the immunohistochemistry optimisation.

Egyptian University

I would also like to thank members of my department of Obstetrics and Gynaecology in Mansoura University Faculty of Medicine especially Professor Mohamed E. Ghanem, Professor Nasser Ellakany and Professor Elsaid abdelhady for their encouragement and support.

Family

I would also like to thank my wife Sara, my kids Hadi and Mariam whom has been the source of my inspiration and comfort, my parents for their prayers and very strong emotional support and motivation and my brother and sister for their everlasting support.

Funding

I would also like to express my gratitude to the Egyptian Ministry of Higher Education, Leeds International Research Scholarship and Cerebra charity for funding my research to complete my PhD.

Pregnant women

Last and not least, I would like to thank the pregnant ladies who kindly gave me part of their placentas to complete this project.

Abstract

Background The pathogenetic mechanisms behind placental dysfunction-related complications like preeclampsia and intrauterine growth restriction have remained perplexing till now, in part because of lack of well-defined structural and functional molecular characterisation. There is growing evidence that links trophoblast debris and the existence of syncytial nuclear aggregates (SNA) to the pathogenesis of gestational diseases. Characterisation and quantification of structural and functional parameters of placental dysfunction may give researchers a clearer picture of the mechanisms underlying the development of high risk pregnancy.

Methods Placental samples were obtained from normal term pregnancies, preterm controls, as well as from pregnancies complicated by preeclampsia (PET), intrauterine growth restriction (IUGR) and PET-IUGR. Formalin-fixed, paraffin-embedded sections were visualised with H&E, stained using immunohistochemistry (IHC) and digitally scanned. Using stereological methodology, volumes of placental SNAs, trophoblasts, villi and capillaries were measured. Three dimensional (3D) volume reconstructions of terminal placental villi with SNAs and fibrinoid degenerations were created. IHC-labelled slides were analysed by image analysis algorithms. Differential expression of placental genes and miRNAs, hypothesised to regulate cell death in placental dysfunction, were quantified using RT-qPCR. BeWo cell lines were carried out for *in vitro* validation of the effects miRNAs regulating programmed cell death (PCD) using flow cytometry and western blotting.

Results Specific morphometric patterns of villous, trophoblasts, SNA and capillary volumes were demonstrated with characteristic higher SNAs and lower capillary volumes in PET placentae with reciprocal patterns in IUGR placentae showing a negative correlation pattern between nuclear aggregates and capillary volumes. Image analysis of immune-labelled slides showed a higher autophagy marker expression in PET and a positive correlation to SNAs as well as a balanced reciprocal expression patterns with apoptosis. Moreover, miR-204 transfected BeWo cells showed a similar balanced reciprocal regulation of autophagy and apoptosis expressions.

Conclusion We have demonstrated that applying stereology-based and image analysis on digitised placental sections can be useful in quantifying and dissecting structural and functional patterns in normal and abnormal placental function. 3D reconstruction model are a novel approach towards placental characterisation in normal and complicated pregnancies. The study also showed that miR-204 plays a vital role in the regulation of placental autophagy and apoptosis, critical in the pathophysiology of placental dysfunction.

Table of content

List of figures

List of Tables

List of Abbreviations

∑P	total number of points
3'UTR	3' untranslated region
8OHdG	8-Hydroxydeoxyguanosine
AGA	Appropriate for gestational age
AEDF	Absent end diastolic flow
ANOVA	Analysis of variance
ATG	Autophagy
Bcl-2	B cell CLL/lymphoma-2 protein
cDNA	complementary deoxyribonucleic acid
CE	Coefficient of error
CI	Confidence Interval
CK	CytoKeratin
CRR	Congo red retention
CTB	cytotrophoblast
DAB	3, 3’-diaminobenzidine
DE	Differentially expressed
dH_2O	Deionized water
EOIUGR	Early-onset intrauterine growth restriction
EOPET	Early-onset pre-eclampsia
EOPET/IUGR	Early onset pre-eclampsia with growth restriction
ER	Endoplasmic Reticulum
EtOH	Ethanol
FACS	Flow Cytometry
FCS	Fetal calf serum
FFPE	Formalin-fixed, paraffin-embedded tissue
GA	Gestational age
GAPDH	Glyceraldehyde-3-phosphate dehydrogenase
H&E	Haematoxylin and eosin
HELLP	Haemolysis, elevated liver enzymes, low platelet count
HKG	Housekeeping gene
IGF	Insulin growth factor
IHC	Immunohistochemistry
IQR	Interquartile range
IUGR	Intrauterine Growth Restriction

MAPLC3	Microtubule-associated protein light chain 3
LGA	large for gestational age
LOPET	Late-onset Pre-eclampsia
LOPET/IUGR	Late onset pre-eclamspia with growth restriction
miRNA	MicroRNA
mRNA	messenger ribonucleic acid
mTORC1	mammalian target of rapamycin complex 1 or mechanistic target of rapamycin complex 1
NGS	next-generation sequencing
NP	number of positive pixels
NSP	number of strong positive pixels
NSR	Ratio of strong/total pixel number
NWP	number of weak positive pixels
NWR	Ratio of weak/total pixel number
OD	optical density
PARP	nuclear poly (ADP-ribose) polymerase
PBS	Phosphate-buffered saline
PC	Placental capillary
PCD	programmed cell death
PET	Pre-eclampsia
P-MP	Pregnancy-Microparticles
PPC	Positive Pixel Count algorithm
PrR	Prevalence ratio
qRT-PCR	quantitative Real Time-Polymerase Chain Reaction
REDF	Reversed end diastolic flow
ROS	reactive oxygen species
RT	Room temperature
RTase	Reverse Transcriptase
SD	Standard deviation
SEM	Standard Error of the Mean
SGA	Small for gestational age
SNA	Syncytial nuclear aggregates
SRS	Simple Random Sampling
STB	Syncytiotrophoblast
STP	Staurosporine
SURS	Systemic Uniform random Sampling

TBS	Tris-buffered saline
TOP1	DNA topoisomerase 1
TUNEL	Terminal deoxynucleotidyl transferase (TdT) dUTP nick-end Labelling
VAR	Variance
VD	Volume Density
YWHAZ	tyrosine 3-monooxygenase/tryptophan 5-monooxygenase activation protein, zeta polypeptide

Chapter 1
General Introduction

1.1 High risk pregnancy

1.1.1 Preeclampsia (PET)

1.1.1.1 Definitions

Preeclampsia is a multisystem pregnancy-associated syndrome unique to humans clinically characterised by the new onset of hypertension and proteinuria after 20 weeks of gestation. It affects 3% to 8% of all pregnancies (1). The American College of Obstetricians and Gynaecologists (ACOG) and the International Society for the Study of Hypertension in Pregnancy (ISSHP) defines PET as a new onset hypertension (>140/90 mm Hg) and proteinuria (>0.3 g per day) after 20 weeks of gestation. According to the latest ACOG guidelines in November 2013, the detection of high levels of protein in the urine (proteinuria) is no longer essential for the diagnosis of preeclampsia. Preeclampsia may be now diagnosed by persistent hypertension that develops during pregnancy or during the postpartum period that is associated with proteinuria OR thrombocytopenia, renal or hepatic dysfunction, pulmonary oedema and seizures (2).

The definitions of preeclampsia are not only decisive for the clinical practice, in which clinical judgment and timely intervention has significant importance, but also for research, in which unbiased data and uniform criteria adopted by different researchers are equally important. Different variants of the definition have been proposed (ACOG, ISSHP, Australian College) in an attempt to encompass all the different aspects of the syndrome. Strategies such as “The Core Outcomes in Women’s health” (CROWN) initiative, an international initiative led by journal editors to harmonise outcome reporting in women’s health research, may seek to address these variations (3).

1.1.1.2 Classification

Preeclampsia has been sub-classified into mild, moderate and severe, depending on blood pressure measurements, and additionally by gestational age into

early onset (prior to 34^{+0} weeks) and late onset (after 34^{+0} weeks) preeclampsia (PET) (4). Early and late-onset PET have shown differences in clinical risk factors that made it tempting to speculate that those are two different conditions in terms of pathogenesis, aetiology and therefore clinical phenotypes but this remains a subject of extensive research.

1.1.1.2.1 Late-onset preeclampsia (LOPET)

LOPET constitutes around 80 % of PET world-wide. Delivery is usually at term with normally grown newborns that are appropriate size for gestational age (AGA) with lower incidence of growth restriction. Also, the placental weights and volumes are usually in the normal range (5). The umbilical artery blood flow to the fetus usually remains normal in line with the normal growth projection of the fetus leading to a normal or slightly altered umbilical Doppler waveforms and/or a minimal increase in the pulsatility index (PI) (6). Pregnant women displaying increased placental mass or volumes due to diabetes or multiple pregnancies were found to be more prone to this subtype of preeclampsia (7).

1.1.1.2.2 Early-onset preeclampsia (EOPET)

Less than 20% of all preeclampsia cases can be categorised as early-onset (8). This group usually shows evidence of inadequate trophoblast invasion of the maternal spiral arteries leading to uterine artery flow perturbations evidenced by notches and increased PI of the Doppler waveforms. Moreover, EOPET pregnancies show abnormalities in the umbilical artery Doppler like increased systole/diastole (S/D) ratio if end diastolic flow is still preserved (PEDF), or absent (AEDF) and even reversed end diastolic blood flow (REDF) velocity (9). Interestingly, pregnancies diagnosed with EOPET frequently co-present with another major pregnancy complication, fetal or intrauterine growth restriction (FGR or IUGR). IUGR shares the characteristic features listed above for EOPET, such as poor trophoblast invasion leading to insufficient maternal spiral artery transformation. This may be followed by uterine artery blood flow changes as well as umbilical artery blood flow changes like absent or reduced end-diastolic flow (AEDF, REDF) (10).

Intriguingly, the classification of preeclampsia into mild and severe does not mirror the classification of early and late onset preeclampsia (10). That is to say, both early and

late (preterm and term) PET pregnancies have mild and severe cases. Nonetheless, it is observed that the more severe cases in respect to clinical relevance are usually early onset in nature. This might be related to the additional pathology of IUGR added early on and linked to the pathogenesis of PET (10).

1.1.1.3 Complications

Severe pre-eclampsia remains a major cause of severe maternal and perinatal morbidity and mortality (11, 12). Reported maternal complications include placental abruption, eclampsia, stroke, HELLP (haemolysis, low platelets, and elevated liver enzymes) syndrome, disseminated intravascular coagulation, liver haemorrhage or rupture, pulmonary oedema, acute renal failure, adult respiratory distress syndrome, and death (11).

Pre-eclampsia is still also a leading cause for maternal mortality worldwide; where the World Health Organization (WHO) estimates that worldwide ~63,000 women die annually because of pre-eclampsia related complications (13). In developing countries, it amounts to as high as 15% as compared with 0% to 1.8% in developed countries. That may be due to the lack of health access to appropriate maternity care (14). Moreover, hypertensive pregnancy disorders account for around 26% of maternal deaths in Latin America and the Caribbean and 9% of deaths in Africa and Asia (13). Other hypertensive disorders in pregnancy include pre-existing essential hypertension and pregnancy induced hypertension (PIH).

Adverse perinatal outcomes include preterm delivery, Intra uterine growth restriction (IUGR), stillbirth and neonatal morbidity (15). A third of babies born to preeclamptic pregnancies are born preterm, and quarter of them growth-restricted. Long-term maternal risks include chronic hypertension, ischaemic heart disease and diabetes mellitus (16). An unfortunate detail that adds to the problematic and often late diagnosis is that most pregnant women with preeclampsia show no symptoms until late or complicated.

System	Complications of PET
Central Nervous System (CNS)	Eclampsia (seizures) Cerebral oedema Cerebral haemorrhage Cortical blindness Retinal oedema
Renal system	Renal tubular and cortical necrosis
Respiratory system	Pulmonary and laryngeal oedema
Hepatic system	Haemolysis, elevated liver enzymes, low platelets (HELLP) syndrome Jaundice Disseminated intravascular coagulation Haemolysis
Placenta	Placental infarction Placental abruption
Fetus	Growth restriction Preterm delivery Death or stillbirth

Table 1-1 Maternal, placental and fetal complications of pre-eclampsia. Adapted from Duley et al (12)

1.1.1.4 Pathogenesis

The precise aetiology of the pathogenesis of preeclampsia is still unclear and remains a subject of extensive research. Though it is anticipated that a multifactorial background is involved, it has become obvious that the placenta rather than the fetus is a prerequisite for the syndrome development (17). The clinical features of PET are thought to arise from various pathophysiological processes related to impaired implantation, endothelial dysfunction and systemic inflammation (18). Moreover, shallow cytotrophoblast invasion of maternal endometrial spiral arteries leading to their inadequate remodelling with consequent placental hypoxia and/or ischemia has been linked to the pathogenesis of preeclampsia early on (19).

Remodelling is a multistep process commencing around the implantation period (20). Any aberrations at this stage could raise the risk of pre-eclampsia, and might explain why women with recurrent miscarriage and unexplained subfertility have higher rate of PET (21).

Moreover, this process of inadequate remodelling is not specific to pre-eclampsia. Similar initiating placental dysfunction pathways may also lead to IUGR with or without PET. Furthermore, IUGR is not a consistent feature in association with PET being more commonly associated with early-onset preeclampsia (EOPET) (22) raising the question whether the typical pathological features of EOPET with IUGR are caused by PET or are simply the features of the combined and overlying syndrome, IUGR.

It has also been speculated that pre-eclampsia is a syndrome resulting from an inadequate interaction of two genetically distinct organisms, sometimes known as Haig's maternal-fetal conflict hypothesis (23). The maternal–fetal conflict hypothesis suggests that there is a selective gain to fetuses who can selfishly maximize their own growth at the expense of the their mother and siblings, whereas there is an opposing benefit to mothers who can counter these adaptations by maintaining equal investment in all offspring (24). A complex interplay of proteins from the mother and the fetus, at the maternal–fetal interface, mediates nutrient and waste exchange, immunoregulation, and other pregnancy-related physiological processes. These interactions are likely to lead to an evolutionary conflict between maternal and fetal genes (25). It has also been proposed that atypical or excessive maternal immune response to trophoblasts (26) and either impaired decidualisation or lack of proper preconditioning of the uterine decidua (27) might be linked to the pathogenesis of the first (placental) stage of pre-eclampsia.

This apparently inexplicable heterogeneity of the pathophysiology of pre-eclampsia may be explained partly by the resulting placental response to the initial insult. This may include the release of debris from the placental syncytiotrophoblast, variable in quantity and function, into the maternal circulation, which may induce maternal vascular and immunological responses characteristic of PET (Figure 1-1).

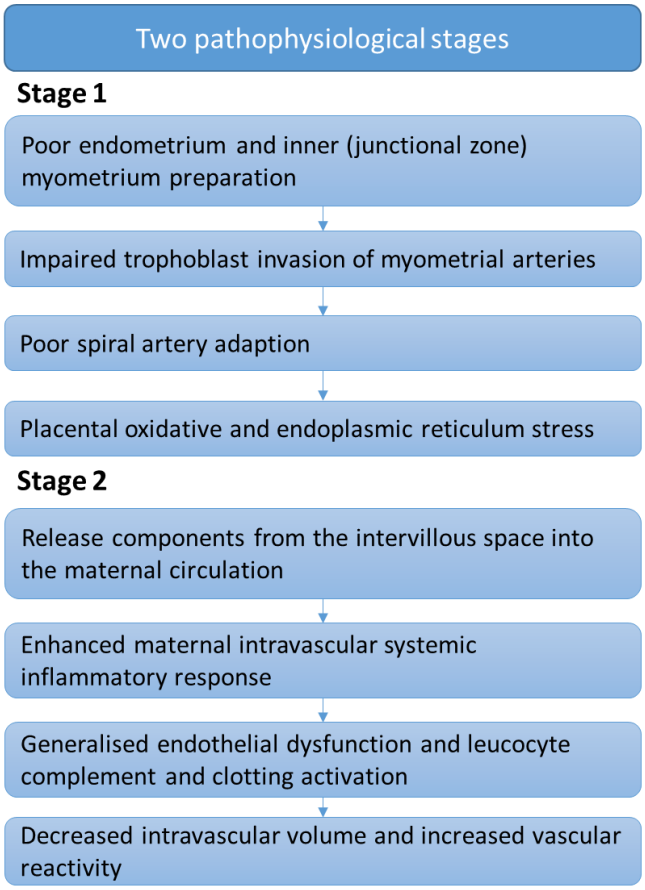

Figure 1-1 Possible pathophysiological processes in pre-eclampsia, adapted from Steegers, 2010 (28)

1.1.2 Intrauterine growth restriction (IUGR)

1.1.2.1 Definition

Growth restriction is a term given to describe infants of low birth weights for the gestational age. Several other terms are also used including small for gestational age (SGA) and IUGR. Although both terms are interchangeably used to describe the same clinical phenotype, they are not the same.

1.1.2.2 Small for gestational age (SGA)

SGA is defined as newborns with a birth weight below the 10th percentile for gestational age (29), however, this definition does not differentiate between those who are constitutionally small due to factors such as ethnicity, maternal height and weight and those who are small due to growth restriction. It is sometimes referred to as

physiological smallness, where during examination the placenta may be normal except for its small size (30) (31).

1.1.2.3 Intrauterine growth restriction

Fetal growth restriction refers to the fetus that does not achieve its expected growth potential *in utero* at a given gestational age. Clinically, most newborns with IUGR are diagnosed because they are born SGA with a birth weight below the 10th percentile for gestational age. However, the switch of SGA for IUGR is inaccurate. This is because using the SGA criteria does not discriminate the constitutionally small fetus that reaches its normal growth potential from similarly small infants with IUGR whose birth weight is lower than the predicted optimal birth weight. Moreover, using SGA as the indicator for growth restriction will not include newborns with IUGR who have birth weights that are greater than the 10th percentile. This has led to the development of customized fetal growth curves based on constitutional factors to help differentiate between SGA infants who are normally small from those with IUGR (32).

Growth restriction can occur alone or in combination with pre-eclampsia. Their combined appearance of growth restriction with early onset preeclampsia has led to questions whether the blood flow and pathological changes indicative of growth restriction are also relevant to the aetiology of early onset preeclampsia. Moreover, ultrasonography diagnostics measuring changes in fetal growth, uterine and umbilical arteries blood flow changes have shown exactly the same features in isolated early-onset growth restriction compared to growth restriction associated with early onset preeclampsia (9). Moreover, studies have shown that abnormal uterine dopplers at 11-14 weeks identified one-third of women with severe early onset preeclampsia, and all fetuses with early-onset IUGR (9, 33). Hence, it is tempting to speculate that these changes are mainly due to growth restriction and not preeclampsia. However, pathological changes in their placenta, which is incriminated in both pathologies and thought to reflect upon the clinical and radiological parameters, may be required to be adequately assessed in those two groups to either prove or refute this hypothesis.

1.1.2.4 Epidemiology

The incidence of intrauterine growth restriction differs among populations and rises with decreasing gestational age. It is estimated that IUGR is more prevalent in

developing and resource limited countries where studies have shown that around 23 % of term infants are SGAs compared to only 10 % in developed countries (34).

1.1.2.5 Aetiology

Maternal, fetal and placental factors can be implicated in the development of growth restriction. However, 40% of IUGR pregnancies appear to be idiopathic with no identifiable underlying cause. It is estimated that one-third of the cases are genetic in origin and is related to the fetal environment in the other two-thirds (35).

1.1.2.6 Complications

Newborns with IUGR are at higher risk of premature delivery, perinatal asphyxia, impaired thermoregulation, hypoglycaemia, polycythaemia and impaired immune function (36). Perinatal mortality rates are also increased in small for gestational age (SGA) compared with appropriate for gestational age (AGA) infants in both term and preterm infants, and increases more as growth restriction becomes more severe (37-40). Fetal growth restriction is also associated with long-term morbidity; where severely affected infants frequently are shorter and weigh less than their AGA peers throughout childhood and adolescence with heights more likely to be less than the 10th percentile (41). Moreover, IUGR infants appear to be at increased risk for adverse neurodevelopmental outcomes and decreased intellectual performance (42). More alarmingly, growth restriction also seems to be a contributing factor for later-on-in-life adult diseases including ischaemic heart disease, hyperlipidaemia, hypertension, and chronic kidney disease (CKD) (43, 44).

1.2 Role of the placenta

The importance of the placenta as the nutritional and immunological gateway to the normal fetal development is well established. Moreover, different pregnancy complications such as PET and IUGR are conditioned on placental dysfunction and that its delivery results in its resolution. Furthermore, PET is more common in disorders associated with hyperplacentation such as hydatidiform mole, diabetes, and multiple pregnancy (7). Hence, placenta-related events are believed to be a central factor in the pathogenesis of gestational disease like PET and IUGR.

A key problem encountered by clinicians and researchers is that PET is a heterogeneous pool of disease manifestations with varying severity, that share some common features but also show fundamental discrepancies indicating that a single mechanism cannot explain all preeclampsia presentations (45). In preeclampsia, shallow cytotrophoblast invasion of maternal endometrial spiral arteries leads to inadequate remodelling of uterine spiral arteries with placental hypoxia and/or ischemia (19, 28). However, the same pathology may commonly lead to the development of IUGR and even preterm labour without developing preeclampsia (22). It is likely that placental dysfunction triggers the release of factors, which are variable in quantity and function, into the maternal circulation which interacts differently with the mother's immune and vascular systems leading to a heterogeneous range of gestational disease.

1.3 Placental development and maintenance

Embryologically, the trophoblast is the first cell lineage to differentiate during human development at around six days post conception (pc) when the morula develops into the blastocyst. Within the next two weeks, consecutive differentiation steps lead to the development of two trophoblast sub-populations, the villous and extravillous trophoblasts (46). At around day 12 pc, when the extravillous trophoblast has not yet been developed, the villous trophoblast develops into two layers, cytotrophoblasts and syncytiotrophoblasts. At or soon after day 15 pc, the early cytotrophoblasts come into contact with the decidual stroma in the maternal side of the developing placenta. The extravillous trophoblast population is developed in week 3 pc. During the next two weeks, consecutive differentiation of the villous and extravillous sub-populations continues (46).

The villous trophoblast shell is the epithelial layer covering the villous tree of the placenta. It is formed of a basal layer of mononucleated cytotrophoblasts covered by unicellular multinucleated syncytiotrophoblast with no lateral cell borders. Syncytiotrophoblast is maintained by syncytial fusion of underlying cytotrophoblasts representing a typical syncytium covering the entire placental villous tree. Thus, there is only single syncytiotrophoblast unit per placenta (47).

The villi at the feto-maternal interface are connected of the basal plate by trophoblast cell columns forming the anchoring villi. The overlying basement membrane is covered by continuously proliferating cytotrophoblasts (48, 49) which serve as source of extravillous trophoblasts which then invade into maternal uterine interstitial and vascular tissues of the placental bed finally reaching the inner third of the myometrium (50).

1.4 Placental dysfunction and failure

1.4.1 Placental perfusion

Compromised remodelling of the spiral artery in the developing placenta has particularly been considered as an early pathological sign leading to preeclampsia (51). In the inner myometrium, vascular changes in the decidua arise as well followed by trophoblast invasion with accompanied remodelling (52). At 7-8 weeks gestational age, intervillous flow begins by forming channels connecting the lacunae in the wall of the implanted blastocyst with the spiral arteries (53). Trophoblast invasion and the deplugging of spiral artery outlets begins in the centre and spreads to the periphery. This trophoblast invasion leads to wider calibre vessels with increased laminar blood flow to the placental chorionic villi. Inadequate lateral spread could lead to widespread chorionic regression and a smaller placenta, leading to IUGR, PET, or both (54).

Since spiral arteries in the myometrium have distinct muscular and elastic layers than the corresponding decidual vessels, inadequate or failed remodelling results in reduced diameters and uteroplacental flow with periods of irregular placental perfusion. Such episodes of hypoxia/reoxygenation could produce reactive oxygen species (ROS), thus increasing the placental oxidative stress and therefore placental dysfunction (Figure 1-1)(55).

1.4.2 Trophoblastic debris

1.4.2.1 Introduction

The placental villous tree is covered by a continuous, uninterrupted, unicytoplasmic, multinucleated syncytial layer called syncytiotrophoblast (STB). It is the only fetal layer that is in direct contact with the maternal circulation and hence regulates gas and

substrate exchange between the mother and the fetus, as well as synthesising and secreting growth factors and hormones (56).

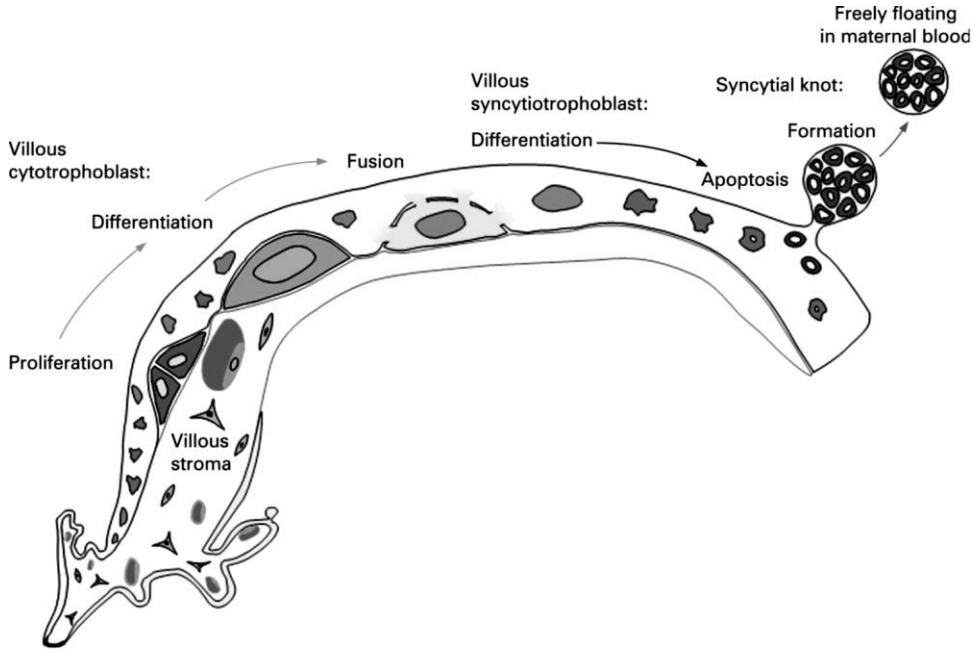

Figure 1-2 Trophoblast lifecycle. Cytotrophoblasts on the left proliferate as daughter cells and then leave the cell cycle as they differentiate and fuse with the syncytiotrophoblast layer (STB). The syncytiotrophoblast then differentiates further till the aged nuclei starts the process of apoptosis and compacted into an SNA which is then released from the apical membrane and enter the maternal circulation. Adapted from Huppertz, 2008 (57).

During the course of normal pregnancy, large multinucleated aggregates of the syncytiotrophoblast called syncytial nuclear aggregates (SNAs) develops reaching a size greater than 100 µm in length with a diameter of 60–200 µm (58), as well as much smaller Pregnancy-Microparticles (P-MP) (59) including exosomes (30-100 nm), microvesicles (0.1-1 µm) and apoptotic vesicles (1-5 µm), together with necrotic debris, collectively called trophoblast debris. They are shed into the maternal circulation (60) in a process called trophoblast deportation. Under normal circumstances, this process increases with gestational age and labour, with few detectable by 48 hours post-delivery (61).

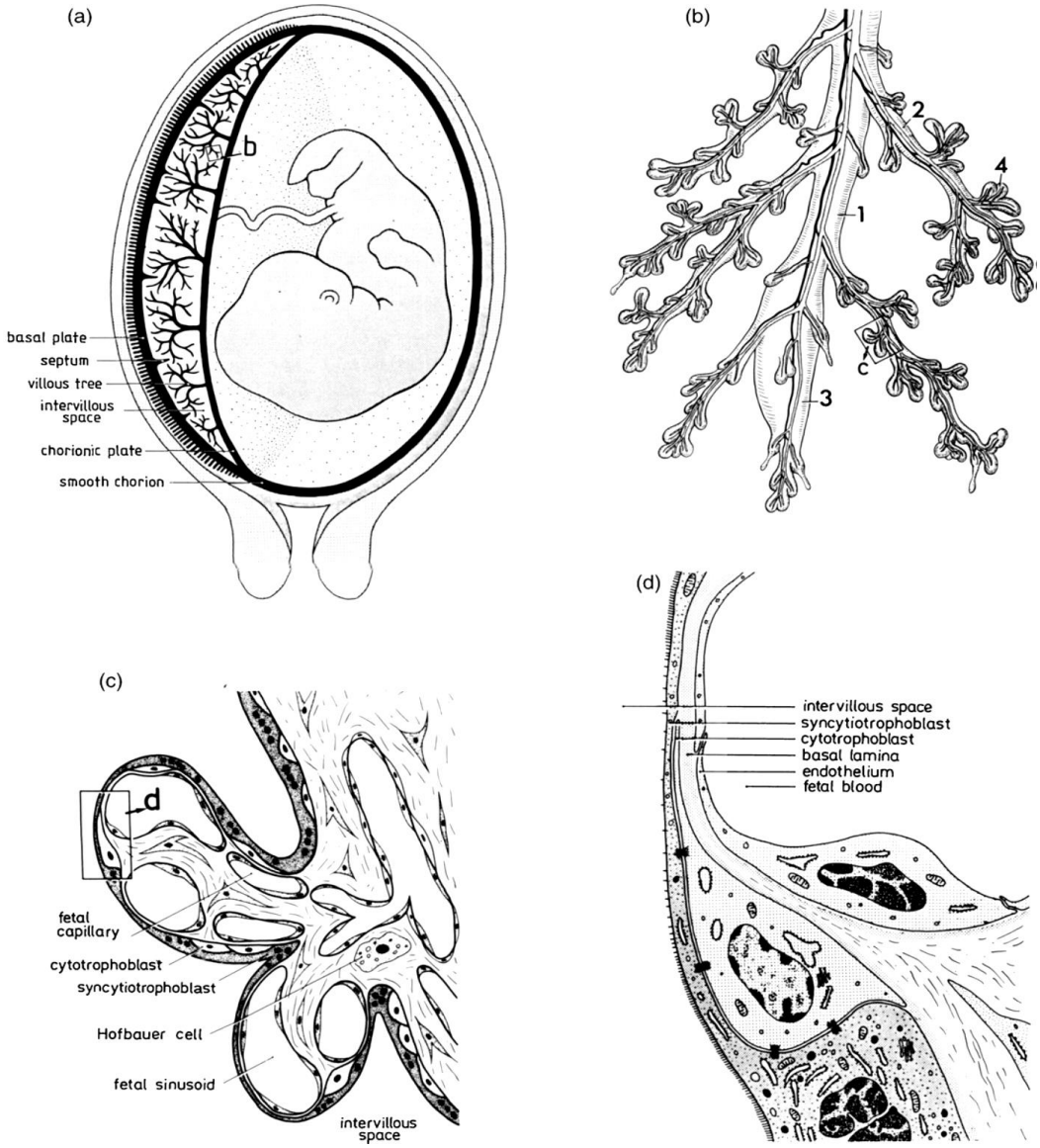

Figure 1-3 Basic Anatomy and histology of the human placental villous architecture. (a) A longitudinal section across the uterus, placenta, and membranes. (b) Peripheral arborisation of villi starting from stem villi (1), and into a bulbous immature intermediate villus (3); then slender side branching (2) are the mature intermediate villi, densely covered with grape-like terminal villi (4). (c) Light microscopic (LM) section of two terminal villi, branching off a mature intermediate villus (right). (d) An electron microscopic representation of the placental barrier with its typical layers. Image from Benirschke and Kaufmann (62, 63).

In 1893, Schmorl first reported the occurrence of large multinucleated syncytiotrophoblasts trapped in the pulmonary capillaries in women who had died of eclampsia (64). Later, it also became evident that trophoblastic deportation occurs in

normal pregnancy as well (46, 59, 65, 66) starting from 6 weeks of gestation and onwards (67).

Trophoblastic debris can travel from the placenta along the draining uterine veins, into the inferior vena cava via the heart and into the pulmonary arteries, where most of them become lodged in the pulmonary capillaries and into the peripheral circulation (58, 60, 66) where an effective mechanism of phagocytosis is ready to remove them from the maternal circulation (46).

1.4.2.2 Functions of the deported debris

The biological significance of this deported trophoblastic debris is still unclear. Recently it has been shown that trophoblast deportation is not merely a waste disposal system from the fetus to the mother (68, 69) but serves as an immunomodulatory role towards the growing fetus by being an ongoing source of paternal antigens to the maternal immune system.

A constant process of trophoblast layer remodelling occurs throughout the placental development. It is characterized by the functional loss of trophoblast cells by apoptosis, a physiological process of programmed cell death, and the fusion of new cytotrophoblasts (70). It has been suggested that in normal pregnancy, a predominantly apoptosis-type cell death leads to SNA shedding. Whilst in the placenta of preeclampsia and/or IUGR, a dysregulation in the mode of programmed cell death might lead to the shedding of more necrotic SNAs (71).

There is growing data that suggests that phagocytosis of apoptotic cells leads to a more tolerogenic immune response (72, 73), whereby the release of phagocytosed necrotic cells or those that did not complete the apoptotic cascade results in an inflammatory response. Thus the maternal vascular and immune system response to the deported SNAs may be dependent on the underlying mode of cell death (72, 73).

1.4.3 Syncytial Nuclear Aggregates

Syncytial nuclear aggregates (SNA) are clusters of densely-packed, degenerate syncytial nuclei on the villous surface that are released into the intervillous space in the form of tightly-sealed membrane-bound vesicles, possibly in an attempt to prevent an adverse inflammatory response in the mother (74). The mechanisms involved in

the formation and shedding of SNAs are still unknown, however, it is hypothesised that shear mechanical stress from the flow of blood through the intervillous space drives the aggregation of these degenerate nuclei toward the tips of villi where they congregate into SNAs (74).

It is also hypothesised that programmed cell death is involved in the shedding of these nuclei in the form of apoptotic bodies into the maternal circulation so as to avoid a maternal inflammatory response (75). One of the hallmarks of apoptosis is that cells undergoing programmed death are normally phagocytosed by macrophages and dendritic cells without activating an inflammatory or immune response (76). Moreover, the mechanism of clearance after shedding of the SNAs is still unclear, though fragments of SNAs have been identified in the capillary beds of maternal lungs, suggesting that this first capillary system is responsible for their phagocytosis after their release from the placenta (77).

SNAs are sometimes referred to as syncytial knots (SK). They were first described by Tenney and Parker in 1940 (78). The increased SNA formation in placentas from complicated pregnancies, continue to be referred to as Tenney-Parker changes (78). They described it on nearly all terminal villi in preeclamptic placentas, whereas they were only found on 10% to 15% in normal placentas. They described them on examination of two-dimensional histologic sections, which has since been recognised later that viewing a single section in a highly branching and tortuous villi (as in PET and IUGR) can increase the incidence of tangential sections through the STB, which can also give an impression of increased prevalence (79, 80).

SNAs are the only component of the trophoblastic debris that are histologically amenable to study. Currently, our knowledge of SNAs is based mainly on describing them in histological slides. It would be a great benefit if researchers would be able to quantify their most basic features across different placental pathologies (69). A stereologically-based volume estimation of such SNAs in different correlating placental pathologies may help researchers understand the role they play in the pathogenesis of PET and/or IUGR.

1.5 Apoptosis

1.5.1 Apoptotic cascade

Apoptosis is a tightly regulated, well-characterised, energy-dependent programmed cellular demise mechanism associated with cell shrinkage, membrane blebbing, nuclear condensation and DNA fragmentation (81, 82). Caspases represent a family of cysteine proteases that have essential regulatory function of apoptosis (Figure 1-4). Initiator caspases (including caspase-2, -8, -9, -10, -11, and -12) are closely tied to pro-apoptotic signalling. Initiator caspases cleave and activate downstream effector or 'executioner' caspases-3, -6, and -7 that modify proteins eventually responsible for programmed cell death. Targets such as nuclear poly (ADP-ribose) polymerase (PARP) are cleaved by executioner caspases and serve as markers of apoptosis. PARP is believed to be involved in DNA repair as a result of environmental stress (83, 84).

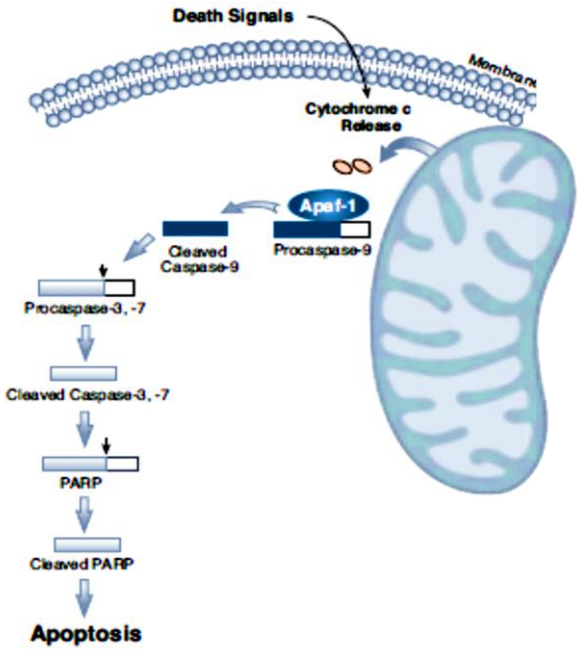

Figure 1-4 A schematic diagram of the apoptotic cascade.

1.5.2 Apoptosis in trophoblasts

Apoptosis is known to play a crucial role in trophoblast differentiation and syncytial fusion of villous cytotrophoblasts with the syncytium, a fusion which is known to be coupled to the early stages of the apoptotic cascade (Figure 1-5) (85). Studies have

reported an activation of the initiator stages of apoptosis, and is linked to the temporal and spatial regulation of the cytotrophoblastic fusion to the syncytium (86) and are believed to be restricted to the cytotrophoblast cells that are designated to fuse to the STB, thereby preserving a reservoir of progenitor proliferating cytotrophoblast cells required for further syncytial growth and regeneration during pregnancy (87). For example, active caspase 8 has been found to be expressed in cytotrophoblast cells before syncytial fusion. Moreover, its blockage by antisense oligonucleotides or peptide inhibition resulted in significant inhibition of trophoblast fusion to STB in villous explant cultures and the build-up of cytotrophoblast cells (86) thus leading to expression of some of the apoptotic-related proteins in post-proliferative cytotrophoblast cells that are destined for syncytial fusion (88). In turn, this leads to phosphatidylserine (PS) flip from the inner to the outer plasma membrane of the trophoblast, and acting as a trigger for syncytial fusion which is believed to be followed by the transfer of the apoptosis machinery from the cytotrophoblast to syncytiotrophoblast (89, 90). These measures, though are the hallmarks of apoptosis, are still this far reversible.

Although details of induction of the apoptotic machinery is not well understood in the placenta (91, 92), cytotrophoblasts, after syncytial fusion, are thought to go through the 'executional' or final stages of the apoptotic cascade in STB leading to the induction of caspases 8, 9 and 10 responsible for the degradation and cleavage of the cytoskeletal proteins vimentin, actin and fodrin, resulting in membrane blebbing (82).

These initial phases of apoptosis, which are believed to be reversible, appear not to advance to the late final stages of apoptosis, but rather are suspended thus preventing the premature death of STB nuclei (74, 93). Nonetheless, effector caspases 3, 6 and 7 activation commonly, but not unavoidably, follow these focal apoptotic inhibitions. This leads to cleavage of the cytoskeletal filament proteins and formation of an immunohistochemically detectable neo-epitope (M30) (88, 94). It is hypothesised that several weeks later, the apoptotic cascade is reactivated by irreversible activation of the executional caspases leading to DNA condensation (pyknosis), fragmentation, change in the nuclear and cellular shape, and finally forming SNAs (74).

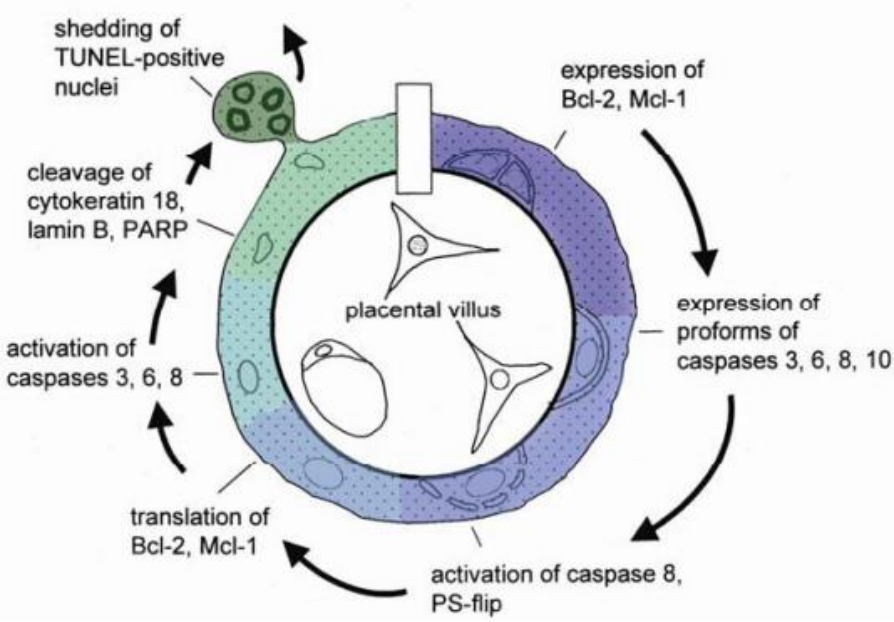

Figure 1-5 Apoptosis cascade progression in villous trophoblasts. Molecular markers for the apoptotic machinery present in the cytotrophoblast; where prior to syncytial fusion only the reversible early stages of apoptosis takes place. After syncytial fusion, the cascade is paused where it is restarted several weeks later. Lastly, late apoptotic nuclei are packed in SNAs and shed into the intervillous space (74)

However, in a typical apoptotic cascade, once the cascade is activated the cell will die within 24 hours but the turnover from syncytial fusion to shedding of syncytial knots in normal pregnancy may take around 2-3 weeks (88). It may be that after syncytial fusion, the cascade is paused then restarted several weeks later in separate areas of the syncytiotrophoblast. Lastly, late apoptotic nuclei are packed in SNAs and extruded into the maternal circulation (74).

One of the factors believed to assist in this focal apoptotic suspension is the upregulated expression of the anti-apoptotic proteins Bcl-2, Mcl-1, and Mdm2 in the STB compared to the cytotrophoblast (74, 93). However, the half-life of Bcl-2 is only a fraction of the supposed period of suspension (95).

Another trophoblast apoptotic discrepancy is that it is not associated with typical apoptotic morphological appearances as nuclear blebbing, or karyorrhexis (74) and given that widespread apoptosis in villi would be devastating to the placenta, and the developing fetus. Hence, it is tempting to speculate that the human villous trophoblasts display other prosurvival mechanisms to maintain homeostasis and protect from

dysregulated apoptosis. One mechanism by which cells protect themselves from stressors is autophagy (96), known to have an antiapoptotic role in other systems, which may play a role in orchestrating trophoblast survival in the placenta with antiapoptotic proteins. Moreover, autophagy vacuoles has been reported to be seen in the vicinity of SNAs and may be linked to delaying the already initiated apoptotic machinery (97).

1.6 Autophagy

1.6.1 Introduction

Autophagy is a Greek term coined by Christian De Duve to indicate “self-eating” (98). It is a tightly regulated process through which dysfunctional proteins, organelles, and invading microorganisms are confined within double membrane-bound vesicles called autophagosomes, which then fuse with lysosomes, leading to cargo degradation in the resulting autolysosome and hence recycling of biomolecules (99).

The autophagy process begins in response to an intracellular milieu that strays from normal homeostasis (100). Induction of autophagy and recognition of the cargo leads to formation of a C-shaped double membrane organelle called the phagophore. When a phagophore closes around the cargo forming a double-membrane organelle, it is called the autophagosome, which then fuses with lysosomes via the help of the cytoskeleton. Merging the autophagosomal outer membrane with the lysosomal membrane results in the lysis of the autophagosome’s inner membrane by lysosomal enzymes like specific acidic hydrolases in addition to the cargo therein contained, liberating monosaccharides, free fatty acids, and amino acids into the cytoplasm for re-use (99).

The phagophore membranes are initially derived from the endoplasmic reticulum (ER), trans-Golgi network and late endosomes (101), but *de novo* synthesis of membranes is also thought to be involved in the phagophore expansion. The newly formed autophagosomal membranes are modified by a ubiquitin-like system that facilitates the processing of microtubule-associated protein light chain 3-I (LC3-I) into the LC3-II isoform. Microtubule associated protein 1 light chain 3 (MAP1LC3) is the mammalian homologue of the yeast autophagy protein ATG8 with three mRNA isoforms currently

known, LC3A, LC3B, and LC3C (102). LC3-II is a useful and flexible marker for accurate autophagy flux assessment. It is the active membrane bound form processed from the cytosolic LC3-I by posttranslational modification. LC3-II, which is characterised by a covalent attachment to phosphatidylethanolamine (PE), fuses into PE-rich lipid membranes with the relative amount of LC3-II reflecting the autophagic activity, thus constituting a specific and reliable marker for autophagosome formation in mammalian cells (103, 104).

Autophagic flux refers to the progression of the autophagy process to completion. It is critical to discriminate autophagosome development that signposts the induction of autophagy, and the autophagy flux, which governs if the autophagy process goes to completion or not. Because a complete autophagy flux cycle will commonly exhibit a cytoprotective effect, autophagy inhibition can lead to the build-up of autophagosomes, therefore leading to physiologic dysfunction (105).

Even though previously labelled as a cell death pathway, autophagy is now considered to be a key pro-survival phenomenon from environmental stresses facing most physiological systems (106). It is a process that declines in animal cells with aging *in vivo* and *in vitro*, associating the process to longevity (107). Indeed, caloric restriction was reported to both induce autophagy and promote longevity as well (108).

There are growing evidence that autophagy (ATG) proteins, in addition to regulating the autophagy pathway, are also involved in different immunologic and metabolic pathways, emphasising the intricate and coordinated relationship of autophagy with other signalling pathways (109).

The way the recycling function of autophagy impacts the cellular physiology varies depending on the circumstances. Cellular homeostasis is maintained by basal autophagy via removal of dysfunctional organelles and misfolded protein aggregates (110). Moreover, acute induction of autophagy, as a result of cellular stresses like nutrient deprivation, hypoxia, and pathogen infection, provides a cytoprotective response leading to a better survival and cellular adaptation. Moreover, it acts as a vital natural defence mechanism towards infectious, inflammatory, neoplastic and degenerative disorders, and the dysregulation of which is linked to the pathogenesis of several human diseases (110, 111).

1.6.2 Autophagy regulators

1.6.2.1 Nutrient deprivation

Starvation or nutrient deprivation is a well-known and effective autophagy inducer, where reducing the availability of amino acids results in inhibition of the mammalian target of rapamycin (mTOR) complex1 thus inducing autophagy. Conversely, mTOR is stimulated by increased availability of essential amino acids in skeletal muscle, which is shown to both increase amino acid transporter expression and mTOR signalling (112).

1.6.2.2 Growth factors

Growth factors are major regulators of autophagy, where autophagy is known to be induced on withdrawal of growth factors from the extracellular environment (113). These effects are probably mediated through different signalling pathways. One of them is through insulin and insulin-like growth factors regulating the mTOR signalling pathway (114, 115). Furthermore, growth factors are known to inhibit Tuberous Sclerosis Complex (TSC) function by both Phosphatidylinositol-4,5-bisphosphate 3-kinase (PI3K) dependent and independent pathways (116).

1.6.2.3 Energy levels

Similarly, energy levels detected by the 50-AMP-activated protein kinase (AMPK), which detects reduced ATP levels inside the cell, can regulate autophagy pathway. A reduced ATP/AMP ratio stimulates AMPK through phosphorylation of the TSC1/2 complex, which inhibits mTOR activity and thus activating autophagy (117). Moreover, cellular ATP production is known to increase during the autophagic process (118). The final consequence of the induced autophagy process is a continued cellular existence despite starvation through this partial self-eating, and evading apoptotic cascade activation.

1.6.2.4 Hypoxia

Autophagy is also known to be activated by hypoxia by at least two mechanisms. First, sustained hypoxia diminishes levels of ATP and thus stimulates AMPK. Secondly, hypoxia stabilises hypoxia-inducible factor 1 (HIF-1), an important transcription factor

regulating cellular response to hypoxia, thus activating TSC1/2 and inhibiting mTORC1 activity and resulting in autophagy activation (119, 120).

1.6.2.5 Oxidative stress

Oxidative stress is known to have an important role in autophagy induction, especially by formation of superoxide anions (121). Multiple reactive oxygen species (ROS) as well as hydrogen peroxide are released from the mitochondrial electron transport system during energy generation. Nevertheless, the cell antioxidant defences try to remove such oxidant metabolites to avoid cell damage by induction of autophagy. Whereas, induced mitophagy was found to degrade dysfunctional mitochondria and diminishe ROS formation, thus promoting cell survival (122, 123).

1.6.3 Role of autophagy in cell survival and death

Autophagy is now believed to play an important role in the process of aging, neurodegeneration, infection, cancer, and autoimmune diseases like Crohn's disease and rheumatoid arthritis (124-126). Whether the role of autophagy at the cellular level involves a pro-survival or pro-death function usually depends on the context (126, 127).

The most well-defined autophagy function at the cellular levels is the pro-survival one, helping cells adapt to stressful events by clearing dysfunctional organelles, misfolded proteins and pathogens or by providing the cell with anabolic building elements and energy during periods of nutritional deprivation. Nonetheless, other studies have also identified autophagy as a mechanism of an apoptosis or caspase-independent cell death (106, 128). The quest for understanding when and where these incongruent functions of autophagy apply are the principal goals in this field as controlling autophagy could potentially help researchers modulate cell death making it a potential target for therapeutics in several diseases (129-131).

1.6.3.1 Autophagy and apoptosis

One way to reach such a goal is to understand the intricate and multifaceted molecular networks between autophagy and cell death (apoptosis and necrosis). Though it is widely recognised that autophagy functions as a pro-survival mechanism against cellular stresses like starvation, nevertheless, the molecular mechanisms regulating

autophagy are just starting to be understood. Furthermore, though there are many reported connections between autophagy and cell death, still there are big gaps in our understanding of even the most simple questions concerning the relationship between autophagy, cell death and disease (132).

1.6.3.2 Linking of autophagy and apoptosis

There are two possible ways that autophagy could be linked to the apoptotic pathway: the first being that autophagy could regulate the probability of the cell entering into apoptotic cascade and the second being that apoptotic activation of caspases could modulate the autophagy response by its up or downregulation (133).

Several mechanisms were proposed to explain how autophagy was seen in some studies to be linked to cell death; one is that autophagy can actively degrade essential cellular components like mitochondria to the point that the cell cannot survive any longer (128, 134). Nevertheless, this does not seem to link the autophagy process directly to the cell death machinery. That is to say, autophagy might be responsible for the degradation of some cellular components leading to activation of the apoptotic cascade but that does not necessarily mean that the autophagy process is in fact directly responsible for the apoptotic activation (132).

Studies have also described multiple direct and indirect connections suggesting mechanistic intersections and overlap between the autophagy proteins and the apoptotic machinery (127, 131, 135). For example, an important autophagy regulator that interacts with Bcl-2 is Beclin-1 (136, 137). When the two are bound, Beclin-1 becomes unable to activate autophagy. Only when released from Bcl-2 by pro-apoptotic BH3 proteins is autophagy induced (138, 139). Hence, regulation of Beclin-1 by different proteins of the apoptotic machinery can either inhibit or promote autophagy conditioned by the relative activities of caspases and BH3 proteins. This shows that there might be some sort of reciprocal regulation of both apoptosis and autophagy.

Autophagy can also regulate apoptosis through active degradation of some components of the apoptotic machinery including caspases like caspase-8 as well as some of the mitochondria through their sequestration and degradation in the autophagosomes (140). It has also been suggested that autophagy might adjust the

cell kinetics by controlling the threshold at which stressful stimuli can induce the apoptotic cascade thus regulating whether apoptosis is allowed to proceed or not (133).

1.6.4 Role of autophagy in reproduction

The role of autophagy in reproductive science as an emerging new player is still being elucidated (141). Recent studies have demonstrated its importance in several reproductive fields including implantation failure and embryology as well as placental dysfunction.

1.6.4.1 Autophagy and fertility potential

The maintenance of female fertility is known to depend on oocyte dormancy and survival inside the ovary. The proto-oncogene KIT was found to regulate autophagy during ovarian development in neonates via activation of the PI3K-Akt-mTOR pathway (142). Moreover, this gene's mutation resulted in fewer germ cells in mice ovaries, and KIT-mTOR inhibition was shown to lead to infertility (142). Thus, indicating the importance of autophagy in preserving the viability of the dormant female germ cells during embryogenesis.

Similarly, another study reported that, in the woman's reproductive life, primordial follicles preservation in the dormant state was dependent on autophagy via the inhibition of mTORC1 activity (143). Indicating that autophagy has an essential role to play in fertility preservation from embryogenesis to menopause.

Furthermore, during spermatogenesis a study reported that induced autophagy mediated by activated LC3 was significantly higher in viable stallion spermatozoa (144). Similarly, autophagy is believed to function as a sperm survival mechanism similar to that perceived in the oocyte (145).

1.6.4.2 Autophagy and embryology

Embryology research has revealed that autophagy plays a vital role at different levels of developmental stages (146). Autophagy was recognised in fertilised oocytes from as early as four hours after sperm penetration. Autophagy in mammals is believed to have a role in degradation of the sperm mitochondria following gamete fusion (147). Following initial autophagy induction, the morula and blastocyst display a gradual

decline in transcription of autophagy-related genes (148). The reason behind downregulation of autophagy during this period is still unknown but it is speculated that autophagy suppression at this stage might preserve released nuclear factors needed for further development (149).

Additionally, in mouse models when autophagy-related genes were inactivated, an increase in embryonic and fetal death were reported. These autophagy-deficient embryos died at the four to eight cell stage of development (150). Moreover, mouse embryos deficient in Beclin1 died as early as embryonic day 7.5 (148). The postulated mechanism was the inability of the embryos to remove apoptotic cells with higher levels of reactive oxygen species and inflammation (151) as well as defective gastrulation, the developmental process giving rise to the creation of the three germinal layers (152).

Autophagy was found to be induced in blastocyst artificially maintained in a dormant state (153) and evidence suggests that dormant blastocysts resulted in poorly developed fetal vessels in the chorionic plate and labyrinth, impaired development as well as smaller fetuses (154) suggesting that autophagy is an important mechanism for normal growth development.

1.6.4.3 Autophagy and immunological tolerance

Autophagy inhibition in early pregnancy is also thought to help with immunological tolerance by reduction of the anti-embryonic and anti-fetal immune response as well as playing an essential role in processing of antigens for MHC II presentation to the immune system cells (155). Reduced involvement of autophagy in MHC-antigen presentation might lead to impaired recognition of fetal and embryonic components where during pregnancy, trophoblasts are known to downregulate the expression of MHC-II (156).

1.6.4.4 Placenta, preeclampsia and IUGR

The early human placenta is known to develop under low oxygen and glucose conditions during normal pregnancy. This physiological hypoxia is believed to generate ROS thus contributing to the oxidative stress (157). Placental physiological hypoxia, nutrient deprivation and oxidative stress are inducers of mTOR suppression, therefore stimulating autophagy (99) which is important to preserve a cellular

bioenergetic equilibrium between anabolic and catabolic processes, thus allowing appropriate development of the embryo and placenta (157).

In early pregnancy, villous cytotrophoblast and syncytiotrophoblasts are known to express the active form of LC3, the autophagosome marker, (158) as well as in normal third trimester placental tissue (158, 159) and in amniotic epithelial cells obtained from term gestations (160).

In human placenta, autophagy vacuoles have been detected in normal placenta (159) and it has been suggested that dysregulation of autophagy may have a role in the pathogenesis of placental dysfunction. In early-onset preeclampsia (EOPET), spiral arteries are affected by impaired vascular remodelling and shallow trophoblast invasion, leading to poor placentation, hypoxia and increased anti-angiogenic factors like soluble endoglin, which *in vitro* studies have found to inhibit extravillous trophoblast invasion and vascular remodelling through inhibiting autophagy under hypoxic conditions (161). Moreover, another study also showed that *in vitro* hypoxia-induced autophagy augmented extravillous trophoblast invasion (162).

The role that autophagy plays in the regulation of extravillous trophoblast invasion might allow future research to use pharmacological inducers of autophagy to modulate this process with an aim reduce the incidence of preeclampsia and IUGR (100).

1.6.4.5 Preeclampsia and protein misfolding

The role that autophagy plays in the clearance of misfolded proteins in the human body is vital (163-166). When the chaperone refolding system and the ubiquitin-proteasome pathway's capacities are exceeded by the misfolded proteins production, they are actively transported along microtubules to aggresomes, pericentriolar inclusions that sequester misfolded proteins, thus expediting autophagy clearance (166).

It has been reported that preeclampsia shares pathophysiological characteristics with known protein conformational disorders; for example, urine from preeclamptic women exhibited congophilia, a distinctive feature of protein misfolding (167, 168). This is based on the ability of Congo Red (CR) to form large insoluble oligomers after binding to amyloid proteins with an extensive β sheet structure (169). CR-bound amyloids display bright red fluorescence when illuminated with UV light (170).

Studies have also demonstrated that urine congophilia, measured by CR retention (CRR) carried diagnostic and prognostic potential for preeclampsia as CRR was shown to be different among hypertensive pregnancy disorders and increased with the severity of preeclampsia (168). Moreover, CRR showed a better diagnostic potential for PET than standard used tests and markers. CRR, based on the suggested cut-offs of both American College of Obstetricians and Gynecologists (171) and WHO (172), achieved significantly better than the combination of blood pressure and proteinuria (168). Furthermore, CRR showed significant better performance than urine sFlt-1/PlGF ratio (173), creatinine-normalized urine sFlt-1 concentration, and creatinine-normalized urine PlGF concentration (174).

These studies suggest the potential use of this defective placental clearance of misfolded proteins in diagnostic and prognostic assessment of pregnancy disorders were the clearance mechanisms are not aggregate-specific (175) and have a limited ability to remove dysfunctional proteins. Dysregulation of the placental clearance mechanisms might also explain the common association of PET with pre-existing medical conditions known by its increased load of misfolded proteins like cardiovascular or renal disease, diabetes and autoimmune disease (176, 177). This might indicate that pregnant women with such comorbidities started off with an insufficient reserve of protein misfolding clearance.

1.6.4.6 Autophagy and labour

The role that autophagy plays in the induction of spontaneous labour was suggested by a study that found autophagy inhibition to be more common in spontaneous vaginal births (158). Another study revealed that pregnant women with genetic polymorphism in the ATG16L1 were found to have a reduced capacity to induce autophagy (178) and thus their labour was more rapidly induced than those without the polymorphism (179). Thus emphasising the role that inhibition of autophagy might have in induction of spontaneous delivery.

1.7 MicroRNA regulation of the autophagy pathway

MicroRNAs (miRNAs) are a class of small (usually 21–25 nucleotides in length) naturally occurring non-coding RNA molecules. They exist either as single units in the

genome or in gene clusters and are known to play vital roles to play in post-transcriptional gene regulation (180, 181).

The mechanism by which miRNAs inhibit translation is reliant on the complementarity between a 6-7nucleotide 'seed' region in the miRNA and its targets in the 3` untranslated region of the mRNA leading to either mRNA target sequence degradation or translational repression depending on the complementarity and the mismatch between the seed sequence and the 3` UTR region of the mRNA (182). A synergistic effect can be accomplished when more than one miRNA targets the same mRNA (183). However, the study of tissue specific miRNA expression and function has proven to be challenging because of the fact that a single miRNA might have multiple targets of gene transcripts and each gene might be potentially influenced by multiple miRNA expression (184).

Expression of miRNAs plays an essential role in various aspects of biological processes such as development, signalling and response to stress (185) as well as inflammation, apoptosis, immunity, metastasis and cell transformation (186).

The significant role that miRNAs play as an effective and novel modulators of the autophagy process is now being appreciated. It is also believed that the crosstalk between autophagy and miRNAs has the potential to reprogram and elucidate the physiological and the biological functions of autophagy in normal and abnormal cellular development (187). Interestingly, the miRNA-autophagy interconnections are thought to offer intriguing possibilities in the coming years regarding strategies for future treatment, in view of their significant role in cellular adaptation, stress response and the pathogenesis of human disease (188).

There are several distinctive phases of the autophagy process including induction, vesicle nucleation, autophagosome elongation, fusion with the lysosomes and degradation (Figure 1-6) (102).

MiR-204 was recently found to regulate the process of vesicle elongation in the autophagy pathway, after its role in autophagy has been initially studied in cardiomyocytes (189) and then validated further in renal cell carcinoma (RCC) via its direct modulation of LC3B (190). Other miRNAs, like miR-376b and miR-101, were also identified to regulate the ATG4 proteases (191, 192). This family has important

regulatory elements in vesicle expansion, autophagosome closure (193), fusion of autophagosomes with lysosomes and recycling of LC3 by removing lipid-bound phosphatidyl-ethanolamine (PE) from the outer membrane LC3 (194).

Till now, no studies have identified miRNAs directly regulating the autophagosome-lysosome fusion. Nonetheless, a group of miRNAs, miR-130, 98, 124, 204 and 142, were identified to affect it by a computational systems biology approach (195) with predicted targets like LAMP1, LAMP2 and the v-SNARE protein, known to be involved in the autophagosome-lysosomal pathway, indicating a possible role for these miRNAs in the regulation of such fusion (196).

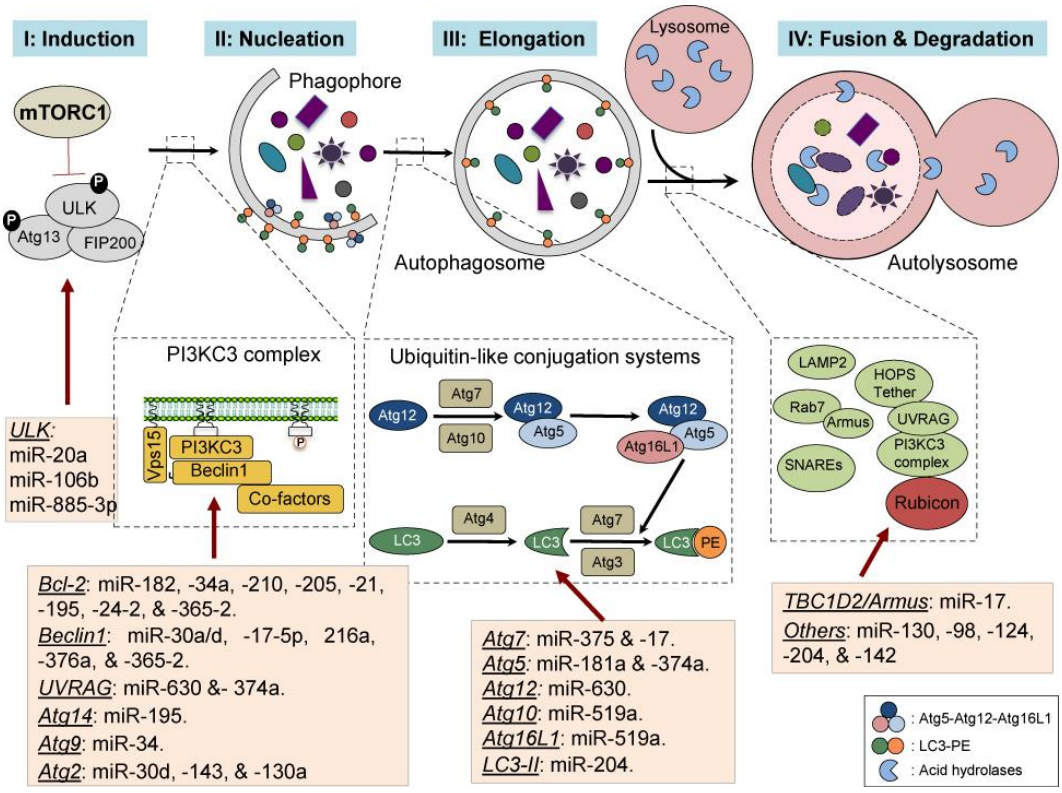

Figure 1-6. Schematic representation of the miRNA regulation of the core autophagy pathway. Autophagy process passes through a sequence of distinctive stages including induction, vesicle nucleation, phagophore elongation, and autophagosome maturation, fusion with the lysosomes and degradation where regulation by miRNAs occurs at each dynamic step**.** Adapted from Yang and Liang, 2015 (197).

Similarly, the role that miRNAs might play in orchestrating selective autophagy, where selective degradation of specific subgroups of the autophagosome cargo takes place, is also a tempting possibility. This was seen with miR-375 and hypoxia-induced

mitophagy (198) and with miR-196 and xenophagy, an autophagic phenomenon specifically involving pathogens and other non-host entities (199, 200).

On the other hand, autophagy appeared to responsible for regulation of the miRNA processing by constructing checkpoints needed for loading of miRNA into the main miRNA effector, eukaryotic translation initiation factor 2C (EIF2C2). Similarly, autophagy exhibited post-transcriptional regulation of the miRNA-processing enzyme DICER mRNA, thus highlighting the role that autophagy plays interchangeably in the fine tuning of the miRNA pathway (201).

1.8 MicroRNAs and the placenta

The discovery of miRNAs has revolutionised the understanding of the mechanisms regulating gene expression, adding a completely novel level of regulatory control (202). Ever since the discovery of the first miRNA, lin-4, in *caenorhabditis elegans* in 1993 (203), miRNAs have been identified in large number in many species adding up to more than 1000 miRNAs discovered to date in humans, and this number is still increasing (204).

The epigenetic process has been shown to play a vital role in the progress and recording of environmental signals through 'fetal programming' (205) or the "Fetal origin of adult disease" hypothesis (206, 207), suggesting that early life programming does have a potential role in adult disease pathogenesis. Studies have also shown differential gene expression in PET involving regulation of epigenetic pathways (208). Moreover, in addition to histone modification and DNA methylation, different placental miRNA expression patterns in different pathologic pregnancies like PET have been reported (209).

1.8.1 Biogenesis and function

RNA polymerase II dependent transcription (pri-miRNAs) takes place from the miRNA encoding genes present in the intron of the host genes; these pri-miRNAs fold into characteristic stem-loop precursors. In vertebrates, these pri-miRNAs are processed in the nucleus (210) and are then transported to the cytoplasm by Exportin 5, where they are additionally processed by DICER, a different RNase III enzyme, into miRNA duplexes (211). Lastly, the miRNA duplex is unwound and the mature miRNA (one strand) combines into the RNA-induced silencing complex (RISC), containing Argonaute (Ago) proteins in its core (212, 213).

MiRNA is known to regulate essentially different features of development as in proliferation, differentiation, apoptosis, metabolic homeostasis and tumourigenesis (214, 215). Abnormal miRNA expression patterns have been linked to several pathologic developments with a miRNA expression profile frequently altered in cancer (216), thus can potentially be used to differentiate cancer from normal tissues or sometimes used to categorise cancers according to their differentiation (217). In

parallel, the use of miRNA expression profiling in placental dysfunction may help clinicians and researchers better understand placental physiological and pathological states especially those related to placental insufficiency.

1.8.2 Placental specific miRNAs

MiRNA expression profile analysis in normal human tissues has shown that some miRNAs are ubiquitously expressed while others are preferentially expressed in specific tissues (218). It is not unexpected the placenta expresses numerous types of miRNAs, playing a potential crucial role in the process of fetal development. Although, large numbers of these miRNAs are universally expressed, certain miRNA families appear primarily distinctive to placental secretion (219)

Research has revealed that many highly expressed placental miRNAs, by sequencing an RNA library from human placental villous tissue, are encoded by the Chromosome 19 miRNA cluster (C19MC)-cluster miRNA genes located in chromosome 19 (220). The C19MC cluster, consisting of 54 predicted miRNAs, is the biggest gene cluster of human miRNA discovered till now. This primate-specific cluster is almost exclusively placental-expressed (218, 221, 222) as well as in trophoblast-derived cell lines, including BeWo, JAR, and JEG3 (with the exception of HTR8/SVneo).

C19MC is known to be modulated by genomic imprinting with placental expression of paternally-inherited allele only, indicating its central role in the development of the human embryo (223). It is still unclear regarding the roles of the placental C19MC cluster, but it is likely, given their high level of placental expression, that they are vital for the preservation and housekeeping of normal placental function (224, 225).

The vital role that miRNAs have in the placental development and function was evidenced when the miRNA machinery was disabled in mice, resulting in midgestational death of mutant embryos with resultant malformed and thinned placental labyrinthine layer (226).

Most of the studies in placental miRNA research, though in its early stage, focussed on cataloguing placental miRNA profiles or studying placental miRNA expression differences between placentas from normal pregnancies compared to those from placental insufficiency-related complications (219). Several reports since 2007 have

used miRNA microarray and real-time PCR assays to outline the human miRNA expression patterns in placentas from normal and complicated pregnancies. These reports have shown that many miRNAs are differentially expressed in human placenta. However, the biological role of these miRNAs in the modulation of placental development and function remains unclear (227).

Placental miRNA profiling studies were mostly carried out using fresh or snap frozen placental samples. Nevertheless, Noack et al. (228) used formalin fixed paraffin embedded (FFPE) tissues for miRNA expression profiling in preeclamptic placentas. Expression profiles of several miRNAs, like miR-26b, miR-296-5p, and miR-223 were in accordance with results from previous studies using microarrays from fresh frozen tissues (229-232). Moreover, high correlation values from results of matched FFPE and frozen samples were also verified in other studies (233, 234).

MiRNAs have been shown to be robust with relative insensitivity to the damage that characterises mRNAs within FFPE due to its small size. Therefore, miRNAs might represent important novel targets for researchers using stored archived material, with an advantage of being linked to a broad clinical background and, more vitally, follow-up data (235).

1.8.3 MicroRNAs and placental dysfunction

Pineles et al. (236), using real-time quantitative RT-PCR, was the first to determine the expression patterns of 157 human miRNAs in placental samples from preeclampsia (PET), small-for-gestational age (SGA), PET-SGA, and spontaneous preterm labour control group. His results showed seven miRNAs (miR-210, miR-155, miR-181b, miR-182, miR-200b, miR-154, and miR-183) to be differentially expressed (DE) between PE-SGA and the control group. Further analysis of the biological processes and target genes of the some of the differentially expressed (DE) miRNAs revealed the potential involvement of antiapoptosis and immune response in the pathogenesis of PET, where miR-182 might potentially downregulate antiapoptotic genes, elevated miR-182 in preeclamptic placenta might lead to a higher apoptosis in PET placentas (236).

Another study assessed the miRNA profiles in placentas from normal, mild and severe PET and found 11 up-regulated and 23 down-regulated in severe-PET placentas

compared with normal controls. Of note, several miRNA clusters on human chromosome 19q13.42 (miR-517*, -518b, and -519e*), 13q31.3 (miR-18a and -19a), Xq26.2 (miR-18b and -363), Xq26.3 (miR-542-3p and -450), and 14q32.31 (a human imprinted region, miR-411, -377, and -154*) were expressed differentially in the severe PET group (231).

Additionally, a study using miRNA microarrays showed differential placental expression patterns between severe PET and control placenta with 13 miRNAs (miR-92b, miR-197, miR-342-3p, miR-296-4p, miR-26b, miR-25, miR-296-3p, miR-26a, miR-198, miR-202, miR-191, miR-95 and miR-204) being upregulated and two miRNAs (miR-21 and miR-223) under expressed in PET placentae compared with normotensive placentae (229). Validated by RT-PCR, miR-92b displayed the largest change (a 12.28 fold change) in PET patients (229). This study also showed that the target genes of some 15 DE miRNAs in PET were related to cell motility, adherens junction, signalling pathways, focal adhesion and TGF signalling. Furthermore, Enquobahrie et al. (208) found eight DE miRNAs, one up-regulated (miR-210), and seven down-regulated (miR-584, miR-139-5p, miR-328, miR-1, miR-500, miR-34c-5p, and miR-1247) from PET compared with control placentas.

1.8.4 Discrepancies of the miRNA profiles in preeclampsia

Surprisingly, a different set of DE miRNAs was reported by each published study (208, 228-230, 232, 236, 237) with minimal overlapping across all the studies. The cause for this noticeable discrepancy is not fully understood yet. Such inconsistencies might be due to heterogeneity in patient populations (different PET phenotypes and severity, gestational age differences, presence or absence of labour, patient ethnicities, and full-term or preterm delivery), mode of delivery (vaginal or Caesarean-section), source materials (plasma, serum, cell, and tissue), data analysis and statistical methods. Furthermore, the location in placenta (decidual or chorionic plate) from where the samples were taken had influence on DE miRNAs (238) as shown by a study by Xu et al (2014) which showed that miRNA expression profiles and functions varied significantly according to their location.

Nevertheless, three studies have found placental miR-210 levels in severe preeclampsia to be elevated (231, 236, 238), and in the maternal circulation at 15 to

18 weeks gestation and at term (238). MiR-210 levels are known to be affected by hypoxia and oxygen tension is a known to regulate the development of the placenta and the differentiation of trophoblasts throughout pregnancy (239). Both PET and IUGR are known to be linked with trophoblast hypoxia and aberrant placental development or function. (240-242). This has resulted in more reports exploring the possibility of miR-210 as a potential diagnostic biomarker for PET (243, 244).

The expression profiles of 820 miRNAs from the first or third trimester placental samples (232, 245) revealed that pregnancy-associated miRNAs concentration were raised throughout gestation (245) and differentially expressed in placentas from preeclampsia or preterm labour (232) suggesting that miRNAs might act as potential serum markers for the placental function.

These discrepancies emphasise the need for more large-scale studies or for those with a homogenous phenotypes, in order to identify more consistent DE miRNAs in placental dysfunction. This approach might have a crucial role in determining the relevant miRNAs that affect the trophoblast dysregulation believed to lead to placental dysfunction-related complications like PET and/or IUGR.

1.8.5 MicroRNAs as biomarkers for placental dysfunction

Dysregulation of placental trophoblast function, known to occur in the first trimester of pregnancy has been presumed to mediate the clinical phenotype later on in pregnancy (246). The ability of researchers to find biomarkers of trophoblast dysregulation and thus early identification of women at high risk of developing PET has always been of critical importance, where vigilant monitoring and early referral to dedicated perinatal care centres could significantly improve fetal and maternal outcomes (247). Up till now, there exist no reliable biomarkers for identifying mothers prior to the development of clinical symptoms.

Circulating nucleic acids (RNA and DNA) in pregnant women have been studied before with still no effective, diagnostic or prognostic, predictive capability for the early diagnosis of PET or IUGR (248). Nevertheless, circulating plasma/serum miRNAs levels in pregnant women could be a novel way to tackle this problem where recent research indicates that miRNAs can be a group of encouraging novel non-invasive markers for placental-dysfunction related complications. They can also be of

diagnostic and predictive importance in placental insufficiency-related diseases as miRNAs are shed into the maternal circulation (183) at levels that may mirror the tissue's physiologic or pathologic state (249).

The exact source of circulating miRNAs is not fully known. MiRNAs are sheathed in cell-derived Microparticles (MPs), including exosomes, microvesicles and apoptotic bodies, possibly shielding them from ribonucleases in the plasma (250, 251). Nevertheless, placental miRNAs are easily detectable in pregnant women's circulation (220, 245) and their levels are known to return to their pre-pregnancy basal levels within 24 hours after delivery thus confirming their placental origin (219).

Several studies have shown that plasma miRNAs are not affected by pH or incubation temperature or even by RNase A treatment (252, 253). These stable characters, as well as the early DE patterns of plasma miRNAs in PET patients, shown in several studies (243, 254) strongly encourage researchers to study the use of miRNAs in the non-invasive prenatal diagnosis of preeclampsia. Nevertheless, their low circulatory level and the specificity and sensitivity in measuring circulating miRNAs impede their identification as biomarkers for pregnancy-associated diseases.

Although there is no standard methodology used to accurately measure circulating miRNAs (245), the three main methods used to analyse the expression patterns of circulating miRNA in serum are microarray, quantitative RT-PCR, and next generation sequencing. Even though quantitative RT-PCR has a limited ability to detect a large number of miRNAs at a time, it is still regarded as the gold standard for miRNA quantification. Microarray array is a high-throughput technology that could identify known miRNA fragments. miRNAs with only single nucleic acid polymorphisms can only be detected by the next-generation sequencing (NGS) technology used as well as profiling circulating miRNA in pregnancy (237).

In a study carried out by Hromadnikova and colleagues (255) to quantify previously identified circulatory miRNAs early in pregnancy using real-time PCR, they demonstrated substantial rises of extracellular miRNA expression levels during early gestation (within the 12th to 16th weeks) in the women's plasma who later developed PET and/or IUGR. This suggested that screening for extracellular miRNAs in early gestation could discriminate between normally developing pregnancies and those who

developed placental insufficiency-related complications later on in pregnancy. However, miRNA concentrations at the time of clinical manifestation of PET and/or IUGR did not reveal significant difference from the controls, indicating the need for other studies with higher number of samples to calculate and confirm the diagnostic power of miRNAs as biomarkers for placental dysfunction.

A study using NGS technology to profile circulatory serum small RNAs showed that miRNAs were the major contributor of the circulatory small RNAs, thus supporting the ability to profile analysis of circulating small RNA using next generation sequencing technology (237). Differentially expressed miRNAs in the circulation were then compared to those placental-expressed miRNAs in PET. Three of these (hsa-let-7d, hsa-let-7f and has-miR-223) were shown to be consistent in both placenta and maternal serum (230, 231, 236).

Xu et al. (238) also studied several circulating miRNAs in severe PET (sPET) patients previously sampled at 15th to 19th weeks of gestation, and found that circulating levels of miR-18a, miR-19b1, and miR-92a1 were significantly lower, while those of miR-210 were higher in sPET patients than in normal controls. This emphasised their aberrant expression in sPET placenta at the first half gestation and their contribution in the early pathological events of sPET (238). Another study found that miR-1301, miR-223 and miR-224 expression was downregulated in early-onset PET, but not in late-onset PET, compared to controls (256).

Meanwhile, identifying more circulating candidate miRNAs with altered concentration early in pregnancy requires a more inclusive and comprehensive systematic microarray/sequencing review of miRNA expression profiles before the onset of PET and/or IUGR (247). This work may help researcher identify women at high risk of developing PET and/or IUGR, and also in the stratification of the severity of PET. Further standardised research on the biologic properties of miRNAs dysregulated in gestational diseases might deliver novel targets for further exploration of the ultimate molecular pathophysiology of PET/IUGR.

1.9 Hypothesis and aim of the study

It is evident that placental dysfunction manifest itself in different spectrum of pregnancy complications. Dissecting such differences has proven difficult using standard qualitative methodologies.

1.9.1 Hypothesis

It is my hypothesis that this spectrum of placental dysfunction, though has similar pathogenetic mechanisms, are essentially different on the structural and the molecular level leading to different pathways which is then reflected in the clinical phenotypes. It is also hypothesised that a normal placental housekeeping and homeostatic function is dependent on a balance between different mechanisms of programmed cell death. A balance that is vital in determining which pathway the placenta will follow and that autophagy is an essential biological player in regulating trophoblast apoptosis. It is also hypothesised that miRNAs can modulate the biological functions of autophagy and thus trophoblast apoptosis.

1.9.2 Aim of the study

The aim of this research is to structurally and functionally characterise and quantify elements of placental dysfunction found in normal and in pathological placentas, believed to be implicated in the pathogenesis of PET/IUGR. Structural characterisation involves the use of novel digital quantifiable approaches to assess the morphometric features of the placenta in 2D and 3D in health and disease. Whereas, functional characterisation involves quantification of programmed cell death-related proteins, genes and miRNAs in normal and in placentas from complicated pregnancies. This is followed by an *in vitro* validation of those functions in a trophoblast cell line.

The expected outcome of completing the proposed aims is an in-depth understanding of placental dysfunction and the role that structural and molecular intricateness yields its different forms. This can be translated into a better understanding of “normal” and “abnormal” pregnancy, from which will have direct clinical translational effects to prevent or treat PET/IUGR-related morbidities and optimize patients’ outcomes.

Chapter 2 Materials and Methods

2.1 Ethical approval

This study was approved by the Leeds Bradford NRES committee York and Humber, reference: 13/YH/0344 granted in November 2013 (Ethical Approval document).

2.2 Patient recruitment and demographics

Women with singleton pregnancies were recruited for research in the Department of Obstetrics and Gynaecology, Leeds Teaching Hospital Trust. Informed written consent was obtained from all study participants. Eight patient groups were pre-specified: Full-term normal pregnancies, normotensive idiopathic intrauterine growth restriction (IUGR), late onset preeclampsia (LOPET), LOPET with IUGR, preterm controls, early-onset IUGR (EOIUGR), early-onset preeclampsia (EOPET) and EOPET with IUGR.

Term control pregnancies were defined as those delivering a normal birth-weight baby or appropriate for gestational age (AGA) babies at greater than 37 weeks with no comorbidities. IUGR pregnancies were defined as those delivering a baby with an individualized birth-weight ratio below the 10th percentile (257) in the absence of maternal disease (hypertension, diabetes, or autoimmune disease) or underlying congenital, chromosomal, infectious, metabolic or structural abnormalities in the baby. Preeclampsia (PET) was defined as hypertension (>140/90 mmHg on two occasions four hours apart) and proteinuria (>300 mg/day) after 20 weeks gestation (258); whilst LOPET was defined as that requiring delivery after 37 completed weeks; whilst EOPET requiring delivery before 34 weeks. Individualised birth weight ratios were calculated using the GROW centile calculator v5.15 (Perinatal Institute, www.gestation.net).

	Normal (n=16)	IUGR (n=20)	LOPET/IUGR (n=18)	LOPET (n=20)
Maternal age	30± 1.2	28.2± 3.5	31.4± 2.4	30.75± 3.7
Gestational age (wks.)	39.1± 1.5	38.9± 0.8	38.6± 0.9	37.9± 0.6
BMI	28.4± 2.6	21.14± 3.7*	27.23± 2.4	28.76± 6.3
Birth weight (kg)	3.512± 0.53	2.133± 0.18****	2.349± 0.83****	3.248± 0.623
Placental volumes (cm^3)	432.9± 96.4	322.3± 50.4**	292.8±54.01****	381.9± 105
Highest Systolic Blood pressure (mmHg)	121± 4.84	118.5± 4.24	155.0± 4.7*	157.5± 3.8*
Highest Diastolic Blood pressure (mmHg)	66.55± 4.6	69.5± 5.4	99.3± 7.5*	106.6± 4.5*

Table 2-1 Table showing demographic criteria in control, idiopathic IUGR, LOPET/IUGR and LOPET. * denotes *p <0.05, ** p<0.01.*

	Preterm control (n=8)	EOIUGR (n=10)	EOPET/IUGR (n=20)	EOPET (n=12)
Maternal age	28.56± 4.7	27.33± 4.770	31.25± 2.1	25.50± 4.0
Gestational age (wks.)	31.35± 1.76	33.72± 0.96	32.5± 2.5*	31.94± 1.6
BMI	26.33± 2.062	26.56± 2.920	22.13± 2.7	27.63± 2.5
Birth weight (kg)	1.933± 0.301	1.202± 0.3***	1.249± 0.29****	1.711± 0.308
Placental volumes (cm^3)	298.4± 42	224.2± 49.79*	189.3± 41.89****	271.6± 49.61
Highest Systolic Blood pressure (mmHg)	116.6± 5.044	118.3± 5.1	164.0± 8.64*	166.5± 6.32*
Highest Diastolic Blood pressure (mmHg)	70.44± 7.055	69.11± 8.838	112± 4.8*	110.5± 4.4*

Table 2-2 Table showing demographic criteria in preterm control, EOIUGR, EOPET/IUGR and EOPET. * denotes *p<0.05. ** p<0.01. *** p<0.001.*

Only placentas from AGA births where the babies were within the normal range (≥10th≤90th centiles) were included in the pure preeclamptic groups (LOPET & EOPET). Preterm controls were defined as those delivering before 34 weeks gestation AGA babies, while EOIUGR was defined as growth restriction developing early and delivering before 34 weeks gestation in the absence of preeclampsia. All term and preterm controls exhibited no clinical or pathological signs of preeclampsia, IUGR, or any noteworthy maternal co-morbidity. Placentas were collected within 30 minutes of delivery and tissue stored in accordance with the Human Tissue Act 2004.

2.3 Tissue processing

Each placenta was trimmed of its membranes and umbilical cord before weighing. Four full-depth (maternal to fetal) placental columns (Figure 2-1) were randomly sampled (259). The placental samples were washed in PBS, fixed in 10% formalin for 24 hours, and then the placental tissue was dissected into smaller, 1 x 2 x 2 cm segments. These were then re-submerged in formalin for a further 72-80 hours to ensure complete fixation, then into 70% ethanol, before being processed in a Leica ASP300 tissue processor for 48 hours and embedded in paraffin wax at random orientation. Paraffin-embedded tissue blocks were cut into 5µm sections using a Leica RM2235 microtome and mounted on Plus Frost slides (Solmedia®, London, UK). Slides were then incubated overnight at 37°C to dry and then placed in a hot plate at 70°C for 6 hours to ensure complete adhesion.

2.4 Haematoxylin and Eosin (H&E) staining

Slides were dewaxed, rehydrated and stained with Mayer's haematoxylin and eosin (H&E) for 2 minutes each, so that nuclei stain blue while the cell cytoplasm and extracellular matrix stain pink. Slides were then mounted with cover-slips (24x40mm, VFM®, Powys, UK) using DPX mounting (Solmedia®).

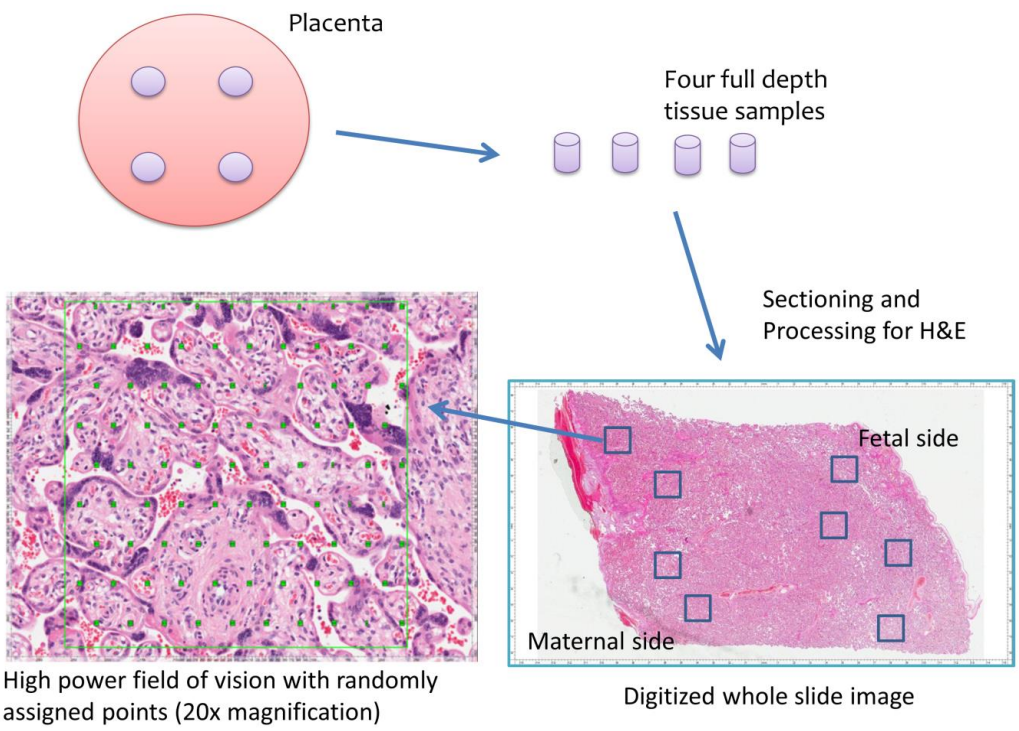

Figure 2-1 Multistage random sampling of placenta. Image showing representative sampling with four full-thickness placental tissues diced to make FFPE blocks. One section was chosen at random, mounted and stained with H&E, scanned and overlaid with virtual fields of vision (FOV). A known number of points were then overlaid inside each FOV using RandomSpot software. The points hitting the area of Interest (SNA or capillaries) were scored and counted.

2.5 Virtual pathology and digital scanning

Advances in technologies used to study histopathology as in virtual pathology are currently limited to research, education and training. Digitised slides have been used for about two decades and, as a technology, are growing in maturity and increasingly becoming a vital tool in research practice (260).The digitisation of a glass slide is achieved by using specific whole slide scanners with high resolution generating very large images (virtual slides) of about one gigapixel in size, necessitating specialist software for hosting. They are typically scanned at 20x (0.5 microns per pixel) magnification, but have capacity to scan at 40x (0.25 microns per pixel) and 80x (0.125 microns per pixel).

Virtual slides have a principal advantage in their ability to rapidly scan through the slide by clicking on the area of interest. They also can be stored and retrieved easily, without breaking, diminishing in quality, a feature absent in conventional light microscopy.

Moreover, the viewing software has additional functions, such as taking snapshots, side-by-side comparison of images, making annotations and image analysis features (261).

The ability to use, validate and reproduce a sound unbiased quantifying methodology, like stereology, on digital slides would be a helpful tool in the pursuit of a precise method to structurally characterise and quantify different constituents of placenta pathology.

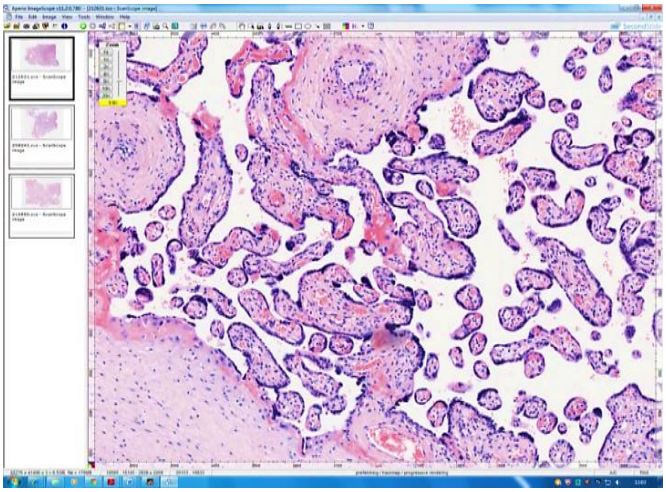

Figure 2-2 A Virtual slide hosting software. A placenta stained with H&E is examined using Aperio's ImageScope software (Aperio Technologies Inc, San Diego, CA, USA).

Following H&E staining, slides were then digitally scanned at x20 magnification using the ScanScope™ system (Aperio Technologies®, Aperio, Vista, CA, USA) producing images with a final resolution of 0.23 microns per pixel (262). After coding the scanned slides, images were opened in ImageScope software and examined blind to the clinical diagnosis. All placental specimens were subject to conventional pathological examination by a perinatal pathologist, and those with evidence of infection or metabolic disease excluded.

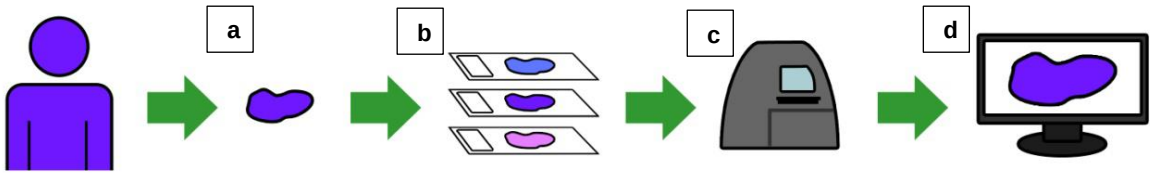

Figure 2-3 Simplified process of obtaining tissue from patient to virtual slide. A biopsy (a) is processed, sliced and placed onto glass slides (b), which are then scanned (c), and examined on a computer screen (d)

2.6 Serial sectioning for SNA follow-up

SNA-containing serial images were manually opened (200x magnification), aligned side by side using ImageScope software to structurally characterise SNAs through consecutive serial sections.

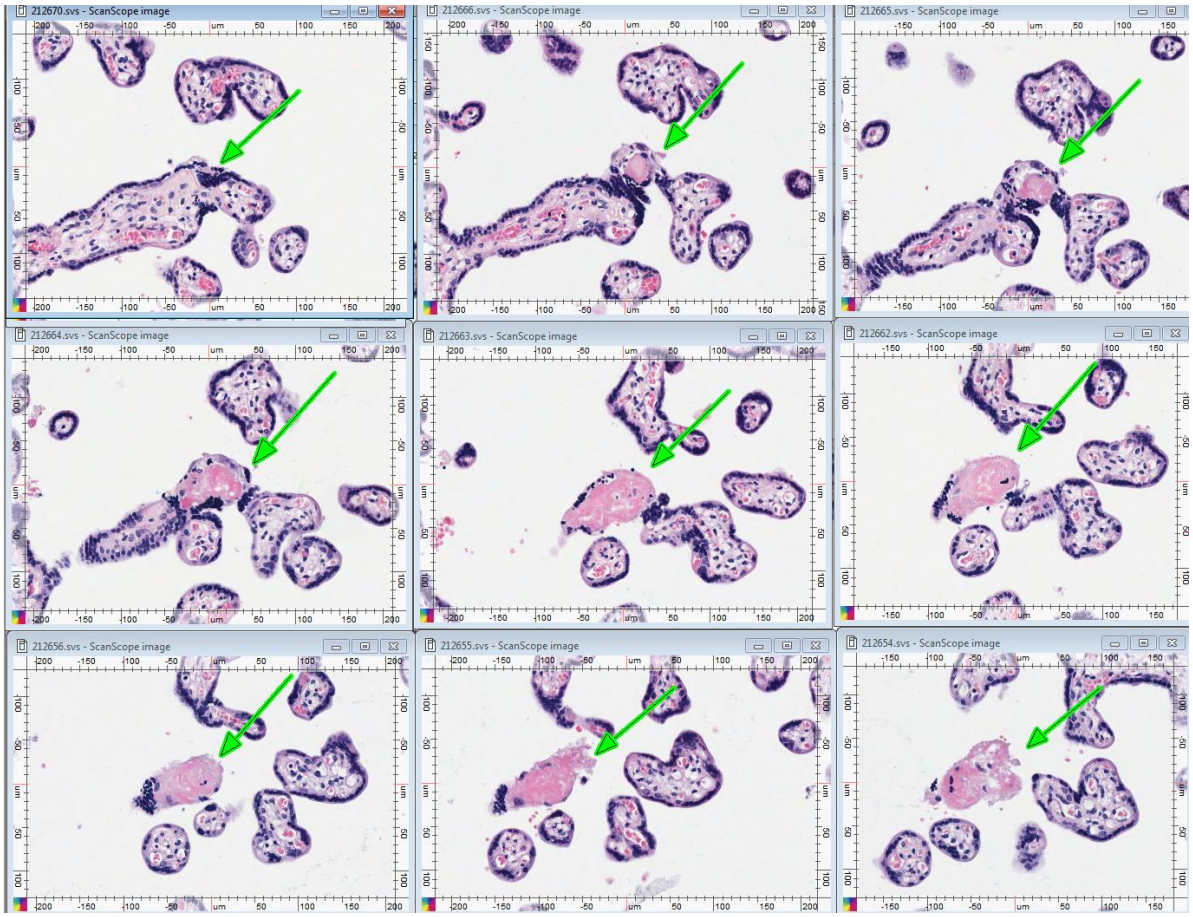

Figure 2-4 SNA serial follow-up in digital slides. Serial images showing a surface villus SNA as a part of the terminal villi, then continuous in space with isolated islands of SNAs and fibrinoid degeneration (green arrow) in the intervillous space and isolated from villi.

2.7 Stereology

Biological systems and organs exist and function in 3D space. Although taking sections of them is indispensable to disclose their internal structure at an acceptable resolution, this comes on the account of reducing 3D space to fundamentally a 2D image (263), which would obscure analyses of spatial relations, volumes and sizes (264). However, 2D sections can be converted to a three dimensional reality through stereology (265).

Stereology is a powerful tool for morphometry. It encompasses strict sampling procedures with simple and reproducible assessment tools that allow impartial and efficient quantification of 3D structures such as volumes, surface areas and numbers of cells from histological 2D sections. It delivers total volumes as well as information regarding the local features of the organ of interest, both of which are decisive to our comprehension of how biological systems function at the whole organ level (266, 267). This “2D effect” is only overcome by randomising the sampling procedure, the orientation and sectioning direction through the organ. That is why stereology generates more consistent and precise 3D measurements in comparison to *ad hoc* 2D quantification practices (268). Thus allowing researchers to collect data effectively and efficiently (269, 270). Moreover, the provision of discrete, quantifiable targets ensures higher reproducibility and more consistent inter-observer scoring. In placental research, stereological methods offer the only way, till now, to obtain a reliable, quantitative measurement of the volume, surface area, number and length of the microscopic structures from 2D images (259).

2.7.1 The stereological design

The principal requirement of stereological assessment is that all areas within the organ of interest have an equal likelihood of being sampled (271). Multistage random sampling is the first element in stereological design. Randomising selected blocks then sections and then fields of vision at every stage of a hierarchical design is essential for the final sample to be a good representative sample. This gives all placental regions a chance to be chosen in an equal and independent way (272) and mimicking the biological reality of the organ of interest (273).

Robust stereological assessments aim to achieve the desired precision of the calculations from the data gathered from sampling protocols, whilst using as few measurements as possible to increase work efficiency. This precision or reproducibility, often known as the coefficient of error of the estimate (274), is indicative of the measurement variability if it were repeated several times similar to the 'margin of error' related to opinion polls.

Stereological assessments are impartial and efficient. Accuracy and precision symbolise two statistical aspects used to label the value of the result measurement. In the stereology context, accuracy refers to ‘without systematic deviation from the true value’ (inherently unknown) and precision refers to ‘with low variability after spending a moderate amount of time’ (275). This degree of bias is therefore correlated to the degree of deviation from the true value. Stereology computes this deviation, which is known as the coefficient of error (CE), allowing the researcher to judge how accurately the stereological measurement represents the true value. This is also helpful in ensuring that the sampling error is less than diverse biological variation of the organ which can rarely be eliminated (276).

2.7.2 Volume measurement in 3D

A crude measure of the organ growth based on mass and physical structure in 3D is volume. Since the placenta is a three dimensional organ, a much better representation of placental change in compromised pregnancies is gained through stereological assessment of volumes (17).

The volume of the placenta (in cm^3) can be measured either from fluid displacement or from weight in grams (gm) and tissue density in gm/cm^3, the volume density can be converted into an absolute volume (in cm^3) through this equation (277):

$$\text{Total quantity} = \text{Density} \times \text{Reference volume}.$$

Density will indicate how much change within a unit volume, which is essential in the comparison between different conditions, but the absolute value will be useful to determine the adaption of the whole organ and measure the organ’s functional capacity (278). The volume density of any structure at high magnification, in relation

to the reference volume may be measured by counting points hitting the relevant structure and points hitting the reference volume (259).

Equation 2-1

$$\mathrm{V(structure)} = \frac{\sum \mathrm{P(structure)}}{\sum \mathrm{P(reference)}} \times \mathrm{V\ (reference)}$$

$\sum \mathbf{P}(\mathbf{struc})$ is the sum of number of points hitting the desired structure (e.g. SNA).

$\sum \mathbf{P}(\mathbf{ref})$ is the sum of number of points hitting the reference organ (e.g. placenta).

Volume measurements were performed according to the Cavalieri principle (272, 279) on single thin (4–6 μm) histological sections. Volume density was calculated by the technique of point counting, so that volume density (fraction) was equal to the number of points falling within the area of interest divided by the total number of points inside the reference space (placenta) (273). This methodology calculates volume densities which were allocated to the villous tree (stratified by the villous stroma, vessel lumen, endothelium, and trophoblast), trophoblast layer and syncytial nuclear aggregates.

Absolute volumes were then calculated by multiplying each of the volume densities with the placental volume (This is is defined by the placental weight (PW) divided by the density of placental tissue. The placental specific density is about 1.04 (280, 281). Volumes of SNAs, trophoblasts and capillaries in each placenta were then divided by their own villous volumes as ratios ($V_{SNA}/V_{Villous}$) so that differences between villous volumes across disease groups could be accounted for when comparing different components of interest.

Since the human placenta represents a heterogeneous organ varying in spatial and temporal structure, an attempt was made to determine whether fetal and maternal sides of the placenta have a role in this heterogeneity either in structural or functional measurements. Each digitised placental slide was categorised into two virtual halves: a fetal half, the half on the side of the chorionic plate and the fetal membranes (amnion and the chorion), and a maternal half nearer to the basal plate (Figure 2-1). They were then compared to each other (maternal vs fetal-side measurements) within each group and across different groups to determine site specific differences in different groups of

placental dysfunction. All the scanned slides were number coded, relevant volumes in every slide and placenta quantified and examined blind to the clinical diagnosis.

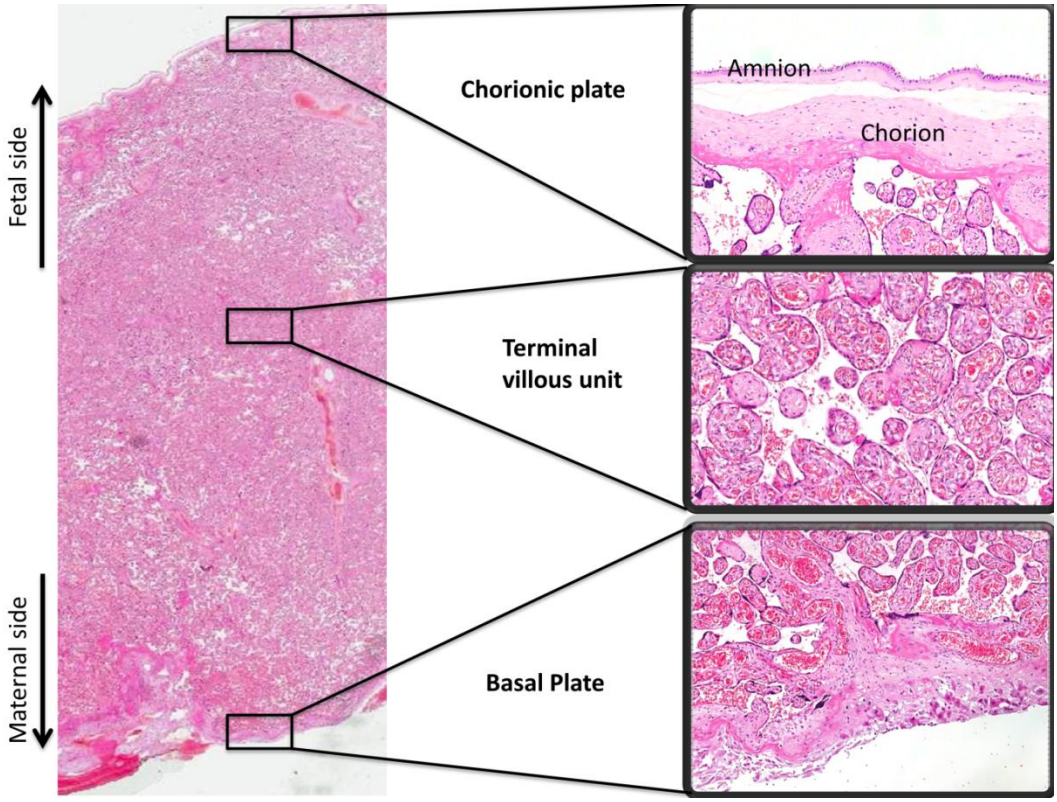

Figure 2-5 Histological structure of the placenta and membranes.

2.7.3 Coefficient of Error (CE)

The extent of sampling error made by a stereological measurement (the difference between a measurement and a true value) is unknown. By calculating the co-efficient of error (CE), it can be determined how close the stereological calculation is from the true value. Thus, the CE is essentially a measure of 'how accurate' the stereological measurement is.

The independent noise, which is the expected variance of point counting with a grid of systematic points on slides, was calculated from the following equation:

Equation 2-2

$$\text{Noise} = 0.0724 \times \left({}^{b}/_{\sqrt{\text{a}}}\right) \times \sqrt{n.\sum \text{P}}$$

Where $\sum \mathbf{p}$ is sum of points counted, **n** is the number of slides used, the value 0.0724 is a constant for point lattices with a quadratic arrangement. $\boldsymbol{b}/\sqrt{\mathbf{a}}$ is an average shape factor for a set of sectional profiles. In this study, a shape factor of 10 was used, which was attained by comparing the overall sectional profile shape with those available in the nomogram, which predicts the number of points needed to perform counts (272, 282). The variance of areas (VAR_{sur}) among the systematic random sample of slides used to measure the volume of area of interest (etg. SNAs) was computed with the formula (283) as follows:

Equation 2-3

$$\mathrm{VARsur} = \frac{3(\mathrm{A} - \mathrm{noise}) - 4\mathrm{B} + \mathrm{C}}{240}$$

Where A= Pi x Pi, B= Pi x (Pi+1), C= Pi x (Pi+2). A, B, and C can be calculated from the number of points (Pi) counted on each section. The variable A is the sum of the squares of the number of points counted on each section [Pi x Pi]. The variable B is the sum of the product of the number of points counted on each section and the number of points counted on the next section in the series [Pi x (Pi+1)]. The variable C is the sum of product of the number of points on each section and that counted on the second next section in the series [Pi x (Pi+2)]. See Table 2-3 for an example of the calculations

Section no.	∑P	A= P_i x P_i	B=P_i x(P_i+1)	C=P_i x(P_i+2)
1	28	784	896	1036
2	32	1024	1184	1184
3	37	1369	1369	1332
4	37	1369	1332	999
5	36	1296	972	0
6	27	729	0	0
7	0	0	0	0
8	0	0	0	0
9	0	0	0	0
SUM	197	6571	5753	4551

Table 2-3 Table calculating showing how variance and noise is calculated from ∑P, where P_i is the number of points hitting the area of interest (SNAs, Capillaries, trophoblasts and villi). A= P_i x P_i, B= P_i x (P_i+1), C= P_i x (P_i+2).

The total coefficient of error for the Cavalieri estimate of the placental constituents was estimated as follows:

Equation 2-4

$$CE = \frac{\sqrt{\text{noise} + \text{variance}}}{\sum \text{Pi}}$$

Where ∑Pi was the sum of the number of points that landed on the area of interest in all the slides.

2.7.4 Villous volume measurement

For the villous tree (distal and intermediate villi) volume estimation, four slides were randomly sampled. In each slide, eight fields of view were randomly assigned; four of these were from the fetal (subchorionic) side and the other four from the maternal (parabasal) side of the placenta. For each field of vision, a grid, with 30 randomly assigned points, was overlaid (using RandomSpot software (284)) and the points hitting the villous tree were counted, annotated and exported to an Excel sheet. The total number of points hitting the villous tree was counted to calculate the volume density (VD) and the absolute volumes were calculated by multiplying the VD with the placental volume (Equation 2-1).

2.7.5 Trophoblast volume estimation

Volumes of the trophoblast layer were stereologically measured using four slides from each placenta. In each slide, eight fields of vision were randomly assigned, four of them were in the fetal side and the other four were in the maternal side of the placenta (Figure 2-1). For each field of view, a grid with thirty randomly assigned points was overlaid and the points hitting the trophoblast layer were counted, annotated and exported to an excel sheet. The total number of points counted in each placenta in this protocol was 960.

2.7.6 Placental capillary vessel volume estimation protocol

The protocol for placental fetal capillary vessel volume estimation included four slides from the whole placenta through stratified random sampling. For each slide eight fields of vision are randomly assigned, four of them were in the fetal side and the other four were in the maternal side of the placenta. In each field of vision, a grid with thirty randomly assigned points was overlaid (using RandomSpot software (284)) and the points hitting the fetal capillaries were counted, annotated and exported to an Excel sheet. The CE, noise and surface variance were manually calculated in each case (Equation 2-2, Equation 2-3, Equation 2-4). The total number of points counted in each placenta was 960.

2.7.7 Syncytial nuclear aggregates (SNA) volume estimation protocol

The final protocol for SNA volume estimation had four randomly-assigned slides, each had eight FOVs. In each field of vision, a grid with 50 randomly assigned points was overlaid and the points hitting the SNAs were counted. Volume densities (VD), absolute volume ratios to villous volumes were calculated. The total number of points counted in each placenta in this protocol was 1600.

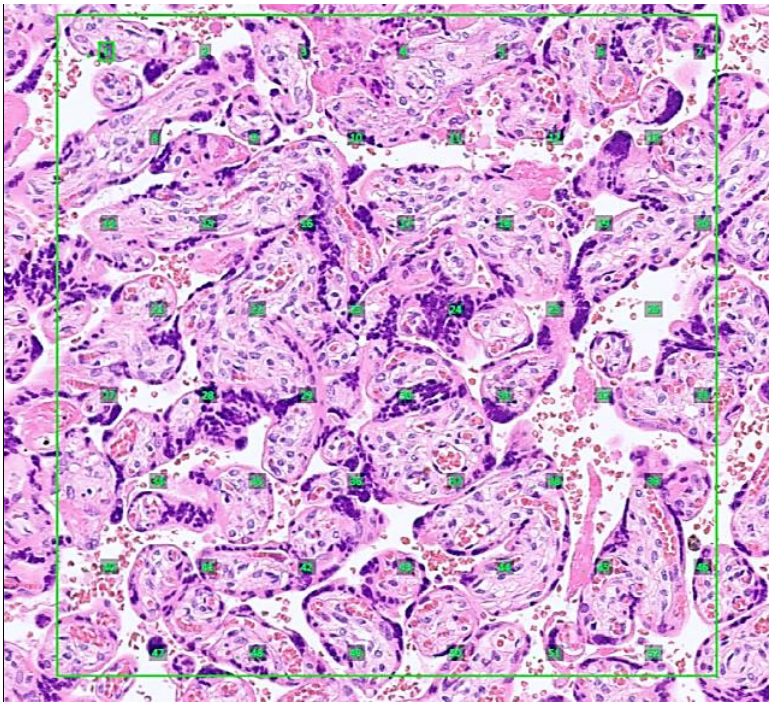

Figure 2-6 Placental villi with SNAs as a sample field of vision overlaid by a randomly assigned 50 point-grid. The points hitting the SNA are counted annotated and exported for analysis.

2.8 Novel 3D reconstruction model of the spatial arrangement of SNAs around the terminal villi

A novel technique developed at The University of Leeds that uses an algorithm combining multiple 2D dynamic programming to create a 3D volume out of serial histopathological sections (285) was used to develop a reconstruction of the spatial arrangement of SNAs, fibrinoid degenerations and villus branching in normal and preeclamptic placentas.

2.8.1 Registration

The scanned images were registered, that is to align digitised serially sectioned placental slides (262), using Slice Registration Application which uses a slice to slice image-based registration algorithm to automatically align the images. Virtual slides were first rigidly registered, with each subsequent slide being aligned to its neighbouring slide. It is designed to allow the alignment of multiple serial sections from a single sample into a volumetric stack. This works by sequentially aligning to a reference image (usually at the centre of the stack). Colour inconsistencies were also corrected, and volumetric data suitable for visualisation in a number of standard packages generated.

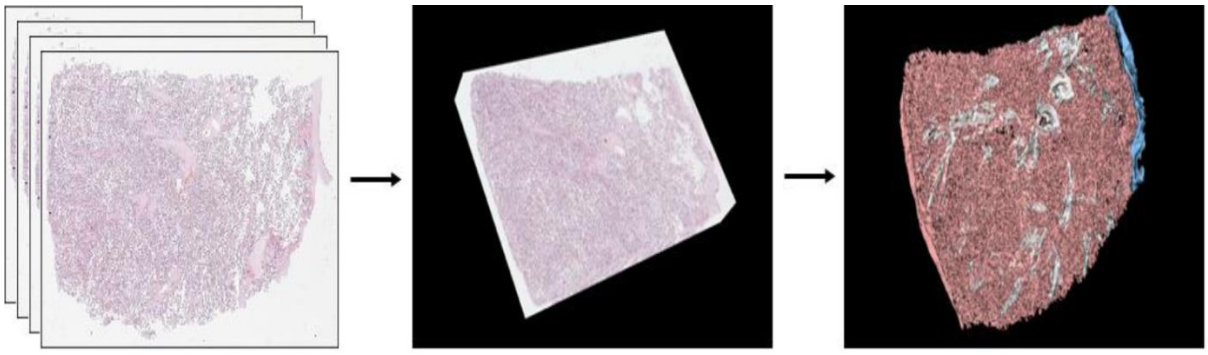

Figure 2-7 3D reconstruction process of the placenta. Series of images illustrating the way in which scanned and aligned slides were used to create a volume, which is then reconstructed and iso-surfaced.

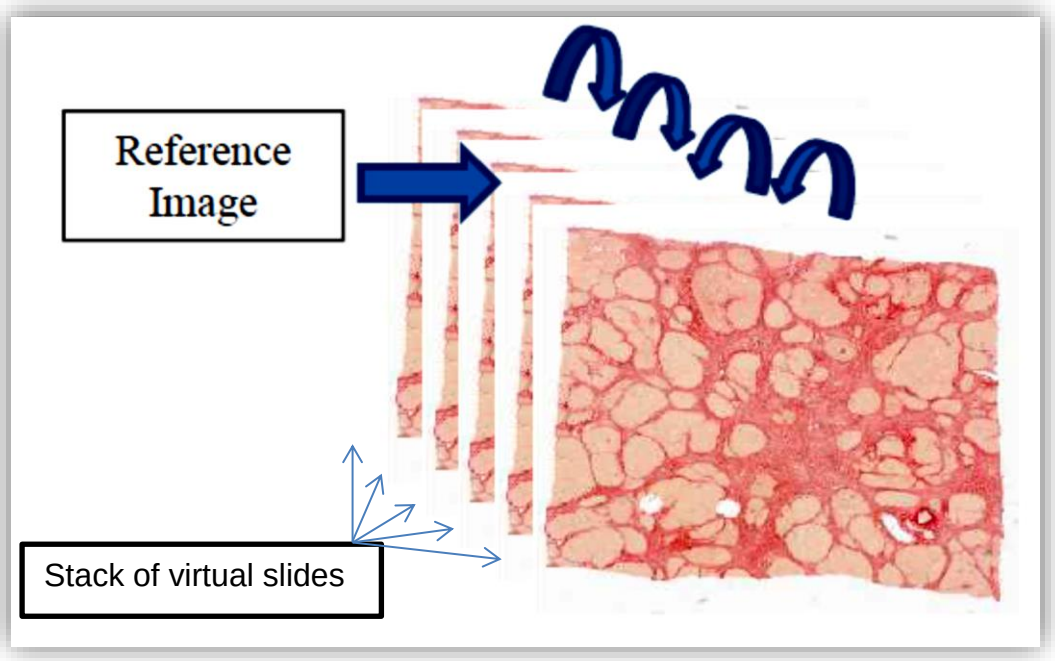

Figure 2-8 A schematic representation of the slice registration process for virtual images. A stack of virtual slides from serial sections aligned in relation to a reference image (in the middle of the stack) using Slice Registration Application (262).

2.8.2 Volume rendering

Non-rigid registration at increasing image resolutions was then carried out producing a dataset that could generate a volume, then subvolumes from the whole slides taken with higher magnification performing multilevel registration at successive image magnifications at a resolution of zoom 1/32, whereby axial, coronal and sagittal views could be studied (Figure 2-9).

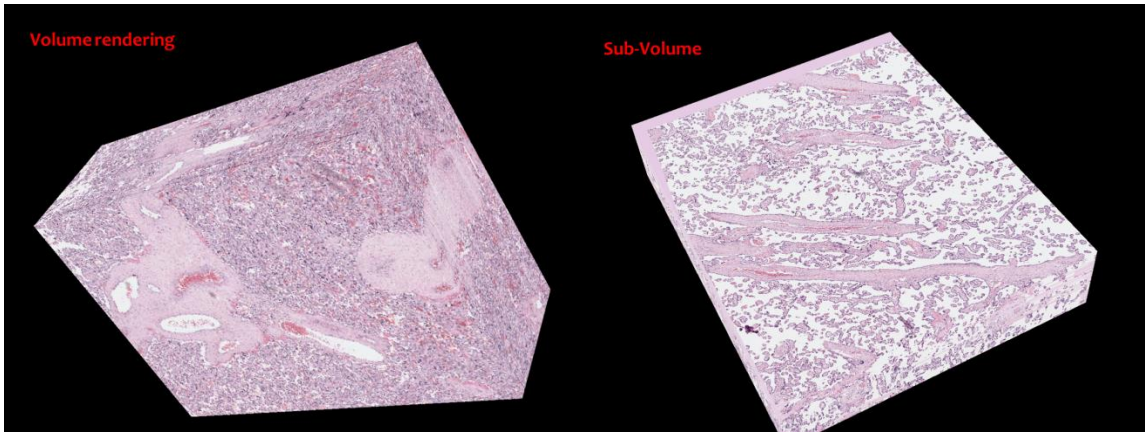

Figure 2-9 Images of generated volumes from scanned 2D slides of the placenta forming a volume and a sub-volume with a higher resolution with axial, coronal and sagittal views.

2.8.3 Segmentation

This was followed by manually segmenting the terminal and intermediate villi, fibrinoid degeneration and SNAs in 48 virtual images and then using the Volume Viewer software to form 3D reconstruction of the villi and spatial arrangement of the fibrinoid degeneration and SNA around them.

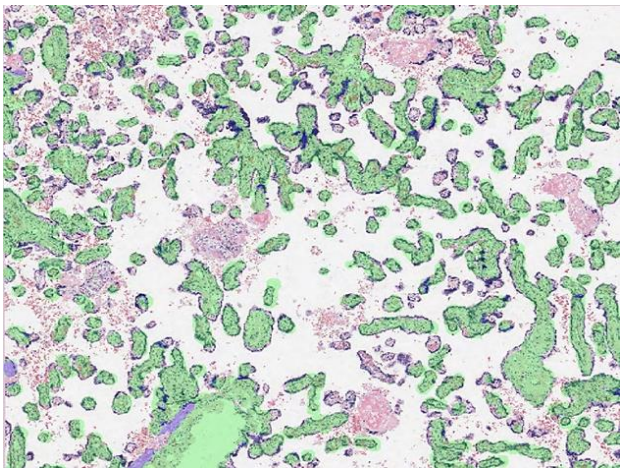

Figure 2-10 Image depicting segmentation of branching villi of the placenta for one slide (Green). This is manually done for each slide to annotate the areas of interest and then followed by 3D reconstruction of the segmented volumes.

2.8.4 3D reconstruction

Virtual slides were then reconstructed using volume viewer software forming a 3D volume.

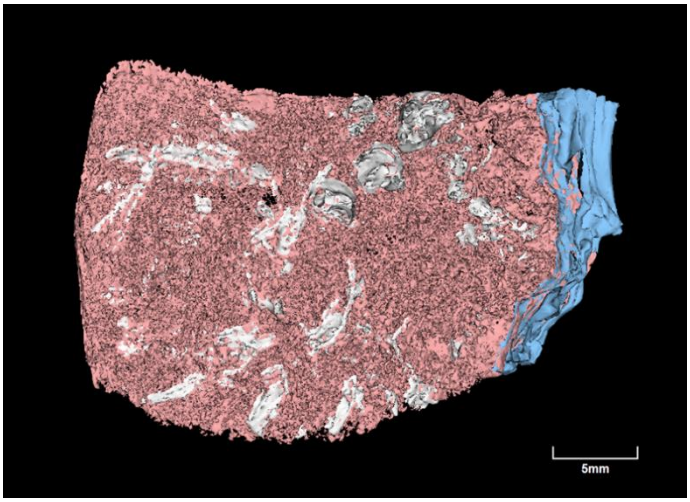

Figure 2-11 Image of a reconstructed placental block. Grey areas represent stem and intermediate villi, while the pink displays the peripheral villi and the pale blue represents fetal membranes.

2.9 Immunohistochemistry

2.9.1 Antibody optimisation

All antibodies were optimised by serial dilution on appropriate tissues that were known to express the specific antigen (http://www.proteinatlas.org/). Human multi-tissue blocks containing tonsil, colon, kidney, thyroid, oesophagus and spleen, provided by the Section of Pathology and Tumour Biology, University of Leeds, were used as positive controls. Slides with no primary antibody, but with added secondary antibody, were used as negative controls. The optimal concentrations for each antibody were determined by an optimal signal with no background staining.

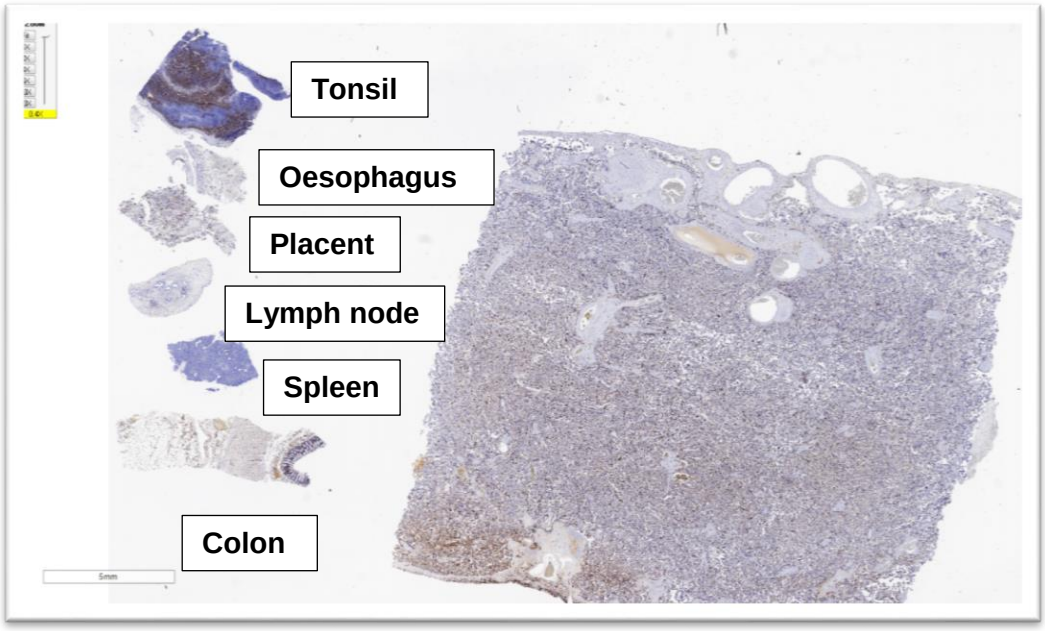

Figure 2-12 Multi-tissue slides containing tonsil, colon, kidney, thyroid, oesophagus and spleen used for optimisation of the primary antibodies. Each antibody was optimised by serial dilution against its appropriate positive control tissue.

2.9.1.1 The M30 CytoDEATH™

A staining was performed using M30 antibody (ALX-804-590), a mouse monoclonal IgG2b antibody that recognizes caspase-cleaved cytokeratin 18 (CK18) in epithelial derived cells. CK18 cleavage generates a neo-epitope detected by the monoclonal antibody M30. This antibody does not identify uncleaved CK18 and is thus specific for apoptotic epithelial cells. Moreover, apoptosis detection using M30 CytoDEATH™ has been referred to in several publications to function as a superior technique in comparison to TUNEL (286, 287).

The apoptotic M30 antibody was then preliminary optimised at 1:50, 1:100 and 1:200, and the 1:100 M30 antibody concentrations was chosen on the basis of its specificity (optimal signal and no background staining).

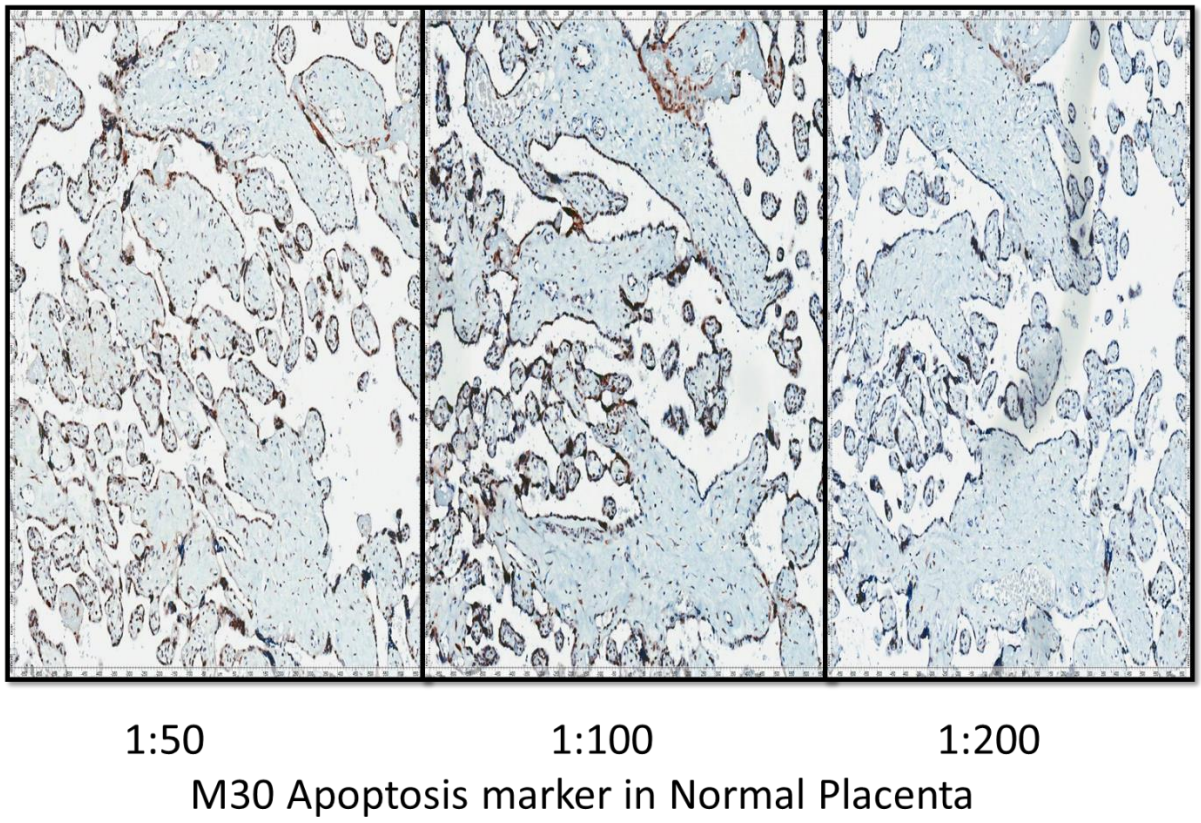

Figure 2-13 Different M30 antibody concentrations used for optimisation in placenta in serial sections

2.9.1.2 LC3B/MAP1LC3B Antibody

A rabbit polyclonal anti-LC3 antibody (NB100-2220, Novus Biologicals) was used as an autophagosomal marker. The autophagy LC3 antibody, with a concentration of 1.0 mg/ml), was then initially optimised in kidney (Figure 2-14) at 1:500, 1:1000 and 1:1500, and the 1:1500 LC3 antibody concentration was chosen for the placenta (Figure 2-15).

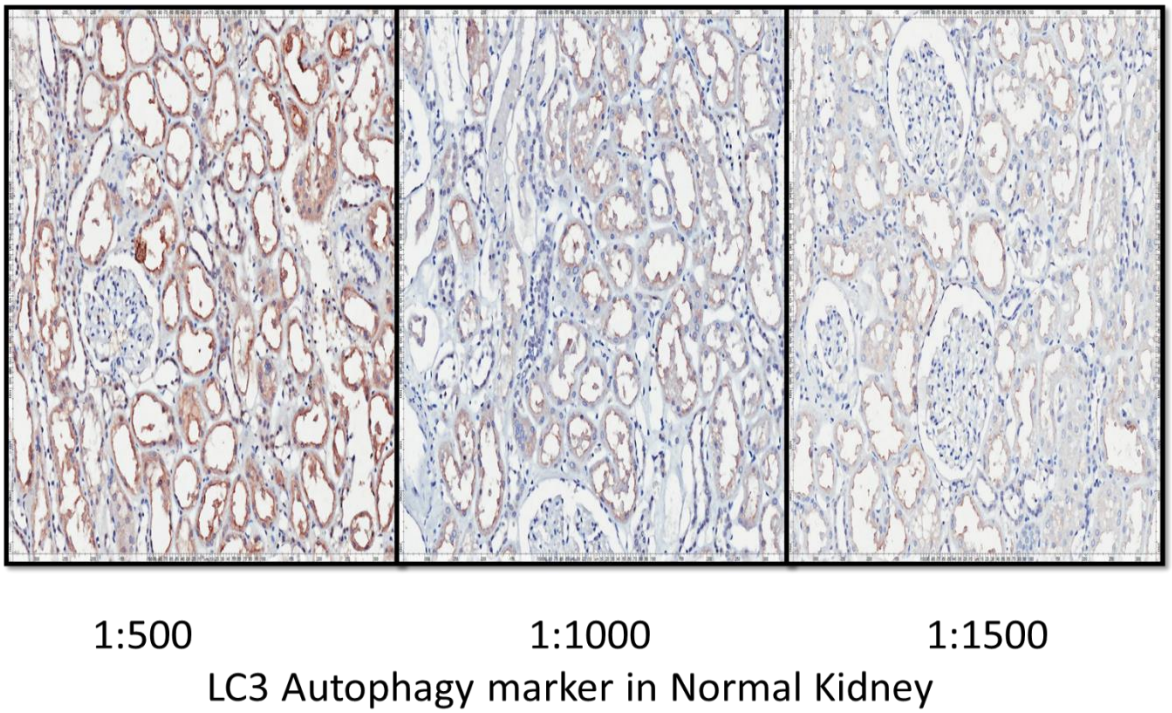

Figure 2-14 Different LC3 antibody dilutions used for optimisation in the Kidney.

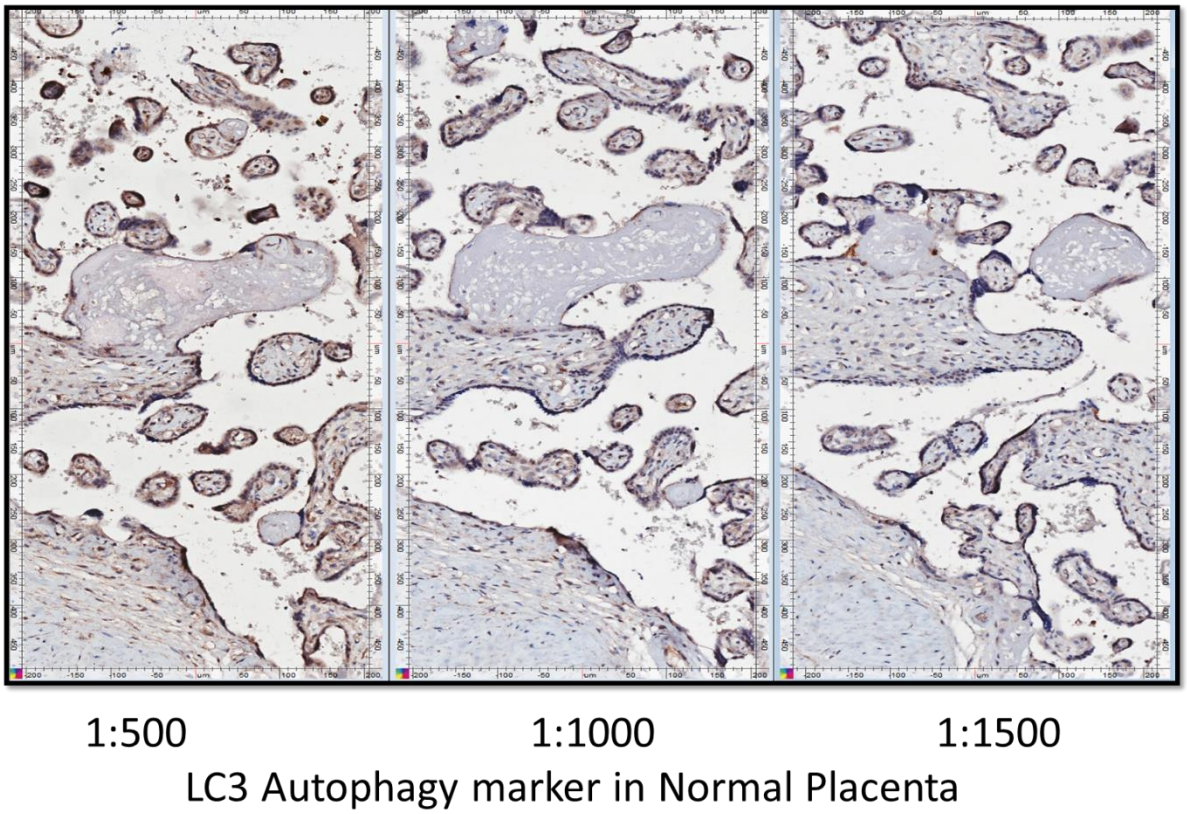

Figure 2-15 Different LC3 antibody dilutions used for its optimisation in normal placenta.

2.9.1.3 Anti-8 Hydroxyguanosine antibody (8OHdG)

A mouse monoclonal [N45.1] antibody to 8 hydroxyguanosine, a modified base that occurs in DNA, detecting DNA damage within cells due to the hydroxyl radicals attack that are formed as by-products and intermediates of aerobic metabolism and throughout oxidative stress. It was optimised by serial dilutions in colon (Figure 2-16) and the placenta (Figure 2-17).

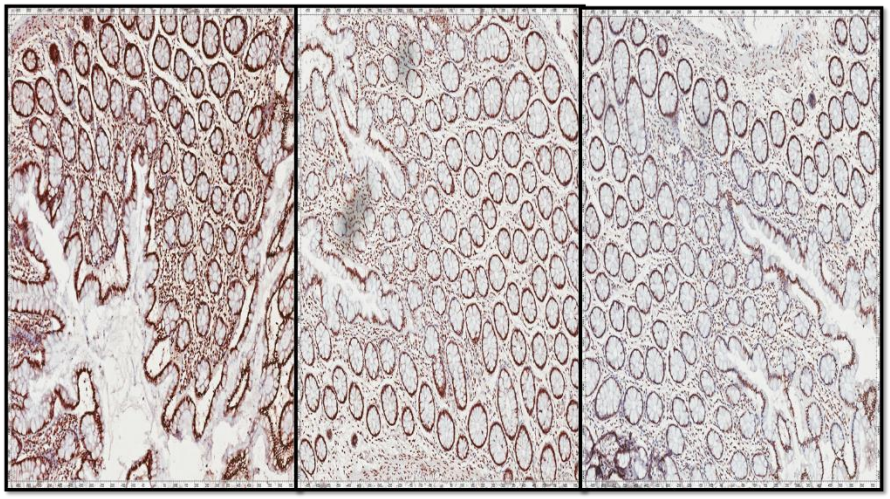

Figure 2-16 Different 8OHdG antibody dilutions used for optimisation in colon.

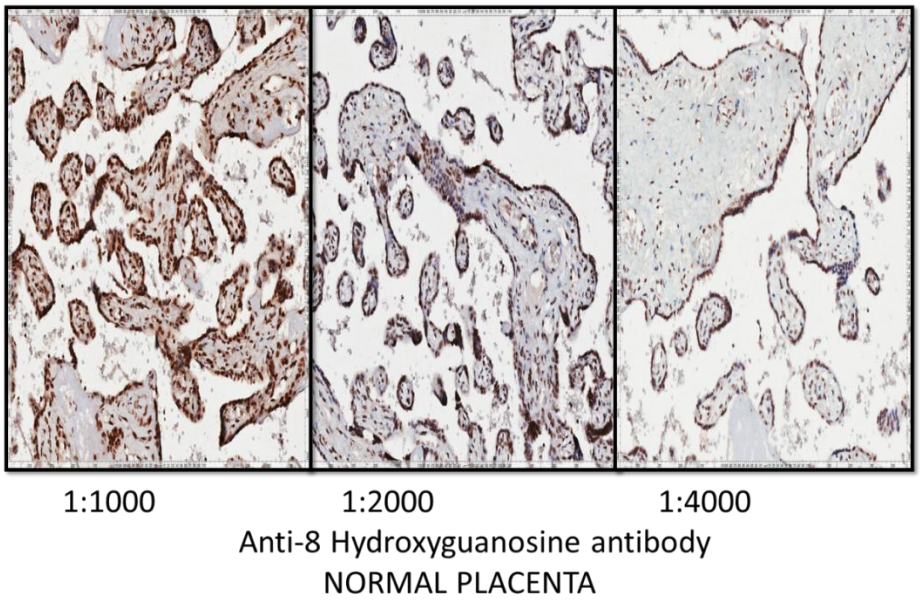

Figure 2-17 Different 8OHdG antibody concentrations used for optimisation in placenta.

2.9.1.4 Uncleaved cytokeratin (8/18) antibody

A monoclonal antibody (NCL-5D3, Novocastra™) clone reacted with human cytokeratin intermediate filament proteins of 52.5 kD and 45 kD, identified as

cytokeratins 8 and 18, respectively. It was optimised by serial dilutions to a concentration of 1:200.

2.9.1.5 CD163 antibody

The monoclonal antibody (NCL-L-CD163, Novocastra™) CD163 molecule is membrane protein limited in its expression to the monocytic/macrophage lineage. Moreover, multi-nucleated cells found within inflammatory lesions are reported not to express CD163 protein. It was optimised by serial dilutions to a concentration of 1:100.

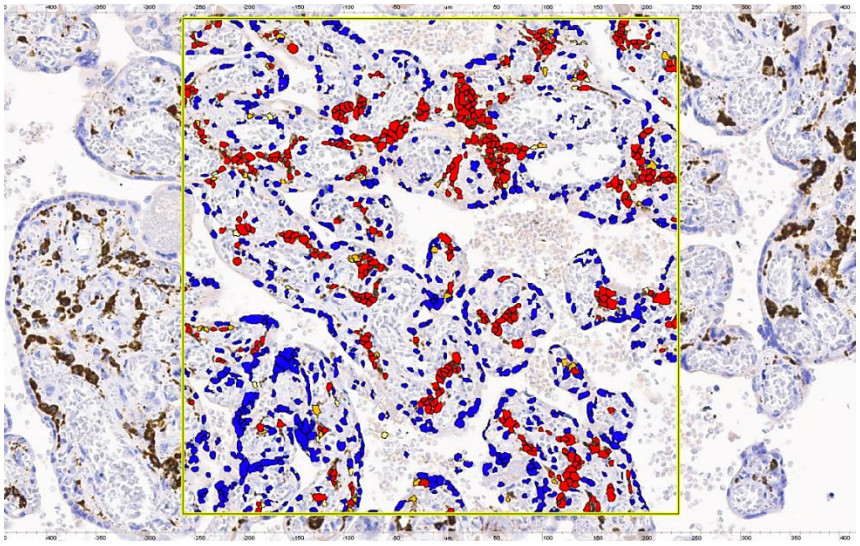

Figure 2-18 Image analysis of a field of vision in a placental slide stained with CD163 antibody with the nuclear algorithm scoring system with a cover-up image formed of colours according to the intensity of staining (red=strong, orange=moderate and yellow=weak staining).

2.9.1.6 Anti-Bcl-2 oncoprotein

Monoclonal Mouse Anti-Human Bcl-2 oncoprotein (Code IR614/IS614, Clone 124, Dako) which reacts with the Bcl-2 oncoprotein and plays a central role in apoptosis.

2.9.2 Immunohistochemistry

Immunohistochemical studies were carried out on 5 µm thick tissue sections from the formalin-fixed, paraffin-embedded tissue samples (FFPE), floated in a 37ºC water bath, and then mounted onto Plus Frost slides (Solmedia®, London, UK). After placing on a hot plate for 30 min, the slides were dewaxed in xylene (4 x 3 minutes) and rehydrated through a series of graded alcohols (absolute, 70%, 50%, 25%; 3 minutes).

Standard heat-mediated antigen retrieval in pH 6.0 using Antigen Unmasking Solution (AUS, H-3300, Vector laboratories, CA, USA) was carried out through pressure cooking, and then the slides were washed in TBS (5mM Trisma Base, 0.3M NaCl, pH 7.6). A liquid wax boundary was applied to the glass microscope slides surrounding the tissue to prevent reagent dispersal (DakoPen, Dako).

Endogenous peroxidase activity was quenched with 3% H_2O_2 in distilled H_2O then the slides were rinsed in running tap water for ten minutes. After blocking non-specific protein binding using 10x Casein (SP-5020, Vector laboratories, CA 94010) , at 1:10 dilution in antibody diluent for 20 minutes, the 5µm sections were incubated with primary antibody at the optimised dilutions for at least 1 hour in a humidified chamber at room temperature (RT). After washing (2 washes of TBS; four minutes each), the sections were incubated with the post primary antibody (Rabbit anti mouse IgG (<10 µg/ml) in 10% (v/v) animal serum in TBS, Novolink™ Polymer Detection System, Novocastra Laboratories, Leica) for 30 min in a humidified chamber at room RT and then after washing with TBS, 2-3 drops of the Novolink polymer (Anti-rabbit Poly-HRP-IgG (<25µg/mL) containing 10% (v/v) animal serum in TBS, Novolink™ Polymer Detection System, Novocastra Laboratories, Leica) were applied per slide for 30 minutes.

After washing the slides (3x TBS, 5 minutes), 100µl of DAB (chromagen diaminobenzidine, 1:20 v/v in its diluent) (ImmPACT™ DAB,Vector Laboratories, Burlingame, CA, USA) was added to each slide and incubated at RT for 5 minutes and rinsed in water. Haematoxylin counterstain was applied for one minute then followed by a further wash in running tap water. The slides were then dehydrated in a series of increasing ethanol concentrations (25% for 15 seconds, 50% for 2 minutes, 70% for 5 minutes, and 100% for 5 minutes) and were submerged in xylene 3 times for 3 minutes. Finally, the slides were mounted with cover-slips (24x40mm, VFM®, Powys, UK) using DPX (Solmedia®). Slides with no primary antibody were used as negative controls (Figure 2-21). Slides were immunostained in the same batch to ensure identical conditions to allow comparison with the appropriate positive control.

2.10 Image Analysis

The image analysis used in this study was from Aperio's technologies which has cleared FDA approval [1] for the company's complete digital pathology platform, including ScanScope® scanners used for creating digital slide images from microscope slides, and analysing digital slides, and the specific image analysis algorithms which performs the automated scoring of IHC used in breast cancer (288).

2.10.1 Scanning and random sampling

Immuno-labelled slides were scanned at 20x magnification (Aperio Technologies). Slides were then opened in Aperio® ImageScope™ software (version 10.2.2.2319, California, USA) to examine four slides in each placenta. Eight randomly assigned fields of vision (FOV), four in the fetal (sub-chorionic) side and the remaining four in the maternal (basal) side were examined in each section, mounting to 32 FOVs examined for each placenta (Figure 2-1).

2.10.2 Automatic scoring algorithms

2.10.2.1 Positive Pixel Count algorithm

The Positive Pixel Count (PPC) v9 algorithm (Aperio® algorithms, University of Chicago, USA) is an image analysis algorithm that counts the amount (pixel number and intensity-sum) of a pre-specified stain in scanned slides, so was used to quantify and score the brown-staining positivity in the examined placenta.

The standard input parameters used for analysis of brown colour were a hue value and width of 0.1 and 0.5 respectively, together with a colour saturation threshold of 0.04 (the required saturation of positive colour; pixels with saturation less than this value were not recorded).

The degree of labelling present in each digitized image was sub-classified into three intensity ranges: weak, positive, and strong (Figure 2-19). For pixels satisfying the brown colour specification (positive pixels), the algorithm counted their number, the ratio of strong/total pixel number (NSR), while the sum of positive/total number of positive and negative pixels calculated the positivity (2.10.2.1.1). The outcome parameters for the PPC algorithm also included the number of weak positive pixels

[1] Aperio-Receives-FDA-Approval-for-Image-Analysis-Applications

(NWP) marked as yellow in the mark-up image, number of positive pixels (NP) marked as orange and number of strong positive pixels (NSP) marked as brown as seen in Figure 2-19. Areas not falling into the positive-colour specification (Blue) were counted as negative stained pixels (Figure 2-18).

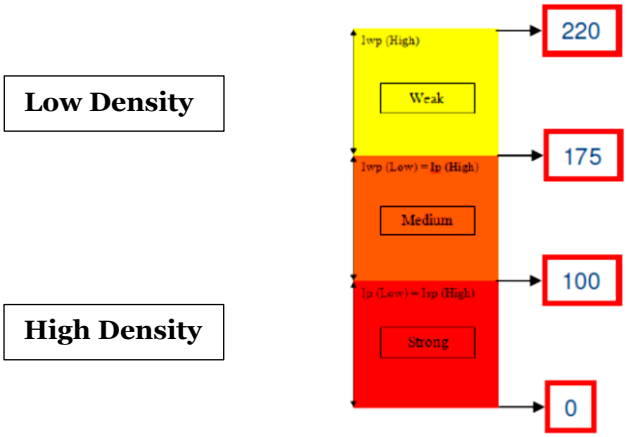

Figure 2-19 Classification of the positive pixels (brown stain) into weak, medium and strong stains according to its intensity. Intensity is the measure of brightness of the pixel, the larger the intensity the brighter the pixel and the lower the density of the stain.

2.10.2.1.1 Algorithm Output Parameters

- Nwp – Number of Weak-Positive pixels (Yellow in mark-up image).
- Np – Number of Positive pixels (Orange in mark-up image).
- Nsp – Number of Strong-Positive pixels (Red in mark-up image).
- Nsr – Ratio of Strong-Positive pixels to total pixels: Nsr = Nsp/(Nwp+Np+Nsp).
- Nn – Number of Negative pixels (Blue in mark-up image).
- In – Sum of Intensity values for all Negative pixels.
- NTotal – Number of Total pixels, Positive + Negative (Nwp+Np+Nsp+Nn).
- Positivity – Total number of positive pixels divided by total number of pixels: (NTotal – Nn)/ (NTotal).

2.10.2.2 Nuclear image analysis algorithm

The IHC Nuclear Image Analysis algorithm was also used to detect the brown IHC staining for the individual cells in different placentas as well as to quantify their intensity to allow comparisons between groups. It classified stained cells as 0, 1+, 2+ and 3+

based on brown staining intensity. A cell was classified 0+ when it had no brown staining, 1+ when it had weak brown staining, 2+ when it had moderate brown staining and 3+ when it had strong brown staining. Based on the percentages of 0, 1+, 2+ and 3+ cells, the percentage of positive stained cells as a percentage of 0 to 100% and the average staining intensity of the positive nuclei as a score of 0, 1+, 2+ or 3+ was determined.

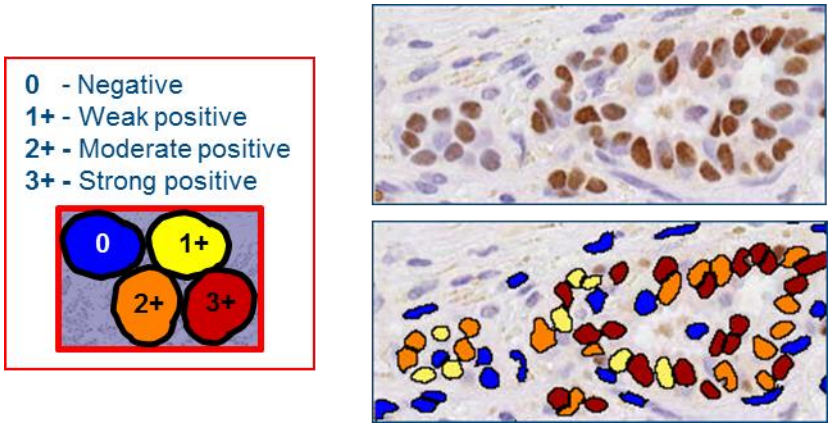

Figure 2-20 Intensity classification of the of the positive stain found in the nuclear pixels (brown stain) into weak, moderate and strong stains[2]

Aperio's IHC Nuclear Image Analysis algorithm can detect nuclear and cytoplasmic staining and corrects for it in the staining intensities and in the segmentation of the nuclei. It also uses a colour de-convolution technique that can split up to three different colour stains, thereby providing a true stain separation otherwise only achievable with multispectral imaging systems. Using this technique, the colours of the stain (brown) and counter-stain (blue) can automatically be calculated and used to standardise the stain colours in Aperio's IHC Nuclear Image Analysis algorithm.

The algorithm provides a mark-up image and an annotation window as its outputs. The mark-up image highlights the detected stain which are colour-coded according to their classification (blue = 0, yellow = 1+, orange = 2+, red = 3+, Figure 2-20). The annotated window delivers the percentage of positive stained nuclei, the average staining intensity of the positive nuclei, the percentages of 0, 1+, 2+ and 3+ nuclei.

[2] IHC Nuclear image analysis user guide

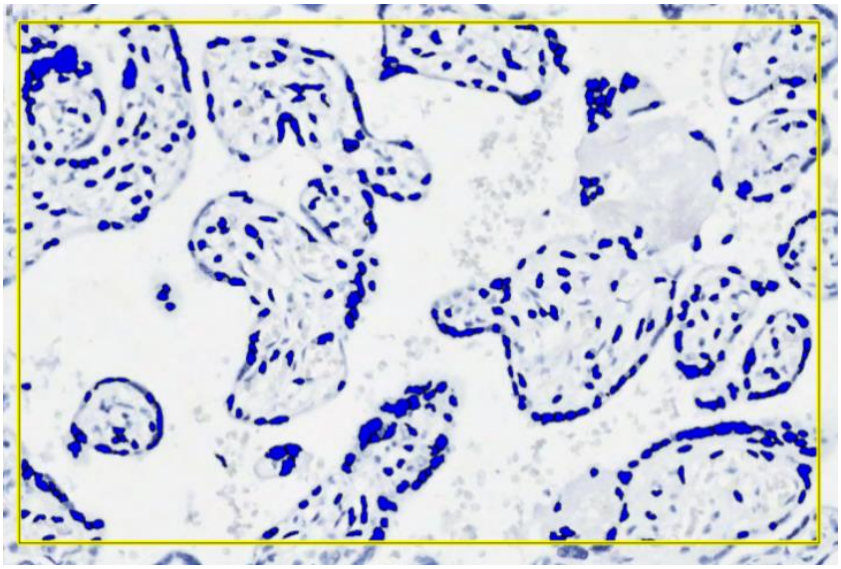

Figure 2-21 Image analysis of a placental negative control showing only blue stained cells with no positive cells (brown).

2.11 Cell culture

BeWo choriocarcinoma cell line, provided by Dr Karen Forbes and obtained from *European Collection* of Authenticated *Cell Cultures* (ECACC) (Porton Down, Wiltshire, UK), were maintained at 37°C under 5% CO_2-humidified incubator and cultured in Dulbecco's modified Eagle's medium-F12 (DMEM; Biological Industries, BI01- 050-1A) supplemented with 10% (v/v) fetal bovine serum (FBS; PAN, P30-3302) and antibiotics (30 mg/l penicillin, 50 mg/l streptomycin and 150 µg/l glutamine; Biological Industries, 03-031-1B), as previously described (289). The medium was changed every 2-3 days and cells were subcultured every 4 days at approximate by 80% confluence, cells were washed with PBS and passaged (1:5) using 0.25 trypsin-EDTA.

2.11.1 Drug treatment

After 24 hr cultures, the cells were treated with drugs that either induced or inhibited autophagy including:

- InSolution™ Rapamycin in EtOH (Merck Millipore)[3]: a known inducer of autophagy and an inhibitor of mTOR signalling supplied as a 10 mM (1 mg/109

[3] http://www.merckmillipore.com/GB/en/product/InSolution%E2%84%A2-Rapamycin-in-EtOH,EMD_BIO-553212?cid=BI-XX-BRC-A-BIOC-INHI-B123-1308&bd=1

µl) solution of Rapamycin (Cat. No. 553210) in EtOH. It was used in a working concentration of 2.5 µM for 24 hrs (191, 290).

- 3-Methyladenine (100mg, CAS 5142-23-4, Merck Millipore)[4]: an autophagy inhibitor, 3-MA, is a cell-permeable autophagic sequestration blocker. Dissolved in 95% ethanol at a stock concentration of 200mM and a working concentration of 5mM for 1 hr (291)
- Bafilomycin A1 (2µg, CAS Number 88899-55-2, Sigma)[5]: a specific inhibitor of vacuolar-type $H^{(+)}$-ATPase, which inhibits acidification and protein degradation in lysosomes of cultured cells, thus interferes with fusion of autophagosomes with lysosomes (292) essential for autophagy flux. At a stock concentration of 10µM and a working concentration of 100nM for 1hr (293, 294).
- Chloroquine: an anti-inflammatory drug used in the treatment or prevention of malaria (295). It suppresses inflammation by increasing lysosomal pH, thereby inhibiting lysosomal activity used in an increasing concentrations of 20, 60 and 120µM[6].
- Staurosporine: an alkaloid, isolated from the *bacterium Streptomyces staurosporeus*, known to induce apoptosis in many cell lines (296-298) was used at a final concentration of 1µM for 4 hours.

2.11.2 Manipulation of miRNA expression in BeWo cells

BeWo cells were transfected with miR-204, pre-miR-145 mimetics and appropriate controls at concentrations of 10nM, 50nM and 100nM to explore their effect on expression on the LC3 and apoptotic proteins. MicroRNA mimetics work by mimicking endogenous microRNAs, allowing microRNA expression and action to be manipulated.

Prior to transfection BeWo cells were plated onto 6 well plates and left for 24 hours in DMEM/F12 medium with 10% FBS and 1% GSP until they reached 55-70% confluency. Culture media was removed and the cells were washed twice with

4 http://www.merckmillipore.com/GB/en/product/Autophagy-Inhibitor%2C-3-MA---CAS-5142-23-4---Calbiochem,EMD_BIO-189490

5 http://www.sigmaaldrich.com/catalog/product/sigma/b1793?lang=en&region=GB

6 http://static.enzolifesciences.com/fileadmin/files/manual/ENZ-51031_insert.pdf

antibiotic-free and serum-free DMEM/F12. Cells were transfected using a 1% solution of DharmaFECT 2 (Dharmacon, GE Healthcare, UK), a lipid-mediated transfection reagent, in accordance with the manufacturer's guidelines (Thermoscientific) in antibiotic-free, serum-free DMEM/F12. Antibiotic-free, serum-free media was used to prevent antibiotic and serum components entering the cell during transfection and damaging the cells.

DharmaFECT contains liposomes composed of cationic lipids, whose basic structure consists of a positive head and two hydrocarbon chains. The positive head interacts with the phosphate backbone of the DNA sequence forming DNA-cationic lipid complexes. The positively charged liposome also facilitates interaction with the negatively charged mammalian cell membrane promoting endocytosis of the complex into mammalian cells. As the transfected DNA is not encapsulated within the liposome, it more readily leaves the vesicle, to diffuse through the cytoplasm and become incorporated within the cell nucleus.

The microRNA mimetics were transfected at concentrations of 10, 50 and 100nM and their effect was compared to controls, including untreated cells and mock transfected cells which were incubated with 1% DharmaFECT 2 in antibiotic-free, serum-free media to monitor the effect of the transfection process. The cells were incubated at 37°C and 5% CO2 for 4-6 hrs with the transfection solution; the following morning the transfection solution was removed and replaced with 2ml of DMEM/F12 with 10% FBS and 1% GSP. 48 hours after transfection the cells were lysed, either for RNA extraction or protein extraction and later qPCR or Western blotting respectively.

2.11.2.1 Transfection efficiency

To screen transfection efficiency BeWo cells were transfected with 10nM, 50nM and 100nM non-targeting CY3 labelled pre-miR negative control (pre C) (Ambion). These are synthetic double-stranded nucleotides intended to mimic naturally-occurring mature microRNAs and specifically designed so that the desired 5p strand becomes incorporated in the RNA-induced silencing complex (RISC) complex. 24 hours after the initial transfection, culture media was removed; cells were washed twice in PBS and stained with Hoechst stain to demarcate cell nuclei. Cells were viewed under an EVOS® Fluorescence live cell imaging microscope and the percentage of nuclei in contact with the red stain of the non-targeting CY3 labelled pre-miR was used as a

measure of transfection efficiency. A total of 6 images per well were captured (n=3 experiments).

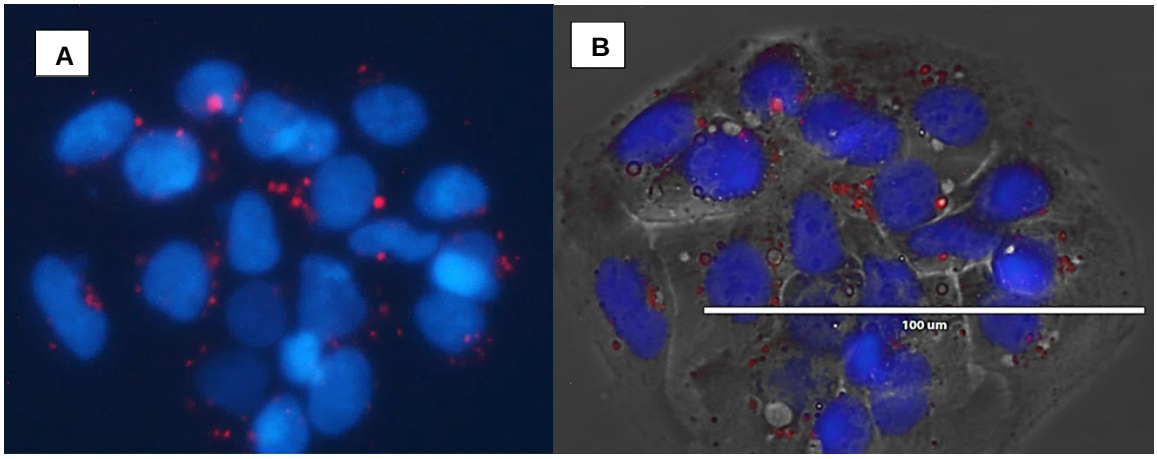

Figure 2-22 A representative image (40x) of BeWo trophoblast cell line transfected with 100nM non-targeting CY3 labeled pre-miR negative control (A) (Ambion) with miRNA appearing as red and nuclei stained blue with Hoechst stain. Image B shows a phase overlay on the stained nuclei with miRNA appearing red within endosomes inside the cells.

2.12 *In silico* data mining of miRNA gene targets

A literature search on the miRNAs related to the autophagy process or proven to affect autophagy-related genes in different body systems was made and then cross-checked with miRNAs differentially expressed in PET and/or IUGR placentae. Shortlisted miRNAs found in both searches were subjected to a stringent data-mining protocol for gene targets using more than one database. These shortlisted genes were then cross-checked again to check whether they had a role in the autophagy pathway in the literature in other organs. Some of the resulting genes were then quantified using polymerase chain reaction in the placenta.

The following sources were used for miRNA data mining:

- TargetScan - http://www.targetscan.org
- PicTar - http://pictar.mdc-berlin.de
- PITA - http://genie.weizmann.ac.il/pubs/mir07/mir07_dyn_data.html
- Microcosm- http://www.ebi.ac.uk/enright-srv/microcosm/cgi-bin/targets/v5/search.pl
- miRDB - http://mirdb.org/miRDB/index.html
- miRNA map - http://mirnamap.mbc.nctu.edu.tw/

2.12.1 TargetScan

After ensuring that ‘Human’ species was chosen, searches were performed using the full miRNA nomenclature e.g. hsa-miR-182-5p and submitted. Results were copied and pasted into a spreadsheet. The best match had the lowest score.

2.12.2 PicTar

PicTar predictions lists in vertebrates, flies, and nematodes (299) were sought, ensuring that species ‘vertebrate and dataset’ based on conservation in mammals’ was selected. ‘Search for targets of a miRNA’ was clicked and the entire table is copied and pasted into the same spreadsheet with their ranks (best match = highest score)

2.12.3 PITA

In this database, the miRNA name was entered with the following options: Minimum seed size: 6, allowing single G: U while not allowing single mismatch; Flank settings: 3 upstream / 15 downstream. The results were copied and pasted into the same spreadsheet with their ranks (best match = lowest score).

2.12.4 Microcosm Targets

After selecting ‘H. Sapiens’, the miRNA ID entered and searched. The results were downloaded and imported into the spreadsheet (best match = highest score).

2.12.5 miRDB

The miRNA name was entered and the results table edited to have the ‘Gene Symbol’ beside the gene name to be easily viewable next to the rank (best match = highest score).

2.12.6 Top results

The top 50 results were copied from each database (the rank and gene name), and pasted into columns A and B of the ‘Top results’ spreadsheet. Then the data were sorted and filtered using a custom sort first on Values, and order Smallest to Largest to have a list with the highest ranking on the top. All data in column B ‘Gene name’ were set to highlight in pink any cells that had duplicates elsewhere in the column. [This was done by selecting column B, going to ‘Conditional Formatting’, then ‘Highlight Cell Rules’, ‘Duplicate Values’ and setting the options to highlight duplicates].

This process gave a clearer picture of any genes from the top 10 of any one dataset which were also reported as likely (top 50) candidates by at least one other dataset.

2.13 Polymerase Chain Reaction

2.13.1 RNA extraction

2.13.1.1 FFPE sections

Ten µm sections were prepared from FFPE placental blocks (Leica RM2235 microtome) to provide more than one cell thickness and maximise the recovery of miRNAs. After the first three sections were discarded (to minimise nucleic acid damaged by exposure to atmosphere during storage), a further 6-8 sections were cut from each placental block and placed in 1.5 ml microcentrifuge tube. RecoverAll™ Total Nucleic acid Isolation Kit (Ambion, Catalogue number: AM1975) was used according to the manufacturer's instructions to extract RNA from FFPE.

Deparaffinisation was achieved by adding 100% xylene to the samples, vortexed to mix, then heated for 3 minutes at 50°C to melt the paraffin, then centrifuged at 10,000 rpm for 2 minutes to pellet the tissue and the xylene discarded. The pellet was then washed twice with 100% EtOH, to remove xylene and accelerate drying of the tissue, and then centrifuged for 2 minutes at 10,000 to pellet the tissue. Residual ethanol was removed without disturbing the pellet. The pellet was then air-dried for 45 minutes at room temperature, to remove residual EtOH. Protease digestion was then done by adding 200 µl of digestion buffer and 4 µl of protease to each sample. The samples were then incubated in the thermomixer heat blocks overnight at 50°C for 16 hours then at 80°C for 15 minutes.

Nucleic acids were precipitated by adding 240 µl isolation additive and 550 µl 100% EtOH to each sample. Samples were then pipetted to a filter cartridge, to bind to RNA, and centrifuged for 30 seconds at 10,000 RPM and the flow-through discarded. After a series of washing and centrifuging, DNA was digested by adding a DNase mixes (6 µl of 10X DNase Buffer, 4µl of DNase and 50 µl of Nuclease-free water) and incubated for 30 minutes at room temperature. RNA was then isolated by adding RNase free water to the centre of the filter in the final elution step and then centrifuged for 1 min

at 10,000 rpm to pass the mixture through the filter. The RNA was then stored at -80°C.

2.13.1.2 BeWo cell Line

Total RNA was extracted from the BeWo cells using miRNeasy Mini Kit (Qiagen, Hilden, Germany) according to the manufacturer's instructions. The cells were first lysed by adding QIAzol™ lysis reagent (700 µl). The lysate was then collected by a rubber policeman, then pipetted into a microcentrifuge tube, and homogenised by vortexing for 1min. The tube is then left on the benchtop for 5 min at room temperature (RT) to allow dissociation of nucleoprotein complexes. Chloroform (140 µl) was then added to the homogenate and shaken vigorously for 15 sec to allow thorough mixing and then left again on the bench top at RT for 2-3 min. The tube was then centrifuged for 15 min at 12,000 rpm at 4°C. After centrifugation, the sample was separated into 3 phases: an upper colourless aqueous phase containing RNA; a white interphase; and a lower red, organic phase. The upper aqueous phase was transferred to a new collection tube (350 µl) and 100% EtOH (525 µl) added and mixed thoroughly by pipetting up and down several times to precipitate RNA. The sample was then transferred to an RNeasy Mini spin column in a 2 ml collection tube and then centrifuged at 10,000rpm for 30sec at RT and the flow-through discarded. The column is then washed 3 times by EtOH-based buffers, to remove any salts, and then transferred to a new collection tube. RNA was isolated by pipetting 50 µl of RNase-free water directly onto the RNeasy Mini spin column membrane and centrifuged at 10,000 rpm for 1min to elute the RNA.

2.13.2 RNA quantification

The total RNA was collected and quantified using a NanoDrop™ 2000 Spectrophotometer (Thermo, ND-1000, USA). The A260/280 ratios along with total RNA concentration as ng/µl were recorded. This was to measure the purity of the RNA. Ratios of absorption (260/280 nm) were between 1.9 and 2.1.

2.13.3 cDNA synthesis

2.13.3.1 mRNA

AffinityScript Multiple Temperature cDNA synthesis kit (Agilent Technologies, USA) was used to reverse transcribe RNA to cDNA. 100ng of RNA (total volume of 12.5µL in PCR grade H_2O), 3µL of random primers were added, gently mixed, spun briefly and then incubated at 65°C for 5 minutes. The reaction was cooled at room temperature for 10min to allow primer annealing, followed by the addition of 2.0µl 10x AffinityScript RT Buffer, 0.8µl dNTP mix, 0.5µl RNase Block Ribonuclease Inhibitor (40 U/µl) and 1µl AffinityScript Multiple Temperature reverse transcriptase (RTase).

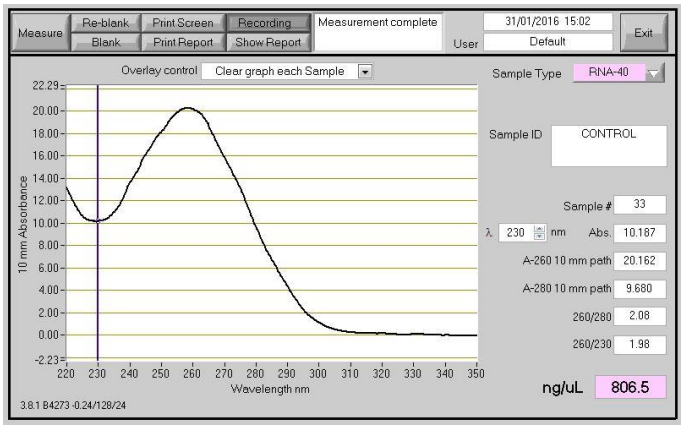

Figure 2-23 Representative example of RNA quantification and purity measurement using Nanodrop Spectrophotometer for BeWo cell line.

The solution was mixed and incubated at 25°C for 10min to allow for primer extension and then 42°C for 60min for cDNA synthesis. The reaction was terminated by incubation at 70°C for 15min to inactivate the enzyme. The completed first-strand cDNA synthesis reactions were then placed on ice for subsequent PCR amplification or stored at -20°C till needed. Alongside each set of reactions, two control samples were also included, one without RTase and one without RNA but with RTase as a No Template Control (NTC) to check for RNA contamination. In addition, human reference total RNA (Stratagene) was used as a calibrator for the RT reaction. These controls and calibrators were subsequently included in each subsequent PCR.

2.13.3.2 miRNA

The miRCURY LNA™ Universal RT microRNA PCR, Universal cDNA synthesis Kit II, Exiqon® was used for microRNA polyadenylation and reverse transcription to cDNA according the manufacturers' instructions. An absolute quantity of 10ng of RNA in a

total volume 7µl (diluted in PCR grade water) was added to 2µl of 5x reaction buffer and 1µl of enzyme mix. Samples were incubated for 60 minutes at 42°C followed by heat inactivation of the reverse transcriptase for 5 minutes at 95°C then immediately cooled to 4°C and stored at -20°C.

2.13.4 Real Time- quantitative Polymerase Chain Reaction

2.13.4.1 mRNA qRT-PCR

mRNA expression was quantified by qPCR using an Applied Biosystems 7900HT Fast Real-Time PCR System machine and Brilliant III ultrafast SYBR® Green QPCR master mix (Agilent Technologies, USA) with 5-carboxy-x-rhodamine (ROX) as a passive reference dye. RT-PCR reactions were prepared under a highly sterile environment. Gene expression was analysed in triplicate in 96 well PCR plates and quantified against standard curves generated (Figure 2-24) from total human placental RNA and human reference total RNA (Stratagene, La Jolla, USA) respectively.

Reagent	Volume (µl)/well
Sterile H_2O	1.44 µl
2x Mastermix (SYBR Green)	6.25 µl
Upstream primer	0.31 µl
Downstream primer	0.31 µl
Reference Dye (ROX)	0.19 µl
cDNA (1:10)	4 µl
Final Volume	12.5 µl

Table 2-4 Summary of the Mastermix used in the RT-PCR reaction for genes.

cDNA samples were diluted 1:10 in sterile water then appropriate volumes of PCR Master Mix, cDNA sample, probes and dH_2O were added in each well as described in Table 2-4. The plate was then sealed, centrifuged for 20 seconds with each plate containing a non-template control and a reverse transcriptase negative control.

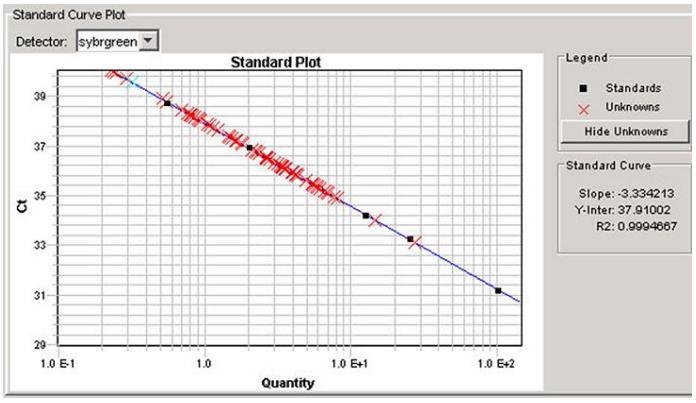

Figure 2-24 An example of a standard curve generated from serial dilution of human reference total RNA for PCR quantification used in the PCR quantification of placental samples.

Primers for gene expression and quantification were designed by a public resource PrimerBank (http://pga.mgh.harvard.edu/primerbank/index.html) and confirmed as specific by BLAST analysis: http://www.ncbi.nlm.nih.gov/tools/primer-blast/

Gene symbol (Accession number)	Primer direction	Sequence (5'->3')	Length	Tm	GC %	Product size
CYC1 NM_001916.4	Forward	CAGATAGCCAAGGATGTGTG	20	55.91	50	93
	Reverse	CATCATCAACATCTTGAGCC	20	54.45	45	
TOP1 NC_000020.11	Forward	GATGAACCTGAAGATGATGGC	21	56.74	47.62	86
	Reverse	TCAGCATCATCCTCATCTCG	20	56.9	50	
GAPDH NC_000012.12	Forward	AGATCATCAGCAATGCCTCC	20	57.73	50	92
	Reverse	CATGAGTCCTCCCACGATAC	20	57.2	55	
YWHAZ NC_000008.11	Forward	ACTTTTGGTACATTGTGGCTTCAA	24	59.6	37.5	94
	Reverse	CCGCCAGGACAAACCAGTAT	20	60.04	55	
TBP NC_000006.12	Forward	TGCACAGGAGCCAAGAGTGAA	21	61.93	52.38	132
	Reverse	CACATCACAGCTCCCCACCA	20	62.13	60	
MAP1LC3B NC_000016.10	Forward	AAACGGGCTGTGTGAGAAAAC	21	59.6	47.62	83
	Reverse	TGAGGACTTTGGGTGTGGTTC	21	60.13	52.38	
BCL2 NC_000018.10	Forward	CGACGACTTCTCCCGCCGCTACCGC	25	72.81	72	319
	Reverse	CCGCATGCTGGGGCCGTACAGTTCC	25	71.62	68	
BCL11B NC_000014.9	Forward	TCCAGCTACATTTGCACAACA	21	58.42	42.86	100
	Reverse	GCTCCAGGTAGATGCGGAAG	20	60.25	60	
PARK2 NC_000006.12	Forward	GTGTTTGTCAGGTTCAACTCCA	22	58.99	45.45	129
	Reverse	GAAAATCACACGCAACTGGTC	21	58.35	47.62	
EGR1 NC_000005.10	Forward	GGTCAGTGGCCTAGTGAGC	19	59.78	63.16	149
	Reverse	GTGCCGCTGAGTAAATGGGA	20	60.39	55	

ATG5 NC_000006.12	Forward	AAAGATGTGCTTCGAGATGTGT	22	58.33	40.91	144
	Reverse	CACTTTGTCAGTTACCAACGTCA	23	59.38	43.48	
YWHAE NC_000017.11	Forward	GATTCGGGAATATCGGCAAATGG	23	60.12	47.83	90
	Reverse	GCTGGAATGAGGTGTTTGTCC	21	59.46	52.38	
PTPN2 NC_000018.10	Forward	GAAGAGTTGGATACTCAGCGTC	22	58.56	50	158
	Reverse	TGCAGTTTAACACGACTGTGAT	22	58.54	40.91	

Table 2-5 Primer characteristics for genes used in the qRT-PCR reactions.

The amplification protocol included 1 cycle at 95ºC for 3 min then 40 cycles of: 95ºC for 20 seconds for denaturation and at 60ºC for 30 seconds for annealing. A dissociation curve (Figure 2-25) was set up after each amplification protocol to ensure the integrity of the PCR reaction and that they have produced single, specific products (Figure 2-25). It included 1 minute at 95ºC, then 55ºC for 30 seconds and increased again to 95ºC, ramping at 0.2ºC/cycle and collecting fluorescent data continuously.

Expression analysis of each sample was calculated from the standard curve (Figure 2-24) and data were normalised to the geometric mean (300) of 4 House Keeping genes (HKG) which were validated in all the placental groups (GAPDH, YWHAZ, TOP1 and β-Actin) for more accurate and reliable normalization of gene expression data.

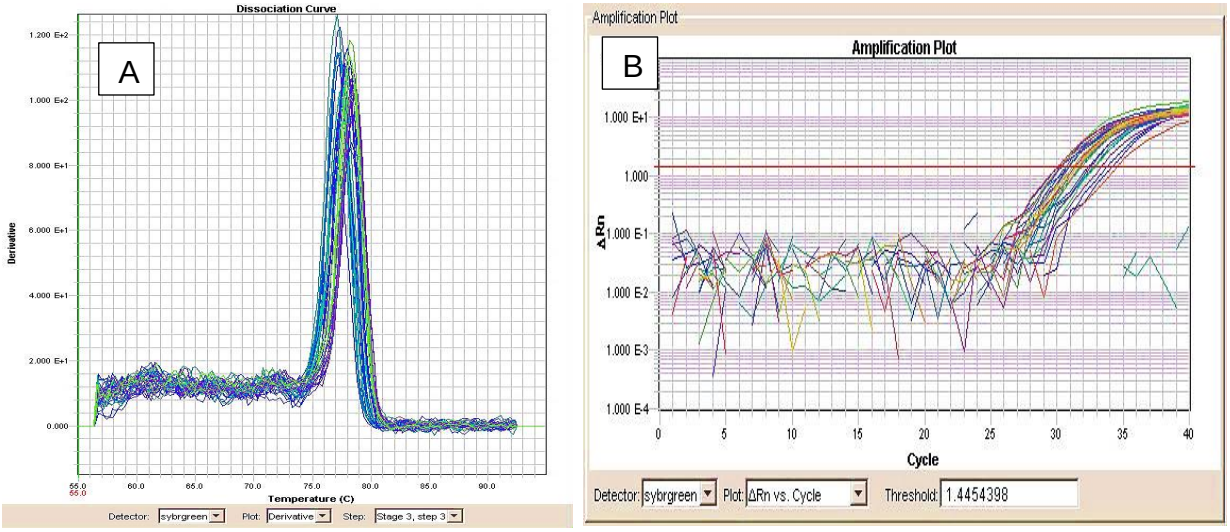

Figure 2-25 Representative example of a dissociation curve of a single PCR product (A) and an amplification plot (B).

2.13.4.2 miRNA qRT-PCR

The miRCURY LNA™ Universal RT microRNA PCR system, a microRNA-specific, LNA™-based system designed for sensitive and accurate detection of microRNA by quantitative real-time PCR using SYBR® Green, was used according to the manufacturer's instructions. PCR Master Mix (5 µL) was added to 1µL of PCR primer mix and 4µL of cDNA diluted 1:80 made a total volume of 10µL for the PCR reaction. The amplification protocol included 1 cycle of polymerase activation/denaturation at 95ºC for 10 minutes and then 40 cycles of: 95ºC for 10 seconds, 60ºC for 1 minute with a ramp rate of 1.6ºC/second. Expression analysis of each sample was calculated from the generated standard curve (Figure 2-24) and data were normalised to the geometric mean 5S and U6 rRNA, that were used in other placental studies (236) and identified as a suitable housekeeping genes (HKG) in this study.

Product name	Target sequence 5'- 3'
hsa-miR-204-5p	UUCCCUUUGUCAUCCUAUGCCU
hsa-let-7a-5p	UGAGGUAGUAGGUUGUAUAGUU
hsa-miR-182-5p	UUUGGCAAUGGUAGAACUCACACU
hsa-miR-145-5p	GUCCAGUUUUCCCAGGAAUCCCU
hsa-miR-192-5p	CUGACCUAUGAAUUGACAGCC

Table 2-6 Primer characteristics for miRNAs used in the qRT-PCR reaction.

2.14 Western Blotting

2.14.1 Protein extraction

Radio immunoprecipitation assay buffer (RIPA) was made from Tris base, sodium chloride (NaCl) in deionised water (dH_2O) and pH adjusted to 7.4. NP40, Na Deoxycholate and EDTA are added as well and volume then adjusted to 100 ml by dH_2O then stored at 4ºC.

Protease Inhibitor Cocktail Tablets (cOmplete™, Mini, Roche) were used to prevent protease inhibitors in the lysis buffer. For protein extraction, the BeWo cells were

placed on ice, the media removed and the washed twice with PBS. A 500 µl of the lysis buffer was added for a T75 flask then the cells were scraped into the buffer, transferred into Eppendorf tubes, and left on ice for 15 minutes where they were vortexed every 5 minutes. This was followed by centrifuging at 13000 RPM for 15 minutes, then the supernatant was removed and placed in fresh tubes and frozen at - 20ºC till ready for protein assay.

2.14.2 Protein standardisation

Protein content of samples was measured using DC protein assay (BioRad), where bovine serum albumin (BSA) standard curve (2mg/ml - 0.1mg/ml) was prepared following the kit instructions for microplate assay. Using a generated standard curve, the protein concentrations of unknown samples were calculated. Forty µg of protein was loaded in each well to run the Western blot.

2.14.3 SDS PAGE Electrophoresis

Western blots were made with Invitrogen NuPAGE® electrophoresis system using NuPAGE® Novex® 4-12% Bis-Tris Gels which are pre-cast polyacrylamide gels. During this step, the proteins in the sample (40µg), using denaturing polyacrylamide gel electrophoresis (PAGE), were separated according to their molecular weight. Once the protein sample has been heated at 70℃ for 10 minutes, the NuPAGE® LDS Sample Buffer was added, loaded with Lithium Dodecyl Sulphate (LDS) to maintain polypeptides in a denatured state.

A reducing agent was also used in conjunction to remove secondary and tertiary structure (to break disulphide bonds). In addition, sample proteins covered in the negatively charged LDS then moved through the acrylamide mesh of the gel toward the positively charged electrode. This facilitated their separation according to molecular weight (measured in kilo Daltons, kDa). 1x SDS Running Buffer was made from adding 50 ml 20x SDS Running Buffer to 950 ml of deionized water. 500 µl of NuPAGE® Antioxidant (Novex™) was added to the upper buffer chamber and the Novex® Sharp Pre-Stained Protein Standard was used as a molecular weight standard for estimation of molecular weight proteins. The running condition included a voltage of 200 V constant for 40-50 minutes.

2.14.4 Protein transfer

NuPAGE® Transfer Buffer (20X) (Novex™) was used to transfer proteins from NuPAGE® Novex® gels to membranes for Western blotting. The transfer buffer (1X with 10% methanol) was prepared and pre-cooled to 4°C in a cold room. Proteins were then transferred by electroblotting from the gel onto a Polyvinylidene Fluoride (PVDF) membrane for 1 hour under 30 volts constant. Protein binding is reliant on hydrophobic interactions and charge interactions between the membrane and protein. The molecular weight of the target protein determines the position of the band, while the band intensity relies on the amount of target protein present (301)

2.14.5 Antigen detection

Subsequently, the membranes were blocked, to avoid non-specific interactions of the antibody with the membrane, with 5% skimmed milk in 0.1% PBST for at least 1hour on a shaker at room temperature. Then the membranes were incubated overnight at RT with the primary antibody (Table 2-7) with 1% skimmed milk containing tween 0.1% PBST. Membranes were washed three times 10 minutes each with PBST and incubated with the appropriate horseradish peroxidase (HRP) conjugated secondary antibody (Table 2-8) for 1 hour at room temperature. The membranes were washed three times, each for 10 minutes with PBST, then the membranes were developed with ECL substrate (1:1 v/v) (Pierce Rockford, IL), a chemiluminescent agent that luminesces when exposed to the HRP on the secondary antibody. The luminescence produced is in place and proportionate to the amount of protein probed.

Primary Antibody	Dilution	Company
Anti LC3 (Rabbit, polyclonal, pAb)	1:1000	Novus Biologicals
Anti actin (Mouse, monoclonal mAb)	1:10,000	Santa Cruz Biotechnology
Caspase-3 (Rabbit, mAb)	1:1000	Cell Signalling Technology
Cleaved caspase-3 (Rabbit, mAb)	1:1000	Cell Signalling Technology
PARP (Rabbit, pAb)	1:1000	Cell Signalling Technology
Cleaved PARP (Rabbit, mAb)	1:1000	Cell Signalling Technology

Caspase-9 (Mouse, mAb)	1:1000	Cell Signalling Technology
Cleaved Caspase-9 (Rabbit, mAb)	1:1000	Cell Signalling Technology
Bcl-2 oncoprotein (Mouse, mAb)	1:1000	Dako Agilent pathology solution

Table 2-7 Primary antibodies used in the western blots.

Secondary Antibody	Dilution	Company
Goat anti-mouse IgG-HRP	1:5000	Santa Cruz Biotechnology
Goat anti-rabbit IgG-HRP	1:5000	Santa Cruz Biotechnology

Table 2-8 Secondary antibodies used in Western blotting.

2.14.6 Protein quantification

Images were obtained on the Gel-Doc imager (Bio-Rad) where relative protein expression bands were quantified by densitometry (OD/mm^2) using Image Lab (Version 5.2.1) image analysis software (Bio-Rad, Segrate, Italy). Protein levels of the treated cells were expressed as densitometry ratio with the control, followed by overall standardisation to actin as a housekeeping protein, thus represented as fold change (increase or decrease) from the control.

2.15 Cytological detection of autophagy and apoptosis by fluorescence microscopy

Autophagy was assayed by CYTO-ID® Autophagy Detection Kit (ENZ-51031-K200, Enzo®) which visualises autophagic vacuoles and displays autophagic flux in live cells using a dye that selectively labels autophagic vacuoles and exhibit bright fluorescence upon incorporation into autophagosomes and autolysosomes (autophagolysosomes). The kit was used according to the manufacturer's instruction. The drug treatments were added when the cells were 70-80% confluent and left for the appropriate time, then the media was removed and cells washed with 1x Assay buffer twice before adding the Cyto-ID green reagent and Hoechst nuclear stain in phenol-free cell growth media. The wells were incubated for 30 min at 37°C in the incubator and then carefully

washed with 1x Assay buffer before being visualised by EVOS® Fluorescence Live Cell Imaging System microscope.

2.16 Flow cytometry analysis

BeWo cells were incubated with drug treatments as previously described in section (2.11.1 Drug treatment), or transfected with miR-204. The cells were dissociated in trypsin and EDTA, pelleted by centrifugation, and resuspended in PBS. The cells were then fixed in 70% ice-cold ethanol, followed by incubation in a freshly prepared staining solution (10mg/ml propidium iodide (PI), 0.1% Triton X-100, and 100mg/ml ribonuclease) at 37°C for 20 min.

Apoptosis was then assayed using an FITC Annexin V Apoptosis Detection Kit II (BD Pharmingen™) and analysed by flow cytometry. The protocol was followed according to the manufacturer's instructions. The cells were stained with 0.5 ng FITC Annexin V (component no. 51-65874X) and 2 ng PI (component no. 51-66211E) for 15 min in darkness at room temperature. The FITC and PI fluorescence were measured at emission wavelengths of 530nm and 585 nm, respectively (FACS VerseTM, BD Biosciences, USA). Cells were considered viable when FITC Annexin V and PI turned out negative; cells that were in early apoptosis were FITC Annexin V positive and PI negative and cells that were in late apoptosis or already dead were both FITC Annexin V and PI positive.

2.17 Statistical analysis

Data were presented as the means ± standard deviation when normally distributed, or medians with interquartile range when not normally distributed. Data were analysed and plotted using GraphPad Prism version 6 (GraphPad Software, La Jolla, CA) with parametric (*t*-test or ANOVA) and non-parametric tests (Mann-Whitney or Kruskal Wallis) as well as *post hoc* tests used as appropriate. Results were considered to be statistically significant if $p < 0.05$.

Chapter 3
Structural characterisation of placental dysfunction in compromised pregnancies

3.1 Introduction

Placental dysfunction has long been regarded as an important signpost in the pathogenesis of several gestational diseases including preeclampsia and/or IUGR (20). Placental dysfunction till now is still a general term used to encompass different entities leading to different clinical phenotypes as seen in IUGR, preeclampsia, or preeclampsia accompanied by IUGR. Aberrant regulation of placental development and invasion can all end up in pregnancy pathologies such as IUGR, preeclampsia and miscarriage (302). Several reports have revealed that this is because dysregulated placental development directly impacts placental function. Altered villous morphology- abnormal trophoblast proliferation and apoptosis and perturbed villous angiogenesis can all result in a reduction in villous growth, (303, 304); this in turn can lead to deficient nutrient transfer to the fetus, and altered release of placental secreted growth hormones and cytokines (305). Another important parameter of placental dysfunction linked to the pathogenesis of PET, owing to its inflammatory and necrotic nature, is the altered shedding of trophoblastic debris; this can be examined histologically by examining levels of placental SNAs.

Whilst it is known that all of these consequences of placental dysfunction are associated with clinical pathologies, the individual or combined mechanisms that lead to the development of distinct clinical pathologies of IUGR, preeclampsia with normal fetal growth, or preeclampsia accompanied by IUGR, is unclear. Moreover, early-onset PET (EOPET<34 weeks), late-onset PET (LOPET>34 weeks) with and without IUGR, have all different clinical outcomes; despite this the distinct histopathology of placentas in these conditions is unclear.

Placental dysfunction has always been an enigmatic term to researchers and perinatal pathologists. It is conventionally assessed through an expert-led process of qualitative

pathological description of the macro and microscopic structure with comments on areas of ischemia and infarction. Though the advantage is that the pathologist would have an overview of the entire placenta, yet the limitations are sometimes the lack of standardisation with the difficulty to grade the severity of the disease. Another limitation is a greater inter-observer variance and experience with consequently a lesser ability to standardise the findings and a considerable heterogeneity of descriptors in placental characterisation from different clinical phenotypes.

So instead of these current methods which examine the overall qualitative histological parameters of placental morphology, a more reproducible and quantifiable histological assessment of the placenta in different clinical phenotypes might allow a better understanding of the mechanisms underlying placental dysfunction in the different pathologies. Furthermore, identification of potential effect modifiers of placental dysfunction and their measurements using a stereological methodology can help us objectively asses the placental pathology.

Volume density, which indicates how much change within a unit volume and is essential in the comparison between different conditions (278), was calculated by the technique of point counting (273). This approach gives volume densities of villous stroma, capillaries, trophoblast, and syncytial nuclear aggregates. Volume densities in each placenta were then divided by its respective villous volumes and expressed as ratios ($V_{SNA}/V_{Villous}$) so that differences between villous volumes across disease groups can be accounted for when comparing different components of interest (Equation 2-1).

Syncytial Nuclear Aggregates (SNA) (78) are focal aggregation, or clumping of nuclei of syncytiotrophoblast on the outer surface of placental villi (306, 307). The potential role of SNAs and other trophoblastic debris shed into the maternal circulation, with their inflammatory/immunogenic nature, leading to a maternal systemic endothelial dysfunction with the hallmark signs of hypertension and proteinuria has increasingly gained more attention recently (68, 69). Furthermore, developing a 3D model for the SNAs, fibrinoid degenerations and villus branching in normal and preeclamptic placentas may help researchers towards a better understanding of the structural arrangement and spatial relationship of SNAs to their surrounding including villi and fibrinoid degenerations.

3.2 Hypothesis

The combined use of quantitative methods such as stereology, together with qualitative approaches such as digitised imaging methods to three-dimensionally reconstruct placental histological sections, will allow the underlying pathological phenotype of placental dysfunction in early and late onset gestational diseases to be defined.

3.3 Aim and specific objectives

The aim of this study was to determine quantitatively through stereology, as well as qualitatively through digital pathology, the structural pathological phenotype of placental dysfunction in early and late onset gestational diseases.

The specific objectives were:

1. To quantify the following parameters in normal pregnancies and those complicated by preeclampsia, IUGR, or PET accompanied by IUGR:
   i) Placental villous volumes
   ii) SNA volumes
   iii) Trophoblast volumes
   iv) Placental capillary volumes
   v) Fetal-side and maternal-side distribution of each of those elements.

2. To perform 3D reconstruction of normal and pathological placental histological sections to determine spatial distribution of placental microarchitecture.

3.4 Results

3.4.1 Serial sectioning classification

3.4.1.1 Artefactual SNAs or Knots

False SNAs are cytotrophoblast nuclei cut tangentially in histological sections and are not aggregated syncytiotrophoblast nuclei. They were identified through serial sections as a bridge between two villi or from tangential sections through the STB layer at points of villous branching and bending. In high magnification, their nuclei appeared as little basophilic separate islands surrounded by a light eosinophilic cytoplasmic syncytium with size similar to nuclei dispersed in the syncytium.

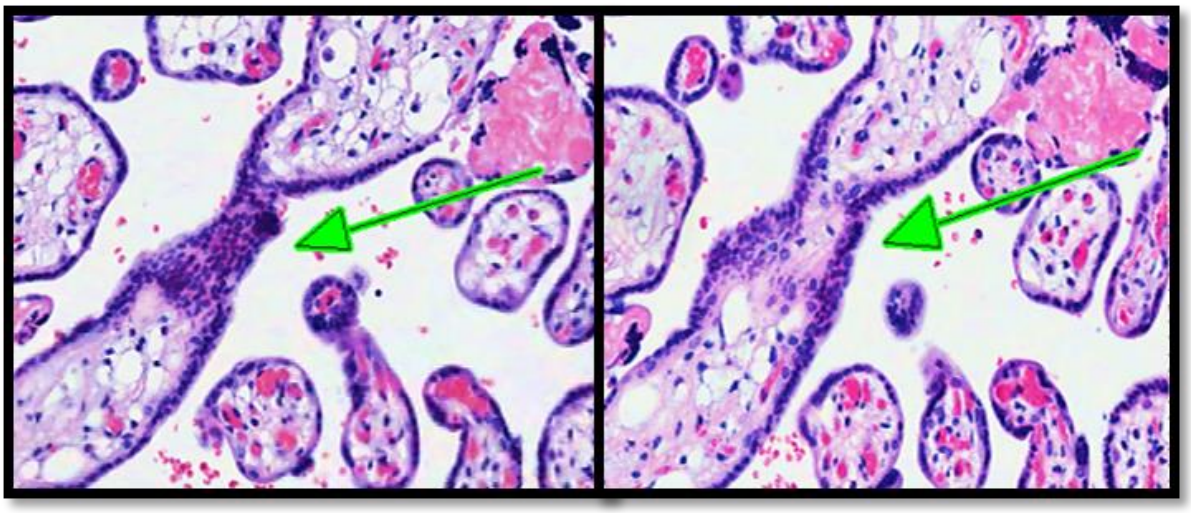

Figure 3-1 Serial sections of 2D placental histological slides showing an artefactual SNA (green arrow), but when followed consecutively is actually revealed to be a trophoblast layer covering the villi, as the sections appeared tangential and attached to the trophoblast lining of the villus.

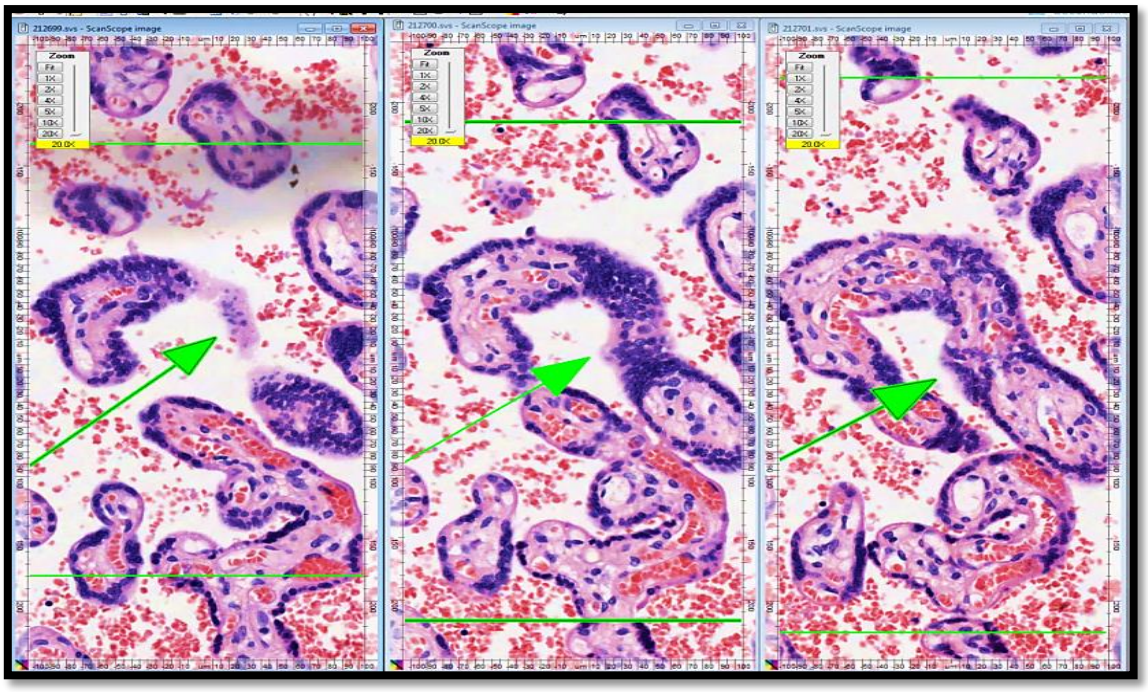

Figure 3-2 Demonstration of an SNA (green arrow) derived from a polar villous end.

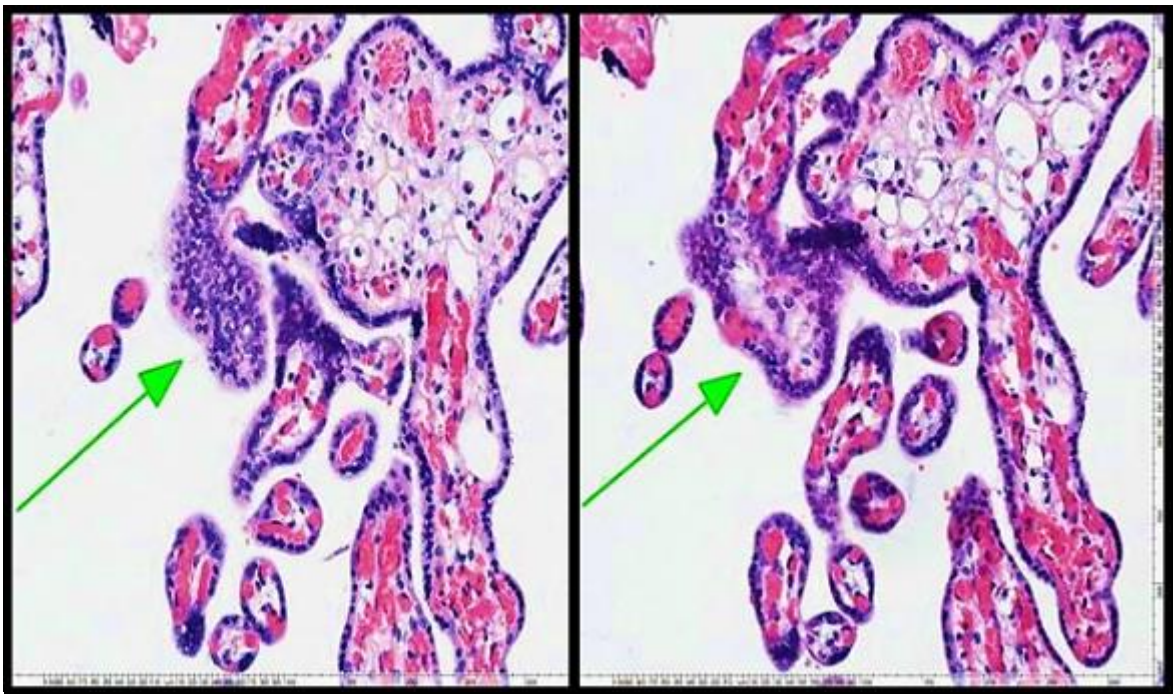

Figure 3-3 Serial images of an artefactual false SNA (green arrow), showing nuclei congregated in proximity to each other from tangential sections.

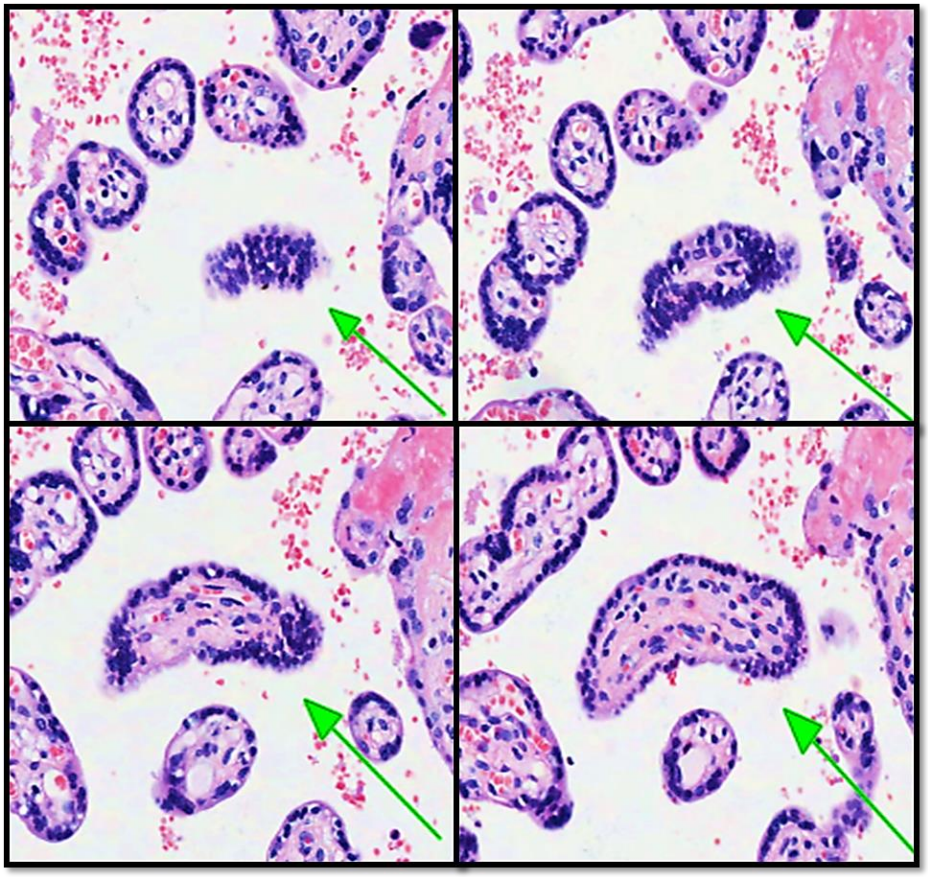

Figure 3-4 Apparent syncytial nuclear aggregation (green arrow) followed in serial sections to show that they are a mere trophoblast lining of a villus.

3.4.1.2 True SNAs

True knots or SNAs, on the other hand, are clumped degenerated nuclei from syncytiotrophoblast that might be shed into the maternal circulation. Their nuclei appeared small, densely basophilic and packed together and in many cases in proximity to or around a core of fibrinoid degeneration (Figure 3-5, Figure 3-6, Figure 3-7, and Figure 3-8).

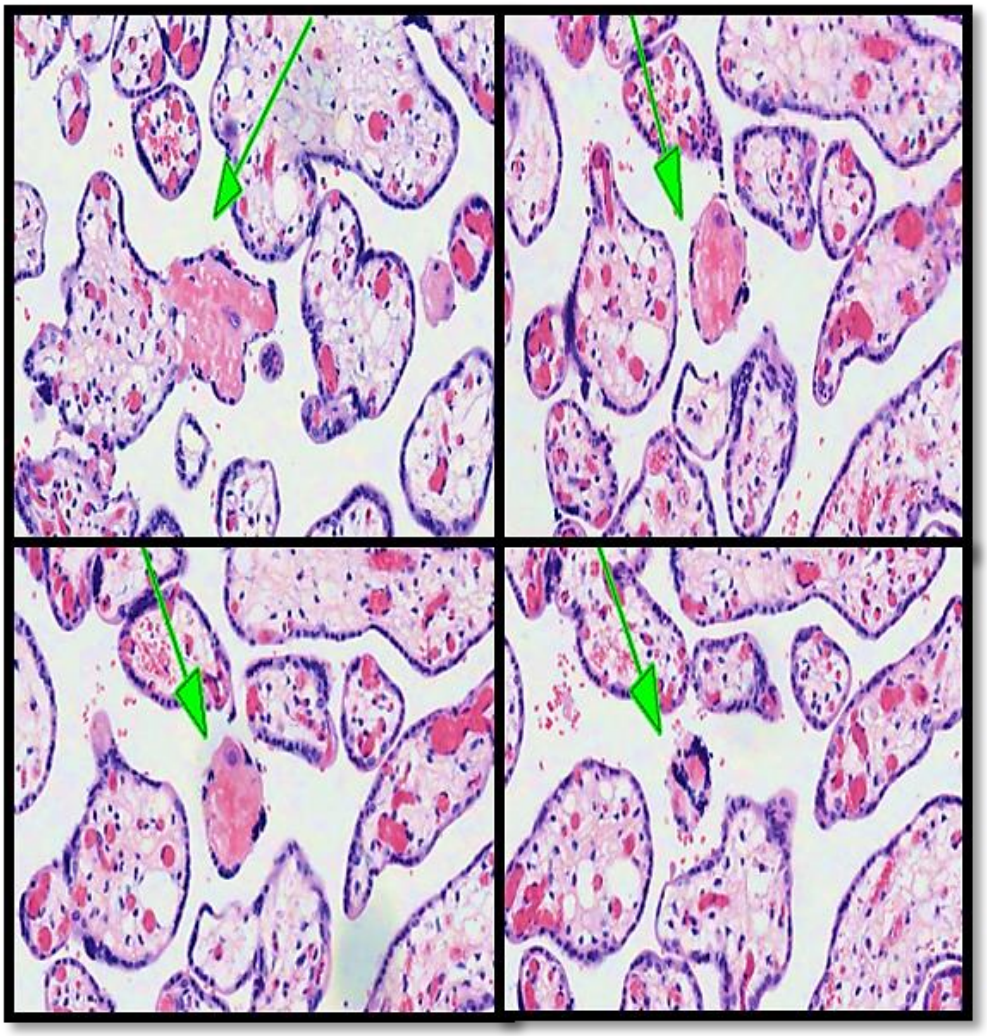

Figure 3-5 Serial sections of a degenerated fibrinoid area and SNA (green arrow). It appears that it is separated from the villous island and shed off into the maternal circulation.

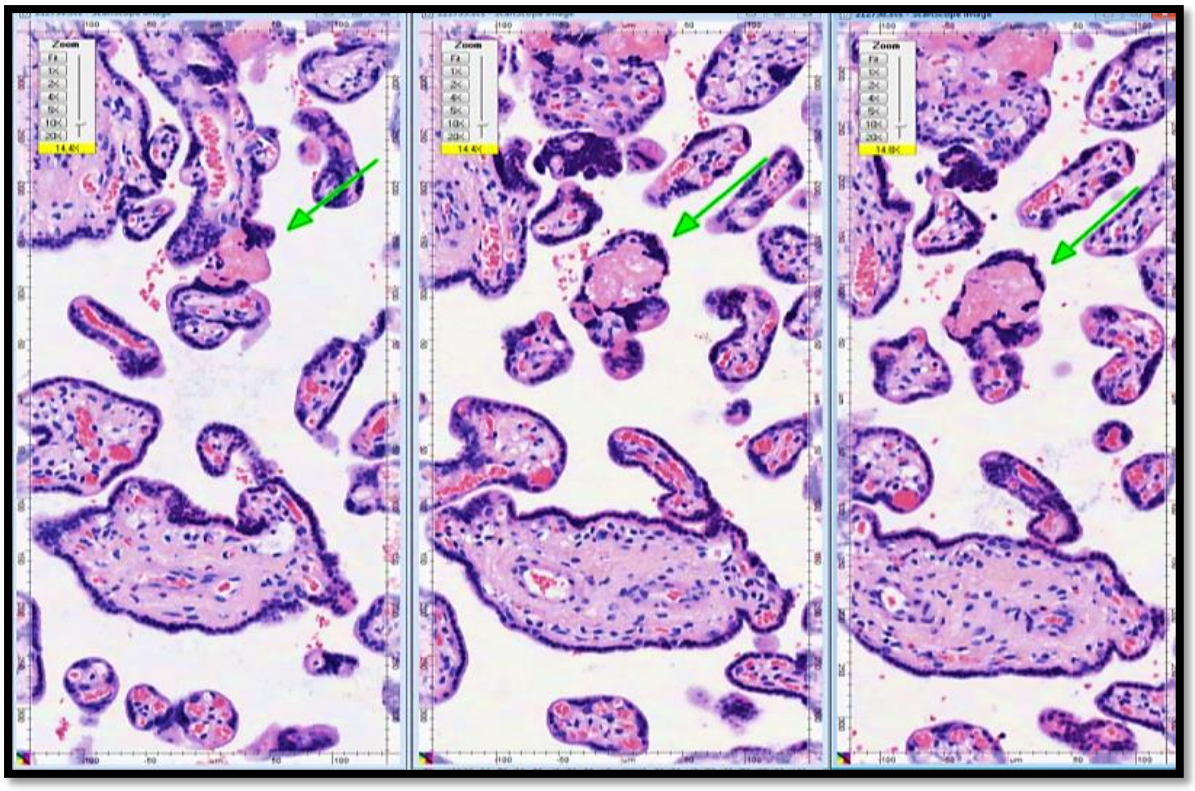

Figure 3-6 Serial images showing intravillous fibrinoid deposition and syncytial denudation and in the following serial sections SNA shedding off the villi (green arrow) around the core of fibrinoid necrosis into the intervillous space (maternal circulation).

These results showed that true SNAs were usually around or adjacent areas of fibrinoid degeneration, that appeared homogenous eosinophilic with no capillaries. This might suggests that SNAs might not be only a feature of trophoblast degeneration but might be linked to features of villous degeneration such as impaired perfusion and degeneration as well and that it might have a role in SNA formation and/or shedding. A more in-depth with a 3D view of the SNAs and their relationship and spatial arrangement around terminal villi and fibrinoid degeneration was therefore warranted (Figure 3-5, Figure 3-6, Figure 3-7, and Figure 3-8).

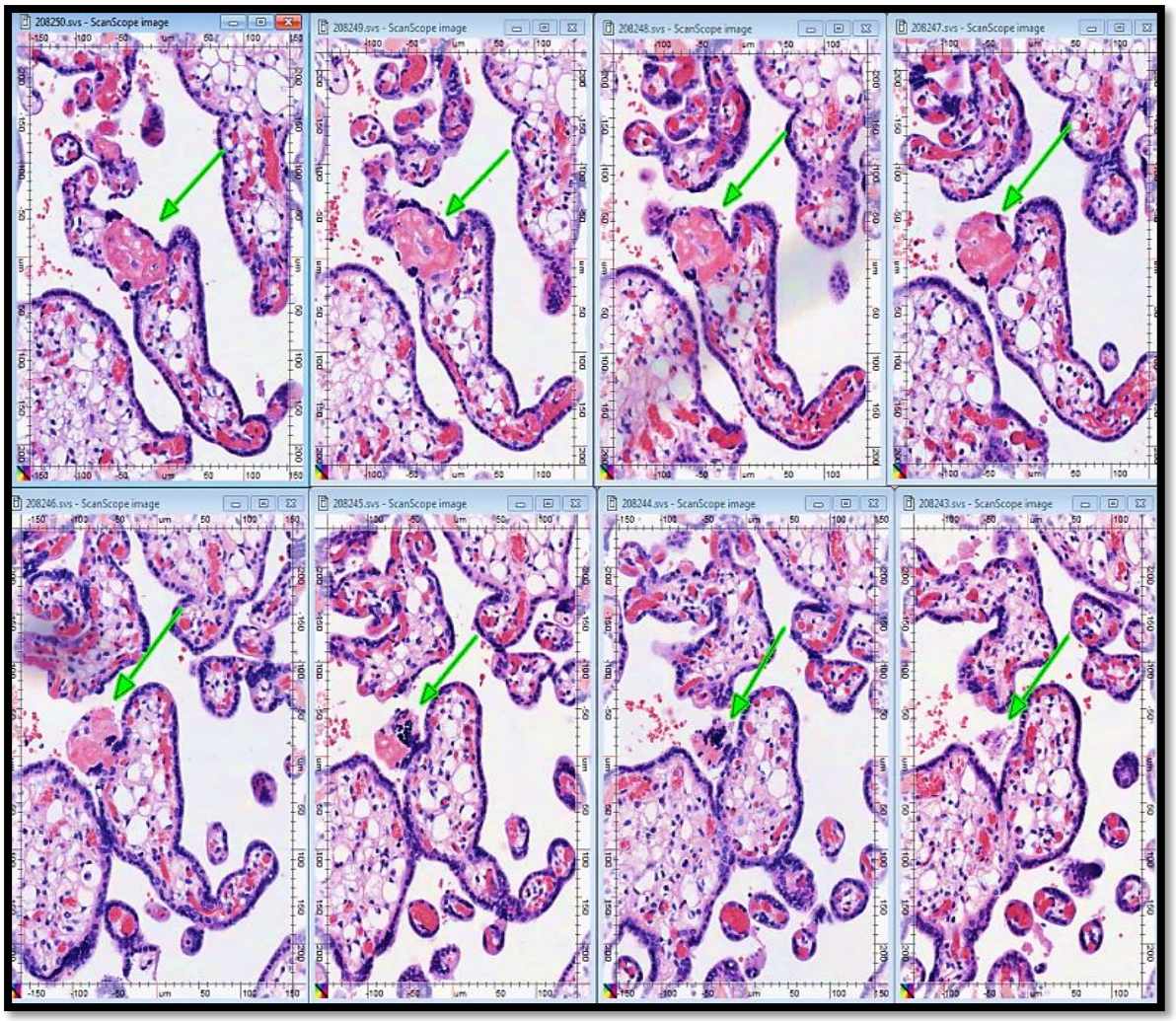

Figure 3-7 A serial sections illustrating intravillous fibrinoid degeneration and syncytial denudation leading to a separation from the terminal villi and shedding into the intervillous space.

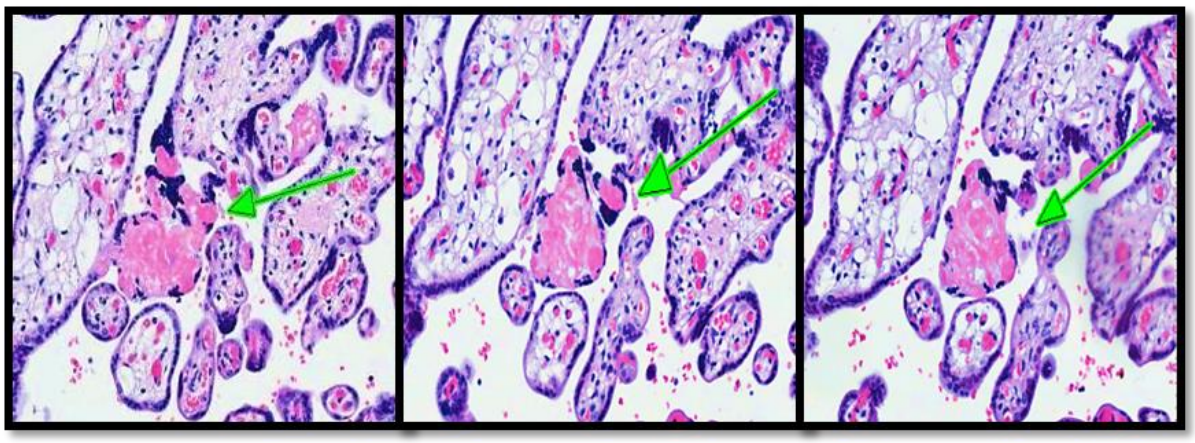

Figure 3-8 Intravillous fibrinoid deposition and syncytial denudation with SNAs detaching from the villi and shedding into the intervillous space.

3.4.2 Novel 3D reconstruction model of the spatial arrangement of SNA around the villi

It was therefore imperative to achieve completeness for the structural classification of the SNAs to explore the 3D and the spatial relationship of SNAs to their surrounding villi and areas of fibrinoid degenerations. Series of digitised scanned placental slides were used to create a volume, which is then reconstructed and isosufaced as shown in Figure 3-9. The reconstructed 3D placental volumes clearly demonstrated that SNAs were scattered through the whole volume with no specific predilections apart from being spatially associated with fibrinoid degenerations (Figure 3-11).

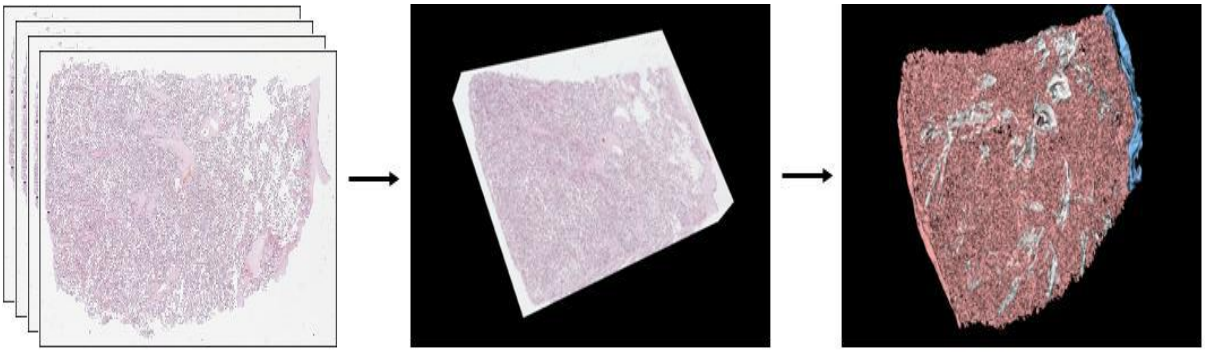

Figure 3-9 3D reconstruction process of the placental histological slides. Series of images, illustrating the way in which slides are used to create a volume (left), which are then reconstructed (middle) and iso-surfaced (right).

The 3D rendition of a given volume allowed the model to be viewed and rotated in all axis/axes and importantly an X, Y and Z slider function can be implemented which allows the user to cut into the tissue volume (Figure 3-10). This function allowed morphological and morphometric changes in different placental structures to be followed throughout the block in all three dimensions/planes.

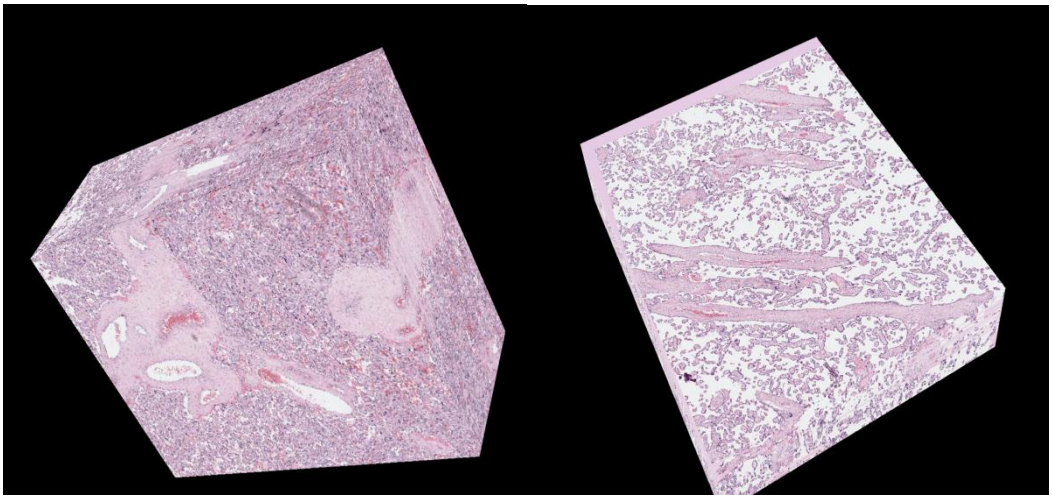

Figure 3-10 Subvolumes are 3D magnified portions of the total placental volumes made from virtual whole serial slides.

3D modelling of the placental microarchitecture proves to be an invaluable tool to assess and characterise placentas from control as well as those from compromised pregnancies. It is able to provide new insights and provoke new hypotheses regarding placental dysfunction appearance and distribution of different elements of placental structure.

Pictures and videos from 3D modelling have provided evidence of villous overcrowding in late onset PET placentas (Figure 3-12), as well as a higher propensity of SNAs surrounding areas of fibrinoid degenerations. It was also evident that the distribution of the fibrinoid degenerations in the placenta from preeclamptic pregnancy was more abundant (Figure 3-12) compared to those found in the control placenta (Figure 3-11), though both were sectioned, volume-rendered and reconstructed from the same number of digitised slides.

Though it is shown to be a promising tool in a proof of concept study, however, the development of its methodology has much more to go in terms of visualising smoother well defined pictures. Moreover, it is designed to reconstruct histopathological scanned slides, thus it is unable to provide a holistic overview of the whole placenta. It is also labour intensive and take considerable amount of time for the whole process to be executed to completion.

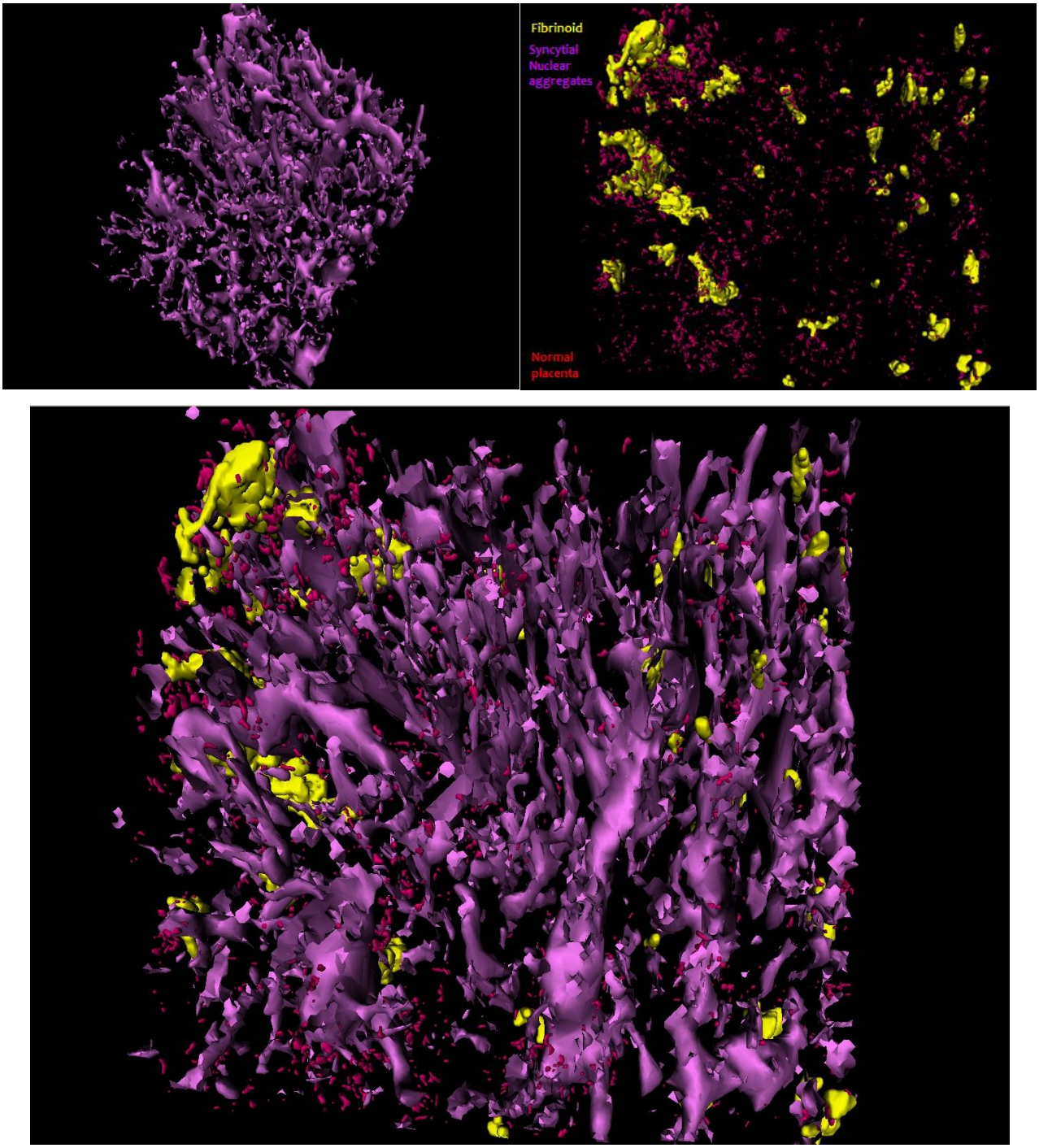

Figure 3-11 Reconstructed 3D volume of intermediate and terminal villi of a placenta from a normal placenta, made from segmenting 48 virtual slides.

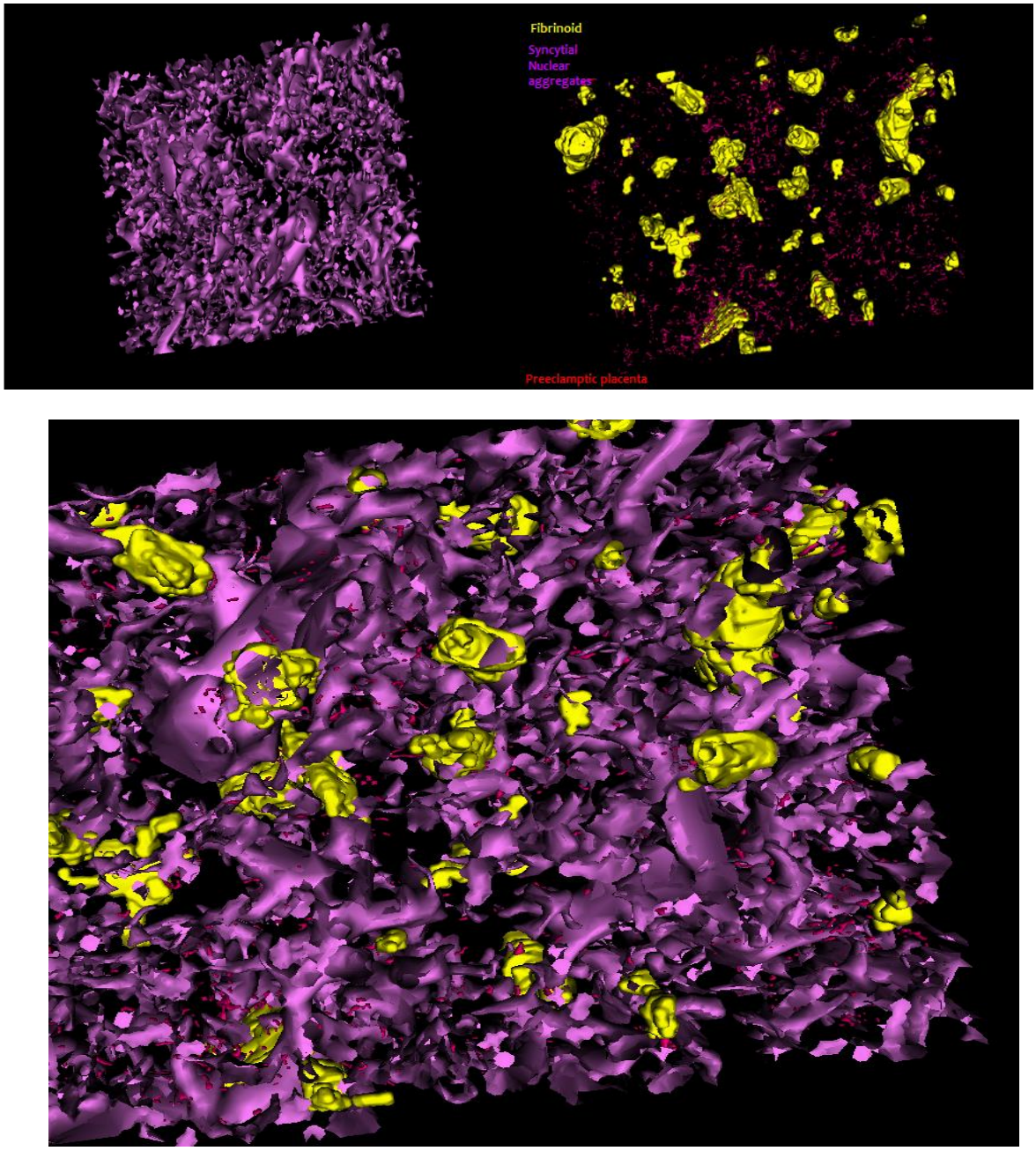

Figure 3-12 Reconstructed 3D volume of villi with areas of fibrinoid degeneration in pale yellow and SNAs in scattered orange dots in a preeclamptic placenta.

3.4.4 Stereology

Placentas from normal pregnancy and those complicated by preeclampsia, IUGR or PET with IUGR were assessed. All of these pregnancy complications can result in delivery at term, but depending on the clinico-pathological severity can lead to delivery prior to 34 weeks gestation. The gestation of delivery may affect placental pathological measurements, or the placental pathology may influence delivery gestation. By classifying each category into those delivered before and after 34 weeks of gestation, an attempt was made to adjust for the gestational age so that any differences would be more a reflection of the disease.

3.4.4.1 Demographics

3.4.4.1.1 Late-onset placental pathologies

No differences in maternal age or gestational age were seen in the participants from the different pathological groups at term (Table 2-1). Both placental volumes and birth weights were significantly decreased in pregnancies with either idiopathic IUGR or IUGR accompanied by term preeclampsia (LOPET/IUGR) compared to full term controls (Table 2-1). Patients with LOPET had no significant differences in placental volumes or birth weights compared to control. Systolic and diastolic blood pressure measurements were significantly higher in LOPET and LOPET/IUGR compared to control (Table 2-1). IUGR, on the other hand, showed no altered blood pressure compared to term controls.

3.4.4.1.2 Early-onset placental pathologies

Similar to patients delivering at term, no differences in maternal age or gestational age at delivery were seen in the participants from the different pathological groups compared to preterm controls (Table 2-2). Placentas from idiopathic early-onset IUGR (EOIUGR) or IUGR accompanied by early-onset preeclampsia (EOPET/IUGR) had lower placental volumes and birth weights compared to preterm controls (Table 2-2). EOPET placentas showed a trend decrease in birth weight compared to preterm control that was not statistically significant. Similarly, mothers with EOPET and EOPET/IUGR pregnancies showed higher systolic and diastolic blood pressure measurements compared to their controls (Table 2-2). All women

delivering as preterm controls or EOIUGR were normotensive throughout gestation and postpartum.

3.4.4.2 Late-onset placental pathologies

Villous volumes were stereologically measured according to the Cavalieri principle (272, 279, 308) where the volume density of villi, at high magnification, in relation to the reference volume (placental volume) was measured by counting points hitting the villi and points hitting the reference volume (259).

3.4.4.2.1 Villous volume measurement

IUGR placenta displayed a significant reduction in total villous volumes compared to term control ($p= 0.004$) with no difference in volume densities. Although, LOPET/IUGR placentas showed an increase in the volume density of the villi ($p=0.01$), their total absolute volume remained less than the term control placenta ($p= 0.04$). On the other hand, LOPET placentas did not display a significant increase in the villous volume density ($p=0.16$) and no difference in total volumes compared to control (Figure 3-13).

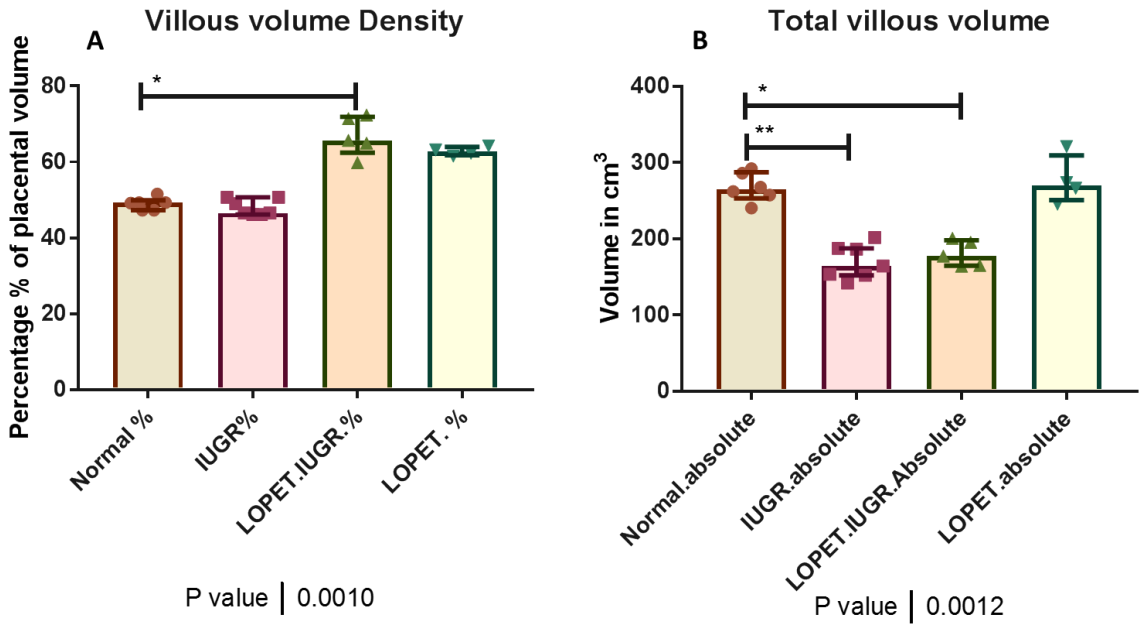

Figure 3-13 Volume densities and total villous volumes in late-onset placental pathologies. (A) Villous volume densities were measured by point counting of the villi in the designated pathologies relative the number of points in the whole placenta, calculated as a percentage % to placental volume. Statistical analysis done by Kruskal-Wallis test with Dunn's post hoc test for multiple comparisons (giving adjusted (adj.) p value). Line is median with Interquartile range (IQR). Results revealed a significantly different villous VD across groups, with higher villous volume densities in LOPET/IUGR placenta compared to term control (*adj. p*=0.01*)*. (B) Total or absolute villus volumes were calculated from the volume densities multiplied by the placental volume in cubic centimetres. Placentas from pregnancies with IUGR and LOPET/IUGR had a significantly lower total villous volumes (adj. *p*=0.004 and = adj. *p*= 0.04 respectively) compared to term controls. IUGR= Term IUGR. LOPET/IUGR= late onset preeclampsia with growth restriction. LOPET=late-onset preeclampsia. * *p*<0.05, ** *p<0.01).*

3.4.4.2.2 Syncytial Nuclear Aggregates (SNAs) volume measurements

Percentages of SNA VD to their respective villous volumes across late onset placental pathologies showed interlinking pathological phenotypes. Placentas from LOPET showed the highest SNA volumes and the lowest in IUGR placentas and LOPET/IUGR placental SNA volumes showing a midway phenotype being higher than IUGR and lower than LOPET (Figure 3-14).

Results showed a significant difference in SNA volumes across placentas of late onset placental dysfunction. LOPET placentas had significantly higher SNA volumes compared to control placenta (*p=0.04*; Figure 3-14). Conversely, IUGR placentas' SNA volumes were significantly lower than control placenta (Figure 3-14). There was no difference between LOPET/IUGR and control placenta regarding the SNA volume densities.

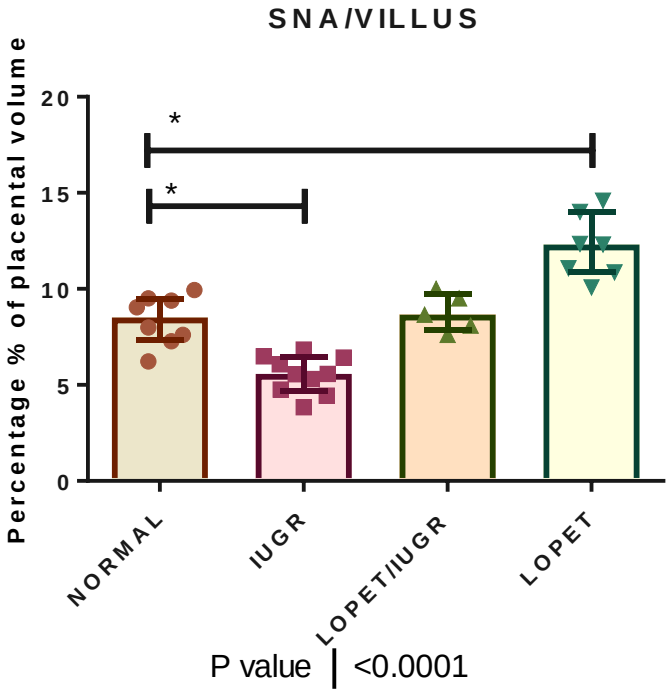

Figure 3-14 Percentages of SNAs volume measurements in relation to villus volumes in late onset placental pathologies. Graph showing percentages of SNA volumes in relation to villous volumes in late onset gestational diseases'; placentas from term control, IUGR, LOPET/IUGR and LOPET. Statistical analysis was done by Kruskal-Wallis test with Dunn's post hoc test for multiple comparisons. Line is median with IQR. SNA volumes were significantly different across groups (*p<0.0001).* LOPET placentas showed significantly higher SNA volumes compared to term control (*p=0.04)*. While IUGR placentas SNA volumes were significantly lower than term control (*p=0.04)*. IUGR=Term IUGR. LOPET/IUGR= Late onset preeclampsia with growth restriction. LOPET=late-onset preeclampsia. * p<0.05.

3.4.4.2.3 Fetal and maternal-side SNA volumes

On comparing the placental fetal/maternal side SNA volumes across all categories, the fetal side of late onset placental dysfunction revealed a significant differences across groups. LOPET placenta showed a higher SNA volumes compared to IUGR placentas (Figure 3-15A). Fetal side IUGR placentas showed a trend lower SNA volumes compared to term control placentas.

In the maternal side, similar trends appeared with much more accentuated differences between groups with normotensive IUGR placentas showed a significant maternal side decrease in SNA volumes compared to control. On the other hand, LOPET placentas showed a consistently higher SNA volumes compared to normotensive IUGR placentas similar to that observed on the fetal side (Figure 3-15B).

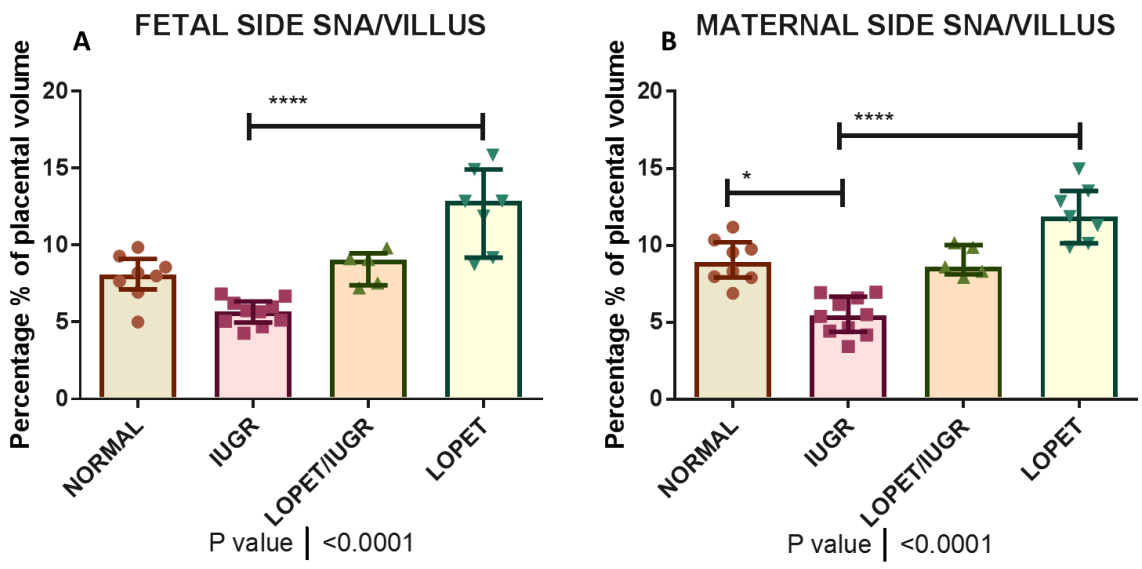

Figure 3-15 Percentages of SNAs volume measurements in relation to villus volumes in fetal (A) and maternal (B) sides in term placentas from Normal, Idiopathic IUGR, LOPET/IUGR and LOPET pregnancies. Statistical analysis was done by Kruskal-Wallis test with Dunn's post hoc test for multiple comparisons. Line is median with IQR. Significant difference were found across groups in both fetal and maternal side of the placenta. IUGR placentas SNA volumes were significantly lower than term control in the maternal side of the placenta (p=0.037) with a trend reduction in the fetal side. IUGR=Term IUGR. LOPET/IUGR= Late onset preeclampsia with growth restriction. LOPET=late-onset preeclampsia. * p<0.05, ** p<0.01, *** p<0.001, ****p<0.0001).

Regarding the proportionate distribution of SNAs in relation to the villus volumes in each category, there were no significant SNA volume differences between fetal and maternal sides in any of late onset placental groups (Figure 3-16).

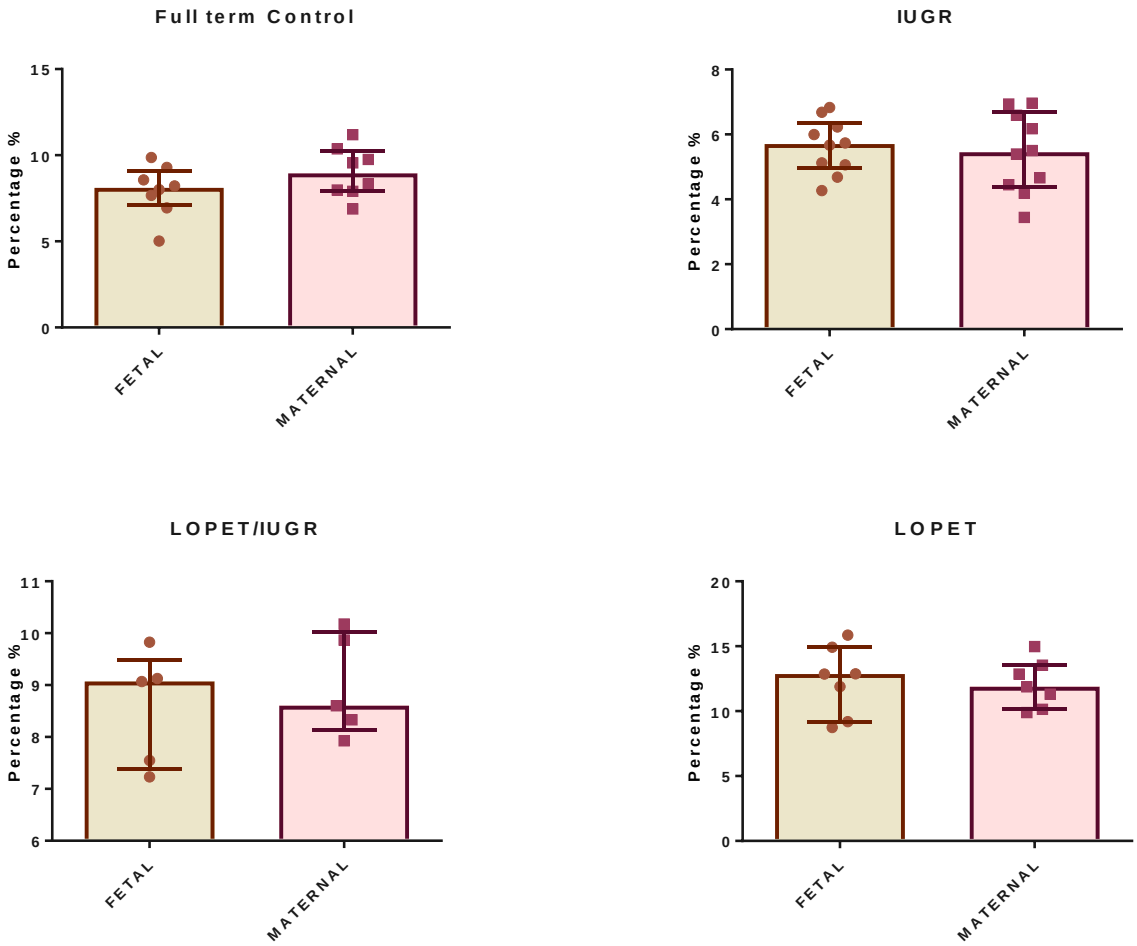

Figure 3-16 Fetal and Maternal side relative distribution of SNA volumes in Control, IUGR, LOPET/IUGR and LOPET placentas. It showed no significant zone predilection of SNAs volumes in any of the placental groups. IUGR=Term IUGR. LOPET/IUGR= Late onset preeclampsia with growth restriction. LOPET=late-onset preeclampsia. Line is median with IQR.

3.4.4.2.4 Trophoblasts volume measurements

Trophoblast volumes in late onset placenta pathologies showed significant differences across groups. IUGR placentas showed a significantly lower trophoblast to villous volume percentages compared to term control (Figure 3-17). LOPET/IUGR placental trophoblast volumes showed also a trend decrease compared to term control placentas (adj. *p*= 0.10). There was no difference between LOPET and control placenta regarding trophoblast volume densities.

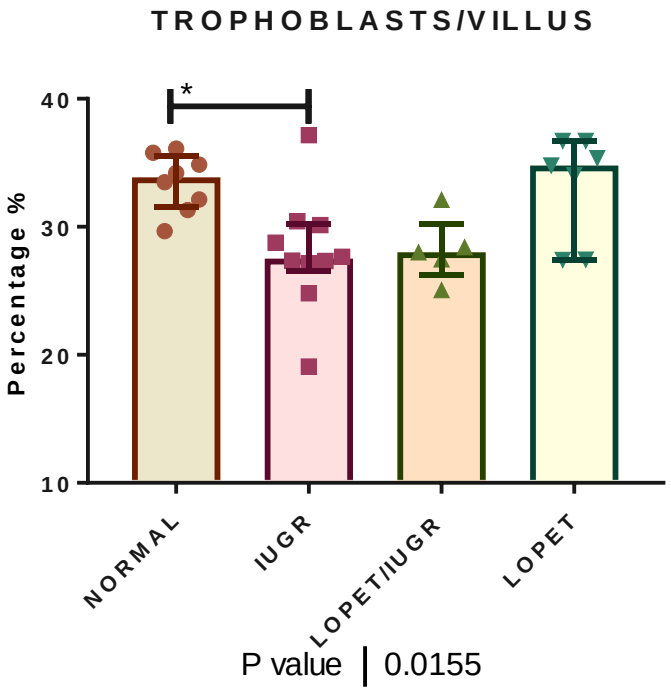

Figure 3-17 Percentage of trophoblast volumes in relation to villous volumes in in late-onset placental pathologies from term control, IUGR, LOPET/IUGR and LOPET. Statistical analysis was done by Kruskal-Wallis test with Dunn's post hoc test for multiple comparisons. Line is median with IQR. * ($p<0.05$). Trophoblast volumes showed significant differences across late onset placental groups (*p=0.01)*. Placentas from idiopathic normotensive IUGR pregnancies showed a consistently lower trophoblast volumes compared to placentas from term control pregnancies (*adj. p*= 0.02). IUGR=Term IUGR. LOPET/IUGR= Late onset preeclampsia with growth restriction. LOPET=late-onset preeclampsia.

3.4.4.2.5 Fetal and maternal-side trophoblast volumes

The total reduction in the IUGR trophoblast volumes compared to term control can be explained by the significant reduction in trophoblast volumes on the maternal side of their placentas (Figure 3-18B). Maternal side trophoblast volumes showed a significant difference across groups on the maternal side of the placenta. On the other hand, the fetal side trophoblast to villous volumes, showed no significant differences across the different groups (Figure 3-18A).

Regarding the proportionate distribution of trophoblast volumes in each category, there were no significant differences across fetal and maternal sides in any of the placental types (Figure 3-19). That is to say, there were no significant differences

between fetal and maternal side trophoblast volumes in any of the late onset placental pathologies.

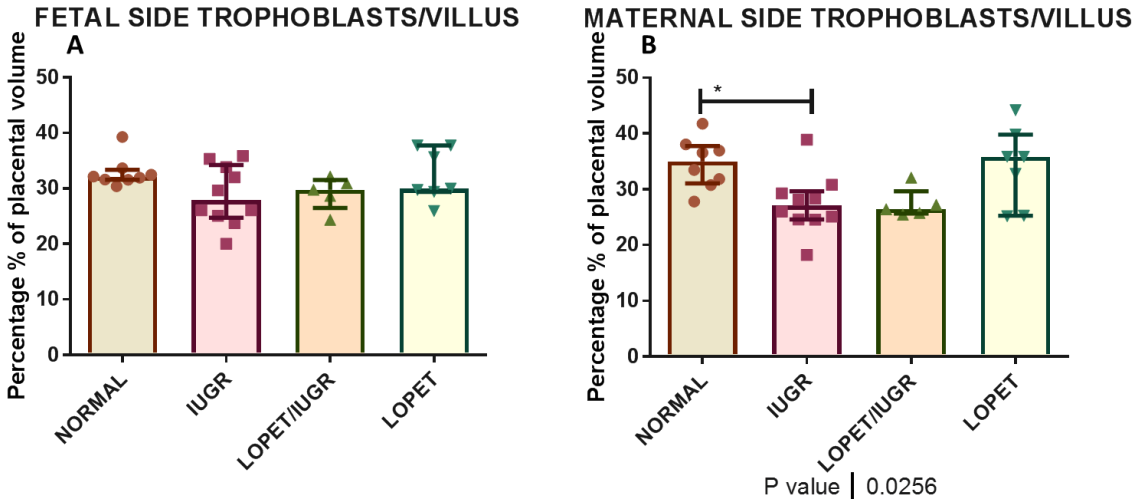

Figure 3-18 Percentages of trophoblast volume measurements in relation to villus volumes in fetal (A) and maternal (B) sides in late onset placental pathologies placentas from Normal, Idiopathic IUGR, LOPET/IUGR and LOPET pregnancies. Statistical analysis was done by Kruskal-Wallis test with Dunn's post hoc test for multiple comparisons. Line is median with IQR. * ($p<0.05$). (A) No differences were observed on the fetal side trophoblast volumes between groups. (B) Maternal side trophoblast volumes showed a significant difference across groups ($p=0.02$). Only the maternal side of the IUGR placentas showed a significant reduction in trophoblasts compared to term control (adj. $p= 0.02$). IUGR=Term IUGR. LOPET/IUGR= Late onset preeclampsia with growth restriction. LOPET=late-onset preeclampsia.

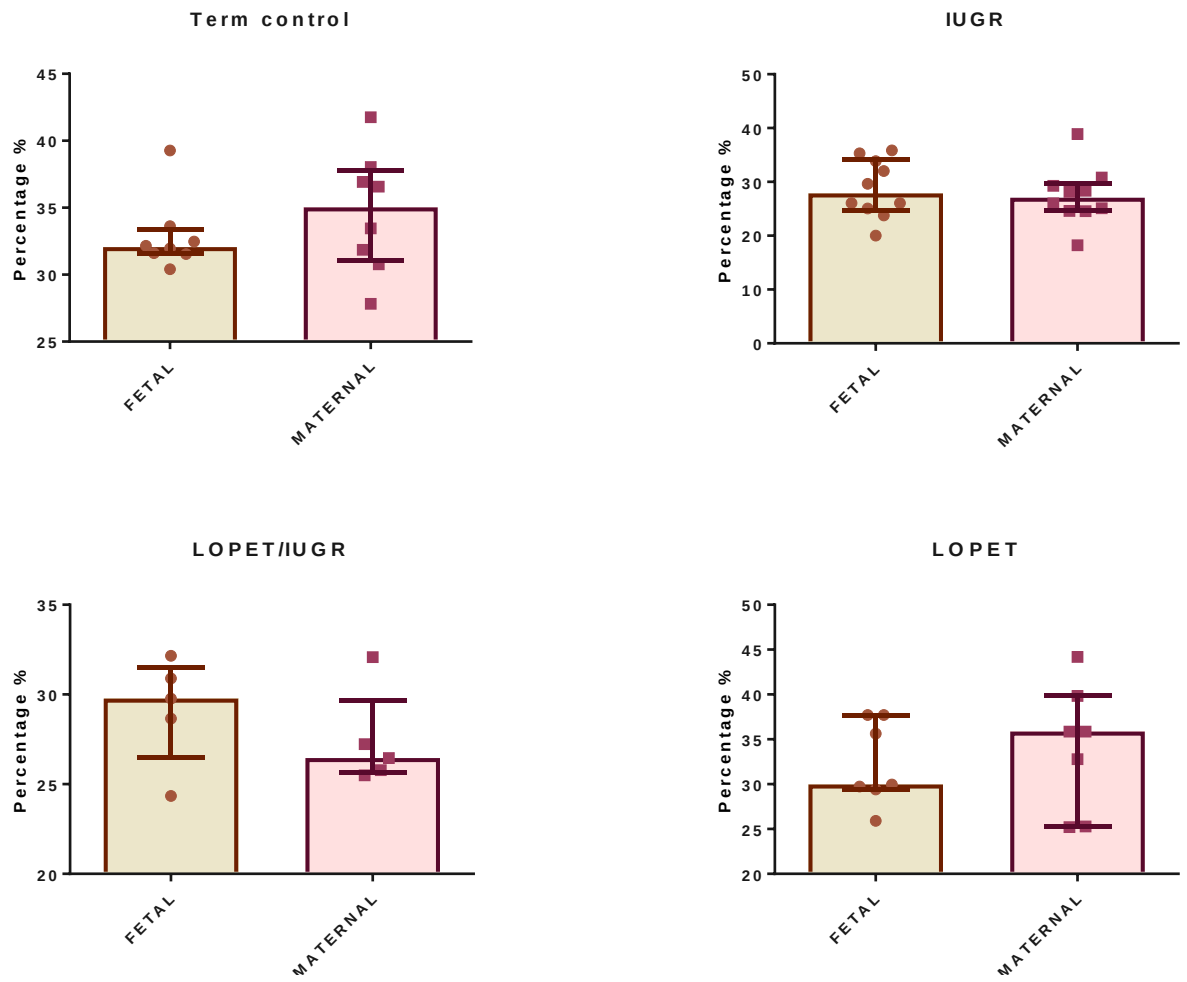

Figure 3-19 Fetal and Maternal side relative distribution of trophoblast volumes in control, IUGR, LOPET/IUGR and LOPET placentas. It showed no significant zone predilection of trophoblast volumes in any of the placental groups. IUGR=Term IUGR. LOPET/IUGR= Late onset preeclampsia with growth restriction. LOPET=late-onset preeclampsia. Line is median with IQR.

3.4.4.2.6 Placental capillary volume measurements

Placentas from late onset placental pathologies showed a significant difference in placental capillary volumes across groups (*p=0.004,* Figure 3-20). Results also showed overlapping pathological phenotypes regarding capillary volumes, with term IUGR placentas having the highest capillary volume percentages (Figure 3-21) compared to all other categories with the lowest being the LOPET placenta (p= 0.001, Figure 3-20). LOPET/IUGR placental capillary volumes showed a midway phenotype being lower than IUGR and higher than LOPET.

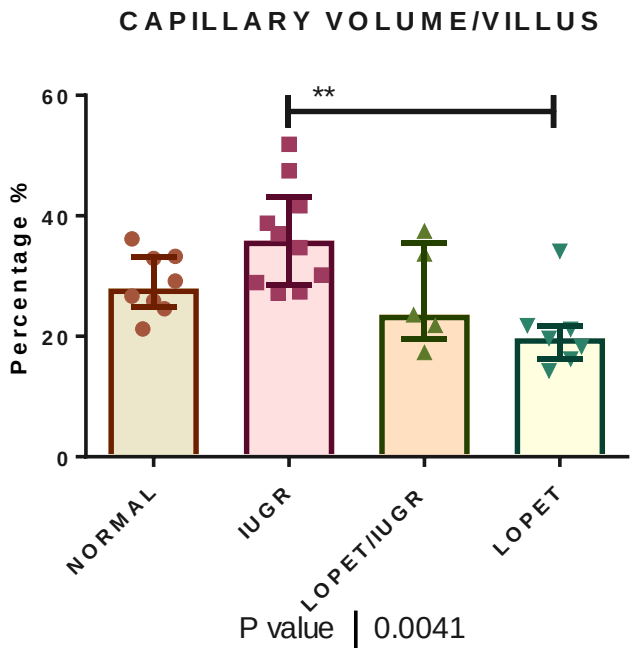

Figure 3-20 Percentage of placental capillary to villous volumes in late onset gestational disease's placentas across Normal, IUGR, LOPET/IUGR and LOPET. Statistical analysis was done by Kruskal-Wallis test with Dunn's post hoc test for multiple comparisons. Line is median with IQR. ** (adj. p<0.01). Placentas from late onset placental pathologies showed a significant difference in placental capillary volumes across groups (*p=0.004).* Placentas from normotensive IUGR pregnancies showed a consistently higher capillary volumes compared to LOPET placentas (adj. p= 0.001). IUGR=Term IUGR. LOPET/IUGR= Late onset preeclampsia with growth restriction. LOPET=late-onset preeclampsia. Bars represent means and SD.

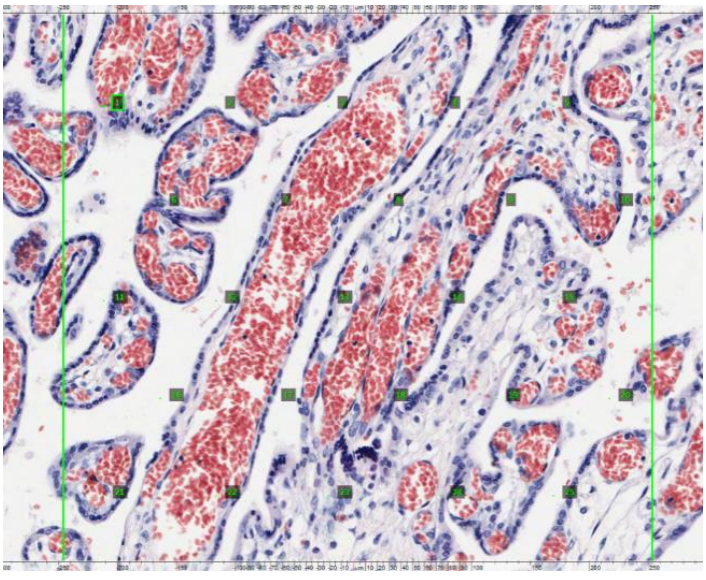

Figure 3-21 A representative image of placental capillary vessels in normotensive full-term IUGR placenta. A grid of random points were assigned in each field of vision. Random points lying on placental capillaries (red in H&E) were counted and volumes measured.

3.4.4.2.7 Fetal and maternal-side capillary volumes

The fetal and the maternal side distribution of capillary volumes showed a significant difference across all groups with a step ladder appearance with IUGR placentas being the highest and LOPET being the lowest in the fetal side (31.1 % vs 19.3 %, adj. p=0.006, Figure 3-22A) and in the maternal side (40.6 % vs 22.15 %, adj. p=0.003, Figure 3-22B).

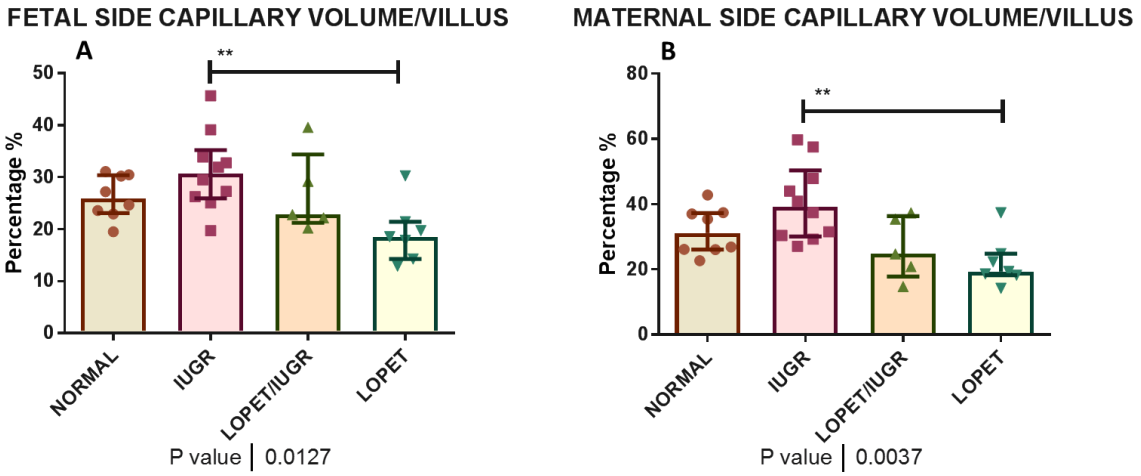

Figure 3-22 Capillary to villous volumes' percentages in (A) fetal and (B) maternal side of placentas in late onset gestational diseases' placentas from Normal, Idiopathic IUGR, LOPET/IUGR and LOPET pregnancies. Statistical analysis was done by Kruskal-Wallis test with Dunn's post hoc test for multiple comparisons showing a persistent higher capillary volumes in term IUGR placentas compared to LOPET in the fetal (A) and maternal (B) sides. IUGR=Term IUGR. LOPET/IUGR= Late onset preeclampsia with growth restriction. LOPET=late-onset preeclampsia. Line is median with IQR, ** (p<0.01).

Late onset placental pathologies did not show a significant zonal (fetal/maternal side) distribution of placental capillaries in LOPET/IUGR and LOPET placentas. On the other hand, fetal side placental capillary volume percentages from term IUGR and term control placentas were significantly lower than the maternal side (Figure 3-23A & B).

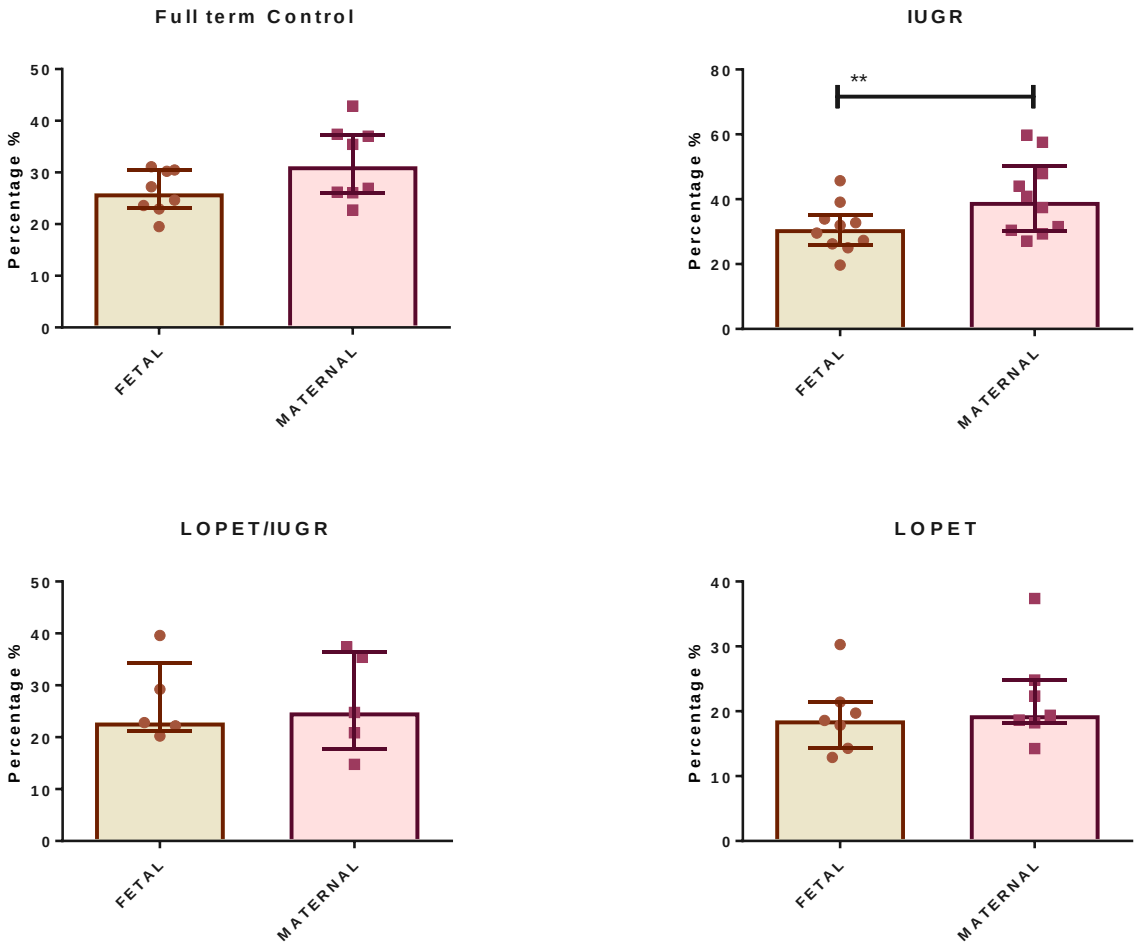

Figure 3-23 Fetal and Maternal side relative distribution of capillary volumes in term control, IUGR, LOPET/IUGR and LOPET placentas. It shows no significant fetal or maternal side predilection of capillary volumes in LOPET and LOPET/IUGR placentas apart from a significantly lower fetal side capillary volumes compared to maternal side in IUGR placentas (Wilcoxon signed rank test, p=0.003) and in term control placenta (Wilcoxon signed rank test, p=0.01). Line represent median and IQR. *(p<0.05), ** (p<0.01).

3.4.4.3 Early-onset placental pathologies

3.4.4.3.1 Villus volume measurement

Villous volume densities in early onset placental pathologies showed a significant difference across groups (p=0.002, Figure 3-24A). Similarly, total absolute volumes were different across groups (p=0.007, Figure 3-24B). EOPET/IUGR placentas were the only placental group to display a significant reduction in both volume densities and total volumes of the villi compared to their preterm controls (p=0.001, p=0.002 respectively, Figure 3-24).

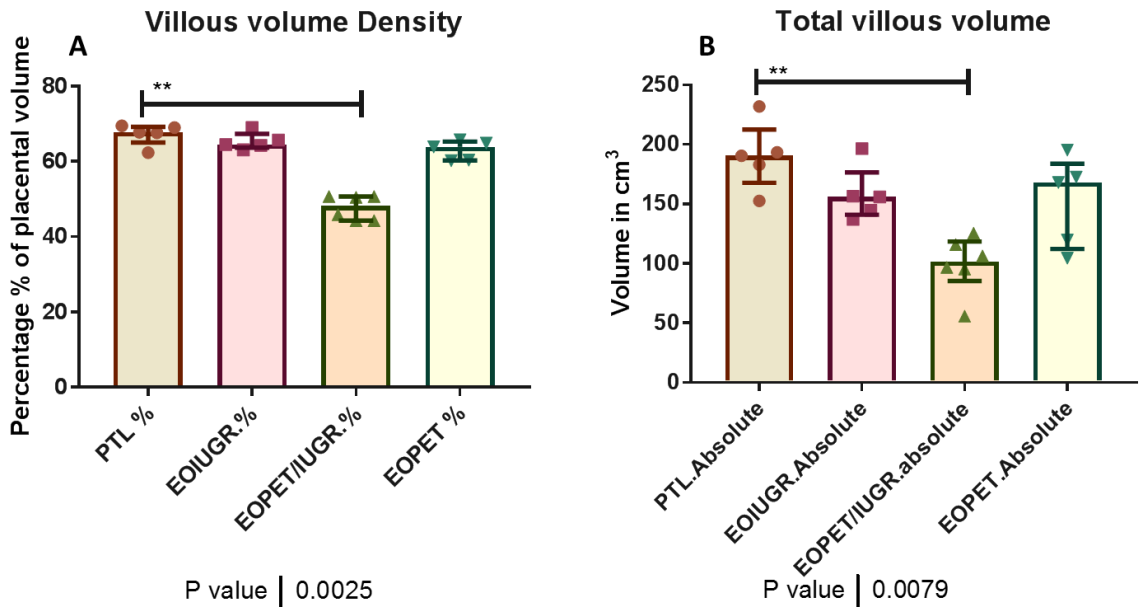

Figure 3-24 Volume densities and total villous volumes in early onset placental pathologies. (A) Villous volume densities were measured by point counting of the villi in the designated pathologies relative the number of points in the whole placenta, calculated as a percentage % to placental volume. Kruskal-Wallis test was used to analyse differences across groups (*p*= 0.002 and *p=0.007 respectively*), Dunn's post-hoc multiple comparisons test revealed a significantly lower villus volumes in EOPET/IUGR placenta compared to preterm control (adj. *p=0.001)*. (B) Total or absolute villus volumes were calculated from the volume densities multiplied by the placental volume in cubic centimetres. Placentas from pregnancies with EOPET/IUGR had a significantly lower total villous volumes (adj. *p*=0.002) compared to preterm controls. PTL= preterm control. EOIUGR= early-onset IUGR. EOPET/IUGR= early onset preeclampsia with growth restriction. EOPET=Early-onset preeclampsia. Lines represent medians and IQR. ** *p<0.01.*

3.4.4.3.2 Syncytial Nuclear Aggregates (SNAs) volume measurement

Early onset placental dysfunction demonstrated a significant difference in SNA volumes across groups (*p*=0.005, Figure 3-25). Similar to results found in the late onset gestational diseases, EOPET placentas showed a significantly higher SNA volumes compared to preterm control (PTL) (11.8 % vs 5.7 %, adj. *p*=0.002; Figure 3-25).

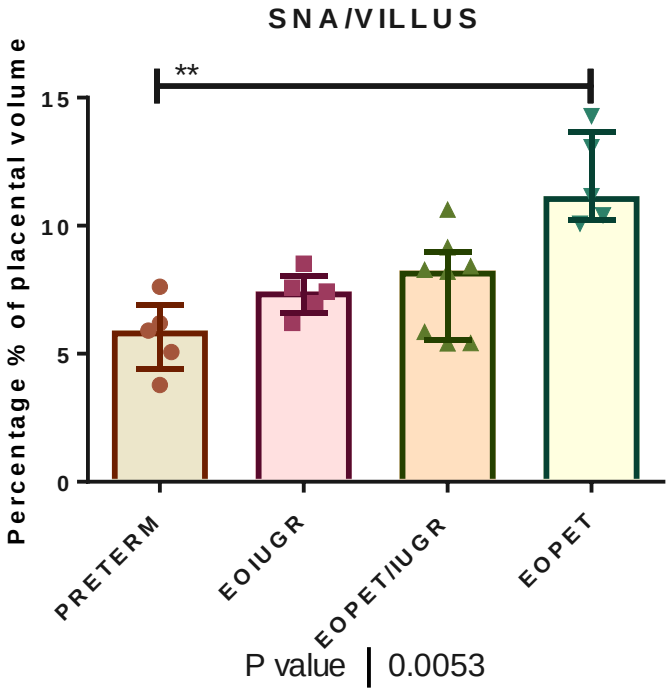

Figure 3-25 Percentages of SNAs volume measurements in relation to villus volumes in early onset placental pathologies. Y axis showing percentages of SNA volumes in relation to villous volumes in early onset gestational diseases'; placentas from preterm control (PTL), EOIUGR, EOPET/IUGR and EOPET. Statistical analysis was done by Kruskal-Wallis test with Dunn's post hoc test for multiple comparisons. Line is median with IQR. ** ($p<0.01$). Early onset placental dysfunction demonstrated a significant difference in SNA volumes across groups ($p=0.005$). EOPET placentas had significantly higher SNA volumes compared to PTC (adj. p=0.002).

3.4.4.3.3 Fetal and maternal-side SNA volumes

In order to test whether the overall increase in the SNA volumes were distributed evenly in both fetal and maternal sides of the placenta, fetal and maternal side SNA volumes were compared across the early onset disease categories showing significant differences across groups (p=0.01 and p=0.002 respectively, Figure 3-26).

EOPET placentas showed higher fetal-side SNA volumes compared to preterm control placentas (11.6 % vs 6.3 %, adj. p=0.004, Figure 3-26A). In the maternal side, similar trends appeared with significant differences between SNA volumes in EOPET placentas compared to preterm control (11.9 % vs 5.2%, adj. p=0.0006, Figure 3-26B)

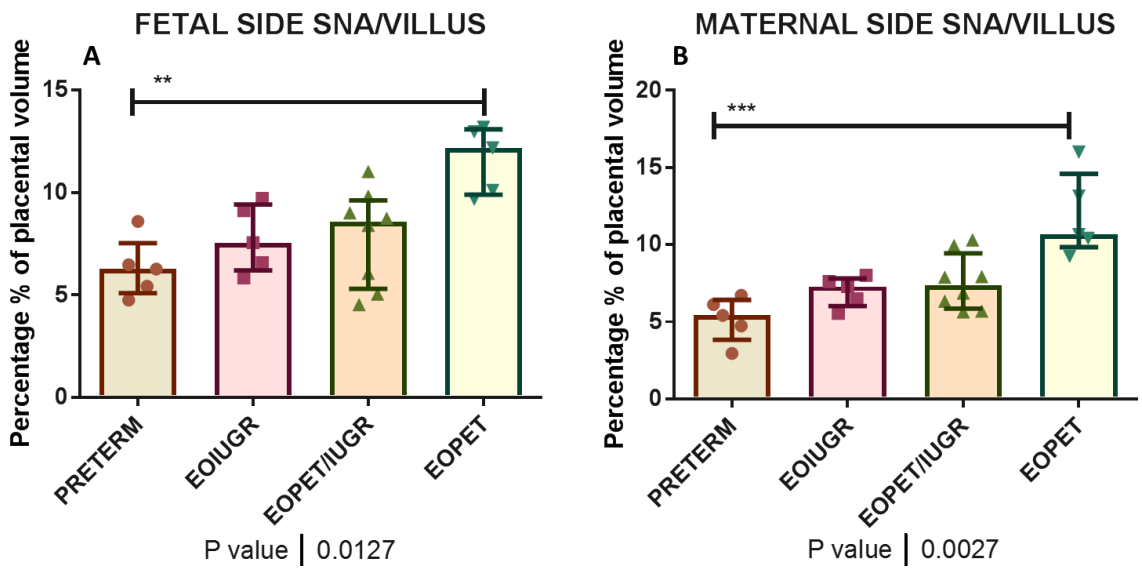

Figure 3-26 Percentages of SNAs volume measurements in relation to villus volumes in fetal (A) and maternal (B) sides in early onset placental pathologies. (A) Percentage of SNA to villous volumes' in fetal side of placentas in early onset gestational diseases' placentas from Preterm control, EOIUGR, EOPET/IUGR and EOPET pregnancies. Statistical analysis was done by Kruskal-Wallis test with Dunn's post hoc test for multiple comparisons. Line is median with IQR. ** ($p<0.01$), *** ($p<0.001$). EOPET placenta showed a higher fetal-side SNA volumes compared to preterm control placentas with adjusted *p* value of 0.004. (B) Percentage of SNA to villous volumes' in maternal side of placentas in early onset gestational diseases' placentas showed a higher SNA volumes compared to PTL, with adjusted *p* value of 0.0006. The fetal and maternal side of EOPET placenta showed a significantly higher SNA volumes compared to the other categories ($p=0.01$ and $p=o.002$ respectively). PTL= preterm control, EOIUGR= early onset idiopathic IUGR, EOPET/IUGR= Early-onset preeclampsia with growth restriction. EOPET= Early-onset preeclampsia.

Similarly, there were no differences between fetal and maternal sides in any of the early onset gestational diseases' placentas regarding the proportionate distribution of SNAs in relation to the villus volumes (Figure 3-27)

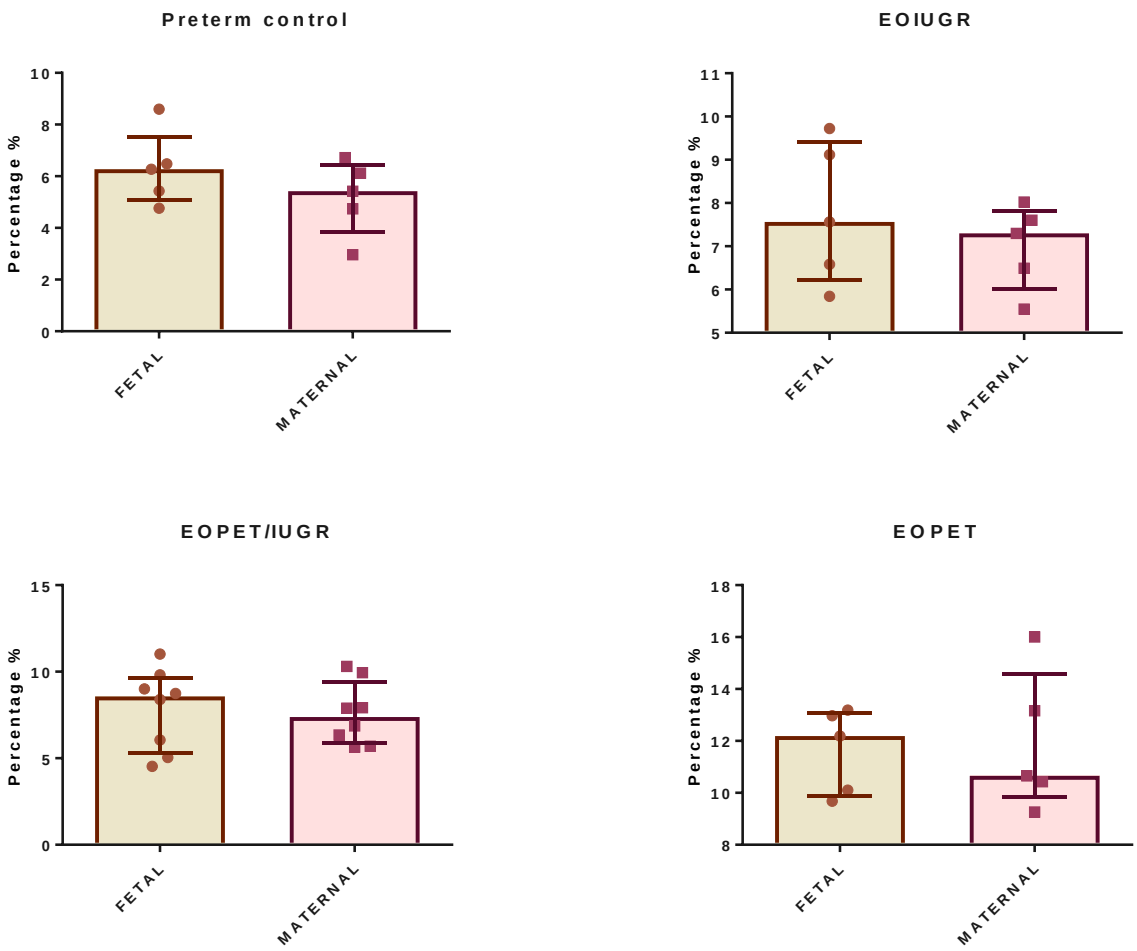

Figure 3-27 Fetal and Maternal side relative distribution of SNA volumes in PTL, EOIUGR, EOPET/IUGR and EOPET. The figure shows no significant zone predilection of SNAs fetal or maternal side distribution in any of the groups. Line is median with IQR.

3.4.4.3.4 Trophoblasts volume measurements

Early onset placental dysfunction demonstrated a significant difference in trophoblast volumes across groups (p=0.003, Figure 3-28). In early onset placental pathologies, placentas from EOIUGR pregnancies demonstrated a higher percentage of trophoblast to villous volumes compared to preterm control (29.9 % vs 21.2 %, adj. p=0.001, Figure 3-28). There was also a persistent reduction in the volumes of trophoblasts in preterm control compared to their volumes in EOPET and EOPET/IUGR placentas (adj. p= 0.03 and 0.04 respectively).

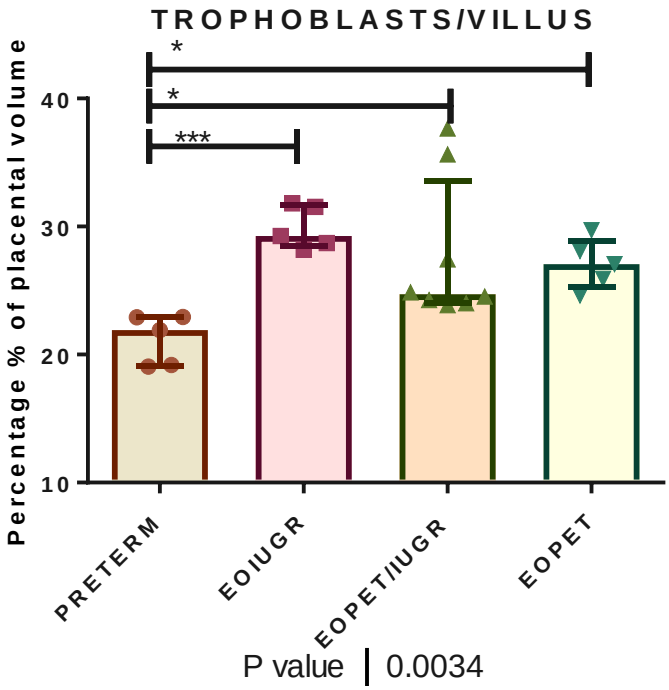

Figure 3-28 Percentage of trophoblast volumes in relation to villous volumes in in early onset placental pathologies from preterm control, EOIUGR, EOPET/IUGR and EOPET. Statistical analysis was done by Kruskal-Wallis test with Dunn's post hoc test for multiple comparisons, * ($p<0.05$), *** ($p<0.001$). EOIUGR placentas had significantly higher trophoblast volumes compared to preterm control (29.91 % vs 21.20 %, adj. p=0.001), while EOPET and EOPET/IUGR trophoblast volumes showed an increase compared to preterm controls (adj. p= 0.03 and 0.04 respectively). Line is median with IQR.

3.4.4.3.5 Fetal and maternal-side trophoblast volumes

Both fetal and maternal side placenta trophoblast volumes in early onset gestational diseases showed significant differences across groups (p=0.02 and p= 0.005 respectively). Fetal side EOIUGR placentas showed significantly higher volumes of trophoblasts compared to preterm controls (30.6 % vs 22.5 %, adj. p=0.009). In the maternal side, EOIUGR placentas showed raised trophoblast volumes compared to preterm controls (adj. p= 0.003) while EOPET/IUGR placentas had a consistently higher maternal side trophoblast volumes compared to preterm controls (adj. p= 0.007, Figure 3-29).

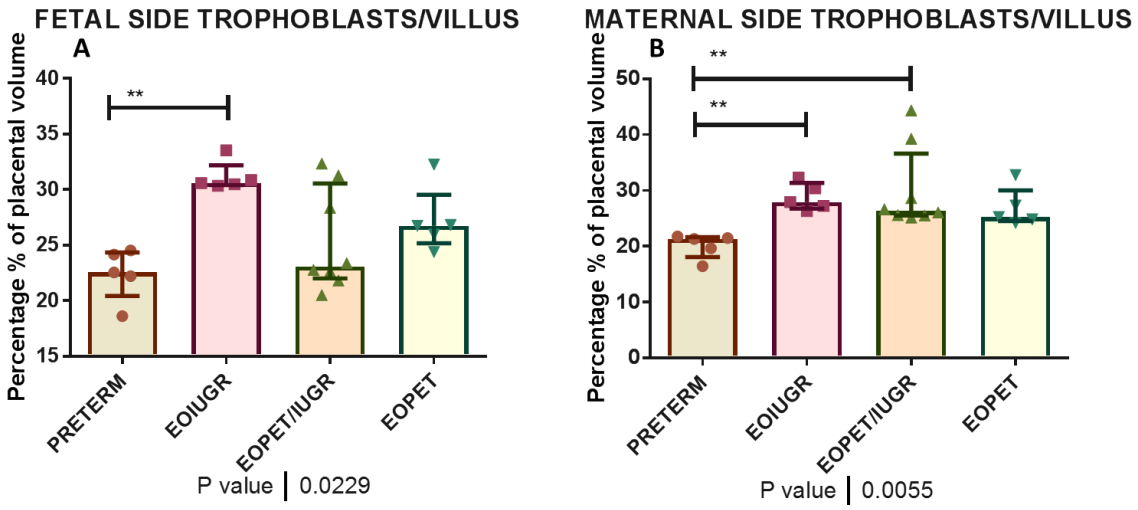

Figure 3-29 Percentages of trophoblast volume measurements in relation to villus volumes in fetal (A) and maternal (B) sides in early onset placental pathologies. (A) Percentage of trophoblast to villous volumes' in fetal side of placentas in early onset gestational diseases' placentas from PTC, EOIUGR, EOPET/IUGR and EOPET pregnancies. Statistical analysis was done by Kruskal-Wallis test with Dunn's post hoc test for multiple comparisons. EOIUGR placentas showed a significant rise in fetal side trophoblast proliferation (Adj. *p*= 0.009) and an increase (adj. *p*= 0.003) in the maternal side compared to preterm control. EOPET/IUGR showed a consistent increase in the maternal side trophoblast volumes (adj. *p*=0.007) compared to preterm control. Where * (p<0.05), ** (p<0.01), *** (P<0.001) and **** (p<0.0001). Lines represent medians and IQR. PTL= preterm control, EOIUGR= early onset idiopathic IUGR, EOPET/IUGR= Early-onset preeclampsia with growth restriction. EOPET= Early-onset preeclampsia.

As regard the relative distribution of the trophoblast volumes, within fetal (sub-chorionic) and maternal side (basal), inside each group, EOPET/IUGR had a significantly lower fetal side trophoblast volume compared to its maternal side volumes (*p*=0.01, Figure 3-30). Otherwise there was no significant zone predilection in any of the other early onset placental groups.

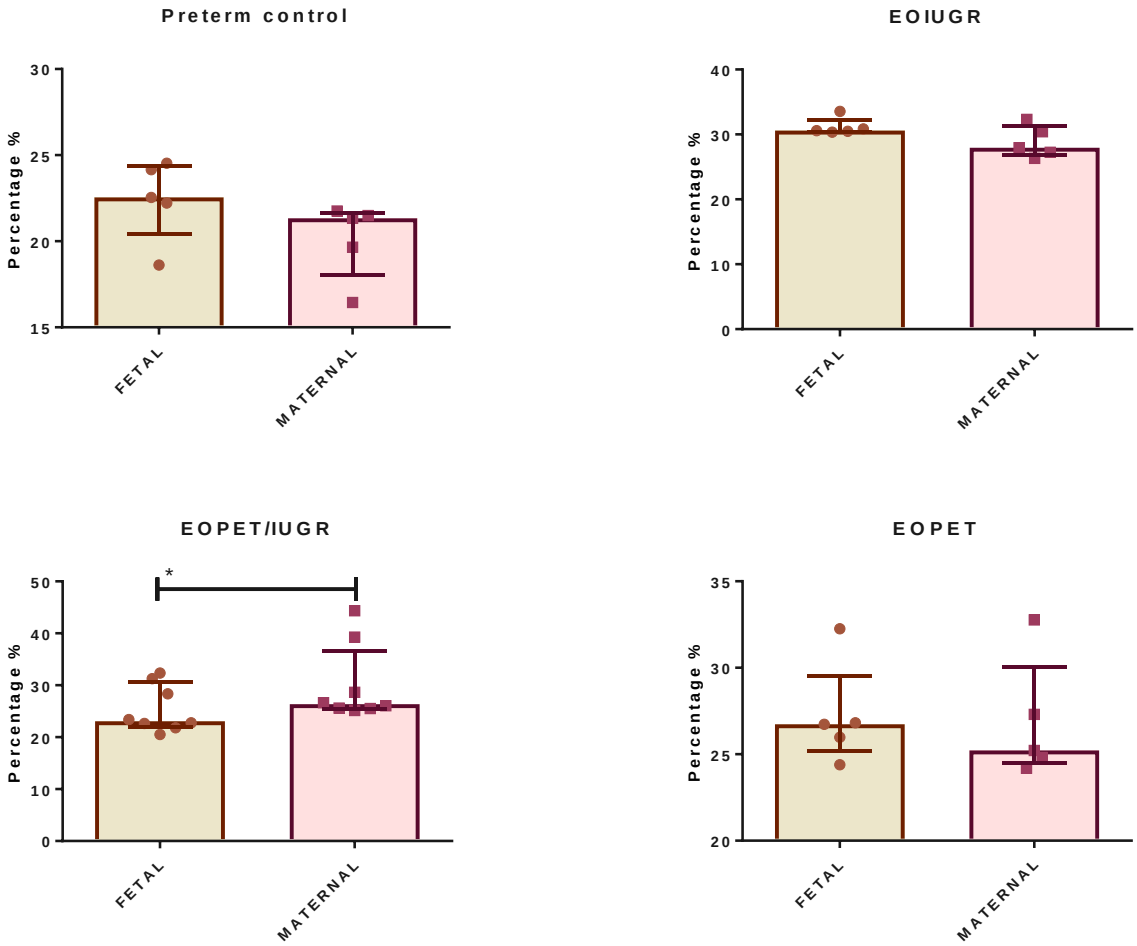

Figure 3-30 Fetal and Maternal side relative distribution of Trophoblast volumes in PTC, EOIUGR, EOPET/IUGR and EOPET placentas. It shows no significant zone predilection except in placentas from EOPET/IUGR that showed a lower fetal side trophoblast volumes compared to the maternal side (Wilcoxon signed rank test, *p*=0.01). Bars represent median and IQR. * (p<0.05).

3.4.4.3.6 Placental capillary volume measurement

In early onset placental pathologies, placentas from EOPET pregnancies demonstrated the lowest capillary to villous volume percentages compared to the other groups. It showed a trend lower volumes compared to EOPET/IUGR (20.5 % vs 29.4 %, adj. p= 0.07, Figure 3-31).

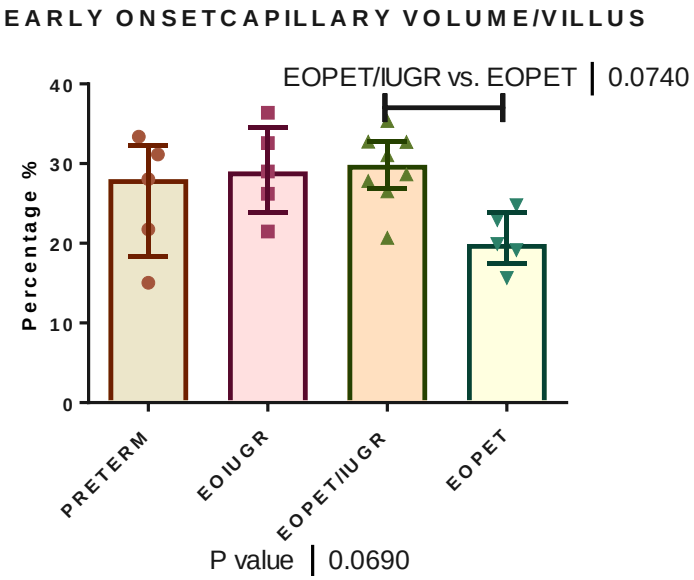

Figure 3-31 Percentages of capillary to villous volumes in early onset placental pathology from preterm control, EOIUGR, EOPET/IUGR and EOPET. Statistical analysis was done by Kruskal-Wallis test with Dunn's post hoc test for multiple comparisons, * ($p<0.05$), *** ($p<0.001$), * ($p<0.05$). EOPET placentas showed a trend lower capillary volumes compared to EOPET/IUGR (adj. p= 0.07). Lines represent median and IQR.

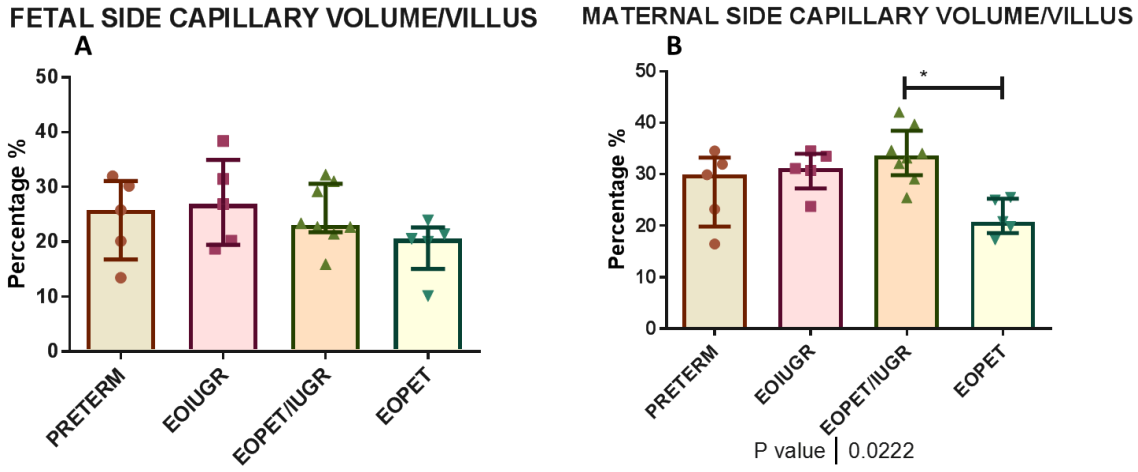

Figure 3-32 percentages of capillary to villous volumes in fetal (A) and maternal (B) side of placentas in early onset gestational diseases' placentas from Preterm control, EOIUGR, EOPET/IUGR and EOPET pregnancies. Statistical analysis was done by Kruskal-Wallis test with Dunn's post hoc test for multiple comparisons. Line is median with IQR. ** ($p<0.01$). (A) Fetal side capillary volumes did not show any significant difference across early onset placental dysfunction groups (B) Maternal side placental capillary volumes showed a significant difference across groups ($p=0.02$). EOPET placenta showed a reduction in capillary volumes compared to EOPET/IUGR placentas (adj. p= 0.01). PTL= preterm control, EOIUGR= early onset idiopathic IUGR, EOPET/IUGR= Early-onset preeclampsia with growth restriction. EOPET= Early-onset preeclampsia.

3.4.4.3.7 Fetal and maternal-side capillary volumes

On comparing the capillary volumes of the fetal sides in early onset gestational disease placentas, although there were no significant differences between groups, but a pattern of reducing percentages was evident from growth restriction to preeclampsia passing by preeclampsia with growth restriction. This pattern was similar to capillary volumes in late onset pathologies (Figure 3-32A, Figure 3-22). On the other hand, maternal side capillary volumes were significantly higher in EOPET/IUGR placentas compared to EOPET placentas (33.8 % vs 21.7%, *adj. p*= 0.01, Figure 3-32B).

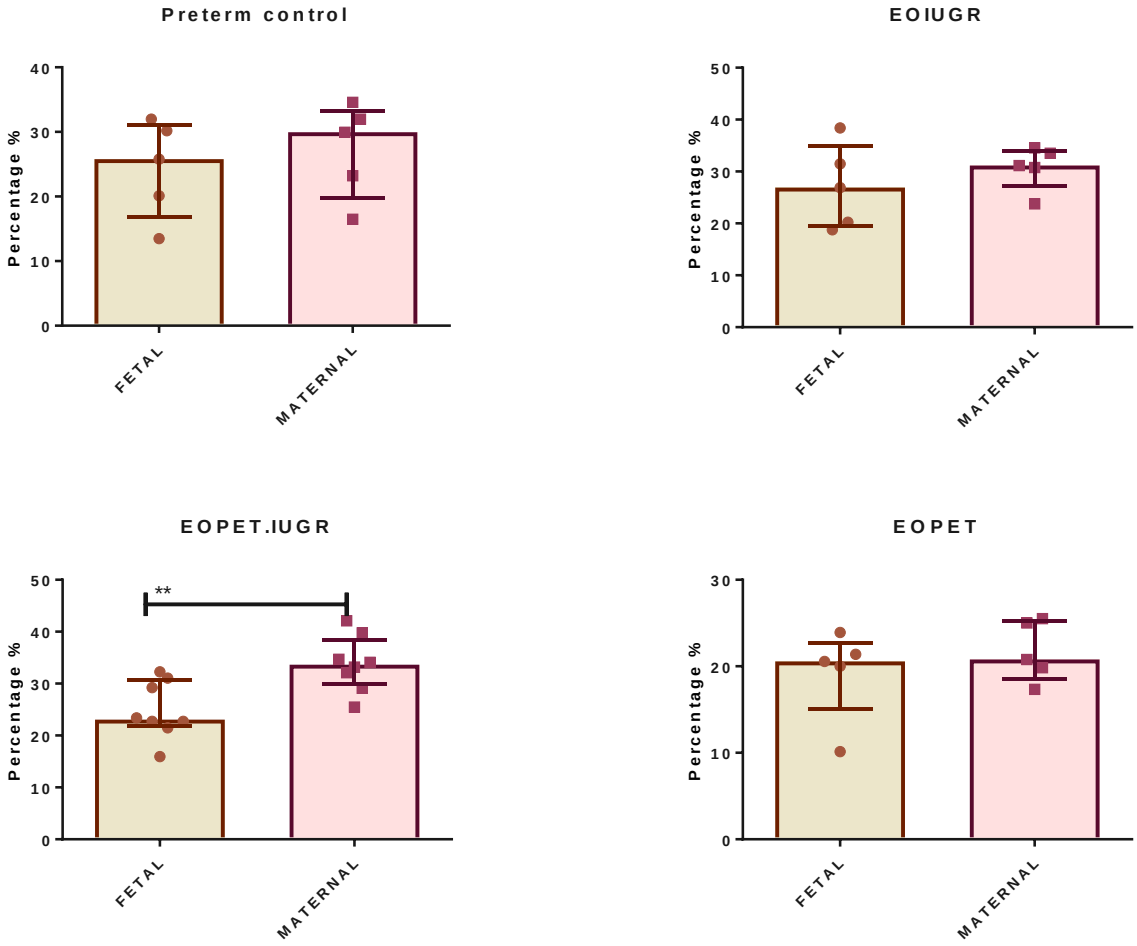

Figure 3-33 Fetal and Maternal side relative distribution of capillary volumes in Preterm Control, EOIUGR, EOPET/IUGR and EOPET placentas. It shows no significant zone predilection except in placentas from EOPET/IUGR that showed a lower fetal side capillary volumes compared to the maternal side (Wilcoxon signed rank test, *p*=0.007). ** (p<0.01). Lines represent medians and IQR. PTL= preterm control, EOIUGR= early onset idiopathic IUGR, EOPET/IUGR= Early-onset preeclampsia with growth restriction. EOPET= Early-onset preeclampsia.

As regard, the relative distribution of the capillary volumes, within fetal and maternal side, inside each group, the fetal-side of the EOPET/IUGR placenta showed a significantly lower capillary volume compared to the maternal side capillary volumes (24.85 % vs 33.81 %, p= 0.007, Figure 3-33). There was no significant fetal/maternal side difference in distribution of capillary volumes in preterm controls, EOIUGR and EOPET placentas (Figure 3-33).

3.4.4.4 Correlations between placental SNAs and capillary volumes

In early onset placental diseases, trophoblast volumes did not correlate with SNAs or with placental capillaries, SNA volumes showed a persistent negative correlation with the placental capillaries in early onset placental dysfunction (Pearson r= -0.45, Figure 3-34). In late onset placental diseases, SNA volumes were negatively correlated to placental capillary volumes (Pearson r = -0.7, Figure 3-34).

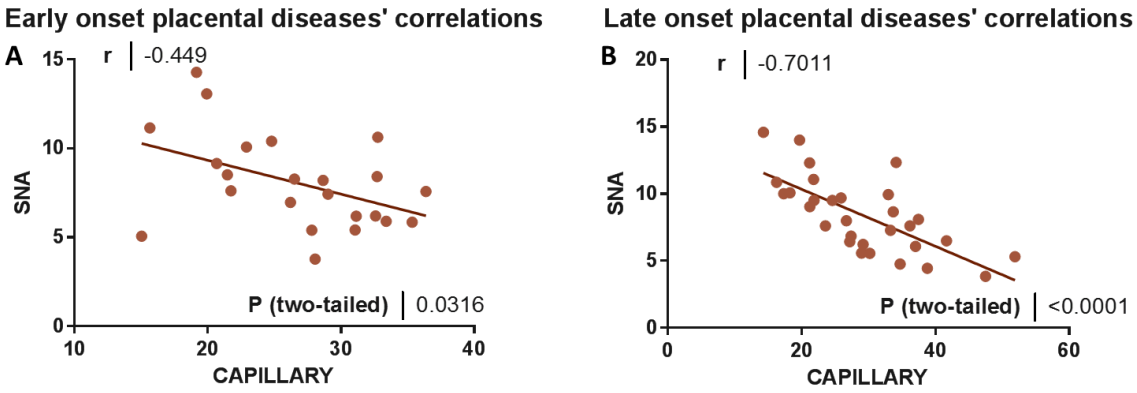

Figure 3-34 Correlations and regression analyses of SNA and capillary volumes in (A) early onset and (B) late onset placental dysfunction. Fig (A) shows a statistically significant negative correlation between SNAs and capillary volumes (Pearson r = -0.45) in early onset placental dysfunction. Fig (B) shows significant strong negative correlation between SNAs and capillary volumes (Pearson r = -0.7) in late onset placental dysfunction.

3.4.4.5 Further statistical analysis

To study the strength of association of reduced capillary volumes (ischaemia) and SNA volumes in depth, we used multiple logistic regression models, accounting for the early-late onset disease status. SNA volume (primary outcome) and capillary volume (primary exposure) were dichotomized into two categories using the median value of 7.9872 and 27.80952, respectively. Given the small sample size of the cohort, we

decided to use Poisson regression with robust variance estimation to calculate the Prevalence ratio (PrR) of high SNA (as an outcome) comparing those with low capillary volumes (ischemia) to those with high capillary (reference), with 95% confidence interval (CI). In order to identify potential confounders, we ran several simple linear and Poisson regression models. Then, we constructed several regression models in order to identify covariates that should be included in the final model, which informed our decision to only adjust for the early-late disease variable, when studying the association between capillary and SNA volumes. Data management and statistical analysis took place using Stata version 12 (StataCorp. 2012. Stata Statistical Software: Release 12. College Station, TX: StataCorp LP).

3.4.4.6 Exploratory data analysis and identification of confounders

In simple linear regression models, trophoblast volumes were not found to be statistically significantly with capillary in late onset gestational disease, and hence not considered a confounder. On the other hand, early-late disease status was found to be statistically significantly associated with SNA and capillary, and was considered a confounder to the capillary-SNA association. We decided to adjust for early-late disease status in our multiple regression models.

3.4.4.6.1 Placental ischaemia as a predictor of SNA volume

We modelled SNA using Poisson regression with robust variance estimation, the crude PrR (prevalence ratio) of high SNA volume was 2.97 (95% CI: 1.51-5.84) comparing those with low capillary volumes (ischemia) to those with high capillary volumes (reference). When we adjusted for early-late disease status, the measure association was slightly attenuated by the confounding effect of the disease status, but magnitude stayed strong and statistically significant (PrR 2.67, 95% CI: 1.31-5.43).

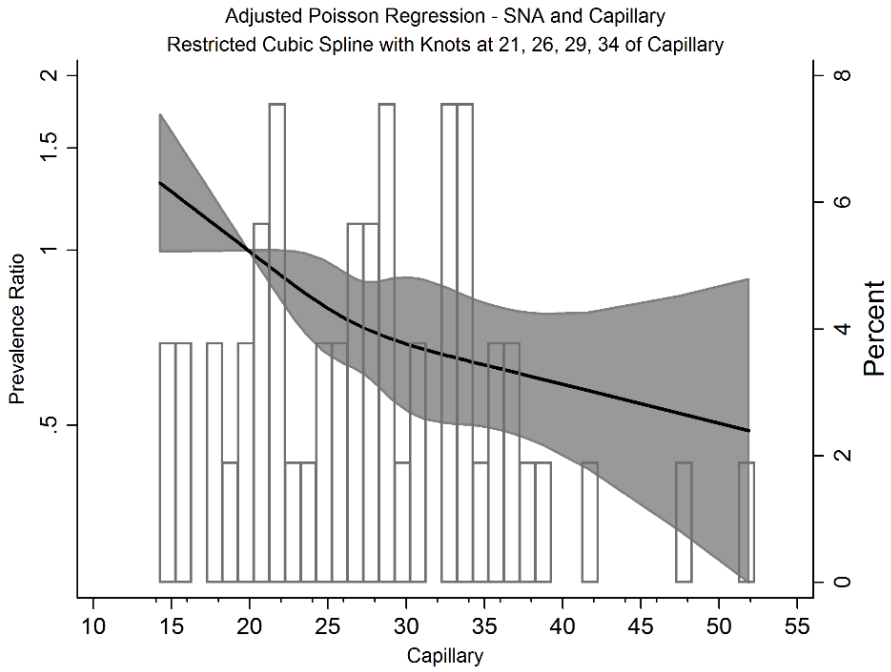

Figure 3-35 Locally weighted scatter plot smoothing (LOWESS) showing a negative relationship of the adjusted association between SNA and capillary volumes in placental dysfunction.

	PrR (95% CI)	p
Model 1	2.97 (1.51-5.84)	0.002
Model 2	2.67 (1.31-5.43)	0.007

Table 3-1 Poisson regression with robust variance estimation of high SNA volume (outcome) comparing low capillary volumes or ischemic villi (below the median) to capillary volumes above the median. Model 1 is unadjusted, Model 2 is adjusted for the early-late disease status. PrR; Prevalence Ratio.

3.5 Discussion

Preeclampsia is an adverse gestational syndrome of diverse aetiology and pathophysiological pathways that occurs in at least two subgroups, one with normal or heightened placental function and another encompassing placental dysfunction (309). This assumption is grounded on the results that early onset PET (delivery <34 weeks) is linked to reduced uteroplacental blood supply (310), leading to reduced birth weight (311). Furthermore, rising evidence shows that in the majority of late-onset PET (delivery>34 weeks), neonates have normal weight (312). Moreover, a study made by Moore and Redman (313) showed that early-onset PET was significantly different from late-onset PET in terms of risk factors.

This study was designed to eliminate the confounding effects of IUGR and PET through matching groups of PET alone, IUGR alone and a combination of both to gestational aged matched controls.

3.5.1 Stereology-based volume estimations

3.5.1.1 Volume estimation

Since volume is a 3D measure of growth and the placenta is a three dimensional organ, a much better representation of placental changes in compromised pregnancies can be attained through stereological assessment of volumes (314). Stereological measurements of the placental volume, villi, trophoblasts and capillaries provide an estimate of the overall growth and development of these structures, delivering an index of placental function. Since the placenta, as gestation advances, must reach a certain size to fulfil the increasing demands of the growing fetus, hence the placental volume, acting as an estimate of the net functional capacity, becomes dependent on its exponential growth of its functional components to maintain normal placental function. Any perturbed patterns of these components will lead to pathologies relevant to PET and IUGR.

The total placental volume change is believed to result from variations in the volume and/or size of placental villi and its subcomponents such as volumes of the capillary vasculature, stromal core and overlying trophoblastic layer. The stereology-based volume estimation protocols of villous stroma, trophoblast layer; placental capillaries

and SNAs were done through the technique of point counting (315), capable of producing volume densities (ratio of placental constituent to total placental volume) and absolute volumes of all the cases with an acceptable coefficient of error (CE). Volumes of SNAs, trophoblasts and capillaries in each placenta were then further adjusted by their respective villous volumes as percentages to neutralise differences due to discrepant villous volumes between groups. Each placental slides were virtually divided to two halves; the fetal half on the side of the chorionic plate and the fetal membranes (amnion and the chorion), and the maternal side nearer to the basal plate, to explore potential heterogeneity in fetal/maternal-side functions related to pathogenesis of placental dysfunction.

Although differences regarding umbilical cord clamping, blood loss due to vaginal delivery can form some degree of bias to vascular volumes inherent to placental collection. Nonetheless, capillaries usually retain their configuration with minimal effects compared to larger veins (316). Furthermore, stereological measurements in this study were comparable to previous researchers.

The use of well-defined and distinct placental study groups with proper controls has enabled a greater appreciation of the effects of isolated PET and IUGR and sub-classification of groups into early- and late-onset based on their gestational ages. This study has revealed that isolated preeclampsia (without IUGR), whether early- or late-onset, had no significant influence on birth weight compared to gestational aged-matched controls. This is in accordance with other published literature that reported normal birth weight new-borns to mothers with LOPET (312) and smaller neonates born to mothers with EOPET (313, 317).

3.5.1.2 Early-onset placental pathologies

In this study, EOPET placentas displayed a significant rise in SNA/villous volumes compared to preterm controls but showed no significant change on birth weight, placental volumes, trophoblast volumes, capillary volumes and total villous volumes and densities compared to preterm controls. The finding that EOPET had no effect on villous volumes in the present study was in agreement with a stereological study made by Widdows (10) which showed no reduction in EOPET placental villous volumes compared to preterm controls. It disagreed with another study which showed that

EOPET placentas had aberrantly developed terminal villi and thus lower villous volumes compared to preterm controls (318, 319). This discrepancy might be explained that the latter study used an EOPET cohort with significantly reduced birth-weights and placental volumes in comparison to preterm controls and IUGR with a less stringently defined group of preeclamptic cases. In contrast, the current study adopted a more homogeneous subset of rigorously defined early onset preeclamptic cases without clinical signs of IUGR and birth-weights above the 10th centile for gestational age.

In the present study, fetal birth-weights from early and late onset IUGR with or without PET were below the 10th centile for gestational age. A birth-weight below that level is an indicator of an inadequate oxygen and nutrient extraction by the 'growth restricted' fetus, such that demand and supply between the fetus and placenta has not been adequately achieved. Indeed, our study has also shown that placentas from growth restricted fetuses with or without PET placentas were associated with reduction in birth weights and placental volumes.

Specifically, EOPET/IUGR placentas showed a marked reduction in volume densities and total volumes of placental villi compared to preterm controls. These morphological findings were similar to other studies reporting a decrease in villous volumes and surface areas of placentas from preeclampsia with IUGR (320, 321). Moreover, stereological studies displayed an increased severity of the changes associated in placentas of IUGR with co-existing preeclampsia; clinically the most severe phenotype (322).

Although overall changes in capillary volumes in EOPET/IUGR compared to preterm control were not noticed, a significant reduction in the fetal-side capillary volumes compared to the maternal-side was evident (p=0.005). This might indicate that a change in the vascular distribution of capillary volumes in the EOPET/IUGR placenta might be a contributing factor to placental dysfunction. A similar reduction in the fetal-side trophoblast volumes was evident compared to maternal-side (p= 0.01), but these changes were not reciprocated on a distribution difference of the SNAs between fetal and maternal sides of the EOPET/IUGR placenta.

Interestingly, placentas from EOPET/IUGR kept a similar pathological signature to EOIUGR placentas in SNAs, trophoblast volumes and highlighted especially in vascular volumes as compared to changes evidenced in EOPET placenta. This might suggest that the pathological signatures of the growth restriction often precede that of preeclampsia. This goes in accordance with clinical studies showing that growth restriction usually comes before the development of the clinical symptoms associated with early-onset PET (309, 311).

3.5.1.3 Late-onset placental pathologies

Placentas from late-onset IUGR in this study exhibited substantial decreases in total placental and total villous volumes compared to full term controls, a result similar to another stereological study reporting a decrease in estimated total villous and placental volumes in late-onset IUGR placentas (10). Nonetheless, late onset IUGR placentas did not show a similar decrease in villous volume density or fraction, which might be explained by a trend rise in the capillary volume fractions in these placenta (p= 0.09) compared to term controls. A phenomenon which can be explained as a form of adaptive angiogenesis in the peripheral villi of IUGR placentas (323) secondary to utero-placental hypoxia from inadequate or failed spiral artery invasion in the first trimester. It also might account for the normal umbilical artery Doppler, only if there was no secondary pathology detrimental to the chorionic villi (i.e. villous infarcts, fetal thrombotic vasculopathy) in IUGR placenta where absolute vascular volumes were reduced whilst volume densities were maintained (324, 325).

Pathologically, placentas from late onset IUGR might go through a compensatory placental capillary vascular response to the growth restriction of the fetus and the placenta in order to counteract chronic fetal nutritive and respiratory deprivation; a response whereby the primary fetal hemodynamic response to this deprivation would involve blood flow redistribution to the brain, heart and placenta at the expense of flow to muscles, viscera, skin, and other less critical organs (326).

The higher capillary volumes observed in placentas from term IUGR pregnancies is also in accordance with other studies that clustered growth restriction into early & late and found out that late onset IUGR had a significantly higher incidence of chorioangiosis, which is a placental pathology characterized by an abundance of blood

vessels within the chorionic villi (327, 328). Placental hypercapillarisation is also suggested by Bacon et al. (329) and Scheffen et al. (330) to be induced by hypoxia.

Moreover, Fox (331) (1976, 1981 and 2000) in several reports observed that in most cases of IUGR, the smaller fetus size could not be elucidated by so-called 'placental insufficiency,' as there was little morphological or other histopathological evidence. He also observed that placentas from cases of idiopathic IUGR were found to be smaller, but placental: fetal weight ratios were usually normal. Histological examination of placentas in IUGR revealed no constant or diagnostic findings (331). Radiologically, a study measured the arterial perfusion using arterial spin-labelling MRI in placentas of severe idiopathic term IUGR pregnancies, even with an average fetal birthweight below the 1st percentile, there was no difference in placental perfusion compared to control placentas (332). This indicates that radiological changes found in placentas of term IUGR may be reflective of pathological and structural differences in their placentas.

In this study, placentas from idiopathic IUGR in normotensive mothers had a significant reduction of SNA volumes by 34% compared to control. This was comparable to another study that showed a reduction of the number of syncytial knots by 50% in idiopathic IUGR placenta compared to the control placentas (333). Another study showed a significantly smaller surface area from IUGR placenta compared to control, with no difference in number of syncytial knots per individual villus (334). A reduction in numbers and surface areas can be indirectly reflected on lower volumes compared to control as in our study. However, other non-stereological studies did not find significant differences of SNA frequencies in IUGR placenta compared to control (335) which supports the need for a more objective stereologically-based approach to quantify SNA volumes. The reduced SNA volume in IUGR placenta in our study could be explained by a reduction in the trophoblast volume in IUGR placenta found in our study compared to control, leading to reduction of recruitment of cytotrophoblast nuclei to the syncytiotrophoblasts and thus reduced formation of SNAs.

The branching pattern of the placental villi and factors controlling it, like vascularity and ischaemia, has also been linked to the altered appearance of SNAs in placental sections with increase the incidence of tangential sectioning of trophoblast layer at

points of villous bending or branching (79, 80). Therefore, the reduced volumes of the SNAs in IUGR placenta may be due to the reduced branching pattern as evidenced by studies (336, 337) showing reduction in number and branching of the fetoplacental vasculature in IUGR placentas.

This study has shown that isolated late-onset PET placentas had a minimal influence on birth weight, placental volumes, trophoblast volumes and total placental villous volumes compared to term controls. This is consistent with previously published reports concluding that isolated PET placentas were similar in structure to gestational age-matched controls (304, 320, 338).

This study also showed that placentas from LOPET pregnancies had significantly higher SNA volumes compared to gestational age-matched control. Similar observations, though non-stereologically based, were reported in the literature showing PE placenta having increased syncytial knots, relative avascular terminal villi, and villous fibrosis (78, 335, 339-342). Nonetheless, these studies were confounded by the inherent bias related to counting the 'number of syncytial knots per unit area' in 2D. Hence, there was always a degree of error associated with morphological estimation of SNAs, which is on the other hand, accurately estimated in stereological studies and can therefore be kept to a minimum. A greater volume of SNAs in isolated PET (early and late-onset) may reflect either an increase in the addition of nuclei into the syncytiotrophoblast and their subsequent hastened ageing process through a programmed cell death (PCD) pathway, or a reduced shedding phenomenon, or both of them.

On examining the LOPET/IUGR placenta, we demonstrated a midway pathological phenotype between the LOPET and the normotensive IUGR placenta, having more capillary volume densities compared to LOPET and less compared to IUGR, with a trend reduction in the fetal zone in the LOPET placenta compared to the LOPET/IUGR placenta; indicating that this might be specific to the "preeclampsia" effect. Our study also demonstrated that SNA volumes were reduced in placentas from mothers with LOPET/IUGR compared to pure LOPET without IUGR. A similar pattern was observed between placentas from IUGR normotensive mothers and LOPET/IUGR placentas,

highlighting a potential effect of pure PET on the placenta raising SNA volumes as this was consistent in early and late-onset preeclampsia placenta.

This study also demonstrated a significant inverse relationship seen between SNAs and placental capillary volumes. Those with capillary ischemia had two and half times the likelihood of having high SNA than those with higher vascularity, after adjustment for the disease status. Moreover, the results from the multiple linear regression adjusting for early-late disease status showed that the lower the capillary volume, the higher the SNAs.

This was consistent with another study showing SNAs as a prominent feature in areas with avascular villi and regressive villous changes (343). Moreover, Ali et al, (80) showed that the volume density of the villous tree occupied by SNAs was higher in term placentae delivered at altitudes over 3000 meters than in controls. This showed how ischaemia and structural vascular changes might have a role in the change in villous architecture and SNA volumes.

This negative correlation found in this study might suggest that reduced capillary volumes or ischaemia in placental dysfunction might have a role in regulating the pathogenesis of SNA formation and/or shedding. This might emphasise a potential role of programmed cell death (PCD) related to SNA formation and/or shedding. There is growing evidence of SNAs being a consequence of subcellular stress in the syncytiotrophoblast (STB) leading to the release of anti-angiogenic factors in the maternal circulation which have an important role in the widespread endothelial dysfunction observed in such cases (5).

A limitation to this study, in addition to the relatively small number of placentas, is the absence of placental phenotypes in stillborn newborns, which might have elucidated the role the SNA may have in the pathogenesis of stillbirth. A possible reason for this absence is the well-known common placental post-mortem regressive changes that commonly preclude a meaningful histological diagnosis (327).

3.5.2 Structural classification

This study suggests that the virtual pathology platform, with its very high resolution, can be used to structurally classify SNAs in 2D digital images into false and true SNAs.

False SNAs are those aggregates bridging between villi with nuclear size and dispersion similar to the rest of the syncytial nuclei. Conversely, true SNAs showed aggregates of dense basophilic compacted smaller nuclei. Moreover, its close proximity to areas of fibrin-type fibrinoid was clearly demonstrated. This came in accordance to previous studies showing that STBs didn't show evidence of apoptosis except in regions of fibrin-type fibrinoid (344).

3.5.3 3D reconstructed villi, fibrin-type fibrinoid and SNAs

Three-dimensional (3D) reconstruction of placenta with microscopic resolution might have an enormous potential to enhance our understanding of normal and disease processes, mainly those involving structural villous changes and those showing spatial relationship of different placental features. This new platform has the advantage of allowing for conventional histopathological staining and interpretation techniques using an automated whole slide scanner. It is also able to make high-resolution digital images and yield 3D reconstructions at a cellular resolution level (262).

This was the first attempt, to our knowledge, to reconstruct villi, fibrin-type fibrinoid and SNAs together using histopathological slides and convert them into 3D volume to explore the spatial relationship between them. This methodology has enabled us to visualise the distribution of the SNAs clustering around areas of fibrinoid degenerations which were highly abundant in the preeclamptic placentas evaluated.

3.5.4 Summary and conclusions

This study, through assessment of the structural components of placentas from complicated pregnancies, has identified certain parameters that can be associated to placental dysfunction. Stereological methods were used to provide quantifiable estimates of volumes of placental structures. Volume densities of placental components were then adjusted for their respective villous volumes.

In late onset disease, villous volumes in placentas from IUGR and LOPET/IUGR were reduced compared to control. Similarly, trophoblast volumes were lower in IUGR placentas. SNA volumes were persistently higher in LOPET and lower in IUGR placentae compared to control. On the other hand, capillary volumes showed a trend

increase in IUGR placentas compared to control. Conversely, LOPET showed a trend decrease in capillary volumes compared to term control.

In early onset disease, our study has demonstrated that placentas from pregnancies complicated with EOPET/IUGR had lower villous growth compared to control and a trend higher placental capillary volume compared to EOPET. EOPET placentas showed a consistently higher SNA volumes compared to preterm control.

The study revealed that SNA volumes showed a significantly negative correlation with capillary volumes in early and late placental pathologies, a finding that might suggest a pathogenestic link between placental ischaemia and regulation of SNA formulation/shedding. A link that might involve a potential role of programmed cell death (PCD) and placental dysfunction, which will be studied in the next chapter.

Chapter 4
Molecular characterisation of programmed cell death in placental dysfunction

4.1 Introduction

Programmed cell death (or PCD) is the cell death mediated by an intracellular program which is carried out in a biological process, and usually confers advantage during an organism's life-cycle serving fundamental functions during both plant and animal tissue development (345). Apoptosis and autophagy are both forms of programmed cell death. The concept of "programmed cell-death" was used by Lockshin & Williams in 1964 in relation to insect tissue development, around eight years before "apoptosis" was coined (346).

Autophagy was first described in the 1960s in hepatocytes (347). Jones and Fox were the first to describe the presence of trophoblast vacuoles in the 1970s (348). Though initially identified as lysosomes, it seems likely that they would now be described as autophagy vacuoles. Autophagy is known to have a crucial recycling function that affects the cellular physiology. In basal conditions, autophagy is vital for maintaining cellular homeostasis through recycling old and dysfunctional cellular organelles and protein aggregates (110).

Autophagy is induced following cellular stresses like starvation, hypoxia and pathogen invasion providing a cytoprotective response thus helping cellular survival and adaptation (110). One of the major autophagy inducers is oxidative stress, including superoxide anions (121), other reactive oxygen species (ROS) and hydrogen peroxide generated from the mitochondrial electron transport system during energy production. Cell damage is usually prevented by cellular antioxidant defences, which if low will lead to damage of lipids, proteins, DNA and organelles like mitochondria. Autophagy induction is known for its ability to remove dysfunctional organelles as in mitophagy thus reducing the generation of ROS and contributing to cell survival (122, 123).

A dysregulation in the physiological induction and assembly of the autophagic pathway has been linked to a broad range of diseases such as neurodegenerative disorders,

cardiomyopathy, autoimmunity and cancer (349). Its involvement in reproduction, and especially in placental dysfunction, has not been extensively studied. Moreover, it is essential to study and understand the role that autophagy plays in the context of placental dysfunction and whether that role is ancillary or antagonistic to the apoptotic pathway, thus favouring a balance towards survival.

A useful and flexible marker for accurate autophagy flux assessment is the Microtubule-associated protein light chain 3-II (LC3-II). It covalently attaches to phosphatidylethanolamine (PE), thus when LC3-II fuses into PE-rich lipid membranes. The relative amount of LC3-II will reflect the steady state autophagic activity, thus represents a specific and reliable marker for autophagosome formation in mammalian cells (103, 104).

The early human placenta is known to develop under low oxygen and glucose conditions in normal pregnancy. This physiological hypoxia is believed to generate ROS thus contributing to the oxidative stress (157). Placental physiological hypoxia, nutrient deprivation and oxidative stress are inducers of mTOR suppression, therefore stimulating autophagy (99) which is important to preserve a cellular bioenergetic equilibrium between anabolic and catabolic processes, thus allowing appropriate development of the embryo and placenta (157).

In human placenta, autophagy vacuoles have been detected in normal placenta (159) and it has been suggested that dysregulation of autophagy may have a role in the pathogenesis of placental dysfunction. In early-onset preeclampsia (EOPET), spiral arteries are affected by impaired vascular remodelling and shallow trophoblast invasion, leading to poor placentation, hypoxia and increased anti-angiogenic factors like soluble endoglin, which in *in vitro* studies has been found to inhibit extravillous trophoblast invasion and vascular remodelling through inhibiting autophagy under hypoxic conditions (161). Moreover, another study also showed that *in vitro* hypoxia-induced autophagy augmented extravillous trophoblast invasion (162).

There are growing evidence that autophagy (ATG) proteins, in addition to regulating the autophagy pathway, are also involved in different immunologic and metabolic pathways, emphasising the intricate and coordinated relationship of autophagy with other signalling pathways (109).

Understanding the role that autophagy plays in the regulation of extravillous trophoblast invasion might allow future research and inform therapeutic strategies to use pharmacological inducers of autophagy to modulate this process with an aim to reduce the incidence of preeclampsia and IUGR (100).

4.2 Hypothesis

The combined use of random sampling and novel image analysis tools will attain a more objective quantification method of molecular markers of programmed cell death in placental dysfunction. Moreover, the markers of programmed cell death will be differentially expressed across placentas from early and late onset gestational diseases.

4.2.1 Specific hypotheses

- Oxidative stresses in placental dysfunction that can lead to trophoblast cell apoptosis are modulated by placental autophagy.
- Image analysis can help quantify immunolabelled markers essential in understanding placental dysfunction.
- Fetal and maternal sides' distribution of PCD markers in the placenta is different.

4.3 Aim and specific objectives

The aim of this study was to determine, quantitatively through image analysis and qualitatively through localisation of immune-labelled markers of programmed cell death, the molecular pathological phenotypes characteristic of placental dysfunction in early and late onset gestational diseases.

The specific objectives were:

1. To quantify molecular markers of programmed cell death (autophagy and apoptosis) in different groups of placental dysfunction
2. To explore relationship between markers of apoptosis (M30 and Bcl-2), autophagy (LC3), oxidative metabolism (8-OHdG) and the anti-inflammatory scavenger macrophage-specific protein CD163 and the effect of the disease status on that role
3. To seek correlations between structural (SNAs and placental capillaries) and molecular markers of programmed cell death in placental dysfunction

4.4 Results

Placentas from early and late gestations with different clinical diagnoses were serially sectioned and immunolabelled with several markers of programmed cell death i.e. M30, Bcl-2, LC3, 8-OHdG and CK18. They were then digitally scanned and virtually retrieved for annotation and analysis using Aperio ImageScope software.

4.4.1 Apoptosis-related markers

4.4.1.1 M30 Antibody optimisation

The M30 CytoDEATH™ antibody has been reported in several studies to serve as a superior technique in apoptosis detection compared to TUNEL (286, 287). M30 monoclonal antibody identifies only caspase-cleaved cytokeratin 18 in epithelial-derived cells and does not recognise uncleaved CK18, thus is specific for apoptotic epithelial cells. Early and late placental pathologies were initially immunolabelled with uncleaved CK18, human cytokeratin intermediate filament protein, to measure their levels of expression in different placental pathologies in order to account for any differences in M30 expression not due to differences in uncleaved CK18 levels (Figure 4-1).

4.4.1.2 Specificity and expression pattern

Uncleaved cytokeratin 18 was abundantly expressed in the trophoblast layer (Figure 4-1A). Its expression levels did not show any significant differences across groups of the early and late placental pathologies (Figure 4-3A). Placental slides were then stained with the apoptotic M30 marker using adequate positive and negative controls (See 2.9.1, Antibody optimisation).

The M30 marker, being an epithelial-specific marker, only stained the trophoblast as expected (Figure 4-1B & C), being the only epithelial component of the placenta. Immunolabelled slides were then analysed using image analysis algorithms (Figure 4-2) that scored the percentage of positivity and the staining intensity of the slides. Positivity, which is the proportion of the positive (brown) stains (strong, intermediate and weak positive) taken from all the positive and negative stains (villous area as seen in Figure 4-2B), was the main output analysed. The ratio of strong staining (NSR), which is the proportion of strongly stained pixels from the whole positive pixel range, was also analysed when appropriate.

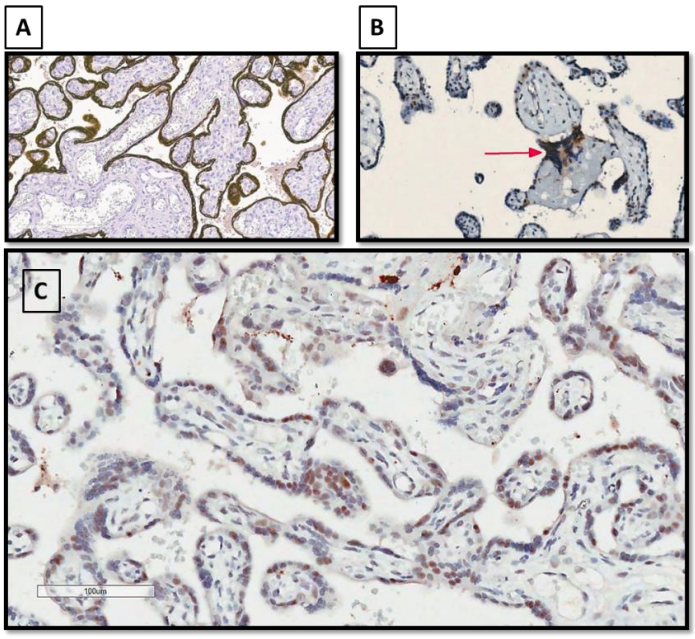

Figure 4-1 Specificity of M30 stained slides of placental dysfunction. (A) Representative image of uncleaved CK-18 in the placenta, showing staining specific to the epithelial element of the villi (trophoblast). (B) Representative image of M30-stained SNA adjacent to an area of fibrinoid degeneration. (C) Representative image of M30-stained IUGR placental slide showing brown stained trophoblasts.

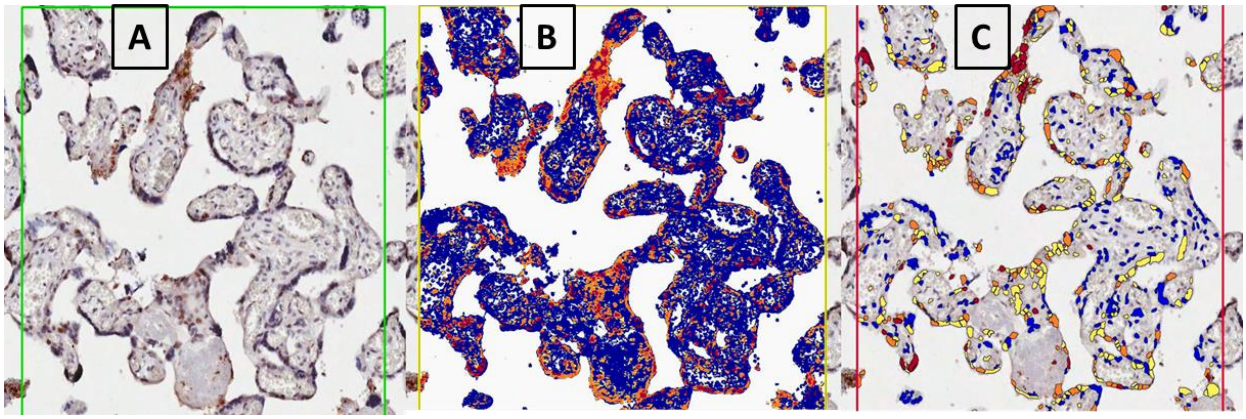

Figure 4-2 Examples of the application of image analysis algorithms used for assessing placental slides stained by immunohistochemistry. (A) Unstained representative image of placental field of vision (FOV). (B) A cover-up image after applying the Positive Pixel Count (PPC) algorithm where yellow represents the weak positive stain, orange the medium positive stain, brown the strong staining and blue the negative (unstained). (C) A cover-up image after applying the nuclear image analysis algorithm where yellow represents weakly stained, orange represents moderately stained and brown represents intensely stained cells.

4.4.1.3 Scoring of apoptotic marker M30 in placental dysfunction.

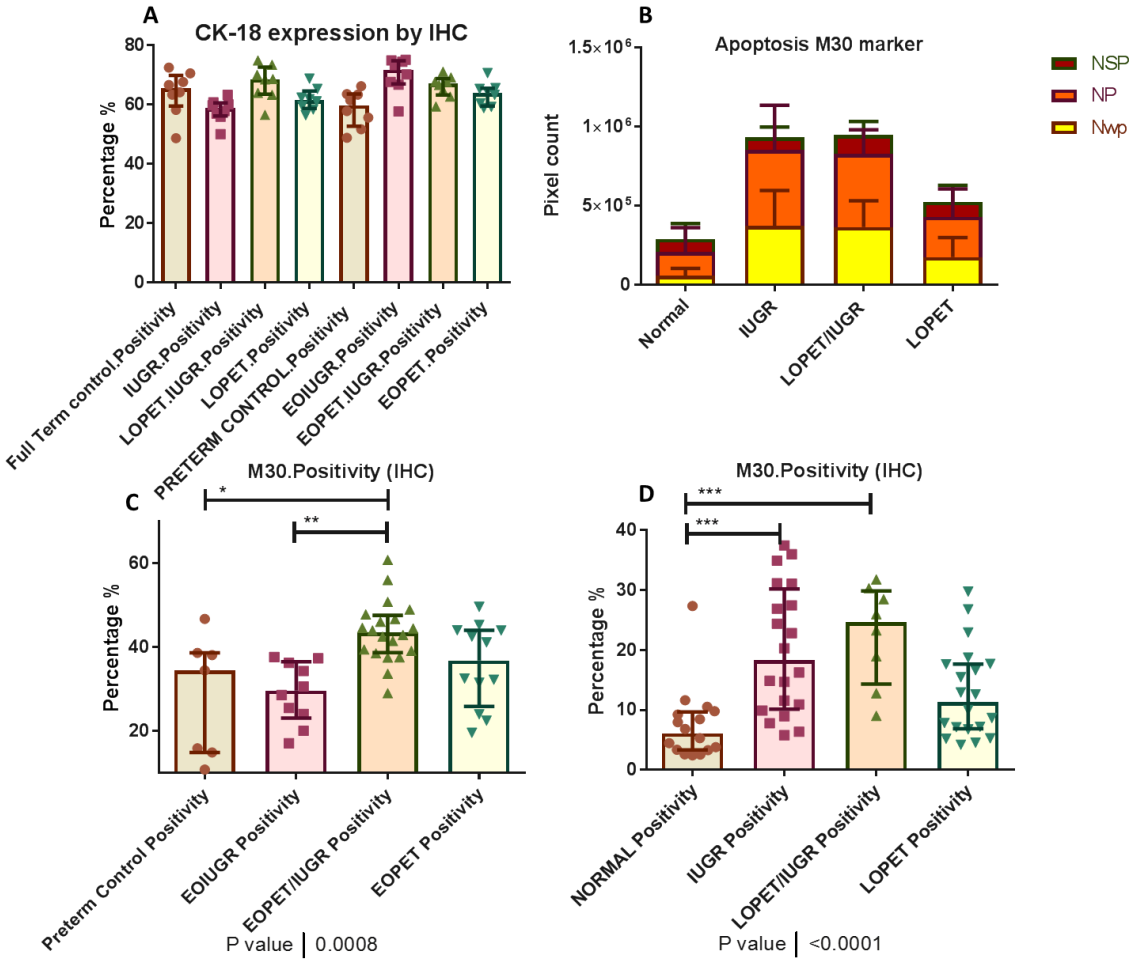

Figure 4-3 Apoptotic marker quantification in early & late-onset placental dysfunction stained with Cytokeratin 18 and M30 apoptosis marker. (A) Cytokeratin-18 (CK-18) positivity staining percentages in the different placental pathologies. It shows no significant differences in CK-18 staining across different pathologies. (B) M30 apoptotic marker staining intensity (in pixel count) in placentas from control (n=16), IUGR (n=20), LOPET/IUGR (n=8) and LOPET (n=20) pregnancies. Yellow represents weak staining (Number of weak pixels, Nwp), orange represents moderate staining (Np) and brown represents strong staining (Number of strong pixels, Nsp). Error bars represent SD. (C) M30 apoptotic marker positivity percentages in early onset pathologies as EOIUGR (n=10), EOPET/IUGR (n=20), EOPET (n=12) compared to preterm control (n=8) placentas. Differences across groups were significant (p=0.0008, Kruskal-Wallis with Dunn's multiple comparisons test) where EOPET/IUGR placentas had significantly higher M30 positivity compared to preterm control (43.7% vs 30.9%, *adj. p*=0.03). (D) M30 apoptotic marker positivity percentages in late onset pathologies compared to term control placentas. Differences across groups were significant (p<0.0001, Kruskal-Wallis with Dunn's multiple comparisons test), where IUGR and LOPET/IUGR placentas had a significantly higher M30 positivity compared to term control (20%, 23% vs 7.5%, *adj. p*=0.004 and p=0.0009 respectively). IUGR=Term IUGR. LOPET/IUGR= Late onset preeclampsia with growth restriction. LOPET=late-onset preeclampsia. EOIUGR= Early-onset IUGR, EOPET/IUGR= Early-onset preeclampsia with IUGR, EOPET= Early-onset preeclampsia. Lines represent medians and IQR. * p<0.05, ** p<0.01, ***p<0.001, **** p<0.0001.

In early onset placental pathologies, apoptotic burden was significantly different across groups. Apoptotic trophoblasts were significantly higher in placentas from pregnancies diagnosed with early onset severe preeclampsia with IUGR compared to placentas from control term pregnancies (Figure 4-3C). Placentas from EOIUGR and EOPET did not show significant differences in M30 expression compared to the gestational age matched preterm control.

Similarly, placentas from late onset gestational diseases demonstrated significant differences of trophoblast apoptotic burden across groups. Placentas from IUGR and LOPET/IUGR pregnancies had a significantly higher M30 positivity compared to term control (20%, 23% vs 7.5%, *p=0.004 and p=0.0009 respectively,* Figure 4-3D). Although LOPET placentas showed a higher trend of apoptotic M30 expression compared to control placenta, but it did not reach statistical significance in the post-hoc multiple comparison's test (Figure 4-3D).

4.4.1.4 Bcl-2 immunostaining

Bcl-2 protein, a potent anti-apoptotic protein that plays an important role in impeding the mitochondria-operated pathway of apoptosis (350), was immunolabelled in our placentas to identify differences in expression across placental dysfunction.

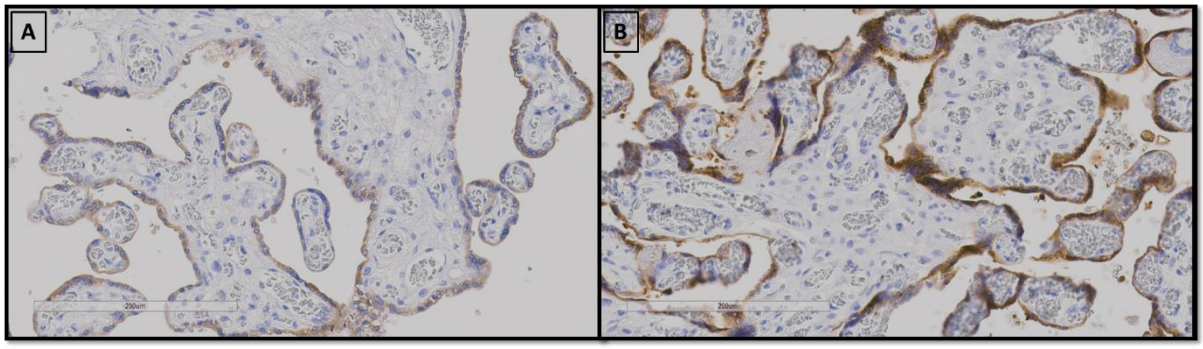

Figure 4-4 Representative images of placental slides immunolabelled with Bcl-2 antibody. (A) Representative image of placental slide from control placenta, showing weak Bcl-2 staining. (B) Representative image of a placental slide from Late-onset preeclampsia (LOPET), showing higher staining intensity compared to (A) control placenta.

Differences of Bcl-2 positivity across early onset placental pathology groups were significant where EOIUGR and EOPET/IUGR placentas had significantly higher Bcl-2

positivity expressions compared to preterm control (52.5% & 63.7% vs 22.6%, with adj. p=0.03 and p<0.0001 respectively, Figure 4-5A).

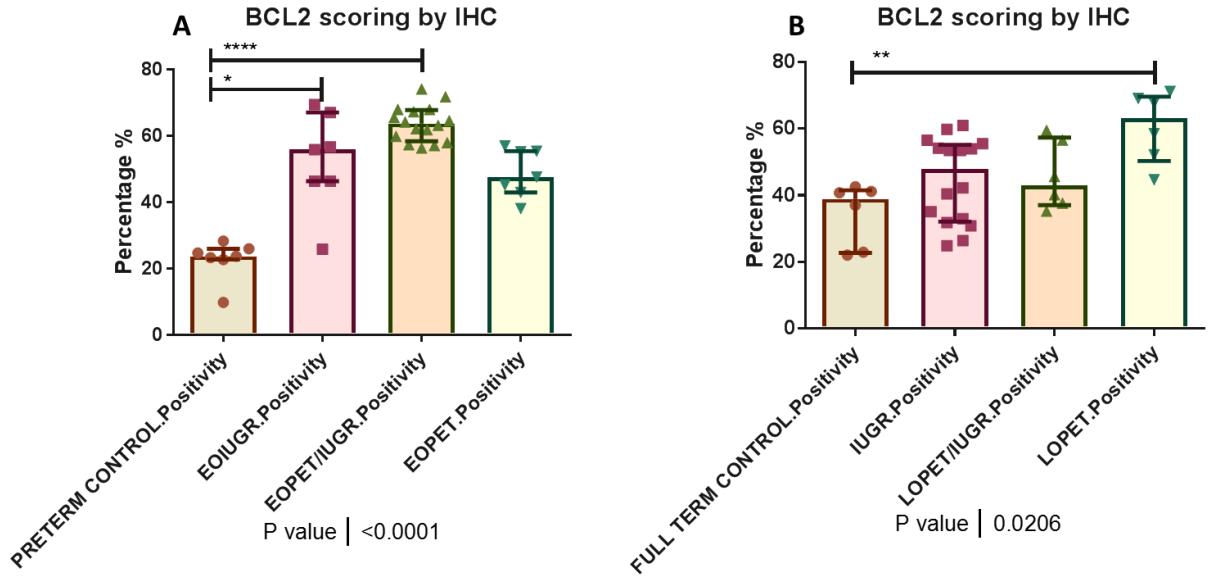

Figure 4-5 Positivity percentages of early & late-onset placental dysfunction stained with Bcl-2 antibody. (A) Bcl-2 positivity percentage in placentas from EOIUGR (n=7), EOPET/IUGR (n=16) and EOPET (n=7) compared to preterm control (n=7). Differences across groups were significant (*p*<0.0001, Kruskal-Wallis test with Dunn's post hoc test for multiple comparisons) where EOIUGR and EOPET/IUGR placentas had significantly higher Bcl-2 positivity compared to preterm control (52.5% and 63.7% vs 22.6%, with *adj. p=0.03 and p*<0.0001 respectively). (B) Bcl-2 marker positivity percentages in placentas from IUGR (n=16), LOPET/IUGR (n=6) and LOPET (n=6) compared to term control (n=6). Differences across groups were significant (*p*=0.02, Kruskal-Wallis test with Dunn's post hoc test for multiple comparisons), where LOPET placentas had a significantly higher Bcl-2 positivity compared to term control (60.5% vs 34.4%, *adj. p*=0.006). IUGR=Term IUGR. LOPET/IUGR= Late onset preeclampsia with growth restriction. LOPET=late-onset preeclampsia. EOIUGR= Early-onset IUGR, EOPET/IUGR= Early-onset preeclampsia with IUGR, EOPET= Early-onset preeclampsia. Lines represent medians and IQR. * p<0.05, ** p<0.01, ***p<0.001, **** p<0.0001.

In late onset placental pathologies, although there was a significant difference in Bcl-2 expression across groups (*p*=0.02), only placentas from LOPET pregnancies showed a significantly higher Bcl-2 expression positivity compared to term control placenta (60.5% vs 34.4%, *adj. p*=0.006).

4.4.1.5 Summary of apoptotic markers

Our study has revealed that there were no differences in expression of uncleaved CK-18 in different placental pathologies. Placentas from EOPET/IUGR showed a higher M30 expression compared to its preterm control. Placentas from normotensive and

hypertensive full-term IUGR pregnancies had significantly higher apoptotic M30 positivity compared to term control. There was relatively lower apoptotic burden observed in LOPET compared to other IUGR pathologies with a higher anti-apoptotic Bcl-2 expression compared to control.

4.4.2 Autophagy marker anti-LC3B

4.4.2.1 Expression patterns

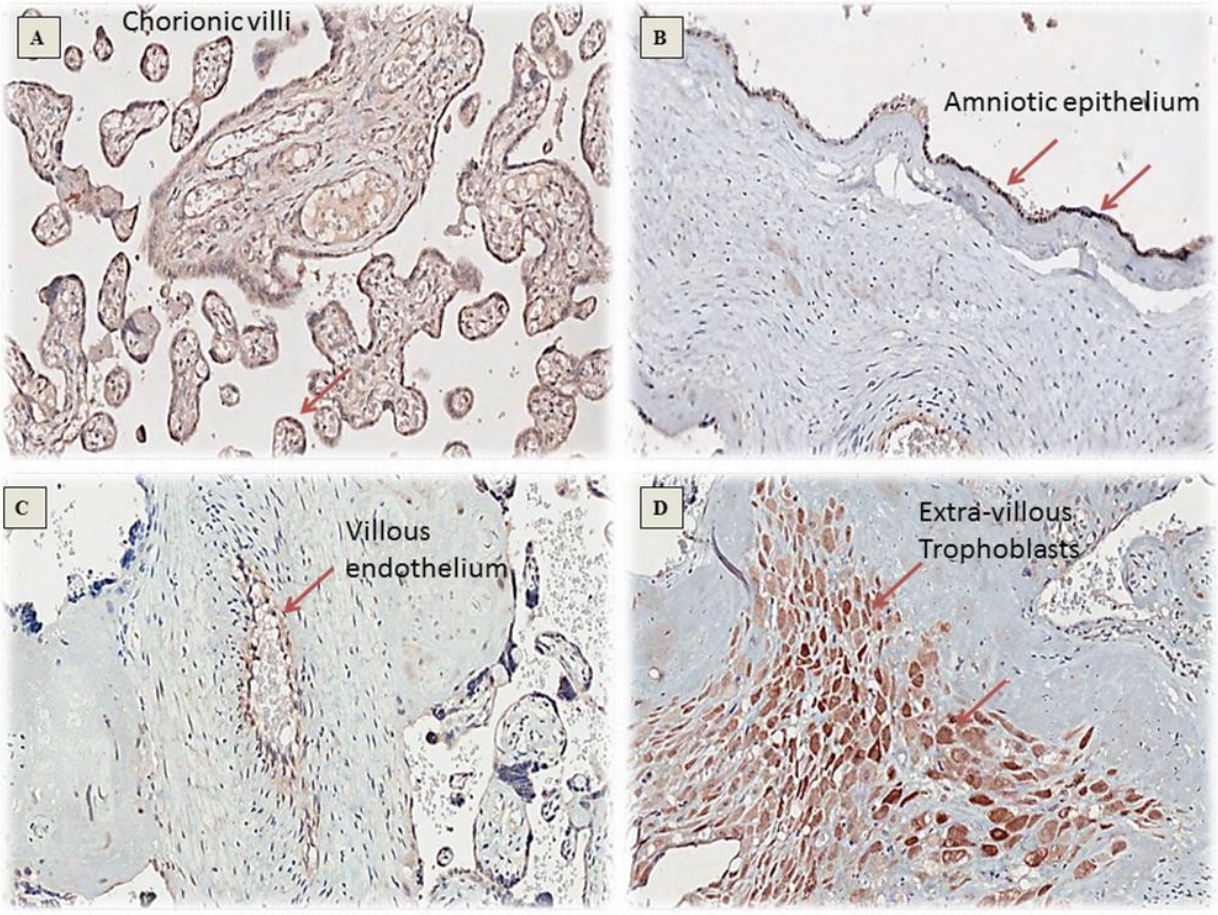

Figure 4-6 Localisation of the autophagy marker LC3 in different parts of the placenta. The IHC staining show localization in the villous trophoblast part (A), amniotic epithelium (B), villous vessels (C) and extravillous trophoblasts (D).

Slides from different placental pathologies were immunostained with anti-LC3B. Its cytoplasmic expression involved different placental cell types: amniotic membrane, endothelial cells and trophoblasts including more prominently in the extravillous trophoblasts (Figure 4-6D).

4.4.2.2 Scoring of the autophagy marker LC3 in placental dysfunction

To control for the villous area in each placental pathology, the total positivity was calculated from the proportion of the positive (brown) stains (strong, intermediate and weak positive) divided by the overall positive and negative stains. The overall pixel count of the LC3 marker across different placental pathologies was raised in placentas from late-onset preeclampsia compared to control (Figure 4-7).

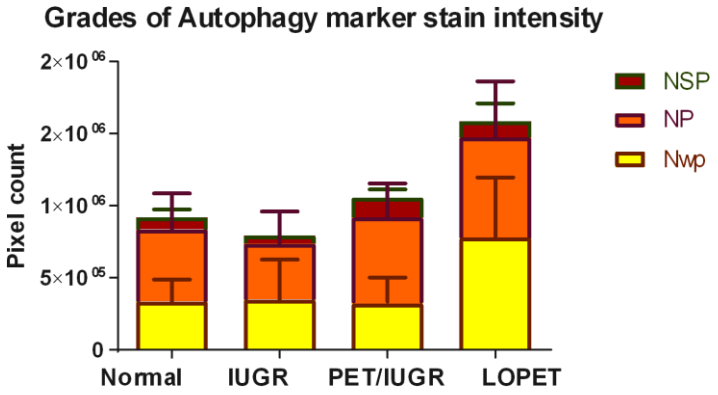

Figure 4-7 Differential stain intensity expression patterns of LC3 autophagy marker immunostaining in placental pathologies. Nwp= Number of weak positive (weak staining), Np= Number of positive (moderate staining), Nsp= Number of strong positive (strong staining). Error bars are SD. IUGR= Intrauterine growth restriction, PET/IUGR = preeclampsia with IUGR, LOPET= late-onset preeclampsia.

Scoring of the immunostained placentas from early and late-onset compromised pregnancies showed that LC3 positivity were differentially expressed across groups ($p<0.0001$ and $p=0.01$ respectively, Figure 4-8A &B). Late-onset preeclampsia had higher percentages of LC3 expression positivity patterns compared to its term control (24.4% vs 18.9%, $p=0.03$, Figure 4-8B), where EOPET/IUGR placentas had significantly higher LC3 positivity compared to preterm control (PTC) (49.9% vs 22.6%, $p<0.0001$, Figure 4-8A).

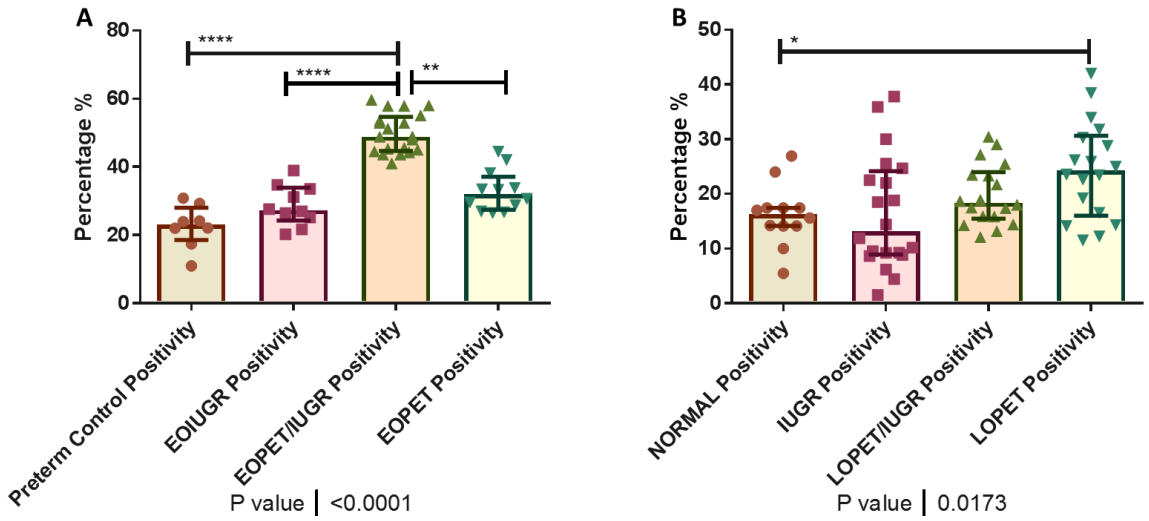

Figure 4-8 Scoring of the autophagy marker LC3 in immunolabelled slides in early and late onset placental pathologies. (A) LC3 autophagy marker positivity percentages in early onset pathologies as EOIUGR (n=10), EOPET/IUGR (n=20), EOPET (n=12) compared to preterm control (n=8) placentas. Differences across groups were significant (p<0.0001, Kruskal-Wallis) where EOPET/IUGR placentas had significantly higher LC3 positivity compared to preterm control (PTC) (49.9% vs 22.6%, *p*<0.0001, post-hoc Dunn's multiple comparisons test) (B) LC3 autophagy marker positivity expressions in late onset pathologies compared to term control placentas. Placentas from late onset placental dysfunction showed a significant difference of LC3 expression patterns across groups (Kruskal-Wallis, p=0.01). Placentas from LOPET pregnancies showed a consistent increase in LC3 positivity compared to full term control, which reached statistical significance (24.4% vs 18.9%, p=0.03, Dunn's multiple comparison's test. IUGR= Term IUGR. LOPET/IUGR= Late onset preeclampsia with growth restriction. LOPET= late-onset preeclampsia. EOIUGR= Early-onset IUGR, EOPET/IUGR= Early-onset preeclampsia with IUGR, EOPET= Early-onset preeclampsia. Lines represent medians and IQR. * p<0.05, ** p<0.01, ***p<0.001, **** p<0.0001.

4.4.2.3 Fetal-Maternal side distribution of LC3 marker

Immunolabelled slides, though undertaken in the same batch, consistently showed differential expression with areas of weaker and stronger staining in fetal/maternal side zones, suggesting differential expression of LC3 and varying levels of autophagy marker expression.

Our results also showed that in placentas from normal pregnancies, the chorionic villous positivity distribution of the LC3 labelling was mainly on the maternal side of the placenta (Figure 4-9A). Whereas, In LOPET placenta, the fetal/maternal zone distribution became comparable with an increase in the maternal side. While in normotensive IUGR placenta, the distribution stayed comparable with a trend decrease of the maternal side distribution. However, in placenta from EOPET/IUGR, the distribution was reversed

compared to normal placenta with a significant reduction in the positivity distribution in the maternal side compared to the fetal zone (*p*=0.02, Figure 4-9C).

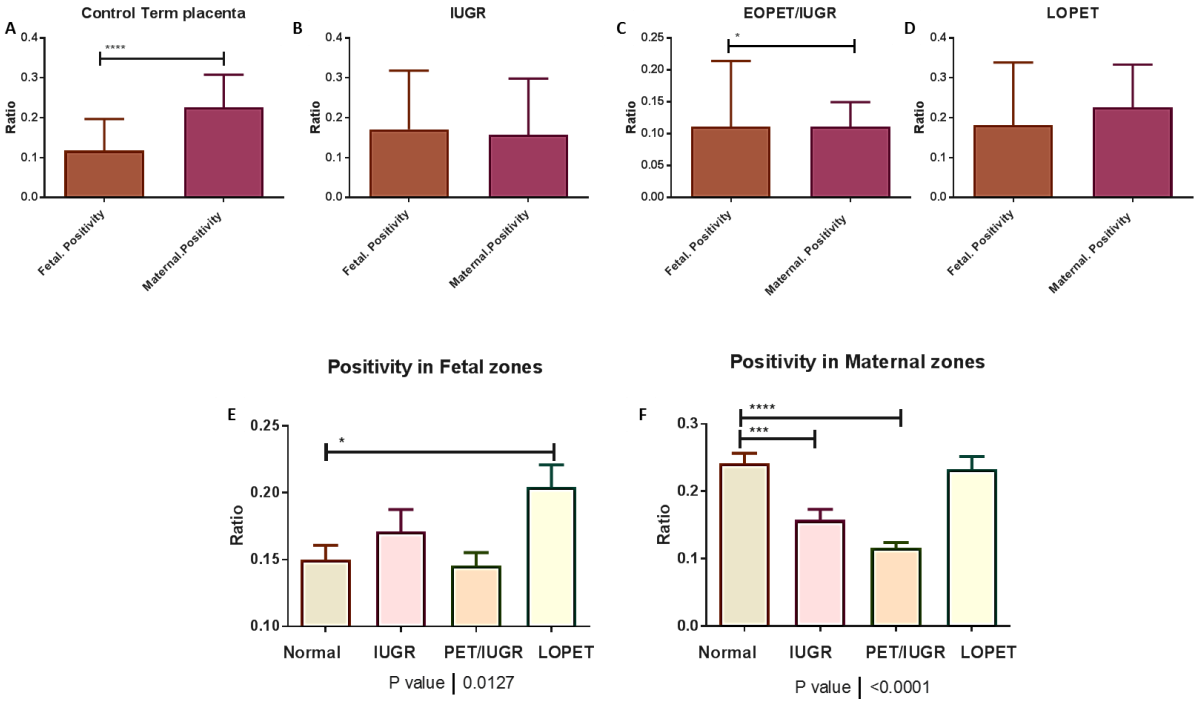

Figure 4-9 Differential fetal/maternal side distributions of the LC3 marker positivity in placental pathologies. (A) Fetal/Maternal side LC3 distribution in the term control placenta. Maternal side expression was significantly higher than fetal side expression (*p<0.0001, Wilcoxon signed rank test)*. (B) Fetal/Maternal side LC3 distribution in the term IUGR placenta. (C) Fetal/Maternal side LC3 distribution in placentas of preeclampsia with IUGR. Maternal side expression was significantly lower than fetal side expression (*p=0.02, Wilcoxon signed rank test)*. (D) Fetal/Maternal side LC3 distribution in the LOPET placenta. (E) Fetal side LC3 distribution showed significant differences across placental pathologies (ANOVA, p=0.01). LOPET placenta had higher fetal-side LC3 expression compared to control (20.4% vs 14.8% *p*=0.02, Dunnett's multiple comparisons test). (F) Maternal side LC3 distribution showed a significant differences across placental pathologies (ANOVA, p<0.0001), and showed a lower LC3 expression positivity in placentas from IUGR and PET/IUGR compared to normal control (15.7% and 11.6% vs 24.5%, *p*=0.0004 and *p*=0.0001 respectively, Dunnett's multiple comparisons test).

Furthermore, the fetal side of the LOPET placenta showed a significant increase in the LC3 expression compared to the fetal side of control placenta. However, IUGR placentas (whether normotensive or hypertensive) exhibited a significant decrease in LC3 expression within the maternal side compared to control (Figure 4-9F).

4.4.2.4 Summary of autophagy marker expression

Our study showed that placentas from early-onset preeclampsia with growth restriction as well as LOPET displayed a higher autophagy marker LC3 expression compared to its respective controls with a higher LC3 staining intensity being a major part of the overall positivity. It also showed that relative differences in biomarker distribution in fetal/maternal zones may constitute a part of the pathological molecular signature of different gestational diseases.

4.4.3 Oxidative metabolism/stress marker

8-OHdG is a nuclear DNA modified base that is formed as a by-product and an intermediate of aerobic metabolism and during oxidative stress. It occurs due to attack by hydroxyl radicals. Oxidative stress has been linked to many diseases like atherosclerosis, cerebral and heart ischaemia reperfusion injury, ageing and Alzheimer's disease (351). The study of the relationship of oxidative stress to the onset of programmed cell death in the placenta is imperative to understand the mechanism of injury in the placenta and whether that interaction is different in different types of placental pathology.

4.4.3.1 Scoring of 8-OHdG in placental dysfunction

Automated scoring of the 8-OHdG marker stained nuclei was carried out in different placental pathologies and compared across groups. These were sub-classified into three categories: 1+ for the weakly stained nuclei, 2+ for the moderately stained and 3+ of the strongly stained nuclei.

In early onset placental pathologies, placentas from pregnancies diagnosed with severe early onset preeclampsia with IUGR demonstrated the highest percentage of cells stained with 8-OHdG marker compared to gestational age matched control (Figure 4-10A). A breakdown of this high overall positivity percentage of the stained nuclei revealed that the biggest difference was in the strongly stained (score 3) nuclei being significantly higher than its control (Figure 4-11F) with a similar trend in the moderately stained nuclei (Figure 4-11E).

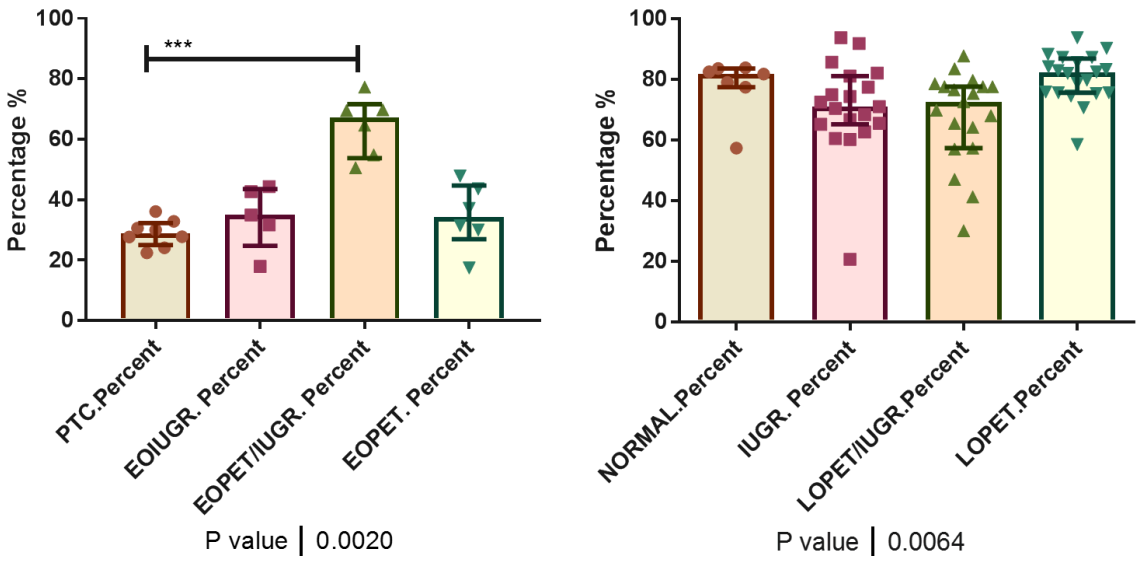

Figure 4-10 Oxidative metabolism/stress marker 8-OHdG overall scoring in immunolabelled slides in early and late onset placental pathologies. (A) Oxidative metabolism 8-OHdG marker positivity percentages in early onset pathologies as EOIUGR (n=5), EOPET/IUGR (n=12), EOPET (n=6) and preterm control (n=8) placentas showed significant differences across groups (p=0.002, Kruskal-Wallis). EOPET/IUGR placentas showed significantly higher 8-OHdG positivity compared to preterm control (PTC) (67% vs 22.6%, *p*=0.0005, Dunn's post-hoc multiple comparisons test). (B) Oxidative metabolism 8OHdG marker positivity percentages in late onset pathologies compared to term control placentas. No differences were found across late-onset gestational disease showed significant differences as well (p= 0.0064, Kruskal-Wallis). Lines represent medians and IQR. ***p<0.001.

Late onset placental pathologies also showed a significant difference of the percentage of cells that displayed oxidative stress expression (Figure 4-10B). However, there were no significant differences between any of the placental dysfunction groups compared to its term control (Figure 4-10B).

On further sub-analysis of the different scoring grades, placentas from late onset IUGR and LOPET/IUGR showed a significant rise in the percentage of cells weakly stained with oxidative stress marker (1+) compared to term control (Figure 4-11A). 8-OHdG marker percentages of strongly stained cells (3+) in late onset pathologies showed significant differences across groups (p=0.02, Kruskal-Wallis), but there were no difference between any of the individual groups compared to control (Figure 4-11C).

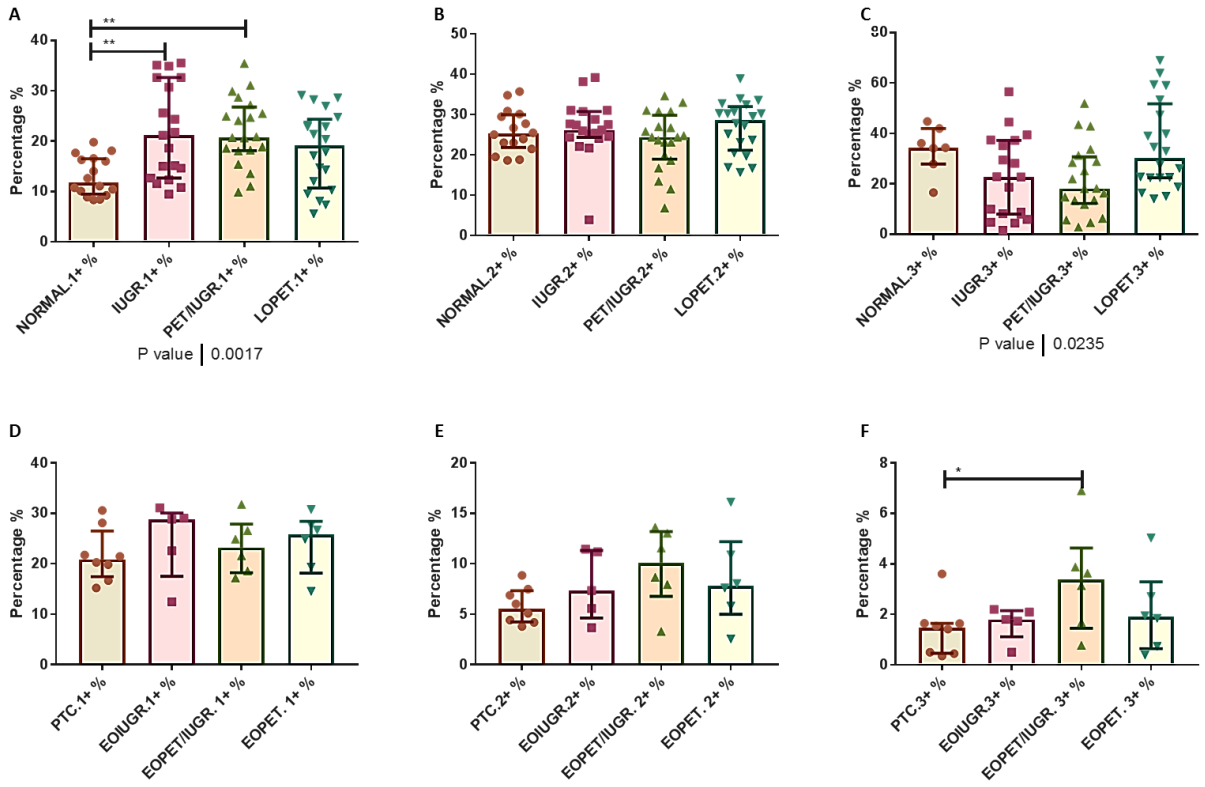

Figure 4-11 Oxidative metabolism/stress marker 8OHdG differential scoring intensities in immunolabelled slides in early and late onset placental pathologies. (A) 8-OHdG marker percentages of weakly stained cells (1+) in late onset pathologies compared to term control placentas. Term control placentas had lower percentages of weakly stained 1+ cells compared to IUGR and EOPET/IUGR placentas (13% vs 21.88% and 21.83% respectively, *adj. p*=0.003 and *p=0.001 respectively)*. (B) 8-OHdG marker percentages of moderately stained cells (2+) in late onset pathologies compared to term control placentas. No difference were found across groups. (C) 8-OHdG marker percentages of strongly stained cells (3+) in late onset pathologies showed significant differences across groups (p=0.02, Kruskal-Wallis), but there were no difference between any of the individual groups compared to control. (D) 8-OHdG marker percentages of weakly stained cells (1+) in early onset pathologies compared to preterm control placentas. No difference were found across groups. (E) 8-OHdG marker percentages of moderately stained cells (2+) in early onset pathologies compared to preterm control placentas. No difference were found across groups except for a trend increase in moderately stained cells in EOPET/IUGR compared to control (10.1% vs 5.5%, *p*=0.08, Mann Whitney test). (F) 8-OHdG marker percentages of strongly stained cells (3+) in early onset pathologies compared to preterm control placentas. Placentas from EOPET/IUGR pregnancies showed a significantly higher percentages of strongly stained cells compared to preterm control (18.1% vs 8.5%, *adj. p*=0.04, post-hoc Dunn's multiple comparison's test). PTC= preterm control IUGR= Term IUGR. LOPET/IUGR= Late onset preeclampsia with growth restriction. LOPET= late-onset preeclampsia. EOIUGR= Early-onset IUGR, EOPET/IUGR= Early-onset preeclampsia with IUGR, EOPET= Early-onset preeclampsia. Lines represent medians and IQR.

4.4.3.2 Fetal/maternal side distribution

The fetal/maternal side zonal distribution of the oxidative marker 8-OHdG, showed a maternal side predominance of 8-OHdG staining in term control and EOPET/IUGR

placentas. Conversely, term IUGR placenta showed a reduction of the maternal side distribution (Figure 4-12) to become similar to the fetal side expression.

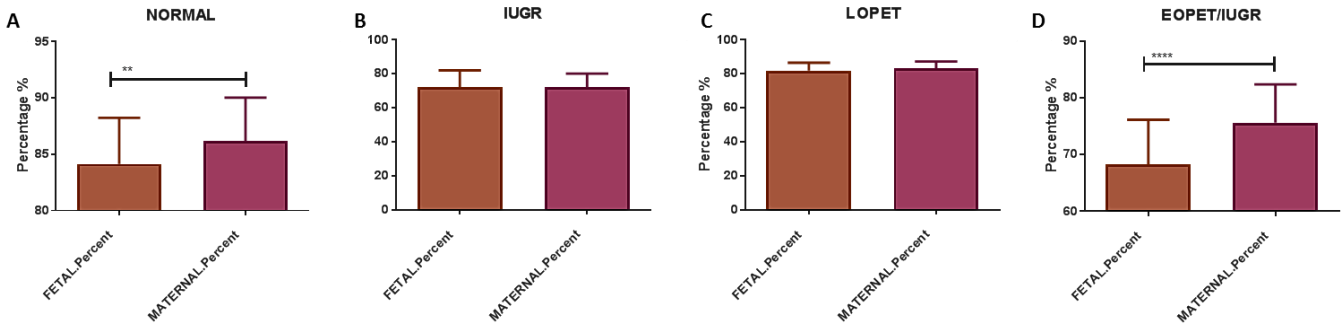

Figure 4-12 Differential fetal/maternal side distribution of 8OHdG marker positivity in placental pathology. (A) Fetal/maternal 8-OHdG marker positivity in term control placenta. Fetal side showed a markedly reduced 8-OHdG marker positivity compared to the maternal side (p=0.003, Wilcoxon test). (B) Fetal/maternal 8-OHdG marker positivity in term IUGR placenta. No differences in zonal distribution was found. (C) Fetal/maternal 8-OHdG marker positivity in term LOPET placenta. No differences in zonal distribution was found. (D) Fetal/maternal 8-OHdG marker positivity in term EOPET/IUGR placenta. Fetal side showed a markedly reduced 8OHdG marker positivity compared to the maternal side (p<0.0001, Wilcoxon test). IUGR=Term IUGR.. LOPET=late-onset preeclampsia, EOPET/IUGR= Early-onset preeclampsia with IUGR. Error bars represent medians and IQR.

4.4.4 Scavenger cell marker CD163

The hemoglobin (Hb) scavenger receptor CD163 is a macrophage-specific receptor protein. Its upregulated expression, in inflammatory tissues, leads to crucial changes in the macrophage switch to alternative activated phenotypes (352). Thus, an upregulated CD163 expression in macrophages is thought to be a feature of tissues adapting to inflammation. It is thus hypothesised that CD163 is indirectly contributing to the anti-inflammatory tissue response via scavenging the oxidative and pro-inflammatory Hb (352). Their study in different entities of placental dysfunction might shed light on one of the adaptation mechanisms by which the placenta responds to the inflammatory stress.

4.4.4.1 Expression patterns and locations

The commonest feature of the CD163 expression in the placenta was its perivascular stromal distribution; it was expressed only in the stroma with predilection around placental vascularity sparing the villous and extravillous trophoblasts (Figure 4-13).

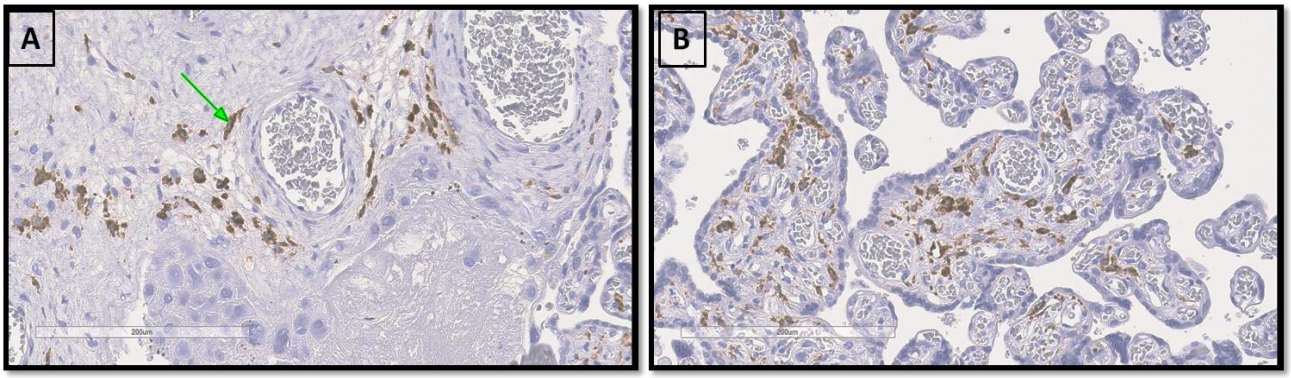

Figure 4-13 Representative image of a placental slides immunolabelled with the macrophage marker CD163. (A) Representative image of the basal plate of the placenta showing perivascular distribution (green arrow). (B) Representative image of the chorionic villi showing the CD163 marker (brown) to be distributed in the villous stroma around placental vasculature.

4.4.4.2 CD163-stained macrophage quantification in placental dysfunction

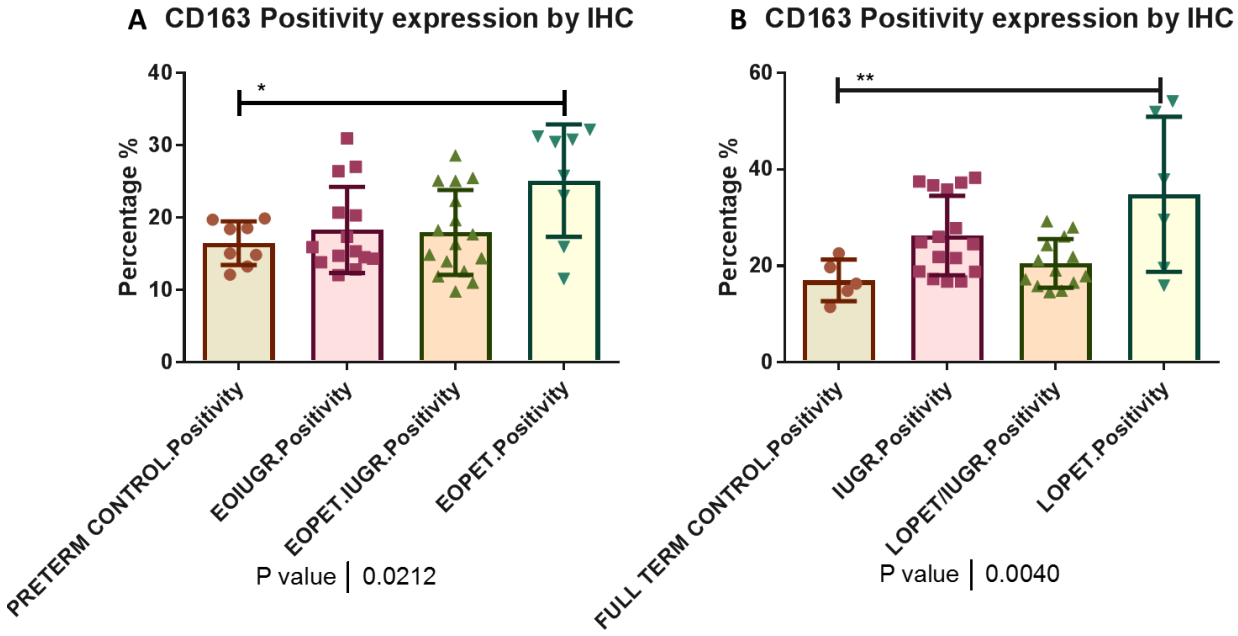

Figure 4-14 Percentages positivity of the macrophage biomarker CD163 in placentas of early (A) & late-onset (B) gestational diseases. Statistical analysis was done by Analysis of Variance (ANOVA) with Dunnett's *post-hoc* multiple comparisons test. Where * ($p<0.05$), ** ($p<0.01$). (A) Significant differences across early-onset placentae were evident (p=0.02, ANOVA). Placentas of EOPET pregnancies showed a significantly higher percentage of CD163 marker macrophages compared to preterm controls (25.1% vs 16.5%, adj. p=0.015). (B) Significant differences across late-onset placentae were evident (p=0.004, ANOVA). The percentage of the CD163 marker macrophage positivity was significantly higher in term preeclampsia compared to term controls (34.8% vs 17%, adj. p=0.004). Lines represent means and SD.

In early onset placental dysfunction, the CD163-stained macrophage expression patterns differed across placental dysfunction groups (*p=0.02)*, with placentas from EOPET pregnancies showing the highest CD163 expression compared to preterm control (25.1% vs 16.5%, *adj. p*= 0.01, Figure 4-14A). A similar expression pattern was found in late onset placental dysfunction, where difference in expression was significantly different across groups (*p*=0.004). Placentas from LOPET pregnancies had a significantly higher CD163 expression compared to term controls (26% vs 17%, *adj. p*= 0.004, Figure 4-14B).

4.4.5 Serial sections of programmed cell death (PCD) markers

The use of virtual pathology platforms has enabled researchers to follow and compare areas of pathological or research interest in serial sections stained with different biomarkers. The expression pattern of the same area of interest for different biomarkers can be studied in serial sections as seen in Figure 4-15.

Terminal placental villi with evident SNAs with or without fibrinous degeneration were examined in serial sections stained with H&E, M30 (apoptosis marker), LC3 (autophagy marker) and 8OHdG (oxidative stress marker) sequentially. The slides were then scanned and digitised to be opened and annotated with Aperio ImageScope.

Serial immunohistochemically labelled placental slides enabled us to study the same region of interest and visualised the patterns of expression of the different markers. It was observed that M30 apoptotic marker was associated with areas of fibrinoid degenerations. SNAs were also associated with areas of autophagy marker LC3 expression (Figure 4-15).

Exploring the correlations of the expression patterns between biomarkers of programmed cell death (PCD) in placental dysfunction, and their biological dependence or independence on the type of the placental dysfunction, was sought using linear regression models and correlation coefficients.

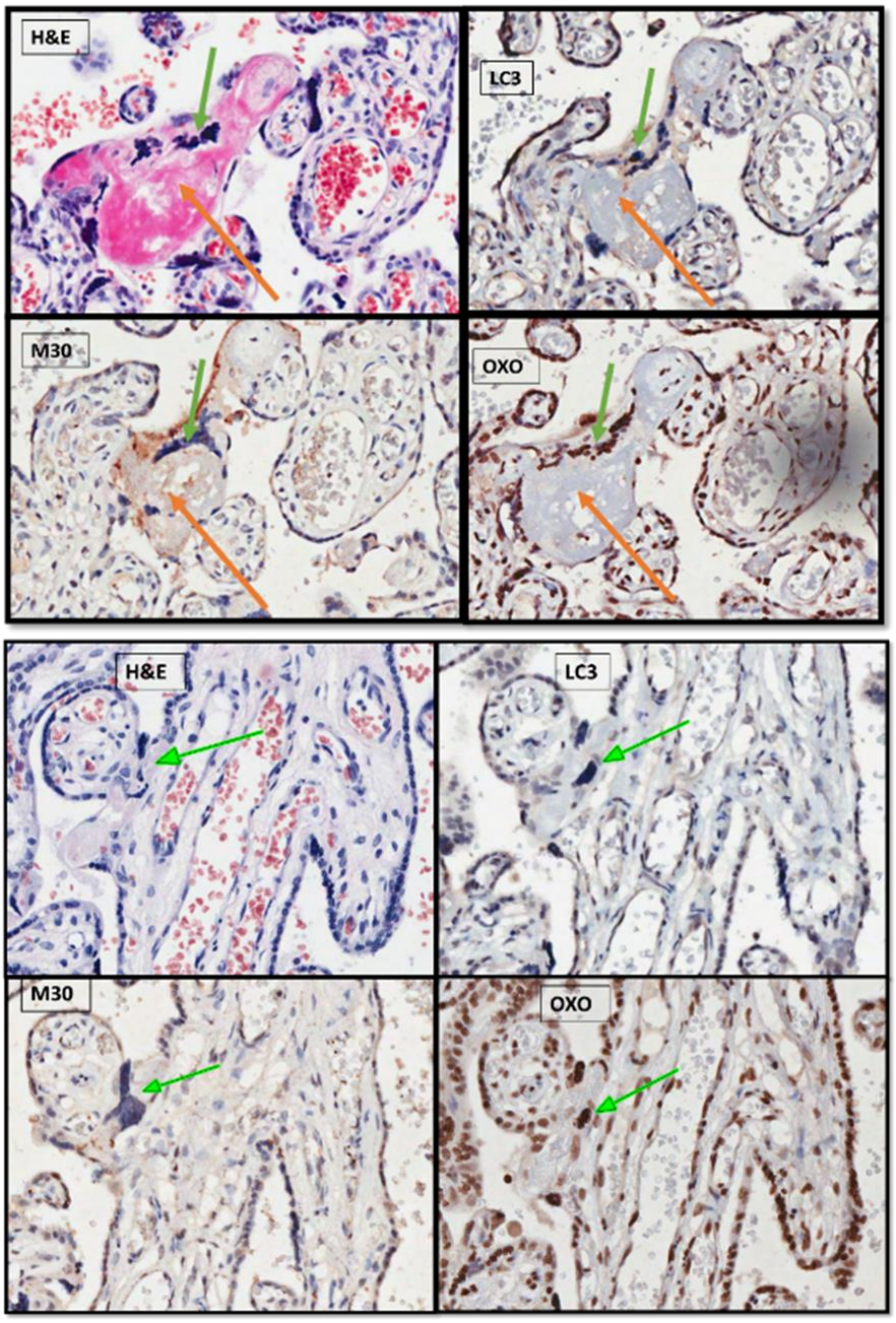

Figure 4-15 Placental serial sections stained by H&E, M30, LC3 and oxidative markers. Green arrows point to syncytial nuclear aggregates, orange arrows point to fibrinous degenerations. H&E= Haematoxylin & Eosin, OXO= oxidative 8-OHdG marker. It shows a higher propensity of LC3 staining in the regions of SNAs as well as fibrinoid degenerations associated with an M30 apoptotic staining.

4.4.6 Correlations between IHC biomarkers

Scoring the percentage of each marker's positivity has helped to identify whether there was a relationship between the studied biomarkers. Linear regression models were constructed to identify correlation coefficients between each and every biomarker.

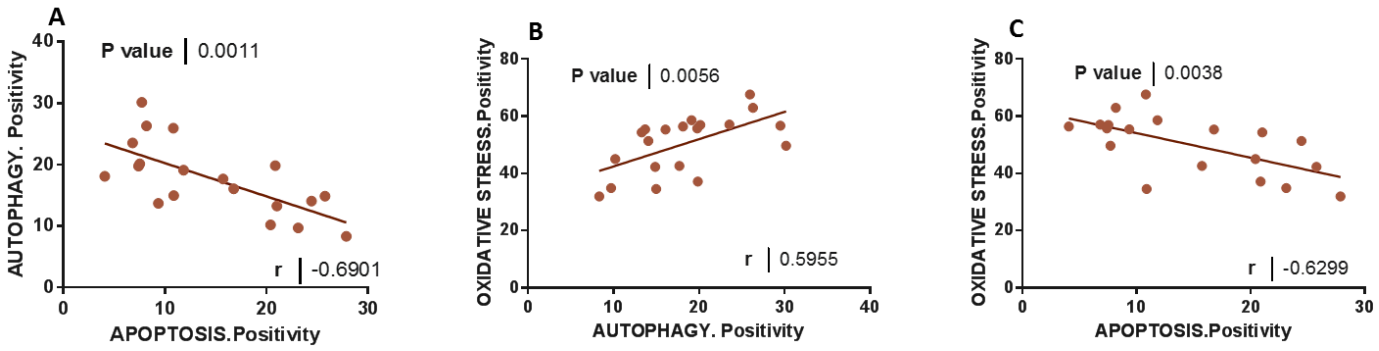

Figure 4-16 Correlation analyses between apoptosis, autophagy and oxidative stress biomarkers in placental samples. The graphs (A) A linear regression analysis between autophagy LC3 and apoptotic marker M30 shows a negative correlation between the two markers (Spearman correlation r= -0.69, *p=0.001)*. (B) A linear regression analysis between oxidative stress 8OHdG marker and autophagy marker LC3 shows a positive linear relationship (Spearman correlation r=0.59, *p=0.005).* (C) A linear regression analysis between the oxidative stress 8OHdG marker and apoptotic marker M30 shows a negative correlation between the two markers (Spearman correlation r= -0.62, *p=0.003)*.

Results showed that placental oxidative stress 8-OHdG marker positivity was positively correlated to the autophagy marker LC3 positivity (Figure 4-16A). Conversely, oxidative stress 8-OHdG marker positivity was negatively correlated to the apoptotic M30 marker positivity (Figure 4-16C). Moreover, results demonstrated that autophagy marker LC3 positivity had a negative correlation to the apoptotic M30 marker positivity (Figure 4-16B).

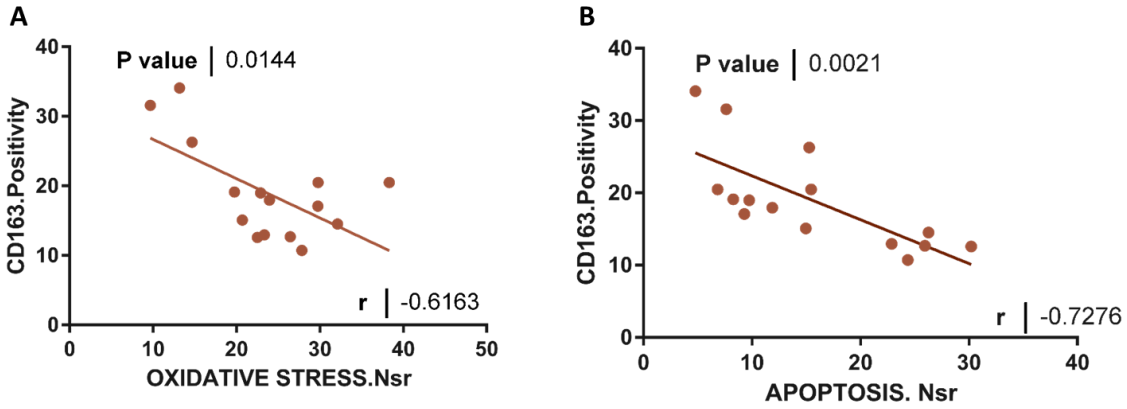

Figure 4-17 Correlation and regression analyses of CD163 marker to apoptotic M30 and oxidative 8OHdG biomarkers. (A) A linear regression analysis between CD163 marker and strong oxidative stress marker 8OHdG positivity showing a negative correlation (Pearson r= -0.61, *p*=0.01). (B) A linear regression analysis between CD163 marker and strong apoptotic M30 marker positivity also showing a negative correlation (Pearson r= -0.72, *p*=0.002).

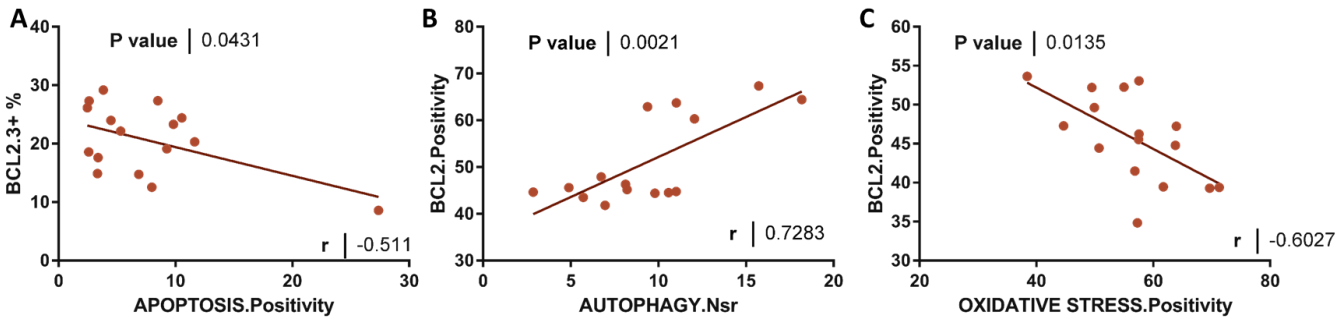

Figure 4-18 Correlation and regression analyses of Bcl-2 marker expression profiles to the apoptotic M30, autophagy LC3 and oxidative 8OHdG biomarkers' expression in the placenta. (A) Linear regression analysis between the percentages of Bcl-2 (2+) stained cells and apoptotic M30 marker positivity showed a negative correlation (Pearson r= -0.51, *p*=0.04). (B) Linear regression analysis between Bcl-2 positivity and LC3 autophagy marker expression found a strong positive correlation between the two (Pearson r= 0.72, *p*=0.002). (C) Linear regression analysis showed a negative correlation between the Bcl-2 positivity and 8OHdG marker positivity in the studied placenta (Pearson r= -0.6, *p*= 0.01).

Furthermore, the expression profile of the macrophage-specific receptor protein, CD163, known for its tissue scavenging function, was found to correlate negatively with the oxidative stress marker 8-OHdG strong staining in the studied placenta (Pearson r= -0.61, Figure 4-17A). A similar trend was also found to the placental apoptosis M30 strong staining expression (Pearson r= -0.72, Figure 4-17B).

Interestingly, our results have illustrated a unique relationship between Bcl-2 expression and the different biomarkers of programmed cell death. That is to say, the anti-apoptotic Bcl-2 expression was positively correlated with the LC3 autophagy marker expression (Pearson correlation r= 0.72, Figure 4-18B). On the other hand, it was negatively correlated with both 8-OHdG and M30 marker expression in our placentas (Pearson, r= -0.61 and r= -0.51 respectively, Figure 4-18).

Using an online TMA navigator software, we were able to construct a heat map (Figure 4-19) of the all the markers of the programmed cell death with their different intensities in a correlation matrix (353). This helped us in visualising the relationship between the different placental biomarkers and their intensities, as well as the strength of such relationships. This relationship can now be further studied in different types of placental dysfunction to check if it is consistent or type specific relationship.

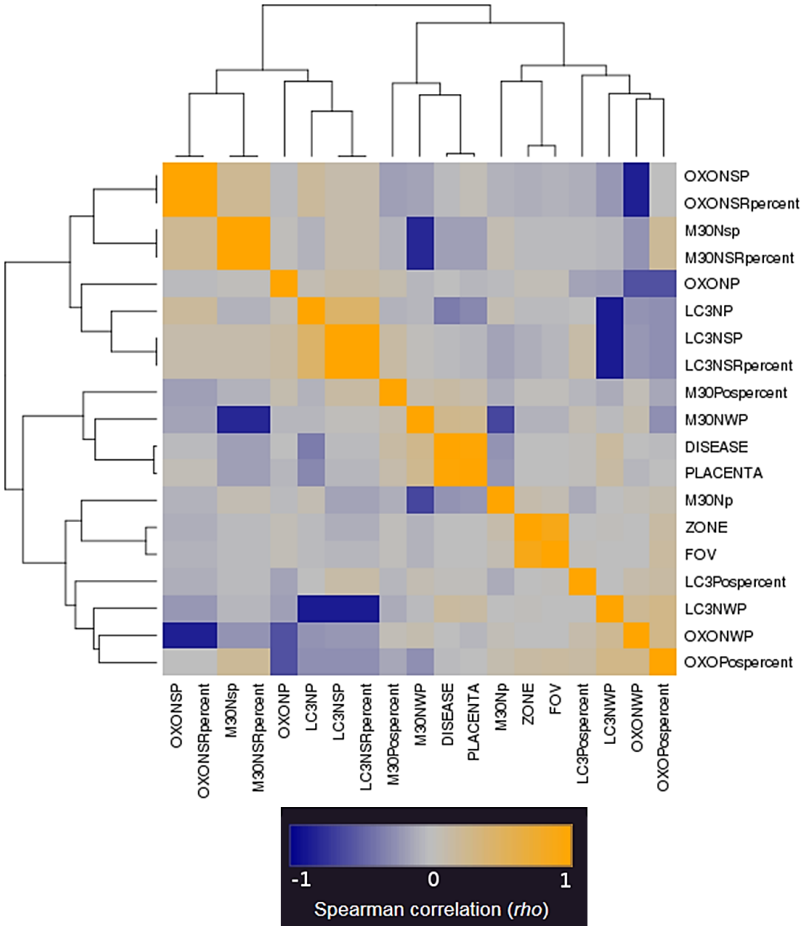

Figure 4-19 Marker heat map and correlation matrix for programmed cell death biomarkers. Each output was entered as a variable including the disease category, placenta, placental zone (fetal or maternal) and the fields of vision (FOV) within each zone. This correlation matrix showed a positive correlation between the disease status and the placenta when put as independent variables confirming that the effect we see is due to the placental pathology and not any confounding variables. Yellow box represent positive correlation while the blue represent negative correlation. Data were visualised using online TMA navigator (353).

4.4.7 Correlations between IHC biomarkers and stereology-derived capillary and SNA volumes

Since slides from each placenta were serial sectioned, they were serially stained with H&E and markers of PCD. Quantified volumes of the placental structures like placental capillary and syncytial nuclear aggregates using stereological techniques were then pairwise correlated to their biomarker expressions. Our results demonstrated that placental ischaemia was associated with a rise in the percentages of the strongly stained oxidative stress marker expression as well as that of the autophagy and apoptotic markers (Pearson r= -0.61, -0.4 and -0.5 respectively, Figure 4-20).

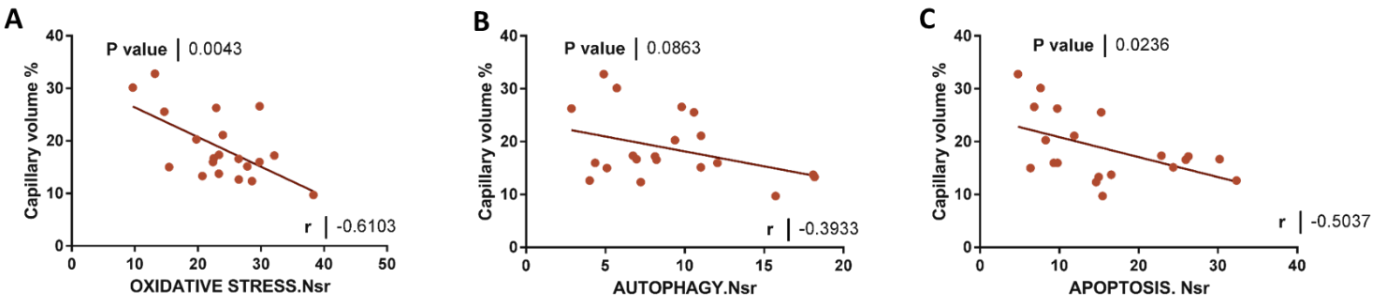

Figure 4-20 Correlation and regression analyses of placental capillary volumes to the apoptotic M30, autophagy LC3 and oxidative 8OHdG biomarkers' expression in the placenta. (A) Linear regression analysis between the percentages placental capillary volumes and 8-OHdG strong marker positivity in the studied placenta showed a negative correlation (Pearson r= -0.61, *p*=0.004) (B) Linear regression analysis between placental capillary volumes and LC3 autophagy strong marker expression found a negative correlation between the two (Pearson r= -0.39, *p*=0.08). (C) Linear regression analysis showed a negative correlation between the placental capillary volumes and the apoptotic M30 strong marker positivity (Pearson r= -0.50, *p*=0.02).

Our results also revealed a statistically significant positive correlation between the placental SNA volumes and the autophagy LC3 marker positivity. That is to say, a higher autophagy activation was associated with abundant SNA volumes in our placentas (Pearson r= 0.45, *p=0.04,* Figure 4-21). On the other hand, placental apoptotic and oxidative marker expression profiles did not show a significant positive or negative correlation to the studied placental SNA volumes (Figure 4-21).

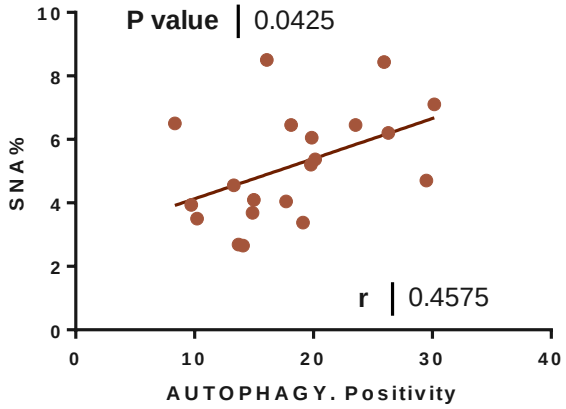

Figure 4-21 Correlation and regression analyses of placental SNA volumes to the apoptotic M30, autophagy LC3 and oxidative 8OHdG biomarkers' expression in the placenta. Linear regression analysis between placental SNA volumes and LC3 autophagy marker positivity found a positive correlation between the two (Pearson r= 0.45, *p*=0.04).

4.4.8 Placental type specific changes

Our results have shown that placental autophagy might regulate the interactions between nuclear oxidative metabolism/stress and trophoblast apoptosis. It is tempting to speculate that the way the placenta reacts to stressful event depends, not only on the intensity and the duration of the accrued stress, but also on the way the placenta is programmed to respond to such stress; different placental dysfunction types might have varying responses to stress events. Our results have shown that there could be a balance between oxidative stress and apoptosis partly regulated by the placental autophagy.

The biological correlations between the oxidative stress, autophagy and apoptosis markers were also studied in the following placentas: control placenta, term IUGR, term preeclampsia and severe early onset PET with IUGR to explore whether these biological relationships is different in each gestational disease (Figure 4-22).

In term control placenta, the expression profiles of the nuclear oxidative metabolism 8-OHdG biomarker did not correlate with either the autophagy marker or the apoptotic M30 biomarker expression (Figure 4-22A, B & C).

Conversely, each placental dysfunction had its unique biological behaviour, where hypertensive preeclamptic placentas from pregnancies diagnosed with LOPET and EOPET/IUGR showed a reciprocal inverse relationship between the LC3 autophagy marker expression and that of the apoptotic M30 expression; the higher the autophagy, the lower the apoptosis. This negative correlation was not consistent in placentas from IUGR complicated pregnancies, where higher autophagy expression was associated with higher apoptotic positivity (Figure 4-22 D, J & G).

Moreover, higher oxidative stress marker expression in LOPET and EOPET/IUGR placentas was associated with a lower apoptotic M30 marker positivity (Figure 4-22 K and E) compared to the opposite effect in IUGR pregnancies that was associated with a higher apoptosis expression (Figure 4-22H). On the other hand, there were no placental specific differences in the correlation between oxidative stress biomarker and the autophagy expression in placentas of hypertensive and non-hypertensive gestational diseases, where placental higher oxidative stress was associated with higher autophagy expression across placental dysfunction (Figure 4-22F, I and L).

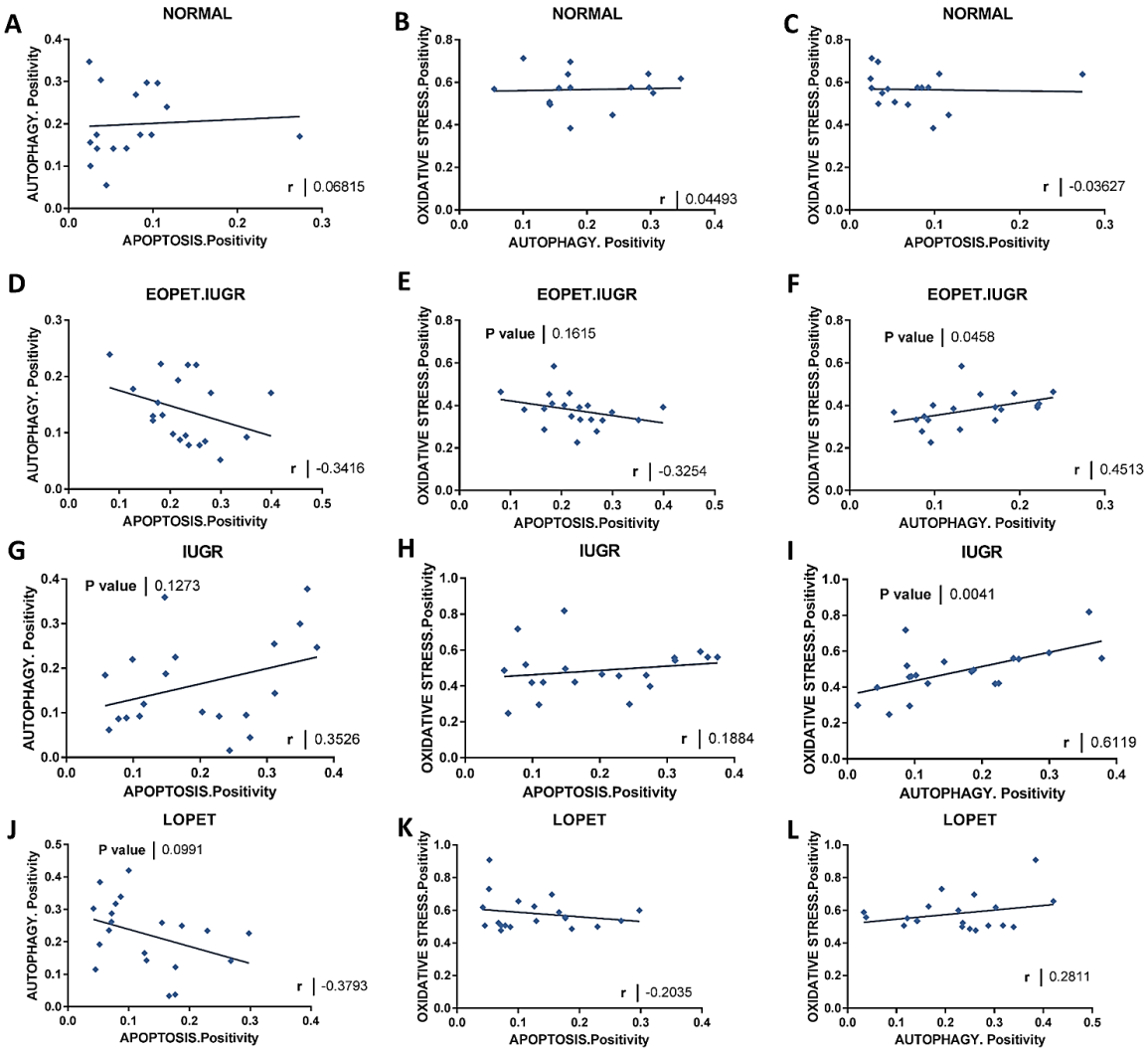

Figure 4-22 **Correlation and regression analyses between apoptosis, autophagy and oxidative stress biomarkers in term control, IUGR, LOPET and EOPET/IUGR placental samples.** (A) Linear regression analysis between apoptotic M30 positivity and autophagy marker LC3 showing no linear relationship in term control placenta (Spearman correlation r= 0.06). (B) A linear regression analysis between oxidative stress 8OHdG marker and apoptotic M30 positivity showing no linear relationship in term control placenta (Spearman correlation r=0.04). (C) A linear regression analysis between oxidative stress 8OHdG marker and autophagy marker LC3 shows no linear relationship in term control placenta (Spearman correlation r=-0.03). (D) Linear regression analysis between apoptotic M30 positivity and autophagy marker LC3 showing negative linear relationship in EOPET/IUGR placenta (Spearman correlation r= -0.34). (E) A linear regression analysis between oxidative stress 8OHdG marker and apoptotic M30 positivity showing negative linear relationship in EOPET/IUGR placenta (Spearman correlation r= -0.32). (F) A linear regression analysis between oxidative stress 8OHdG marker and autophagy marker LC3 shows positive linear relationship in EOPET/IUGR placenta (Spearman correlation r=0.45, p=0.04). (G) Linear regression analysis between apoptotic M30 positivity and autophagy marker LC3 showing a positive linear relationship in IUGR placenta (Spearman correlation r= 0.35). (H) A linear regression analysis between oxidative stress 8OHdG marker and apoptotic M30 positivity showing weak positive linear relationship in IUGR placenta (Spearman correlation r= 0.18). (I) A linear regression analysis between oxidative stress 8OHdG marker and autophagy marker LC3 shows strong positive linear relationship in IUGR placenta (Spearman correlation r=0.61, p=0.004). (J) Linear regression analysis between apoptotic M30 positivity and autophagy marker LC3 showing a negative linear relationship in LOPET placenta (Spearman correlation r= -0.38). (K) A linear regression analysis between oxidative stress 8OHdG marker and apoptotic M30 positivity showing a weak negative linear relationship in LOPET placenta (Spearman correlation r= -0.2). (L) A linear regression analysis between oxidative stress 8OHdG marker and autophagy marker LC3 shows positive linear relationship in LOPET placenta (Spearman correlation r=0.28).

4.5 Discussion

The present study assessed the expression of autophagy, nuclear oxidative stress and apoptotic immunolabelled biomarkers in hypertensive and non-hypertensive placental dysfunction from early and late onset gestational disease. The study also examined the intricate relationship of those markers with each other and with previously studied structural differences. The strength of our study was the examination of a broad range of clinical-pathological placental phenotypes from pregnancies with isolated growth restriction, isolated preeclampsia to preeclampsia with IUGR as well as in controlling for gestational age to minimise a potentially confounding effect on placental expression.

A new dimension of the study was the utilisation of an FDA-approved image analysis system, thus providing an extremely useful tool for the quantification of biomarkers on placental tissue specimens. This approach allowed us to benefit from the most advanced digital pathology system available today in an attempt to characterise placental dysfunction. Manual analysis of immunohistochemistry slides, despite widely used to provide an intensity score, is a time-consuming, variable process that poses a degree of subjectivity with an inherent degree of intra-observer and inter-observer variability (354). This is consistent with other studies that have found image analysis approaches to be objective and successful in identifying appropriate cut-off thresholds for biomarker positivity (354) as well as producing continuous estimates of the IHC data.

Moreover, the positive pixel count algorithm (PPC) utilised in our study was similarly used to quantify protein staining and establish correlations between different markers in both benign and malignant lymphoid tissue highlighting a potential role for viral proteins in the pathogenesis of lymphomas (355). Furthermore, survival was also linked to the immunohistochemically-expressed macrophage infiltration markers using Aperio image analysis (356). In breast cancer, digital image analysis has also showed great improvement in the quantification of protein expression (357) in addition to its success in semi-quantitative assessments of staining levels (358). Studies in breast cancer have also shown that IHC digital image analysis based measurements were in almost perfect agreement with the pathologist's visual scoring and were more accurate in detection of HER2 positive patients, recommending its integration into the routine pathology HER2 testing (359). PPC Image analysis applications were not limited to cancer but also

demonstrated effectiveness as a useful tool for quantifying immunohistochemical expression of inflammatory cells in the diagnosis and follow up of eosinophilic oesophagitis (360).

Our study showed that the apoptotic M30 marker was predominantly immunolocalised in the trophoblast layer and beneath perivillous deposits in relation to areas of fibrinous degeneration. These data were consistent with another study using TUNEL which showed positive apoptotic nuclei in relation to fibrin-type fibrinoid (88). Similarly, another study showed that cleaved CK-18 was mainly present in the syncytiotrophoblast cytoplasm, SNAs, and to a lesser degree in villous cytotrophoblast cells in normal placentas undergoing apoptosis (71).

Our results demonstrated that placentas from term IUGR as well as term and preterm preeclampsia with IUGR had a significantly higher trophoblastic apoptotic burden. This finding agrees with other semi-quantitative immuno-histochemical studies which have showed a higher expression of pro-apoptotic proteins in the syncytiotrophoblast layer, in term (361-364) IUGR placentas as well as in isolated villous cytotrophoblasts from preeclampsia and IUGR at term (365). The intrauterine growth of the fetus is believed to be determined mainly by the availability of nutrients (366) transferred across the syncytium, which is also responsible for hormone production, immune tolerance, as well as the exchange of the gas, nutrients and waste products (341).

Throughout pregnancy, the syncytium is regenerated via continuous syncytial fusion of the underlying proliferative villous cytotrophoblast cells. The trophoblast differentiation and fusion are linked to the initial stages of the apoptosis pathway (86) and counterbalanced by shedding of syncytial nuclei, thus an increase in syncytial nuclei may result from either increased syncytial fusion, or reduced shedding (10).

Since fusion of cytotrophoblast cells seems to retard the apoptotic progression in the syncytiotrophoblast. Thus, the inability to continuously regenerate by syncytial fusion leads to hastened syncytiotrophoblast apoptosis which may explain the high apoptotic burden in growth restriction. These understandings accredit apoptosis a principal role in villous trophoblast turnover (88). Moreover, this was validated by *in vitro* experiments with choriocarcinoma and primary trophoblast cells (367, 368) which demonstrated that this phosphatidylserine flip was integral to syncytial fusion and that antibodies blocking

this step hampered the syncytium formation. Another study using apoptotic staining indicated that apoptosis occurred readily in cytotrophoblasts but was markedly inhibited in the syncytiotrophoblast (369).

Typical apoptosis is well-characterized in its end stages by condensation of cytoplasmic dehydration, nuclear chromatin, and membrane blebbing, but with maintenance of organelle integrity (88). Interestingly, villous cytotrophoblast did not exhibit these typical signs of at any stage of pregnancy (370). Moreover, placental villi exhibited rare annular chromatin condensation which was limited to distinct areas of the syncytiotrophoblast (88). Furthermore, the basal nuclei of SNAs, together with the surrounding syncytiotrophoblast, displayed higher heterochromatin rather than annular chromatin condensations. Another atypical feature of the trophoblast apoptosis is that it is retarded for 3-4 weeks till the “execution stages” of the apoptotic machinery are activated in the syncytiotrophoblast nuclei (88).

A suggested explanation of this retarded syncytiotrophoblast apoptotic cascade is the transfer of the cytotrophoblast organelles to the neighbouring syncytiotrophoblast following syncytial fusion (62) along with the antiapoptotic proteins like Bcl-2 proteins and their mRNAs. However, since Bcl-2 has a limited half-life (371), antiapoptotic proteins, and apparently their corresponding mRNAs, may only be anticipated to impede syncytial apoptosis for a narrow window of time and in a focal manner.

Our IHC results displayed an increase of the Bcl-2 expression in preterm and term preeclampsia without IUGR compared to its gestational age-matched control. This result is consistent with another study where preeclamptic placental slides were immunostained with Bcl-2 then assessed semi-quantitatively. This study revealed that Bcl-2 expression was significantly greater in the villus trophoblast among term preeclamptic women compared with controls (372). Another report also showed an increase in placental expression of Bcl-2 as well in the maternal blood in preterm preeclampsia without IUGR (373).

Given that widespread uninhibited apoptosis in villi would be calamitous to the placenta, and to the developing fetus, therefore it is tempting to speculate that human villous trophoblasts display other mechanisms to maintain homeostasis and protect from dysregulated apoptosis. One mechanism by which cells protect themselves from

stressors is autophagy, which is known to play a prosurvival role in most cells and known to have an antiapoptotic role as well (96).

To decipher the exact role autophagy plays in response to normally occurring events and stresses in “normal” pregnancy and in placental dysfunction. We explored the positivity expression and distribution of LC3 autophagy marker analysed in randomly assigned FOVs in different types of placental dysfunction compared to it respective control. Our results demonstrated that autophagy is constitutively expressed in placentas from normal and abnormal pregnancies in a differential way and distribution. This study confirms reports from earlier studies that identified expression of autophagy in third trimester villous trophoblast (103, 158). These studies suggested that autophagy might be a constitutive process helping to survive periods of moderate nutrient depletion and/or oxidative stress occurring in normal pregnancy (159). Moreover, autophagy was also found to play an important role in placental development and pregnancy maintenance as one of the essential stress response pathways (141, 374).

Our study revealed that placentas from preeclampsia and hypertensive disorders had higher percentages of LC3 expression positivity patterns compared to its control, where EOPET/IUGR placentas had significantly higher LC3 positivity compared to preterm control (PTC) and EOPET had a trend increase compared to PTC (32.9% vs 22.6%, p=0.06, Figure 4-8A). Similarly, placenta from term preeclampsia pregnancies showed a trend increase in LC3 positivity. This was consistent with other studies also revealed that autophagy was induced in placentas with preeclampsia (158, 375). Moreover, in an in vitro study on trophoblasts from placenta with preeclampsia, showed that the expression of autophagy proteins such as Beclin-1, LC3 and the autophagosome formation levels were higher compared to normal placentas (376). Other studies showed that protein expression of LC3 expression using western blots was significantly increased in placentas of women with pregnancy induced hypertension like preeclampsia and gestational hypertension compared to normotensive pregnancies, irrespective of the presence or absence of IUGR suggesting that autophagy was induced in placentas of hypertensive disorders (377).

As regards to fetal/maternal zone distribution, our results showed that placentas from normal pregnancies displayed higher maternal side (towards the basal plate)

autophagic activity compared to the fetal side. This was reversed in placentas from preterm preeclampsia with IUGR, showing a significant reduction in the maternal side autophagic activity compared to fetal side. This suggests that various parts of the placenta are exposed to different kinds of stressors and might also respond differently, and that the placenta might not be a homogenous organ in terms of function. This novel differential fetal/maternal side expression might reflect on the placental maternal/fetal side differences in function. An observation that has been reported in a study set to compare placental elasticity using elastosonography in preeclamptic and normal pregnancies found that the most significant difference was at the fetal side of the placenta towards the umbilical cord compared to the maternal side. The study also suggested that trophoblastic vasculopathy might lead to higher syncytial knots and fibrin deposition, thus increasing the placental stiffness (378). This indicates the importance of the fetal/maternal side structural and functional discrepancies in the placenta and the need for more studies to explore such differences and relate them to the pathogenesis of placental dysfunction.

Moreover, placentas from LOPET pregnancies showed a significantly higher autophagy activity in the fetal and not the maternal side of the placenta compared to the gestational age-matched control placenta (Figure 4-9E) suggesting that this effect might be specific to preeclampsia reflecting the higher stressful events in the fetal side of the placenta. Conversely, autophagy activity seen in normotensive term IUGR placentas showed a significant reduction in the maternal zone with no reduction in the fetal zone compared to control. This observation was replicated in placentas from hypertensive IUGR, indicating that reduction of the maternal side LC3 expression might be a growth restricted associated effect (Figure 4-9). These findings might shed more light on the importance of fetal/maternal zone differences as a part of the pathological signature of gestational diseases.

Regarding oxidative DNA damage in placental dysfunction, our results revealed that placentas from term IUGR, PET/IUGR and preeclampsia showed a significant rise in the percentage of cells weakly stained with 8-OHdG oxidative stress marker compared to term control. This data resembles that of reports showing higher placental levels of 8-hydroxy-2'-deoxy-guanosine (8-OHdG) in preeclamptic compared to normotensive pregnancies (379, 380). Moreover, other studies also showed that 8-OHdG levels were

significantly greater in IUGR or preeclampsia with IUGR than in placentas from normal pregnancy (381).

Our study also examined the expression patterns of the macrophage-specific scavenger receptor protein CD163 that was shown to be involved in anti-inflammatory immune-responses (382). Placentas from preterm and term preeclampsia showed higher expression positivity compared to its respective control. These results were consistent with a study that revealed significant increase in the CD163 expression in preterm preeclamptic decidua basalis compared with preterm control pregnancies (383). These results were also in accordance with another study that found a tendency towards higher soluble CD163 in the circulation of term preeclamptic women compared to healthy women, though not found to be of predictive value (384). This might be explained by the higher and more generalised inflammatory reaction associated with preeclampsia, thus leading to a more abundance of such scavengers of ROS, in an attempt to reduce their levels in the placenta.

Our results have shown a persistently positive correlation between the placental oxidative stress expressions and the autophagy marker LC3 positivity either overall correlation or disease specific correlations, suggesting that autophagy plays an important role in the placental recycling mechanisms of harmful oxidised molecules.

These results agree with several studies that proposed that oxidative stress and the discharge of oxidised macromolecules from the human placenta acted as a driver of cellular turnover in pathologies such as preeclampsia (97, 385). Moreover, failure to curb such oxidative stress and restoring homeostasis might result in tissue turnover and activation of apoptotic and necrotic mechanisms (386, 387). Furthermore, the induction of autophagy as a result of higher oxidative stress has also been demonstrated in several tissues and cell types (388-393).

Moreover, our study results have revealed an overall inverse correlation between placental autophagy and apoptosis. Placental analysis showed the higher the placental autophagy expression, the lower the apoptotic burden expressed. This is consistent with another study that revealed that LC3-II and cleaved poly(ADP-ribose) polymerase, (PARP) an apoptosis marker, expression were inversely related in cultured trophoblasts (96) indicating that there might be a balance between apoptosis and autophagy under

standard conditions. This suggests that autophagy activation in the trophoblasts might have a prosurvival role in an attempt to avoid late apoptotic cascade activation (96). Our study has showed that this inverse relationship was more pronounced in hypertensive preeclamptic placentas as pregnancies diagnosed with LOPET and EOPET/IUGR. This negative correlation was not evident in placentas from IUGR complicated term pregnancies, where higher autophagy expression was associated with a higher apoptotic trophoblastic burden. A relationship that might explain the higher apoptotic M30 expression in placentas of term IUGR pregnancies in response to oxidative stress displayed in our study.

In addition, our study showed that the levels of placental antiapoptotic Bcl-2 expression was associated with higher LC3 autophagy marker positivity, suggesting a possible synergistic role in the prosurvival mechanisms exerted on the syncytiotrophoblast. This might explain the delayed “execution stages” of the apoptotic machinery activated in the syncytiotrophoblast nuclei (88). The synergistic autophagy and anti-apoptotic function proposed by this study was consistent with studies showing that the release of Bcl-2 from activated autophagy protein complexes might free these molecules to block the intrinsic and extrinsic pathways of apoptosis (139, 394).

On the other hand, it is not known whether this prosurvival cascade might constitute a temporary measure to delay the inevitable or if it can avert the apoptotic pathway completely. It is suggested that autophagy might constitute a futile attempt for dying cells to adjust to lethal stress rather than a mechanism for cell death execution (395). However, autophagy inhibition was not found to prevent apoptotic nuclear shrinkage or to suppress the loss of plasma membrane integrity. Nonetheless, secondary necrosis was significantly augmented in numerous cases of autophagy inhibition, thus supporting the idea that autophagy might act mainly as a cytoprotective rather than a cytotoxic mechanism (396). Furthermore, several reports, in cultured human or mouse cells, revealed that depletion of autophagy genes commonly failed to provide long-term shelter against cell death after induction by a range of stressors, and rather accelerated their apoptotic or necrotic demise (113, 397, 398)

It is tempting to speculate that the way the placenta reacts to stressful event depends not only on the intensity of the malicious stress, or the duration of the accrued stress

but also on the way the placenta is programmed to respond to such stress. Our results have shown that there might a sort of balance between oxidative stress and apoptosis partly regulated by the placental autophagy.

In summary, our study was able to discriminate a pathologically distinct placental expression of programmed cell death markers from interlinked clinically-phenotyped gestational diseases. In addition, this study used a novel objective method of analysing the immunostained placental slides using an image analysis algorithm. Furthermore, the use of a hierarchical multilevel representative random sampling technique from the placenta down to the blocks slides and finally to the fields of visions has given strength and precision to this study. This study, to the best of our knowledge, is the first to quantify objectively autophagy expression in fetal/maternal zones of the placenta.

In conclusion, our results showed that each gestational disease has a unique signature pattern of autophagy activity regarding its degrees and distribution in the fetal/ maternal zone (Figure 4-9). Furthermore, the detection of trends across placental groups may help to characterize placentas and provide precincts for sub-phenotyping pathological placentas. Further research is needed to identify the causes of these distinctive effects on the genetic and epigenetic level and whether they can explain differential protein levels of PCD marker seen in placental dysfunction.

Chapter 5
Genes and miRNAs regulating placental autophagy

5.1 Introduction

Chapter 4 has emphasised the importance of autophagy expression in the pathophysiological pathway towards placental dysfunction. It also demonstrated that its biological importance is derived from autophagy's intricate balance with the apoptotic cascade and its interactions with other effect modifiers like oxidative DNA damage and anti-apoptotic proteins like Bcl-2. These observations were made at the protein level. In this chapter we determined whether these changes were due to direct genetic or epigenetic regulation in the placenta.

The miRNA discovery has revolutionised our understanding of the mechanisms regulating gene expression, adding a completely novel level of regulatory control (180, 202). Studies have also shown differential gene expression in PET involving epigenetic pathways regulation (208). Moreover, in addition to histone modification and DNA methylation, different placental miRNA expression patterns in different pathologic pregnancies like PET have been reported (209).

Most of the studies in placental miRNA research, though in its early stage, have focussed on cataloguing placental miRNA profiles or studying the difference in placental miRNA expression between placentas from normal pregnancies and those from placental insufficiency related complications (219). Several reports since 2007, using miRNA microarray and real-time PCR assays, have outlined the human miRNA expression patterns in placentas from normal and complicated pregnancies. These reports have shown that many miRNAs are differentially expressed in human placenta. However, the biological role of these miRNAs in the modulation of placental development and function remains unclear (227).

The significant role that miRNAs play as effective and novel modulators of the autophagy process is now being appreciated. It is also believed that the crosstalk between autophagy and miRNAs has the potential to reprogram and direct the

physiological and the biological functions of autophagy in normal and abnormal cellular development (187). Interestingly, the miRNA-autophagy interconnections are thought to promise intriguing possibilities in the coming years regarding strategies for future treatment, in view of their significant role in cellular adaptation, stress response and the pathogenesis of human disease (188). It will be interesting to further explore and understand these interactions in the reproductive field. Indeed, some may present promising novel possibilities for future treatment strategies.

5.2 Hypothesis

The differential expression of markers of autophagy in placental dysfunction is regulated by the interactions of genetic and miRNA machinery in placenta, and that these miRNAs have a role in the regulation of placental autophagy.

5.3 Aim and specific objectives

The aim of this chapter is to highlight the role of genetic and miRNAs in regulating autophagy in placental dysfunction.

The specific objectives were to quantify:

- The expression of classical autophagy gene (*MAP1LC3B*).
- The expression of autophagy-related genes (*PTPN2, PARK2, EGR1, BCL11B & YWHAE*).
- The expression of the anti-apoptotic gene (*BCL2*).
- The expression of programmed cell death-related miRNAs (miR-204, miR-182, miR-192, miR-145 and miR-let-7a) in placental dysfunction.
- Correlations between miRNAs and levels of protein expression from immunohistochemistry analysis.

5.4 Results

It has been widely acknowledged that a single molecule or a signalling pathway is unlikely to explain the pathogenesis of a complex syndrome like preeclampsia (399). Nonetheless, miRNAs have been found to play indispensable roles in the development of many organs, including the placenta, as well as the pathogenesis of several diseases by targeting panels of genes with their involvement in various biological processes (400). Consequently, the investigations of dysregulated miRNAs in placental dysfunction and genes targeted by those miRNAs are likely to be novel steps into better comprehension of the development and pathophysiology of these pregnancy-specific syndromes (401)

5.4.1 Data mining for target genes of autophagy-related miRNAs

There is a paucity of information available on target genes of placental-operated miRNAs that function in the human placenta, let alone autophagy-related genes. A review of the literature was used to identify miRNAs that were dysregulated in placental dysfunction (i.e. PET and/or IUGR). Following that, a literature search was conducted to check if any of these miRNAs were linked to the autophagy pathway in other organs and systems, hence identify those placental dysfunction-related miRNAs that had links to the autophagy cascade. Each of these miRNAs were searched in five miRNA databases (TargetScan[7], PicTar[8], PITA[9], Microcosm[10] and miRDB[11]) to identify target genes that were mutually found in more than one database. Target genes were cross compared with the Human Autophagy Database[12] to identify common target genes that have been linked to autophagy research and these were later studied by quantitative PCR.

[7] http://www.targetscan.org
[8] http://pictar.mdc-berlin.de
[9] http://genie.weizmann.ac.il/pubs/mir07/mir07_dyn_data.html
[10] http://www.ebi.ac.uk/enright-srv/microcosm/cgi-bin/targets/v5/search.pl
[11] http://mirdb.org/miRDB/index.html
[12] http://autophagy.lu/clustering/

In the miRDB database, all the predicted gene targets had prediction scores between 50 -100 by the computational target prediction algorithm and ordered by prediction score. The higher the score, the more probable it is a genuine target (402).

In the Microcosm database[13], the miRanda algorithm was used to scan the sequences of all present miRNAs against 3' UTR sequences of that genome. This algorithm adopts dynamic programming techniques to scan for optimal local seed complementarity placements, corresponding to a double-stranded anti-parallel duplex with positive scoring given for base pair complementarity and a negative to mismatches.

In PITA miRNA database, the miRNA gene targets are ordered according to their energy score; the lower (more negative) the score, the stronger the microRNA binding to the given site is expected to be. As a rough rule of thumb, sites having “energy score” values below -10 are likely to be functional in endogenous expression levels of microRNAs. Nevertheless, the microRNA concentration determines the actual level of suppression, making sites with “energy score” values above -10 still functional at higher microRNA expression levels (403).

In TargetScan database, the miRNA gene targets are ordered according to a score given from the sum of several contributions from these features: site-type contribution, 3' pairing contribution, position contribution, TA (target site abundance) and SPS (seed-pairing stability) contribution, calculated as in Garcia et al., 2011 (404).

Several miRNAs were identified and their potential target genes were cross checked in more than one database. Genes which appeared in more than one database were examined further using a literature search to check if they were reported to have a role in the autophagy pathway.

5.4.1.1 Hsa-miR-204-5p

Data mining for potential target genes for miR-204-5p revealed that programmed cell death-related genes were among the potential target genes as *MAP1LC3B, BCL2, BCL11B, EGR1, RAB22A*, and *C9orf72*. *MPA1LC3b* and *BCL2* were targets in four

[13] http://www.ebi.ac.uk/enright-srv/microcosm/htdocs/targets/v5/FAQ.html

out of the five searched databases (Table 5-1). Another consistent target of miR-204 in two of the databases was the Insulin growth factor binding protein-5 (*IGFBP5*), an important part of the IGF axis, and suggested to have a role in fetal and placental growth potential in preeclampsia (405).

Possible target genes	**TargetScan**	**PicTar**	**PITA**	**MicroCosm**	**miRDB**
SLC37A3	1				
KLF12		1			
PLCXD3			1		
SCTR				1, 2	
C9orf72	13				1
RAB22A	4	2			2
AP1S2	3				3
TGFBRAP1				5, 6	
NP_997211.2				9, 10	
ADCY6		10, 11			
BCL11B		16, 17			
C2orf68	17				25
EPHB6	21				17
PPM1K	18				26
IGFBP5	43		26		
PIGF				32, 33, 34	
MGAT3	33				23
EGR1			285		560
BCL2	229	33	1348		238
MAP1LC3B	231	174	2626		250

Table 5-1 Potential target genes of miR-204-5p searched in five miRNA databases numbered by their hierarchy of being a potential target gene in each database. Genes in bold were reported in the literature to have a role in the autophagy pathway.

5.4.1.2 Hsa-miR-182-5p

Similarly, miR-182-5p in silico data mining revealed a potential role in programmed cell death by targeting both *MAP1LC3B* and *BCL2* genes (Table 5-2).

Possible target genes	**TargetScan**	**PicTar**	**PITA**	**MicroCosm**	**miRDB**
RGS17	1				39
ADCY6		1,2			
ZFP1			1		
IL1F8				1	
ABHD13					1
MFAP3	3				2
PCNX	37				3
CTTN	4				10
MBNL2		4			30
EDNRB	6				32
PRKACB		6,7			15
ACTR2	7				14

NCALD	13				7
ANK3	35				8
JAZF1		9			38
HOXA9	36				9
TAGLN3	45				11
NRCAM	33				13
BCL2	270	92	1046		
MAP1LC3B	297	431	561		215

Table 5-2 Potential target genes of miR-182-5p searched in five miRNA databases numbered by their hierarchy of being a potential target gene in each database. Genes in bold were reported in the literature to have a role in the autophagy pathway.

5.4.1.3 Hsa-miR-192-5p

The target genes from the *in silico* mining of miR-192 included *MAP1LC3B*, *BCL2L11* and *PARK2* (Table 5-3). *PARK2* is the Parkin Protein Coding gene, that mediates the targeting of substrate proteins for proteasomal degradation and described to be necessary for mitophagy (autophagy of mitochondria) (406). Mutations in this gene are known to cause Parkinson disease (407, 408).

Possible target genes	**TargetScan**	**PicTar**	**PITA**	**MicroCosm**	**miRDB**
PABPC4	1				37
CCNT2	2	1, 2			7
CCDC83			1		
NP_001025167.1				1	
EREG	4				1
DYRK3		20, 21			2
ARFGEF1	3	10			6
DYRK1A		3,4,5,6,	40		
LPAR4	5				3
ZEB2	24				4
MSN			39		5
BHLHE22	6				19
DBT	18	43	7		
RPAP2	9				14
GPR22			22		9
IKZF2			12		11
WDR44	31				13
PARK2			2168	458	
BCL2L11			34		
MAP1LC3B			120	150	

Table 5-3 Potential target genes of miR-192-5p searched in five miRNA databases numbered by their hierarchy of being a potential target gene in each database. Genes in bold were reported in the literature to have a role in the autophagy pathway.

5.4.1.4 Hsa-miR-145-5p

Targets of miR-145-5p included genes related to autophagy and senescence like *MAP1LC3B*, *ATG16L2*, *ATG9B*, *BCL2, BCL11B, PARK2, PTPN2* and *YWHAE* (Table 5-4) as well as genes related to proliferation and growth like *IGF1R* and *IGFBP2*.

Possible target genes	**TargetScan**	**PicTar**	**PITA**	**MicroCosm**	**miRDB**
MAP1LC3B			4373		
BCL2			3519		
BCL11B			2584		
PARK2			5585		
PTPN2			5680		
YWHAE			4765		
ATG16L2				116	
ATG9B				367	
SOCS7			7	1	
FSCN1	2				24
ABHD17C	3				5
RTKN		28	3	12	
KCNA4	17				4
FLI1	5	35			30
ATP6V0B			39	5	
MYO5A	7	43			35
YTHDF2	27				7
IGF1R				42	
IGFBP2				782	

Table 5-4 Potential target genes of miR-145-5p searched in five miRNA databases numbered by their hierarchy of being a potential target gene in each database. Genes in bold were reported in the literature to have a role in the autophagy pathway.

5.4.1.5 Hsa-Let-7a

In silico miRNA database mining demonstrated that miR-let-7a targets were related to cell growth and proliferation like *IGF1R*, *IGFBP4*, *IGF2BP1* and *IGF1*, as well as the autophagy pathway genes (Table 5-5).

Possible target genes	**TargetScan**	**PicTar**	**PITA**	**MicroCosm**	**miRDB**
ATG4B	460				
ATG16L1	857		3177		
ATG9A	1017				
BCL2			2470		
BCL11B			5092		
PARK2			3967		
PTPN2			2888		
ATG12			3576		
ATG16L2			4769		
ATG9B			5098		
ATG10					350
SMARCAD1	11	16			1
HMGA2		1	13		
LIN28B	4				3

TRIM71	5				40
LRIG3	28				5
IGDCC3	6				13
GNPTAB	36				6
BZW1	35	13			7
BCL2L1	438	406, 408	2973	379	
IGF1R	64		1105		67
IGFBP4			1417		
IGF2BP1	94		1300		387
IGF1	829				
IGF2BP2	87				396
IGF2BP3	178		169		38

Table 5-5 Potential target genes of miR-let7a searched in five miRNA databases numbered by their hierarchy of being a potential target gene in each database. Genes in bold were reported in the literature to have a role in the autophagy pathway.

Several target genes of those miRNAs (Table 5-1, Table 5-2, Table 5-3, Table 5-4 and Table 5-5) were cross compared with the Human Autophagy Database[14] to identify common target genes that have been linked to autophagy research and these were later studied by quantitative PCR.

5.4.2 Quantitative real-time RT-PCR for autophagy-related genes

In order to validate if these target genes were differentially expressed in various groups of placental dysfunction, their expression was quantified by real-time qRT-PCR. Selected genes included *MAP1LC3B, BCL2, BCL11B, PTPN2, PARK2, EGR1*, and *YWHAE*. For comparing gene expression in our different groups, it was imperative to use internal controls, known as housekeeping genes (HKG) to ensure validity of our data.

5.4.2.1 Housekeeping genes (HKG) in placental dysfunction

Ideally, a HKG should be stable with comparable abundant expression in all samples, so that the gene of interest can be normalized to the HKG's expression. The use of the geometric mean of multiple HKG of at least two, and preferably three, is appropriate for optimal precision (300). Our study used the geomean of four different HKG expression (β-*actin*, *GABPDH*, *YWHAZ* and *TOP1*) commonly used in placental research for optimal normalisation of the genes of interest (409-411).

[14] http://autophagy.lu/clustering/

The HKG geomean displayed stability across the different groups of early and late placental dysfunction (Figure 5-1).

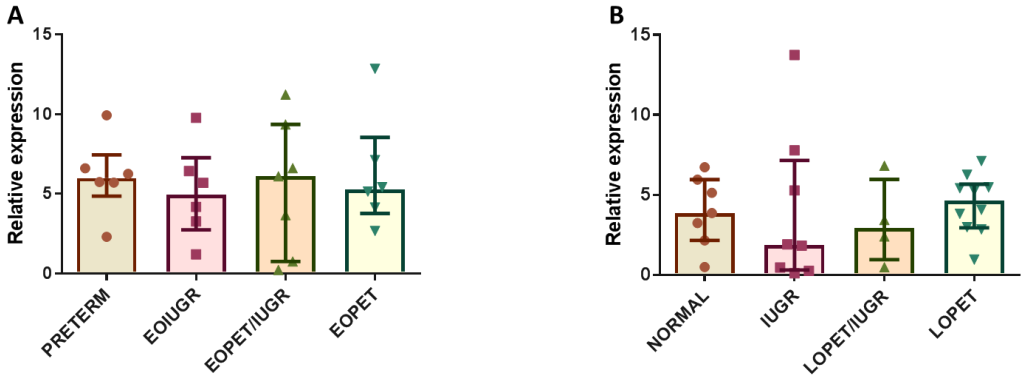

Figure 5-1 Stable expression of the geomean levels of the housekeeping genes (β-*actin*, *GABPDH, YWHAZ* and *TOP1*) in placental dysfunction by qRT-PCR. (A) Early-onset gestational diseases' geomean expression of β-actin, *GABPDH, YWHAZ and TOP1* by qRT-PCR. No differences across groups were found. (B) Late-onset gestational diseases' geomean expression of *β-actin, GABPDH, YWHAZ and TOP1* by qRT-PCR. No differences across groups were found. PRETERM= preterm control (n=6), NORMAL= Term control placenta (n=7), IUGR= Term IUGR (n=8). LOPET/IUGR= Late onset preeclampsia with growth restriction (n=4). LOPET= late-onset preeclampsia (n=10). EOIUGR= Early-onset IUGR (n=6), EOPET/IUGR= Early-onset preeclampsia with IUGR (n=7), EOPET= Early-onset preeclampsia (n=6).

5.4.2.2 Expression of Microtubule-Associated Protein 1 Light Chain 3 Beta (*MAP1LC3B*) gene

Though the differential expression of the *MAP1LC3B* gene expression in the early onset placental pathologies did not reveal significant difference across groups, but a stepwise reduction of gene expression pattern appeared across the groups from isolated early onset IUGR to early onset PET with IUGR and lastly to early onset PET (Figure 5-2A). Moreover, expression levels of the *MAP1LC3B* were higher in early onset pathologies compared to that in preterm control (PTC). Conversely, late onset placental dysfunction displayed lower levels of expression compared to term control placentas (Figure 5-2B).

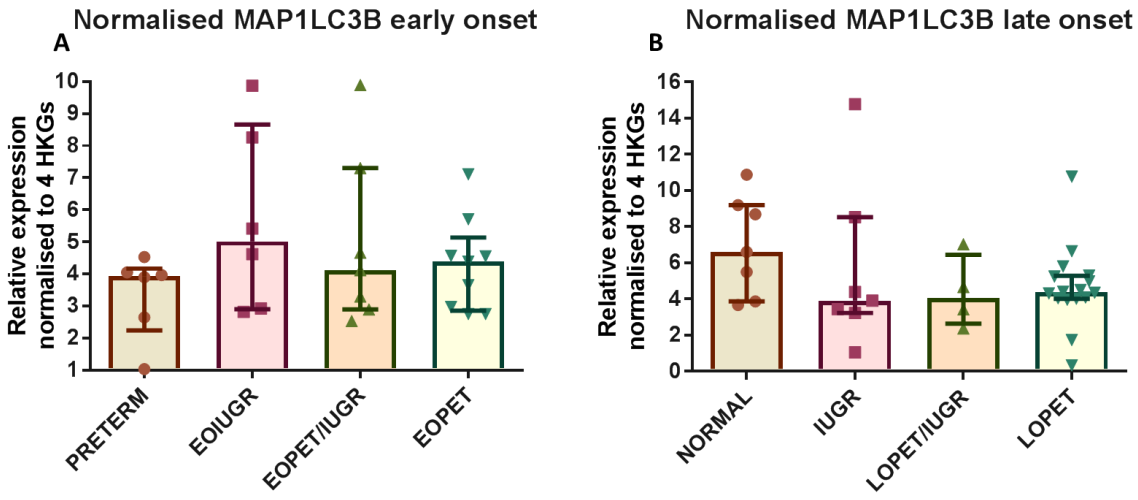

Figure 5-2 Expression levels of *MAP1LC3B* mRNA by qRT-PCR in (A) early onset placental dysfunction and (B) late onset placental dysfunction using specific primers to MAP1LC3B. Expression levels were normalised to the geomean of *β-actin, GAPDH, YWHAZ and TOP1* expression levels. Line is median and data significant if *p<0.05. Data analysed by Kruskal Wallis with Dunn's post-hoc multiple comparison's test. PRETERM= preterm control (n=6), NORMAL= Term control placenta (n=7), IUGR= Term IUGR (n=7). LOPET/IUGR= Late onset preeclampsia with growth restriction (n=4). LOPET= late-onset preeclampsia (n=16). EOIUGR= Early-onset IUGR (n=6), EOPET/IUGR= Early-onset preeclampsia with IUGR (n=7), EOPET= Early-onset preeclampsia (n=9).

5.4.2.3 Expression of selected ATG related genes (*PTPN2, PARK2, EGR1, BCL11B & YWHAE*)

5.4.2.3.1 Parkinson Protein 2 (*PARK2*)

Other autophagy-related genes identified by *in silico* data mining were assessed by qRT-PCR. The expression levels of PARK2 gene also displayed a downward stepwise pattern being the highest in pure EOIUGR and to a lesser degree in EOPET/IUGR and lowest in pure EOPET placentas. Expression levels were significantly different across early onset placental pathologies (Figure 5-3A) with upregulated PARK2 expression in placentas from EOIUGR and EOPET/IUGR pregnancies compared to preterm control placentas (Figure 5-3A).

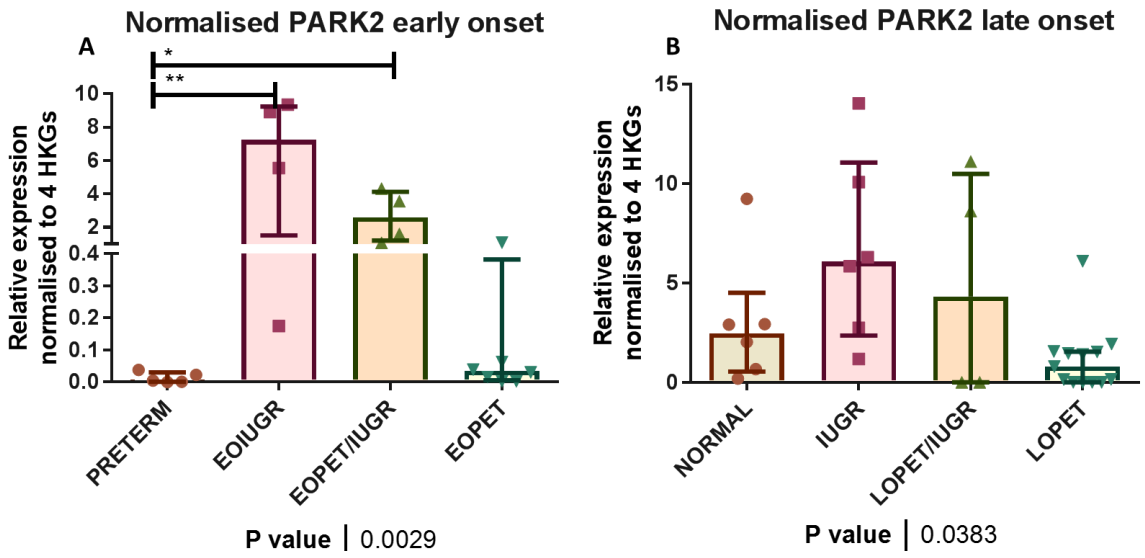

Figure 5-3 Expression levels of *PARK2* mRNA by qRT-PCR in (A) early onset placental dysfunction and (B) late onset placental dysfunction using specific primers to PARK2. Expression levels were normalised to the geomean of *β-actin, GAPDH, YWHAZ and TOP1* expression levels. Line is median and data significant if *p<0.05. Data analysed by Kruskal Wallis with Dunn's post-hoc multiple comparison's test. (A) Expression patterns of PARK2 in early-onset placentae showed a significant difference across groups (p=0.002). EOIUGR and EOPET/IUGR displayed higher PARK2 expressions compared to preterm control (7.22 and 2.58 vs 0.0048, adj. p=0.004 and 0.01 respectively, Post-hoc Dunn's multiple comparisons test). (B) Expression patterns of PARK2 in late-onset placentae showed a significant difference across groups (p=0.03). PRETERM= preterm control (n=6), NORMAL= Term control placenta (n=7), IUGR= Term IUGR (n=7). LOPET/IUGR= Late onset preeclampsia with growth restriction (n=4). LOPET= late-onset preeclampsia (n=16). EOIUGR= Early-onset IUGR (n=6), EOPET/IUGR= Early-onset preeclampsia with IUGR (n=7), EOPET= Early-onset preeclampsia (n=9). Lines represent medians and IQR.

In late onset placental pathologies, stepwise downgrading expression patterns of *PARK2* were evident in placentas from pregnancies with growth restriction to that with preeclampsia, similar to that found in placentas from early onset gestational disease. Though differences across all groups were significant, individual pairwise differences between late-onset placental pathology groups failed to achieve statistical significance by post-hoc multiple comparisons test (Figure 5-3B).

5.4.2.3.2 Protein Tyrosine Phosphatase, Non-Receptor Type 2 (*PTPN2*)

On the other hand, expression patterns of PTPN2 were significantly different across the early onset group (*p=0.001,* Kruskal-Wallis test*)* with a persistent downregulation of *PTPN2* in placentas from EOIUGR compared to gestational aged matched PTC (15.6 vs 6, *adj. p*=0.002, Mann-Whitney test, Figure 5-4A).

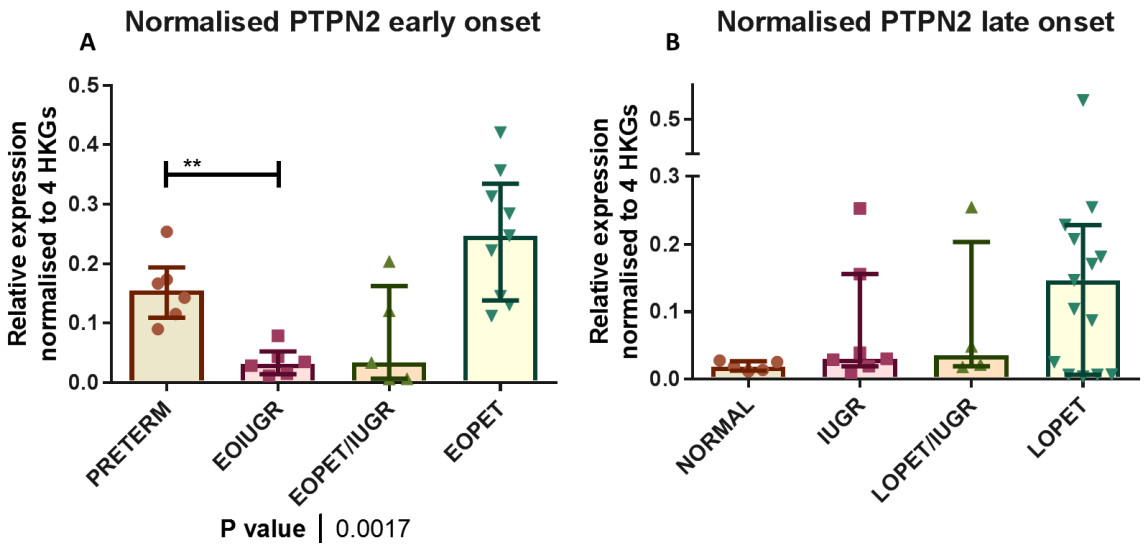

Figure 5-4 Expression levels of *PTPN2* mRNA by qRT-PCR in (A) early onset placental dysfunction and (B) late onset placental dysfunction using specific primers to *PTPN2*. Expression levels were normalised to the geomean of *β-actin, GAPDH, YWHAZ and TOP1* expression levels. Line is median and data significant if *p<0.05. Data analysed by Kruskal Wallis with Dunn's post-hoc multiple comparison's test. (A) Expression patterns of PTPN2 were significantly different across the early onset group (p=0.001, Kruskal-Wallis test) with a persistent downregulation of PTPN2 in placentas from EOIUGR compared to gestational aged matched PTC (15.6 vs 6, adj. p=0.002, Mann-Whitney test). (B) No significant differences were revealed across late-onset placental groups (p=0.38, Kruskal-Wallis test). PRETERM= preterm control (n=6), NORMAL= Term control placenta (n=7), IUGR= Term IUGR (n=7). LOPET/IUGR= Late onset preeclampsia with growth restriction (n=4). LOPET= late-onset preeclampsia (n=16). EOIUGR= Early-onset IUGR (n=6), EOPET/IUGR= Early-onset preeclampsia with IUGR (n=7), EOPET= Early-onset preeclampsia (n=9). Lines represent medians and IQR.

Early onset placental pathologies also had an ascending stepwise pattern of *PTPN2* expression across EOIUGR, EOPET/IUGR and EOPET (Figure 5-4A). In late onset diseases, though a similar stepwise increase in *PTPN2* expression levels was found across placentas from IUGR, LOPET/IUGR and LOPET, no significant differences were revealed across groups (*p*=0.38, Kruskal-Wallis test, Figure 5-4B).

5.4.2.3.3 Early Growth Response 1 (*EGR1*)

The PCR expression profiles of EGR1 gene were significantly different across groups of early onset placental pathologies (*p=0.002*, Kruskal-Wallis test*)* with higher expression in preterm control placentas compared to EOIUGR and EOPET/IUGR placentas (20.67 vs 7.83 and 5.5, adj. *p*=0.005 and *adj. p*=0.0027 respectively, Dunn's multiple comparisons test, Figure 5-5A). Conversely, the PCR expression profiles of EGR1 gene in late onset pathologies were similar with a trend increase in EGR1

expression in placentas from LOPET pregnancies compared to term control (*p*=0.06, Figure 5-5B).

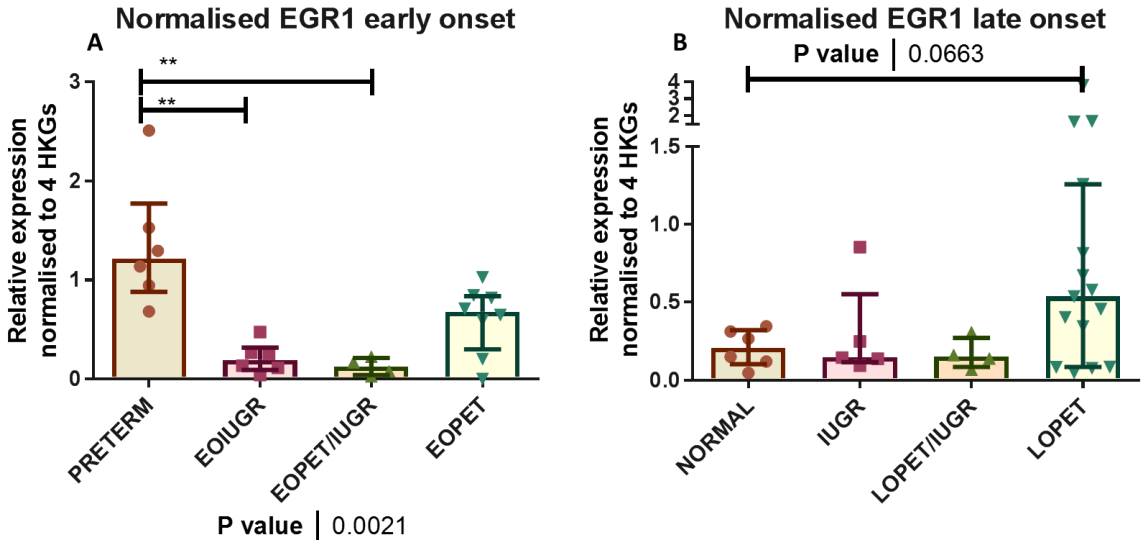

Figure 5-5 Expression levels of *EGR1* mRNA by qRT-PCR in (A) early onset placental dysfunction and (B) late onset placental dysfunction using specific primers to EGR1. Expression levels were normalised to the geomean of *β-actin, GAPDH, YWHAZ and TOP1* expression levels. Line is median and data significant if *p<0.05. Data analysed by Kruskal Wallis with Dunn's post-hoc multiple comparison's test. (A) Expression profiles of EGR1 gene were significantly different across groups of early onset placental pathologies (p=0.002, Kruskal-Wallis test) with higher expression in preterm control placentas compared to EOIUGR and EOPET/IUGR placentas (20.67 vs 7.83 and 5.5, adj. p=0.005 and adj. p=0.0027 respectively, Dunn's multiple comparisons test. (B) Late onset placental pathologies showed no significant difference across them, but LOPET placentas showed a trend increase in EGR1 expression compared to term control (p=0.06, Mann-Whitney test). PRETERM= preterm control (n=6), NORMAL= Term control placenta (n=7), IUGR= Term IUGR (n=7). LOPET/IUGR= Late onset preeclampsia with growth restriction (n=4). LOPET= late-onset preeclampsia (n=16). EOIUGR= Early-onset IUGR (n=6), EOPET/IUGR= Early-onset preeclampsia with IUGR (n=7), EOPET= Early-onset preeclampsia (n=9). Lines represent medians and IQR.

5.4.2.3.4 Tyrosine 3-Monooxygenase/Tryptophan 5-Monooxygenase Activation Protein Epsilon OR 14-3-3 Epsilon (*YWHAE*)

Groups of early onset and late onset placental pathologies demonstrated significant differences in *YWHAE* expression (*p=0.0003 and p=0.038 respectively, Kruskal-Wallis test)*. Both early and late onset gestational diseases also showed a stepwise downward decrease in *YWHAE* expression being highest in pure growth restriction to combined PET with IUGR to their lowest expression in PET. Placentas from preterm control showed a significantly lower expression compared to that in EOIUGR placentas (10.33 vs 25.5, *adj. p=0.006,* Dunn's multiple comparisons test, Figure 5-6A). On the other hand, placentas from LOPET showed a significant

decrease in *YWHAE* expression compared to placentas from normal pregnancies (12.75 vs 24.86, *adj. p=0.02,* Dunn's multiple comparisons test, Figure 5-6B)

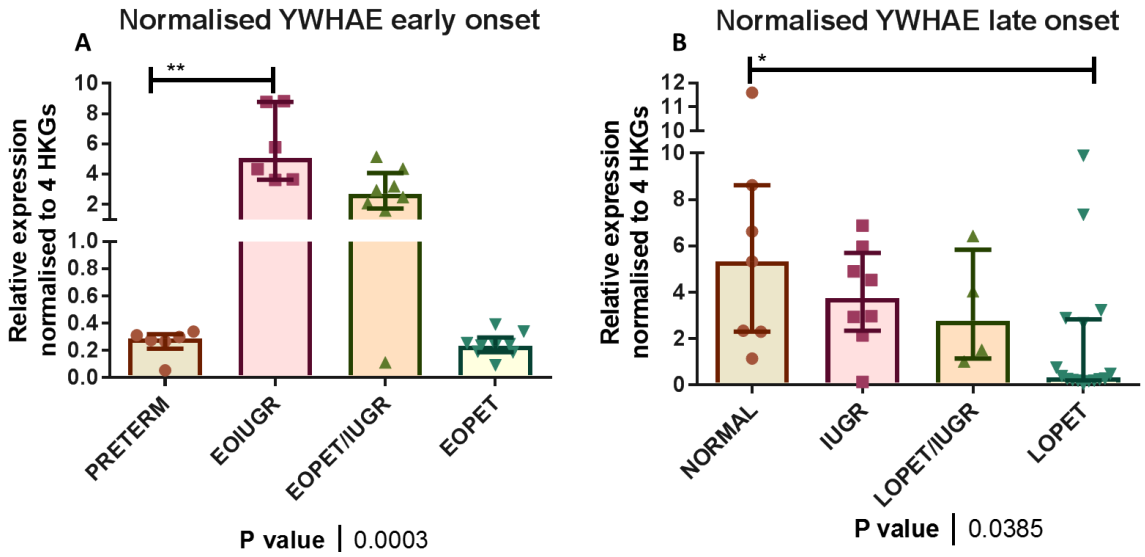

Figure 5-6 Expression levels of YWHAE mRNA by qRT-PCR in (A) early onset placental dysfunction and (B) late onset placental dysfunction using specific primers to YWHAE. Expression levels were normalised to the geomean of β-actin, GAPDH, YWHAZ and TOP1 expression levels. Line is median and data significant if *p<0.05. Data analysed by Kruskal Wallis with Dunn's post-hoc multiple comparison's test. (A) Early onset placental pathologies demonstrated significant differences in YWHAE expression (p=0.0003). Placentas from preterm control showed a significantly lower expression compared to that in EOIUGR placentas (10.33 vs 25.5, adj. p=0.006, Dunn's multiple comparisons test). (B) Late onset placental pathologies demonstrated significant differences in YWHAE expression (p=0.038). Placentas from LOPET showed a significant decrease in YWHAE expression compared to placentas from normal pregnancies (12.75 vs 24.86, adj. p=0.02, Dunn's multiple comparisons test). PRETERM= preterm control (n=6), NORMAL= Term control placenta (n=7), IUGR= Term IUGR (n=7). LOPET/IUGR= Late onset preeclampsia with growth restriction (n=4). LOPET= late-onset preeclampsia (n=16). EOIUGR= Early-onset IUGR (n=6), EOPET/IUGR= Early-onset preeclampsia with IUGR (n=7), EOPET= Early-onset preeclampsia (n=9). Lines represent medians and IQR.

5.4.2.3.5 B-Cell CLL/Lymphoma 11B (*BCL11B*)

The PCR expression profiles of BCL11B gene were significantly different across groups of early onset placental pathologies (*p=0.001, Kruskal-Wallis test)* with a stepwise increase in *BCL11B* expression across early onset pathologies (Figure 5-7A). Moreover, *BCL11B* displayed higher expression in preterm control placentas compared to placentas from EOIUGR and EOPET/IUGR pregnancies (23.3 vs 8.33 and 8.88, adj. *p*=0.006 and *adj. p*=0.005 respectively, Dunn's multiple comparisons test, Figure 5-7A). Similarly, the PCR expression profiles of *BCL11B* gene in late onset pathologies were similar with a significant increase in *BCL11B* expression in placentas

from LOPET pregnancies compared to term control (21.75 vs 11.57, *p*=0.02, Figure 5-7B).

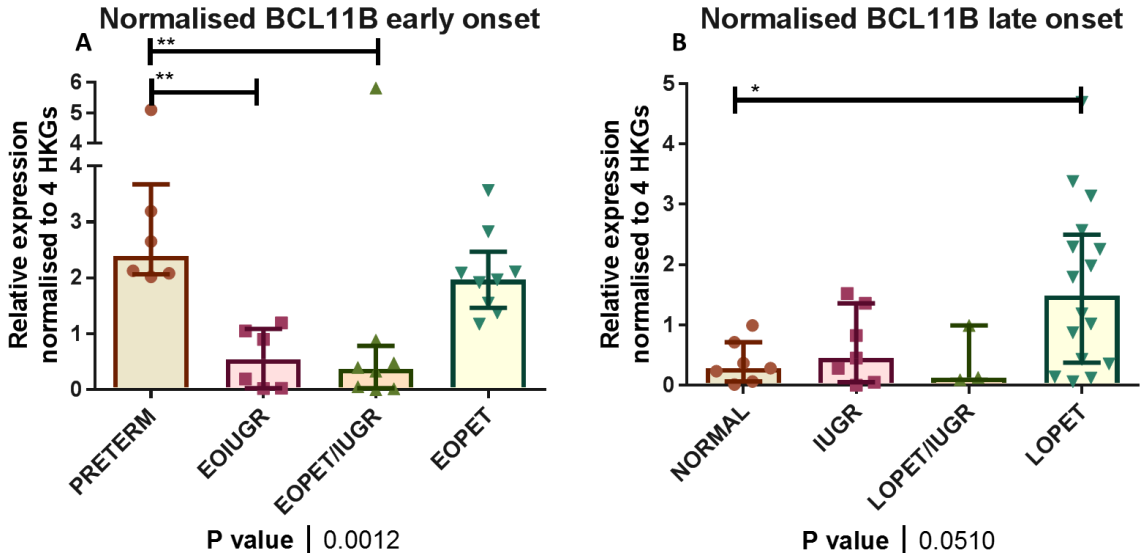

Figure 5-7 Expression levels of *BCL11B* mRNA by qRT-PCR in (A) early onset placental dysfunction and (B) late onset placental dysfunction using specific primers to BCL11B. Expression levels were normalised to the geomean of *β-actin, GAPDH, YWHAZ and TOP1* expression levels. Line is median and data significant if *p<0.05. Data analysed by Kruskal Wallis with Dunn's post-hoc multiple comparison's test. (A) BCL11B gene were significantly different across groups of early onset placental pathologies (p=0.001, Kruskal-Wallis test). BCL11B displayed higher expression in preterm control placentas compared to placentas from EOIUGR and EOPET/IUGR pregnancies (23.3 vs 8.33 and 8.88, adj. p=0.006 and adj. p=0.005 respectively, Dunn's multiple comparisons test). (B) Expression profiles of BCL11B gene in late onset pathologies were similar with a significant increase in BCL11B expression in placentas from LOPET pregnancies compared to term control (21.75 vs 11.57, p=0.02, Mann-Whitney test). PRETERM= preterm control (n=6), NORMAL= Term control placenta (n=7), IUGR= Term IUGR (n=7). LOPET/IUGR= Late onset preeclampsia with growth restriction (n=4). LOPET= late-onset preeclampsia (n=16). EOIUGR= Early-onset IUGR (n=6), EOPET/IUGR= Early-onset preeclampsia with IUGR (n=7), EOPET= Early-onset preeclampsia (n=9). Lines represent medians and IQR.

5.4.2.4 Expression of the anti-apoptotic gene (*BCL2*)

Similar to *BCL11B* expression profiles in early onset pathologies, *BCL2* showed a stepwise increase in expression with the lowest being in placentas from early onset IUGR to almost double in EOPET/IUGR placentas and incrementing to a higher expression in placentas of pure early onset PET. Furthermore, differences across groups were significant (*p*=0.04, Kruskal Wallis, Figure 5-8A) in early onset placental pathologies. In addition, expression levels of *BCL2* in EOPET placenta were upregulated compared to their levels in preterm control placenta (21.56 vs 14.17, *p*= 0.036, Figure 5-8A).

A similar pattern emerged in the late onset group with placentas from LOPET pregnancies showing a higher expression of *BCL2* gene levels by qRT-PCR compared to term control (20.77 vs 11.71, *p*=0.029, Figure 5-8B)

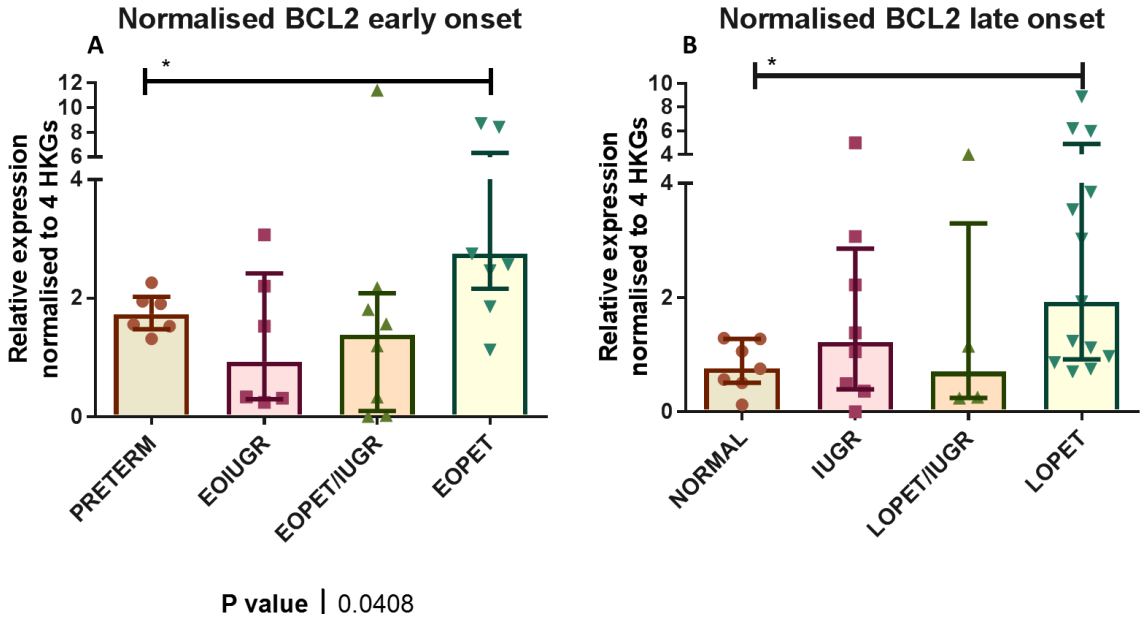

Figure 5-8 Expression levels of *BCL2* mRNA by qRT-PCR in (A) early onset placental dysfunction and (B) late onset placental dysfunction using specific primers to *BCL2*. Expression levels were normalised to the geomean of *β-actin, GAPDH, YWHAZ and TOP1* expression levels. Line is median and data significant if *p<0.05. Data analysed by Kruskal Wallis. Individual pair-wise analysis was done by Mann-Whitney test. (A) BCL2 expression differences across groups were significant (p=0.04, Kruskal Wallis) in early onset placental pathologies. Expression levels of BCL2 in EOPET placenta were upregulated compared to their levels in preterm control placenta (21.56 vs 14.17, p= 0.036, Mann-Whitney test). (B) In late onset group, placentas from LOPET pregnancies showed a higher expression of BCL2 gene levels by qRT-PCR compared to term control (20.77 vs 11.71, p=0.029, Mann-Whitney test). PRETERM= preterm control (n=6), NORMAL= Term control placenta (n=7), IUGR= Term IUGR (n=7). LOPET/IUGR= Late onset preeclampsia with growth restriction (n=4). LOPET= late-onset preeclampsia (n=16). EOIUGR= Early-onset IUGR (n=6), EOPET/IUGR= Early-onset preeclampsia with IUGR (n=7), EOPET= Early-onset preeclampsia (n=9). Lines represent medians and IQR.

5.4.2.5 Correlations of autophagy/anti-apoptotic related genes

Several autophagy and anti-apoptotic genes in our placental groups, though some did not display significant difference across groups, nonetheless showed an interesting resemblance or difference in expression patterns across markers. In order to study and analyse such correlations, an online software (TMA Navigator (353)) was employed to represent genes as a heat map (Figure 5-9A) or a mutual information network (Figure 5-9B).

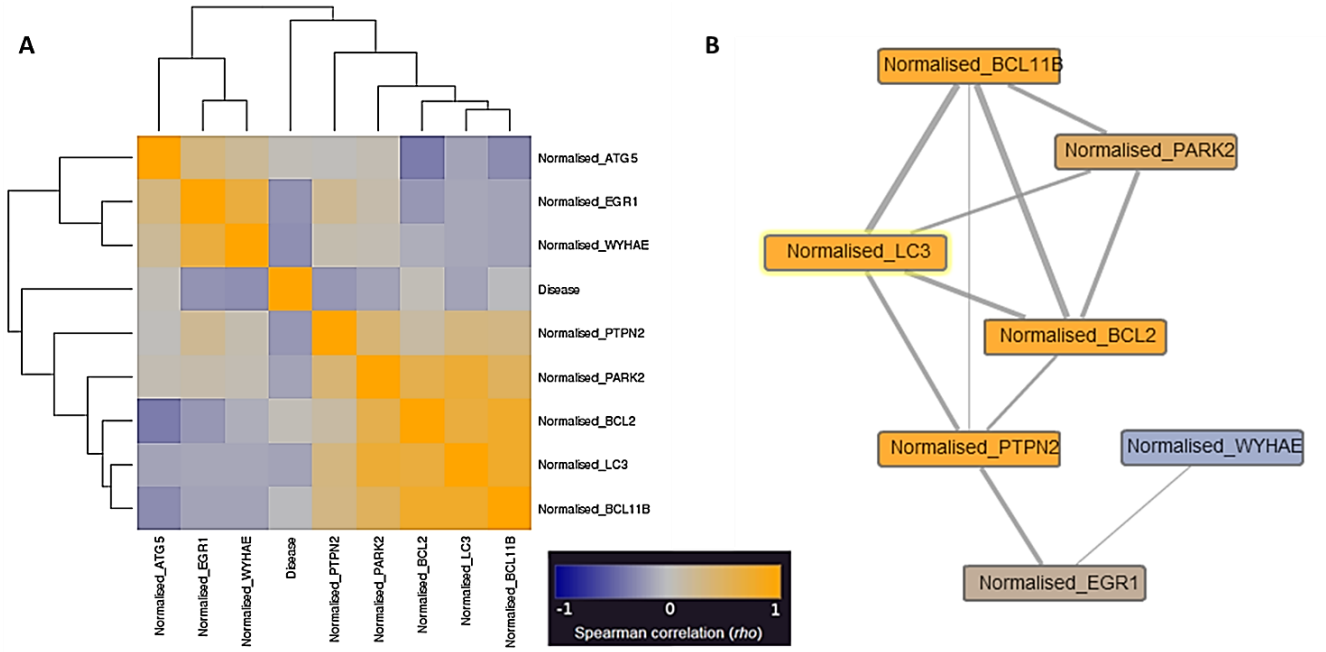

(A) & (B) Lubbock, A. L. R., Katz, E., Harrison, D. J. & Overton, I. M. TMA Navigator: network inference, patient stratification and survival analysis with tissue microarray data. Nucl. Acids Res. 41, W562–W568 (2013). DOI: 10.1093/nar/gkt529 PMID: 23761446

Figure 5-9 Correlation and clustering of autophagy and antiapoptotic genes in human placenta by (A) Heat map and (B) Mutual information network representations of gene expression levels. (A) Marker heat map for the correlation matrix of the selected gene expression levels. Yellow represent positive correlation while the blue represent negative correlation. (B) Mutual information network with a radial layout shows 11 significant connection (edges). The thicker the edge, the stronger the correlation. Network threshold= 0.05 with Benjaminin-Yekutieli multiple hypothesis testing correction. The edge between the LC3B and BCL2 showed a test statistic: 0.69, P-value: 0.006. Data were visualised using online TMA navigator software (353).

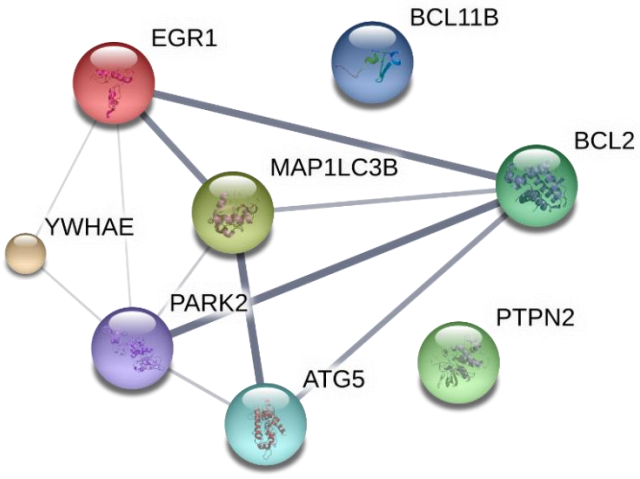

Figure 5-10 Schematic presentation of protein-protein interactions of the selected autophagy related genes identified from our search using STRING online software (412). The line thickness indicates the strength of data support. Sources of active interaction include: Text mining, Experiments, Databases, Co-expression, Neighbourhood and Co-occurrence.

Expression levels in our placentas showed that the main autophagy gene (*MAP1LC3B*) appears to be incorporated in a correlation cluster or a network with other autophagy-related genes like *PARK2* and *PTPN2*, and anti-apoptotic genes like *BCL11B* and *BCL2* (Figure 5-9). That is to say, the levels of these genes are interlinked to form a clustering network irrespective of the placenta dysfunction, which may drive the whole network up or down.

Pathway ID	**Biological process (Pathway description)**	**Observed gene count**	**False discovery rate (FDR)**
GO.0010821	regulation of mitochondrion organization	5	0.000337
GO.0071496	cellular response to external stimulus	5	0.000337
GO.0030217	T cell differentiation	4	0.000356
GO.0000422	mitophagy	3	0.00044
GO.0009267	cellular response to starvation	4	0.00044
GO.0031667	response to nutrient levels	5	0.00044
GO.2000378	negative regulation of reactive oxygen species metabolic process	3	0.000485
GO.2001235	positive regulation of apoptotic signaling pathway	4	0.000485
GO.0043065	positive regulation of apoptotic process	5	0.000508
GO.2001244	positive regulation of intrinsic apoptotic signaling pathway	3	0.000578
GO.0010506	regulation of autophagy	4	0.00105
GO.0010822	positive regulation of mitochondrion organization	4	0.00105
GO.0016236	macroautophagy	3	0.00105
GO.0030154	cell differentiation	7	0.00288
GO.0007005	mitochondrion organization	4	0.00347
GO.1903747	regulation of establishment of protein localization to mitochondrion	3	0.00415
GO.0006995	cellular response to nitrogen starvation	2	0.00687

Table 5-6 Functional enrichments analysis of the selected autophagy related genes in this network.

The search for such selected protein coding genes in STRING database has yielded a string interaction network of strong correlation between *MAP1LC3B, PARK2, EGR1* and *BCL2* (Figure 5-10). Functional enrichment analysis of such network has revealed that it is potentially linked to mitochondrial dysfunctional, organisation as well as mitophagy. Other biological processes included regulation of autophagy, apoptosis and negative regulation of ROS metabolic process as well as cellular response to starvation (Table 5-6).

5.4.3 Quantitative real-time RT-PCR for autophagy-related miRNAs

In order to explore why there was no direct link between the *MAP1LC3B* gene expression and the semi-quantitative analysis of the LC3 autophagy marker protein positivity by IHC, we then explored the role of potential miRNAs, identified from the data mining, in the regulation of autophagy in the placenta. Expression levels of such miRNAs were quantified by qRT-PCR.

5.4.3.1 Hsa-miR-182 expression levels

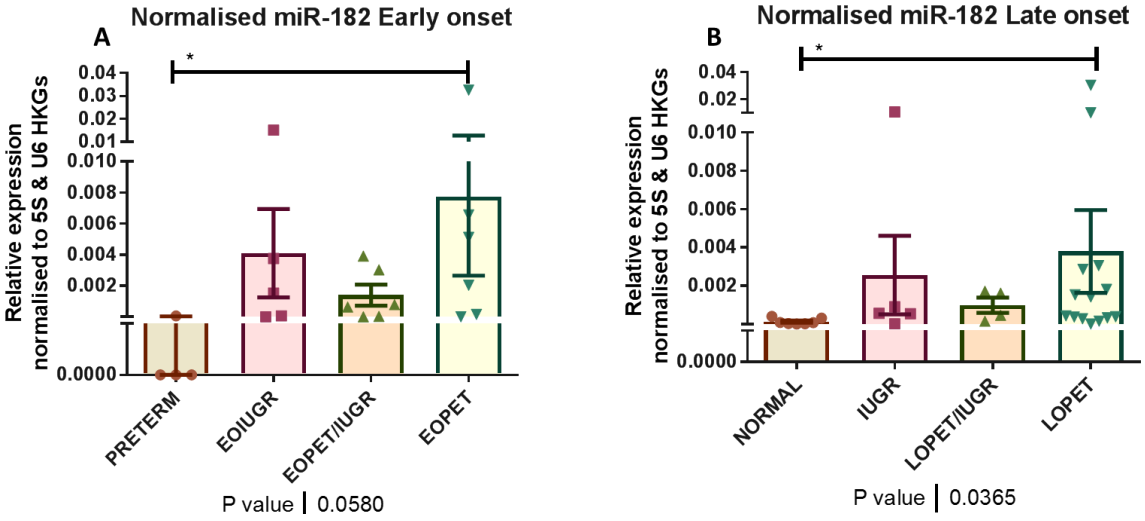

Figure 5-11 Expression levels of miR-182 by qRT-PCR in (A) early onset placental dysfunction and (B) late onset placental dysfunction using specific primers to hsa-miR-182-5p. Expression levels were normalised to the geomean of S5 and U6snRNA. Line is median and data significant if *p<0.05. Data analysed by Kruskal Wallis with Dunn's post-hoc multiple comparison's test. (A) Higher miR-182 levels were evident in placentas from pregnancies complicated with EOPET compared to preterm control (14.33 vs 3.75, adj. p=0.02, Dunn's multiple comparisons test). (B) Levels of expression of miR-182 showed significant differences across groups of late onset gestational diseases (p=0.03, Kruskal-Wallis test). Placentas from LOPET showed a significantly higher expression levels of miR-182 compared to term control (18.07 vs 7, adj. p=0.01, Dunn's multiple comparisons test). Lines represent medians and IQR.

It was evident that term and preterm controls displayed lower levels of miR-182 compared to other compromised pregnancies. Levels of expression of miR-182 showed significant differences across groups of early onset and late onset gestational diseases (Figure 5-11). Moreover, higher miR-182 levels were evident in placentas from pregnancies complicated with EOPET compared to preterm control (14.33 vs 3.75, *adj. p*=0.02, Figure 5-11A). Similarly, placentas from LOPET showed a significantly higher expression of miR-182 compared to term control (18.07 vs 7, *adj. p*=0.01, Figure 5-11B).

5.4.3.2 Hsa-miR-192 expression levels

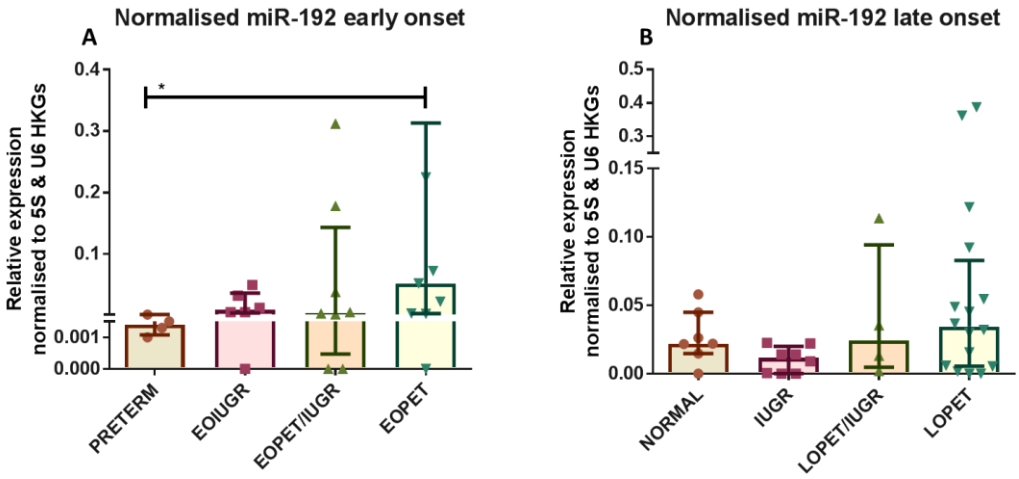

Figure 5-12 Expression levels of miR-192 by qRT-PCR in (A) early onset placental dysfunction and (B) late onset placental dysfunction using specific primers to hsa-miR-192-5p. Expression levels were normalised to the geomean of S5 and U6snRNA. Line is median and data significant if *p<0.05. Data analysed by Kruskal Wallis with Dunn's post-hoc multiple comparison's test. (A) Placentas from EOPET pregnancies showed upregulated expression compared to control (17.94 vs 6.5, adj. p= 0.04, Dunn's multiple comparisons test). (B) In late onset pathologies, there were no significant differences across groups. PRETERM= preterm control (n=6), NORMAL= Term control placenta (n=7), IUGR= Term IUGR (n=8). LOPET/IUGR= Late onset preeclampsia with growth restriction (n=4). LOPET= late-onset preeclampsia (n=13). EOIUGR= Early-onset IUGR (n=6), EOPET/IUGR= Early-onset preeclampsia with IUGR (n=8), EOPET= Early-onset preeclampsia (n=9). Lines represent medians and IQR.

Regarding the expression levels of miR-192 in placental dysfunction, only placentas from EOPET pregnancies showed upregulated expression compared to control (17.94 vs 6.5, *adj. p*= 0.04, Figure 5-12A). In late onset pathologies, there were no significant differences across groups, though there was a stepwise increasing pattern of miR-192 expression from IUGR being the lowest, increasing in LOPET/IUGR placentas and highest in LOPET placentas (Figure 5-12B).

5.4.3.3 Hsa-miR-145 expression levels

Levels of miR-145 expression levels did not display significant differences across groups of early or late onset placental dysfunction (Figure 5-13).

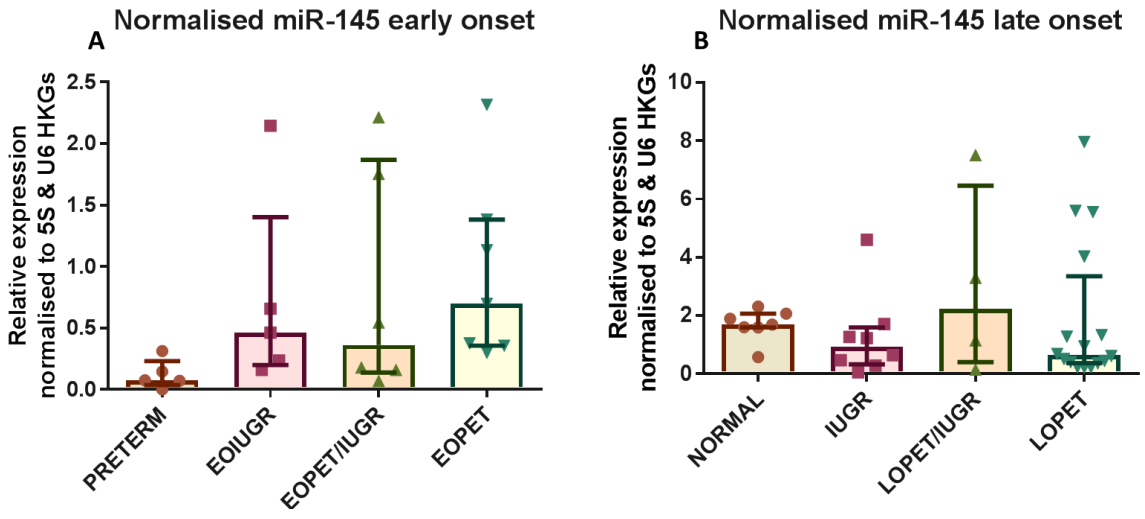

Figure 5-13 Expression levels of miR-145 by qRT-PCR in (A) early onset placental dysfunction and (B) late onset placental dysfunction using specific primers to hsa-miR-145-5p. Expression levels were normalised to the geomean of S5 and U6snRNA. Line is median and data significant if *p<0.05. Data analysed by Kruskal Wallis test. PRETERM= preterm control (n=6), NORMAL= Term control placenta (n=7), IUGR= Term IUGR (n=8). LOPET/IUGR= Late onset preeclampsia with growth restriction (n=4). LOPET= late-onset preeclampsia (n=13). EOIUGR= Early-onset IUGR (n=6), EOPET/IUGR= Early-onset preeclampsia with IUGR (n=8), EOPET= Early-onset preeclampsia (n=9). Lines represent medians and IQR.

5.4.3.4 Hsa-let-7a expression levels

Though no significant difference were found across groups of early and late onset dysfunction in the expression levels of miR-let-7a, but higher levels were observed in placentas from EOPET pregnancies compared to preterm control (18.67 vs 6.75, adj. p=0.03, Figure 5-14A). In late onset placental diseases, levels of miR-let7a showed no significant differences across groups, though a rising trend was evident from across groups towards the pure term preeclampsia (Figure 5-14).

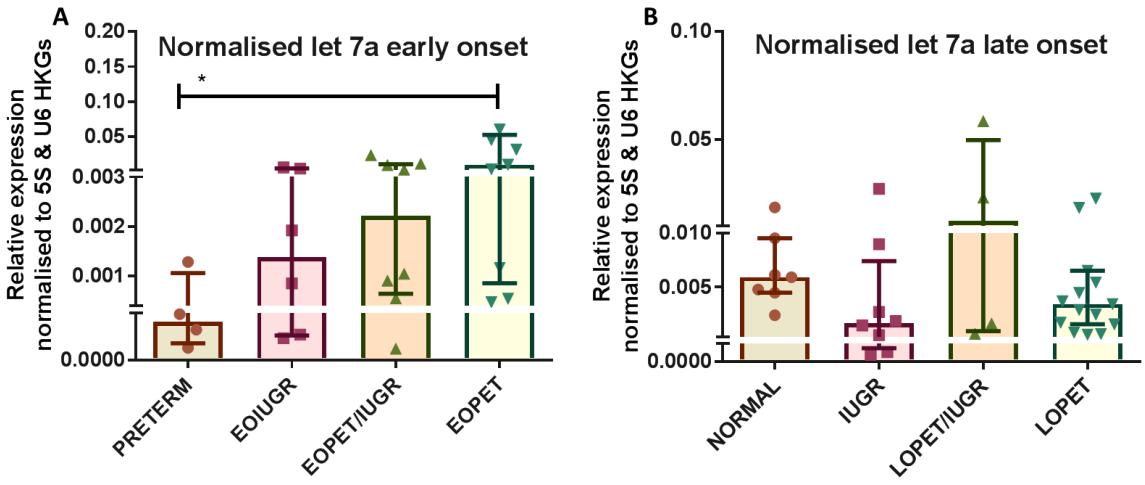

Figure 5-14 Expression levels of let-7a by qRT-PCR in (A) early onset placental dysfunction and (B) late onset placental dysfunction using specific primers to hsa-let-7a-5p. Expression levels were normalised to the geomean of S5 and U6snRNA. Line is median and data significant if *p<0.05. Data analysed by Kruskal-Wallis with Dunn's multiple comparisons test. (A) EOPET placentas displayed a significantly higher let-7a levels compared to preterm control (18.67 vs 6.75, adj. p=0.03, Dunn's test). (B) Let-7a levels in late onset placentas showed no significant differences across groups. PRETERM= preterm control (n=6), NORMAL= Term control placenta (n=7), IUGR= Term IUGR (n=8). LOPET/IUGR= Late onset preeclampsia with growth restriction (n=4). LOPET= late-onset preeclampsia (n=13). EOIUGR= Early-onset IUGR (n=6), EOPET/IUGR= Early-onset preeclampsia with IUGR (n=8), EOPET= Early-onset preeclampsia (n=9). Lines represent medians and IQR.

5.4.3.5 Hsa-miR-204 expression levels

The expression levels of miR-204 in early onset placental dysfunction did not show statistical significant differences across groups (Figure 5-15A), though there were higher levels in severe early onset PET with IUGR. Similarly, no significant difference in the expression levels of miR-204 were measured in the late onset placental pathologies (Figure 5-15B).

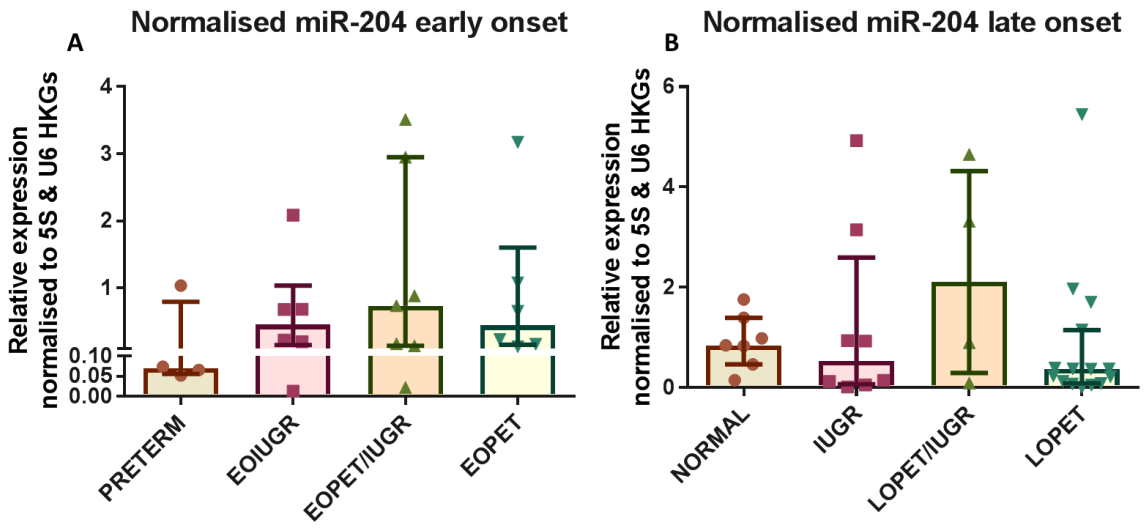

Figure 5-15 Expression levels of miR-204 by qRT-PCR in (A) early onset placental dysfunction and (B) late onset placental dysfunction using specific primers to hsa-miR-204-5p. Expression levels were normalised to the geomean of S5 and U6snRNA. Line is median and data significant if *p<0.05. Data analysed by Kruskal Wallis with Dunn's post-hoc multiple comparison's test. PRETERM= preterm control (n=5), NORMAL= Term control placenta (n=7), IUGR= Term IUGR (n=6). LOPET/IUGR= Late onset preeclampsia with growth restriction (n=4). LOPET= late-onset preeclampsia (n=15). EOIUGR= Early-onset IUGR (n=6), EOPET/IUGR= Early-onset preeclampsia with IUGR (n=8), EOPET= Early-onset preeclampsia (n=6). Lines represent medians and IQR.

Interestingly, though the expression levels of miR-204 in early and late onset placental dysfunction did not show significant differences across groups, nevertheless they showed a resemblance to the pattern of M30 apoptotic marker positivity by immunohistochemistry (Figure 4-3A & B).

5.4.4 Correlations between miRNAs and protein level positivity by IHC

In order to validate such an observation, regression analyses were done to explore the role indicative of miRNAs, as an independent variable, in regulating PCD protein expressions in placental dysfunction. Results have shown that levels of expression of miR-204 in our placentas were positively correlated to the levels of M30 apoptotic marker positivity; higher levels of miR-204 were associated with higher placental apoptotic burden (Pearson r= 0.52, *p*=0.01, Figure 5-16C). Conversely, miR-204 expression levels displayed an inverse correlation to the autophagy marker LC3 positivity (Pearson r= -0.44, *p*=0.04, Figure 5-16A) and the anti-apoptotic marker *BCL2* positivity by IHC image analysis (Pearson r= -0.67, *p*=0.0009, Figure 5-16B).

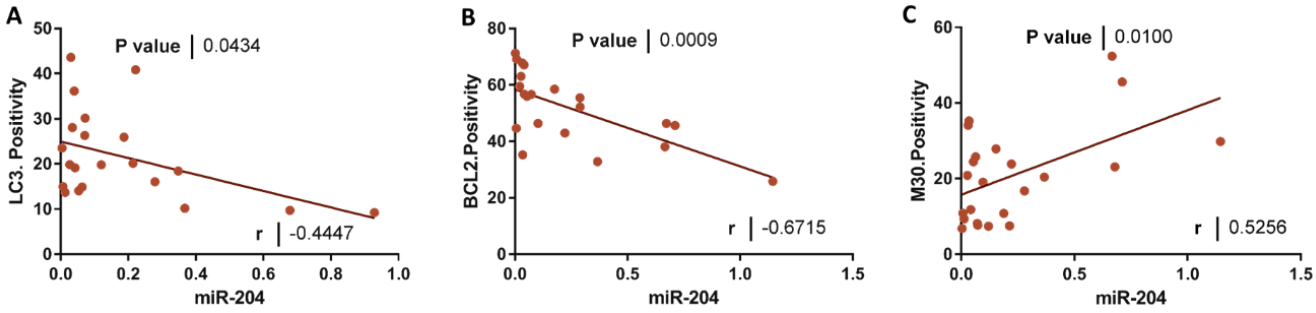

Figure 5-16 Correlation and regression analyses of (A) autophagy marker LC3 positivity, (B) antiapoptotic marker Bcl-2 positivity and (C) M30 apoptosis marker positivity by IHC and expression levels of miR-204 by qRT-PCR. (A) A linear regression analysis between levels of miR-204 by qRT-PCR and autophagy marker LC3 positivity showing a negative correlation with a Pearson r= -0.44 and *p=0.04.* (B) A linear regression analysis between levels of miR-204 by qRT-PCR and antiapoptotic marker Bcl-2 positivity showing a negative correlation with a Pearson r= -0.67, and *p=0.0009*. (C) A linear regression analysis between levels of miR-204 by qRT-PCR and apoptotic marker M30 positivity showing a positive correlation with a Pearson r= 0.52 and *p=0.01.*

This suggests that miR-204 in the placenta might have a pro-apoptotic function in the trophoblasts, thus contributing to placental dysfunction, through regulation of anti-apoptotic protein Bcl-2 as well as inhibiting the prosurvival autophagy process. This is a result that needs to be explored more and validated in an *in vitro* model system, through which we can identify functional changes of miR-204 upregulation in terms of programmed cell death.

5.5 Discussion

Our results have shown that the selected autophagy-related genes (ARG) were differentially expressed across placental groups, especially in early onset placental dysfunction. It was also evident that there was a consistently gradient expression pattern of ARG from growth restriction to preeclamptic pathologies. This might indicate that in addition to the generic interlinking of placental dysfunctional pathologies, there is also evidence of quantitative functional and molecular specificity for each placental disease.

Our results revealed that no single autophagy gene expression with the use of real time qRT-PCR was responsible for the LC3 marker positivity pattern seen in the immunolabelled slides. In addition, our study has characterised the way that the selected autophagy-related genes are expressed in placental dysfunction. The results also illustrated that the autophagy gene *MAP1LC3B* appears to lie in a correlation cluster or network with which autophagy related genes like *PARK2* and *PTPN2*, and other anti-apoptotic genes like *BCL11B* and *BCL2* are incorporated (Figure 5-9). That is to say, the levels of these genes are interlinked to form a clustering network that may dictate the way the placenta behaves in response to stressful events.

BCL2 gene expression in our placentas showed a positively correlated relationship with *MAP1LC3B* gene expression (Figure 5-9B), emphasising the importance of the Bcl-2 anti-apoptotic family of proteins, with the ARGs, in regulating the cell fate decisions. The B-cell lymphoma 2 family of proteins, commonly known as cell fate regulators, usually responds to a range of stimuli, including prosurvival (BCL2L1, BCL2L2, MCL1) and proapoptotic factors (BAK1, BAX, BOK) (413). The differential apoptotic function of the Bcl-2 proteins is dependent on their localisation to the mitochondria; however, they can also be localised to other organelles, like endoplasmic reticulum, triggering other cellular processes like autophagy (414). The way Bcl-2 is involved in catalysing mitochondrial-dependent cell death in the human placenta and the role that these regulatory proteins play in harmony with placental autophagy in normal and pathological pregnancies remains to be elucidated (415). However, it is reasonable to believe that liberating Bcl-2 from activated autophagy protein complexes may unleash these molecules to inhibit the intrinsic and extrinsic

pathways of apoptosis (139, 394). Moreover, these data are consistent with a study that reported that treatment of trophoblast JEG3 cells with Nitric oxide donors, mimicking oxidative stress, activated Bcl-2 family proteins and induced autophagy (416). It is also believed that Bcl-2 modulates cell death by affecting the permeability of mitochondrial membrane through a functioning feedback loop system with caspases, thus blocking caspase activity either by impeding the liberation of mitochondrial cytochrome C and/or by binding to the apoptosis activating factor (APAF-1) (417).

Results from quantitative expression profiles of *MAP1LC3B* gene in our placentas revealed that they cannot explain the upregulated LC3 protein expression found by IHC analysis in LOPET placenta, suggesting there might be an epigenetic layer that has a role to play in the regulation of the placental autophagy through miRNAs.

Through groups of interlinked but clinically distinct subsets of placental dysfunction-related gestational diseases, we were able to study and quantify expression levels of a selected group of autophagy-related genes and miRNAs. Those were selected from a rigorous and focussed data and text mining protocols in order to identify novel programmed cell death regulating miRNAs in the placenta.

The autophagy-miRNA interconnection and its potential physiological significance is only beginning to be clarified; nonetheless, in view of the well-known significance of both miRNAs and autophagy in adaptation, stress response and in the pathogenesis of human disease, further recognition and comprehension of these interactions would be of a great interest, thus presents with promising possibilities for treatment strategies in the future (188).

Different miRNAs were identified having a role in the regulation of growth, proliferation and programmed cell death. Our *in silico* data mining demonstrated that let-7a gene targets were related to cell growth and proliferation like IGF1R, IGFBP4, IGF2BP1 and IGF1, as well as the autophagy pathway genes (Table 5-5). This was consistent with other studies which had predicted let-7a to target placental growth genes. They also showed that hsa-let-7a in first trimester placental explants significantly inhibited cytotrophoblast proliferation and played a role in regulation of endogenous cell growth (418). Moreover, hsa-let-7a mimics inhibited cell proliferation, growth, and metastasis

of hepatocellular cells (HCC), inducing organelle changes, including autophagy (419). This effect was validated by transfecting let-7a-mimics and resulting in a significant reduction of autophagy (420). Furthermore, another study revealed that let-7a through IGF1R down regulation, resulted in enhanced apoptosis, cell cycle arrest and inhibition of cell proliferation (421).

Similarly miR-192 identified by *in silico* analysis to have a potential role in programmed cell death was found by Wang et al., (2012) to be differentially expressed in placentas from severe PET compared to normotensive pregnancies (422). Moreover, miR-192 overexpression in bladder cancer cells was shown to enhance apoptotic cell death and decrease the level of Bcl-2 and other anti-apoptotic proteins (423). It was also found that genotoxic stress causing DNA damage enhanced the p53-dependent upregulation of miR-192 leading to induction of cell arrest, suggesting that it might act as tumour suppressor through cell cycle regulation (424).

Another miRNA of interest and identified in our *in silico* analysis was miR-145, with potential target genes related to proliferation and growth like IGF1R and IGFBP2. These data are supported with another study that reported targets of miR-145 being within the insulin-like growth factor axis, where overexpressed miR-145 in placental explants has displayed its important intermediary role in insulin-like growth factor-induced trophoblast proliferation (418).

Moreover, our results identified potential target genes for miR-145 related to programmed cell death, autophagy and senescence like *MAP1LC3B, ATG16L2, ATG9B, BCL2, BCL11B, PARK2, PTPN2 and YWHAE* (Table 5-4). Its role in autophagy has previously been studied in cardiomyocytes exposed to ischaemia reperfusion injury and revealed that miR-145 induced autophagy, and enhanced the conversion of *LC3B-I* to *LC3B-II*, and reduced the size of the infarcted myocardium (421). Another report revealed that miR-145 also protected cardiomyocytes from hydrogen peroxide (H_2O_2)-induced apoptosis, reactive oxygen species (ROS) production and disruption of mitochondrial structure through targeting the mitochondrial pathway indicating that miR-145 might characterise a potential therapeutic target for treatment of oxidative stress-associated ischemia/reperfusion injury (425).

The expression levels of miR-182 in our study have revealed significant differences across placental groups of early onset and late onset gestational diseases (Figure 5-11). Moreover, higher miR-182 levels were evident in placentas from pregnancies complicated with EOPET compared to preterm controls. Similarly, placentas from LOPET showed a significantly higher expression of miR-182 compared to term control. This result replicated a study showing a marked increase in the expression of miR-182 seen in preeclampsia (236), indicating the potential target genes being down regulated. Identification of such target genes is therefore indispensable for better interpretation of the biologic role of individual miRNAs *in vivo*.

Gene ontology (GO) analysis showed that anti-apoptosis and immune response were enriched among miR-182 target genes (236). Since miR-182 might target and inhibit anti-apoptosis genes, upregulated miR-182 in preeclampsia might have a role to the dysregulated PCD in the placentas of pregnancies with preeclampsia. Furthermore, the targets of miR-182 were also enriched in immune processes, supporting the link between preeclampsia and aberrant immune response (426).

Our *in silico* study has revealed that *BCL2* was a potential target gene for miR-182 in three of the searched databases. This finding was consistent with reports of miR-182 targeting and downregulating *BCL2* expression in uveal melanoma cells (427), glioblastoma cells (428), and was also identified in a study on prostate cancer cells (429). This latter study also revealed a raised miR-182 levels of expression in response to serum withdrawal-induced stress, highlighting that miR-182 overexpression can occur due to nutritional deprivation and stress and suggesting that miR-182 levels were associated with autophagy induction.

Data mining for miR-204-5p revealed that programmed cell death-related genes were among the potential targets as *MAP1LC3B, BCL2, BCL11B, EGR1, RAB22A, and C9orf72. MPA1LC3b and BCL2* were targets in four out of the five searched databases (Table 5-1).

Interestingly, the expression levels of miR-204 by qRT-PCR in early and late onset placental dysfunction, though did not show significant differences between groups, nevertheless showed a strong resemblance across groups to the pattern of M30 apoptotic marker positivity by immunohistochemistry (Figure 4-3). This was assessed

by correlation analysis showing that higher levels of miR-204 were positively correlated with higher placental apoptotic burden. Conversely, miR-204 expression levels displayed an inverse correlation to the autophagy marker LC3 positivity and the antiapoptotic marker Bcl-2 positivity by IHC image analysis. This suggested that miR-204 in the placenta may enhance a proapoptotic role in the trophoblasts, thus contributing to placental dysfunction, potentially through regulation of anti-apoptotic protein Bcl-2 as well as inhibiting the prosurvival autophagy process (Figure 5-16).

These data were consistent with other report that demonstrate that miR-204 play a central role in the regulation of apoptosis, accumulation of damaged proteins and endoplasmic reticulum (ER) stress response (430). A possible mechanism of the enhanced apoptotic effect of miR-204 is its post-transcriptional regulation by direct targeting of the 3′ UTR and thus downregulation of anti-apoptotic *BCL2* gene expression (190, 431, 432). Another possible mechanism of the pro-apoptotic effect of miR-204 is down regulation of autophagy, which plays a pro-survival role, through its direct targeting of the LC3B transcript (189, 190).

A key strength of this study was its robust analysis of the expression levels of five autophagy-related miRNAs normalised to the geomean of two HKGs and seven autophagy related genes normalised to the geomean of four HKGs in eight distinct placental dysfunction groups with the use of real-time qRT-PCR, which is the most sensitive and specific RNA quantification method available. Nevertheless, the limitation of the study was the relatively small sample size and need for an *in vitro* model to validate the pro-apoptotic effect of miR-204 seen *in vivo*. Transfection of *in vitro* cell lines models with miRNA precursors and/or inhibitors with consequent analyses of the cellular morphological and functional molecular changes is, undoubtedly, a well-valued tool in the proper analysis of the biologic and functional implications of a miRNA (236). This will be addressed in the following chapter.

Future studies on the biologic and physiological effects of autophagy-related miRNAs might provide unique targets for further research on the principal molecular pathophysiology of placental dysfunction. Recognition of messenger RNA targets is considered a vital phase in knowing the pathways affected by the miRNAs that are dysregulated in placental dysfunction.

Chapter 6
Modelling autophagy *in vitro* using a trophoblast cell line

6.1 Introduction

Autophagy is a tightly regulated energy-dependent recycling process through which dysfunctional proteins, organelles, and invading microorganisms are confined within double membrane-bound vesicles called autophagosomes, which then fuse with lysosomes, leading to cargo degradation in the resulting autolysosome and recycling of biomolecules (99).

The autophagy process begins in response to an intracellular milieu that strays from the normal homeostasis (100). Though previously labelled as a death pathway, autophagy is now considered a key cell survival phenomenon from environmental stressors facing most physiological systems (106).

Induction of autophagy and recognition of the cargo leads to the formation of a C-shaped double membrane organelle called the phagophore. When a phagophore closes around the cargo forming a double-membrane organelle, it is called the autophagosome, which then fuses with lysosomes via the help of the cytoskeleton. Fusion of the autophagosome's outer membrane with the lysosomal membrane results in the lysis of the autophagosome's inner membrane by lysosomal enzymes like specific acidic hydrolases in addition to the cargo therein contained, liberating monosaccharides, free fatty acids, and amino acids into the cytoplasm for re-use (99).

Autophagic flux refers to the progression of the autophagy process into completion. It is critical to discriminate autophagosome development that signposts the induction of autophagy and autophagy flux, which governs if the autophagy process goes into completion or not. Because a complete autophagy flux cycle will commonly exhibit a cytoprotective effect, autophagy inhibition can lead to the build-up of autophagosomes, therefore leading to physiological dysfunction (105). That is to say, increased LC3 may be due to autophagy induction and activation or might as well be due to accumulation of LC3 resulting from an inhibited autophagy flux. The

understanding of this distinction is paramount to linking autophagy to physiological dysfunction.

The significant role that miRNAs play as effective and novel modulators of the autophagy process is now being appreciated. It is also believed that the crosstalk between autophagy and miRNAs has the potential to reprogram and direct the physiological and the biological functions of autophagy in normal and abnormal cellular development (187). Interestingly, the miRNA-autophagy interconnections are thought to promise strategies for future treatment, in view of their significant role in cellular adaptation, stress response and the pathogenesis of human disease (188).

MiR-204 was recently found to regulate the process of vesicle elongation in the autophagy pathway, after its role in autophagy has been initially studied in cardiomyocytes (189) and then validated further in renal cell carcinoma (RCC) via its direct modulation of LC3B (190), showing a negative correlation between miR-204 and LC3B (190).

Exploring such relationship between miR-204 and autophagy LC3 marker in trophoblasts is much needed in order to identify if the autophagy process in the placenta can be regulated by miRNAs. Moreover, the relationship between autophagy and apoptosis can also be explored *in vitro* to identify if it is similar to that seen in our placentas in an *in vitro* trophoblast cell line model. This study will also shed more light to trophoblast reaction to environmental stressors and the role that autophagy plays in deferring trophoblast apoptosis, a pertinent feature in placental dysfunction.

6.2 Hypothesis

- The BeWo cell line can be used as an *in vitro* cell line model for the study of autophagy.
- MicroRNAs have a role to play in the regulation of autophagy/apoptosis cascade in placental trophoblasts and that miR-204 downregulates autophagy flux by interference with autophagosome turnover, thus enhancing trophoblast apoptosis.

6.3 Aim and specific objectives

The aim of this chapter was to highlight the role that autophagy pathway plays in regulation of the apoptotic cascade in trophoblasts.

The specifics objectives were to:

1. Identify an *in vitro* trophoblast cell line model for the study of autophagy.
2. Explore the effects of autophagy-regulating drugs on BeWo cells.
3. Manipulate miRNAs of interest to regulate trophoblast autophagy/apoptosis.

6.4 Results

6.4.1 BeWo cells and autophagy studies

BeWo choriocarcinoma cell line, provided by Dr Karen Forbes and obtained from European Collection of Authenticated Cell Cultures (ECACC) (Porton Down, Wiltshire, UK), a commonly used *in vitro* model for trophoblast function was used to explore autophagy induction, regulation (291) and manipulation with drugs and miRNAs (433, 434) and its relation to the apoptotic cascade.

6.4.1.1 Western blot optimisation of LC3

Western blotting for LC3 protein was optimised using 20 µg and 40 µg of protein loading and under different starvation condition with fetal calf serum (FCS) under 5% and with 0% FCS to explore the effect of FCS starvation on the LC3 protein expression. Protein loading of 40 µg showed a better and a consistent expression of LC3 compared to the 20 µg protein loading (Figure 6-1). Moreover, the protocol of FCS starvation (0% FCS) yielded a higher LC3 expression compared to 5% FCS. This positive autophagy induction by FCS starvation indicated that BeWo cells might be a suitable model to study autophagy.

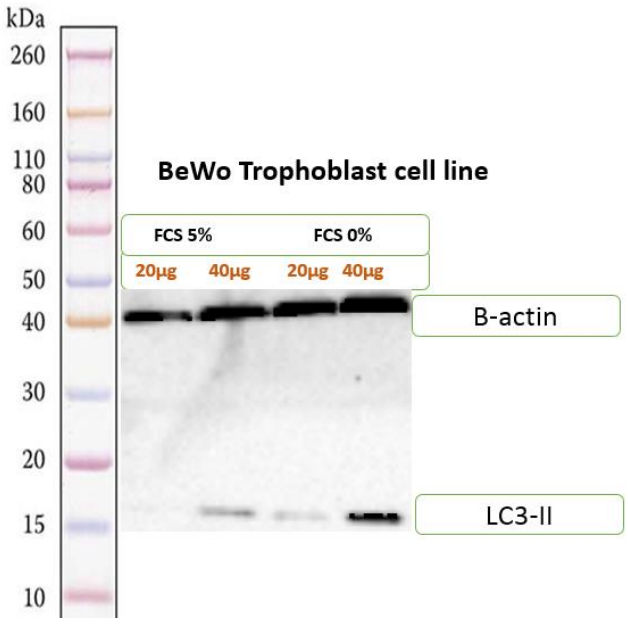

Figure 6-1 Autophagosome membrane LC3 protein expression under different protein loading and FCS starvation.

6.4.2 Drug treatments

6.4.2.1 Western Blotting

Autophagy and apoptosis-related protein expression was assessed using Western blot analysis. BeWo cells were treated with several drug treatments individually and in combination (described in methodology section 2.11.1) to explore their potential effect on the apoptotic and autophagy proteins.

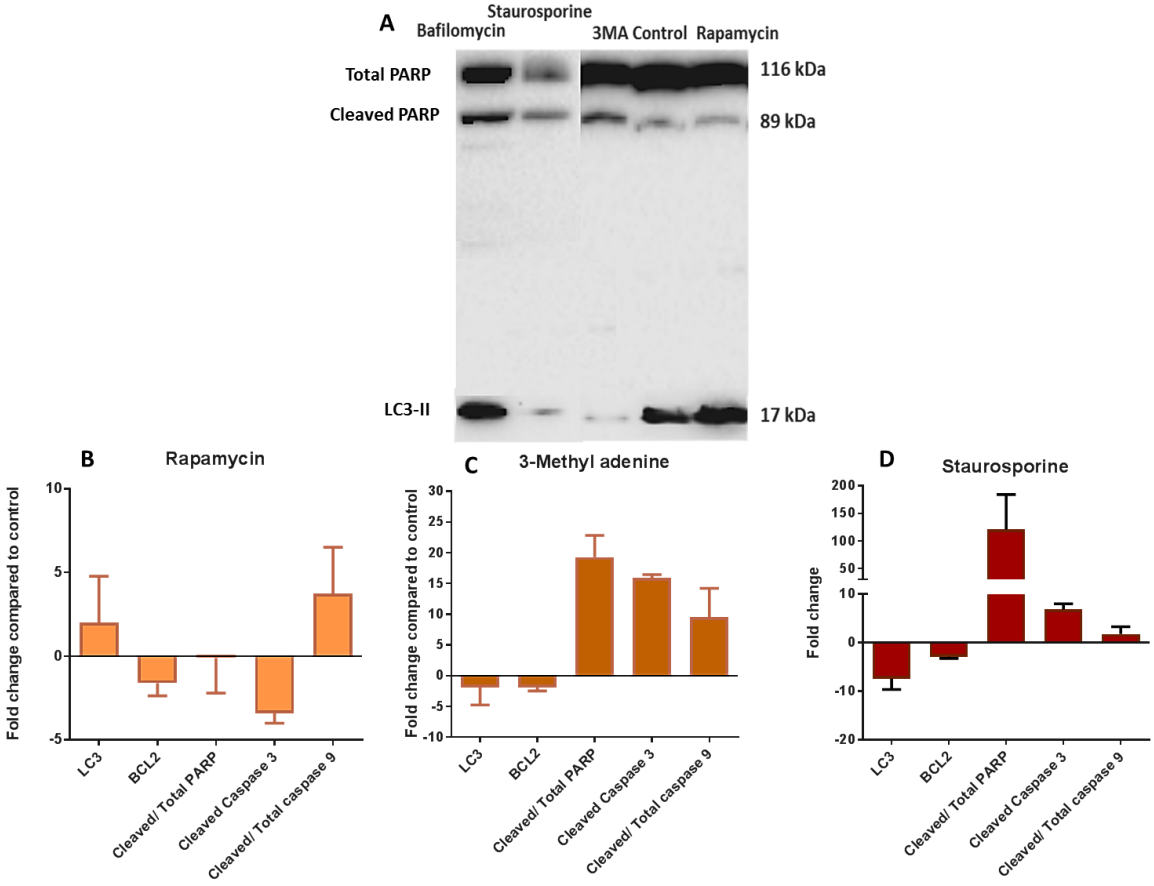

Figure 6-2 Representative Western blotting and relative expression of autophagy and apoptosis-related proteins in drug treated BeWo cells. (A) Representative western blot of LC3 protein expression and cleaved/Total PARP expression in BeWo cells treated with Staurosporine (STP), 3MA and Rapamycin. (B) Relative expression by fold change of LC3, Bcl-2 and apoptotic cascade proteins in Rapamycin (autophagy inducer) treated BeWo cells. (C) Relative expression by fold change of LC3, Bcl-2 and apoptotic cascade proteins in 3MA (autophagy inhibitor) treated BeWo cells. (D) Relative expression by fold change of LC3, Bcl-2 and apoptotic cascade proteins in Staurosporine (apoptosis inducer) treated BeWo cells. It showed a marked increase in the apoptotic proteins with a reciprocal reduction in the LC3 autophagy marker.

Relative protein expression was quantified by densitometry (OD/mm^2) using Image Lab (Version 5.2.1) image analysis software (Bio-Rad). Protein levels of the treated cells were expressed as densitometry ratio with the relative control, followed by overall standardisation to beta actin as a house keeping protein, thus represented as fold change (increase or decrease) from the control.

The addition of Rapamycin (Merck Millipore)[15], a known inducer of autophagy and an inhibitor of mTOR signalling supplied as a 10 mM (1 mg/109 µl) solution of Rapamycin (Cat. No. 553210) and used in a working concentration of 2.5 µM for 24 hrs (191, 290) induced the expression of LC3 and reduced that of the cleaved/total PARP. Conversely, the addition of 3-Methyladenine (3-MA; 100mg, CAS 5142-23-4, Merck Millipore)[16] an autophagy inhibitor, 3-MA, at a stock concentration of 200mM and a working concentration of 5mM for 1 hr (291) resulted in lower LC3 expression and a reciprocal increase in all of the apoptotic pathway proteins (Figure 6-2B).
A similar effect was seen with Staurosporine (STP)**,** an apoptosis inducer, used at a final concentration of 1µM for 4 hours, leading to marked elevation of the cleaved-to-total PARP expression with a reciprocal reduction of the autophagosome protein LC3 and the antiapoptotic protein Bcl-2 expressions (Figure 6-2C). This suggests that both drugs (3-MA & STP) might have similar effects on autophagy/apoptosis and that STP might induce its apoptotic effect by reduction of the pro-survival autophagy flux as well as through downregulating anti-apoptotic Bcl-2 proteins.

6.4.2.2 Flow cytometry analysis (FACS)

FITC Annexin V Apoptosis Detection Kit II was used to quantify the percentage of cells undergoing active apoptosis within the cell population. Its ability to do so depends on the cells' character to lose its membrane asymmetry in the early apoptotic cascade. The membrane phospholipid phosphatidylserine (PS) is flipped from the inner plasma membrane leaflet to the outer leaflet in apoptotic cells, thereby revealing PS to the external environment. Propidium iodide (PI), a standard viability probe, was

15 http://www.merckmillipore.com/GB/en/product/InSolution%E2%84%A2-Rapamycin-in-EtOH,EMD_BIO-553212?cid=BI-XX-BRC-A-BIOC-INHI-B123-1308&bd=1

16 http://www.merckmillipore.com/GB/en/product/Autophagy-Inhibitor%2C-3-MA---CAS-5142-23-4---Calbiochem,EMD_BIO-189490

used to distinguish viable from nonviable cells. PI permeates membranes of dead and necrotic and excluded in viable cells. Annexin V, a calcium-dependent phospholipid-binding protein, binds with high affinity to PS, thus identifying early apoptotic cells. Cells stained positive for FITC Annexin V and negative for PI were labelled as experiencing early-mid stage apoptosis. Cells that stained positive for both FITC Annexin V and PI were either gated in the late stage of apoptosis, or experiencing necrosis, or were already dead. Cells that were negative for both FITC Annexin V and PI were identified as alive and not experiencing quantifiable apoptosis.

In order to validate the effects of autophagy/apoptosis modifying drugs on BeWo cells seen in protein expression, flow cytometry analysis was used to demonstrate their effects in these cell populations. The percentage of each subpopulation was illustrated as fold change relative to the respective subpopulation in the control cells.

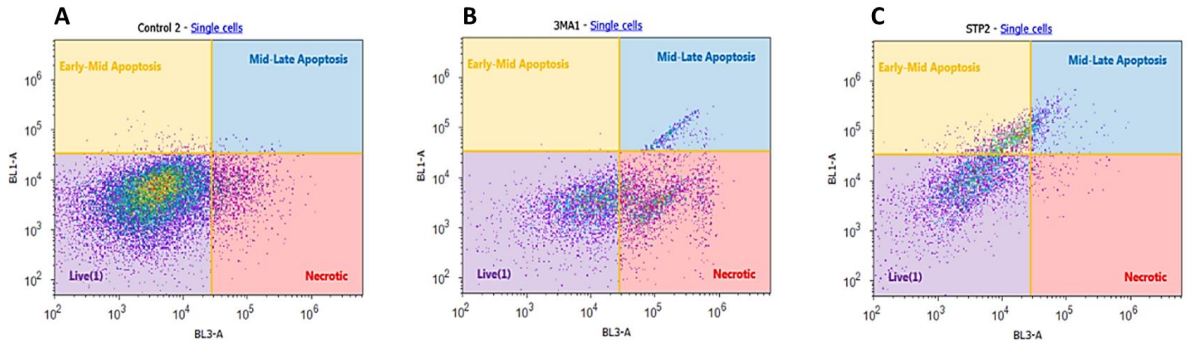

Figure 6-3 Representative images of flow cytometry analysis in drug-treated BeWo cells. The single cell population were segregated into four quadrants (Live, Early, Late apoptosis and Necrotic). (A) Control BeWo cells showing most of its single cell population in the live quadrants with minimal early and late apoptosis sub-population. (B) 3-MA, autophagy inhibitor, treated BeWo, at a concentration of 5mM for 1 hr showed a reduction in the live cell population with an activated apoptosis pathway leading finally into necrosis. (C) STP, apoptotic inducer treated BeWo, used at a final concentration of 1μM for 4 hours, showed a reduction in the live cell subpopulation and activation of the apoptotic cascade.

Staurosporine-treated BeWo (1μM for 4 hours) revealed more than fivefold increase in the early apoptotic cell population and 12-fold increase in the cells undergoing late apoptosis (Figure 6-4A). These findings are consistent with the Western blot analysis of the apoptotic caspase protein expression in STP-treated BeWo (Figure 6-2C).

BeWo cells were treated with 3-MA, an autophagy inhibitor, at a concentration of 5mM for 1 hr (291), to identify whether changes in the cell populations were consistent with

protein expression analysis. Flow cytometry analysis showed that 3-MA treated cells revealed a 30 fold increase in the late apoptotic cell population and fivefold reduction in the live cell population with a reciprocal fivefold increase in necrotic cell population.

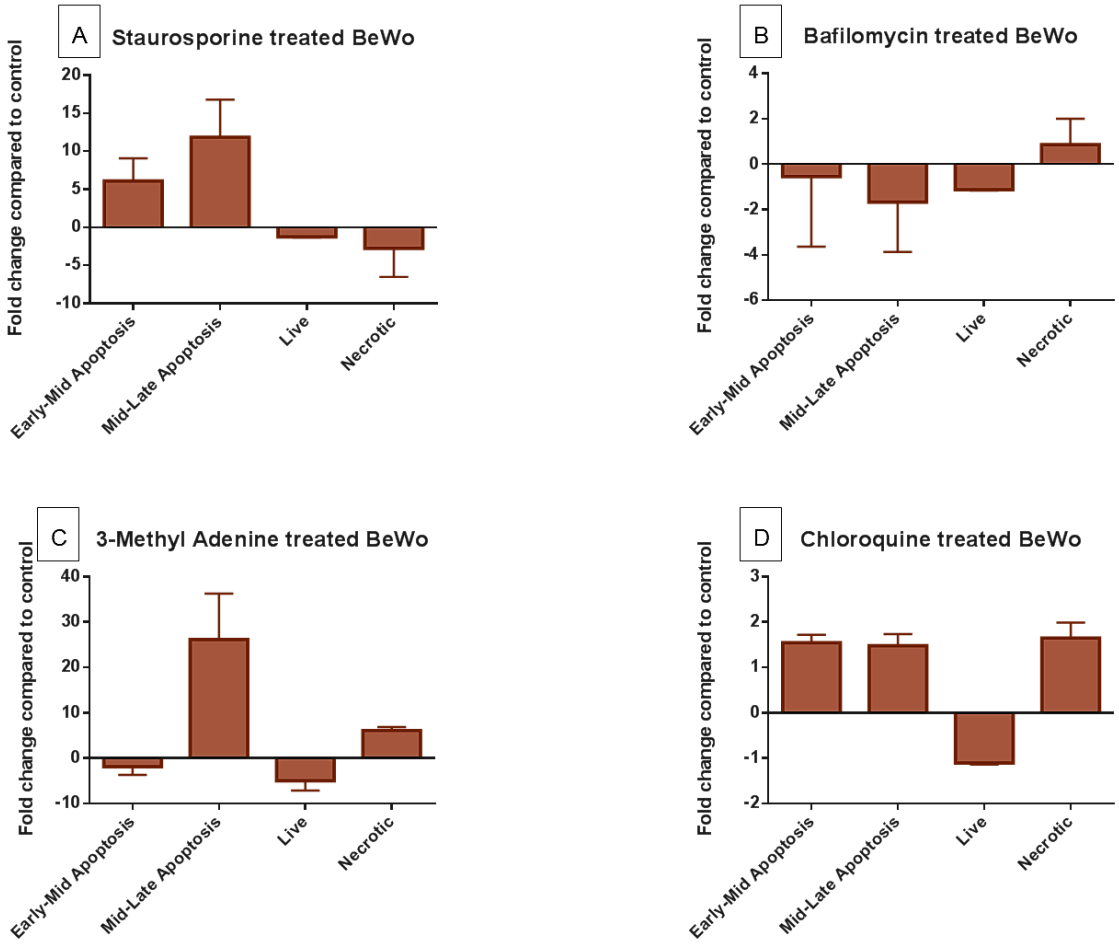

Figure 6-4 Fold changes in cell populations (Early-Mid, Mid-Late apoptosis, Live and necrotic cells) of drug treated BeWo cells compared to control BeWo. (A) Staurosporine (STP), an apoptotic inducer, treated BeWo cells (n=3), used at a final concentration of 1μM for 4 hours, showed a 5 and 12 fold increase in early and late apoptotic subpopulations respectively compared to control BeWo. (B) Bafilomycin treated BeWo showed modest reduction in the live cell population and early-Late apoptosis as well (C) 3-Methyl adenine treated BeWo, and autophagy inhibitor, at a concentration of 5mM for 1 hr showed a significantly higher late apoptotic cell subpopulation (25 folds) with a reduction in the live cell population (5 folds). (D) Chloroquine treated cells (n=3) showed a modest increase in the early and Late apoptosis with a reciprocal decrease in the live cell population.

These data agreed with the Western blot data which showed an increased expression of apoptotic caspase proteins in 3-MA treated BeWo cells (Figure 6-2B). Moreover, BeWo cells treated with chloroquine at 60 μM concentration demonstrated a rise in

early, late and necrotic apoptotic cell populations with a proportionate reduction in the live cell population (Figure 6-4).

After quantification of protein expression using western blotting and the percentage of the cell populations using flow cytometry analysis, a qualitative assessment of autophagy in drug-treated BeWo was used to visualise the autophagy vesicles, their size, numbers and localisations.

6.4.2.3 Fluorescence microscopy

Autophagosomes are essentially cellular vacuoles intended for waste recycling and disposal. The study of their localisation, size and numbers using live cell fluorescence microscopy, in addition to the protein expression, is essential for a complete, quantitative and qualitative, evaluation of the autophagy function.

Autophagy vacuoles were assayed using the CYTO-ID® Autophagy Detection Kit (ENZ-51031-K200, Enzo®), showing autophagic vacuoles in live cells using a proprietary dye specific for staining autophagic vesicles and exhibiting a bright fluorescence upon incorporation into pre-autophagosomes, autophagosomes, and autolysosomes (autophagolysosomes), and visualised by EVOS® Fluorescence Live Cell Imaging System microscope.

6.4.2.3.1 Control BeWo cells

Autophagosomes were seen as bright green vacuoles in BeWo cells (control) as multiple small fluorescent green vacuoles (Figure 6-5).

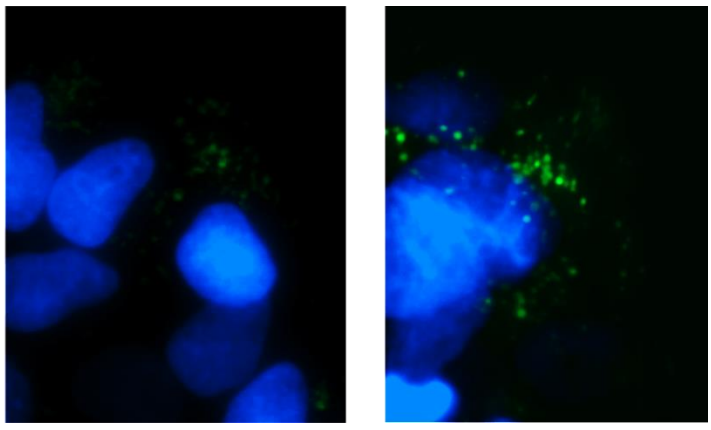

Figure 6-5 Representative images of autophagosomes (bright green) in control BeWo cells. Cells were stained with Hoechst stain (blue) to demarcate cell nuclei and autophagy vacuoles appear bright green.

6.4.2.3.2 Rapamycin-treated BeWo cells

Treating the cells with Rapamycin, an autophagy inducer, for 24hrs led to a marked increase in the numbers of autophagy vacuoles (Figure 6-6), demonstrating the specificity of the dye to autophagosomes and validity of the BeWo cells as a good *in vitro* model for trophoblast autophagy.

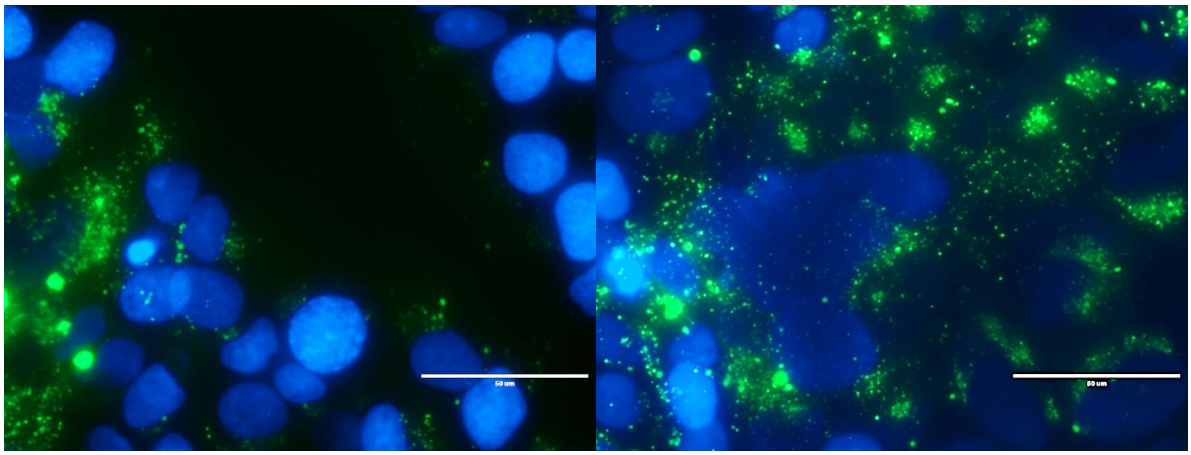

Figure 6-6 Representative images of fluorescent labelled autophagosomes in rapamycin (autophagy inducer) treated BeWo. Rapamycin-treated BeWo, used in a working concentration of 2.5 µM for 24 hrs, showed a markedly increased number of autophagy vacuoles (bright green). Cells were stained with Hoechst stain (blue) to demarcate cell nuclei and autophagy vacuoles appear bright green.

6.4.2.3.3 Chloroquine-treated BeWo

BeWo cells were also treated with chloroquine (CLQ), an immune modulator, known to inhibit autophagy flux by increasing lysosomal pH, thereby inhibiting lysosomal activity leading to accumulation of autophagosomes without proper digestion by lysosomes, thus reducing the turnover of the autophagolysosomes and inhibiting the autophagy flux (435). CLQ-treated BeWo showed an increase in the size of the autophagosomes. The chloroquine-induced increase of autophagosome size occurred in a dose-dependent manner between working concentrations of 20µM, 60µM and 120µM (Figure 6-7 and Figure 6-8). Transmission microscope image overlay was used to identify perinuclear cellular vacuolar appearances that overlaid with green fluorescently labelled autophagosomes (Figure 6-7B & Figure 6-8B).

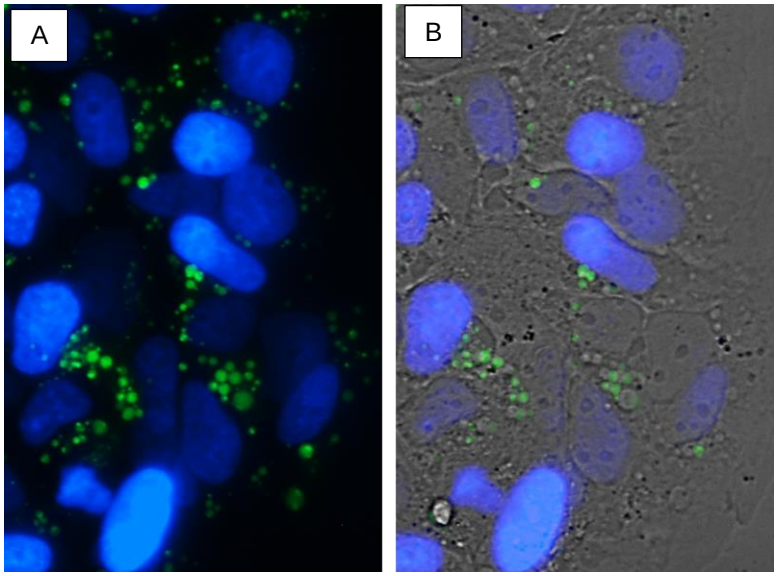

Figure 6-7 Representative images of Chloroquine (CLQ)-treated BeWo (60µM concentration). (A) CLQ-treated BeWo cells demonstrated an increase in size of the autophagy vacuoles. (B) A phase overlay of the same image showing the green autophagosomes in their designated cellular vacuoles. Cells were stained with Hoechst stain (blue) to demarcate cell nuclei.

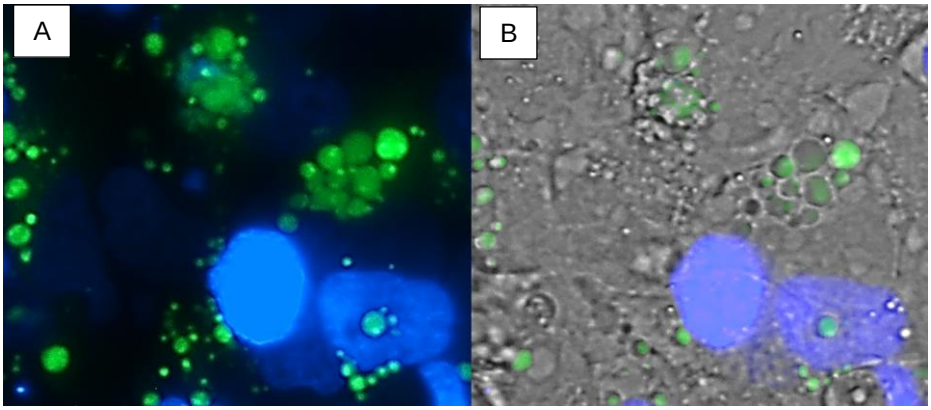

Figure 6-8 Representative images of Chloroquine-treated BeWo (120µM concentration). (A) CLQ-treated BeWo cells demonstrated an increase in size of the autophagy vacuoles becoming more coalescent. (B) A phase overlay of the same image showing the green autophagosomes in their designated cellular vacuoles. Cells were stained with Hoechst stain (blue) to demarcate cell nuclei.

6.4.3 MicroRNA manipulation of BeWo cells and its effect on autophagy

The combined approach of the *in silico* analysis of miRNA targets in different databases together with the focused literature search of those miRNAs, with their potential role in the autophagy/apoptosis cascades, resulted in five miRNAs of potential importance, differentially expressed in some of the placental dysfunction related literature. These miRNAs were miR-204, miR-182, miR-192, miR-145 and let-

7a. To explore the potential role that some of these miRNAs play in trophoblast function, their expression levels were quantified using RT-qPCR in different trophoblast cell lines (Figure 6-9).

6.4.3.1 Expression levels of autophagy-related miRNAs in cell lines

The expression levels of the chosen miRNAs were quantified in RNA extracted from purified stroma and cytotrophoblasts derived from human placental explants (**Error! eference source not found.**). They were also measured in different human tumour-derived trophoblast cell lines including BeWo, JEG-3, JAR and the placental cell line Swan-71 (Figure 6-9).

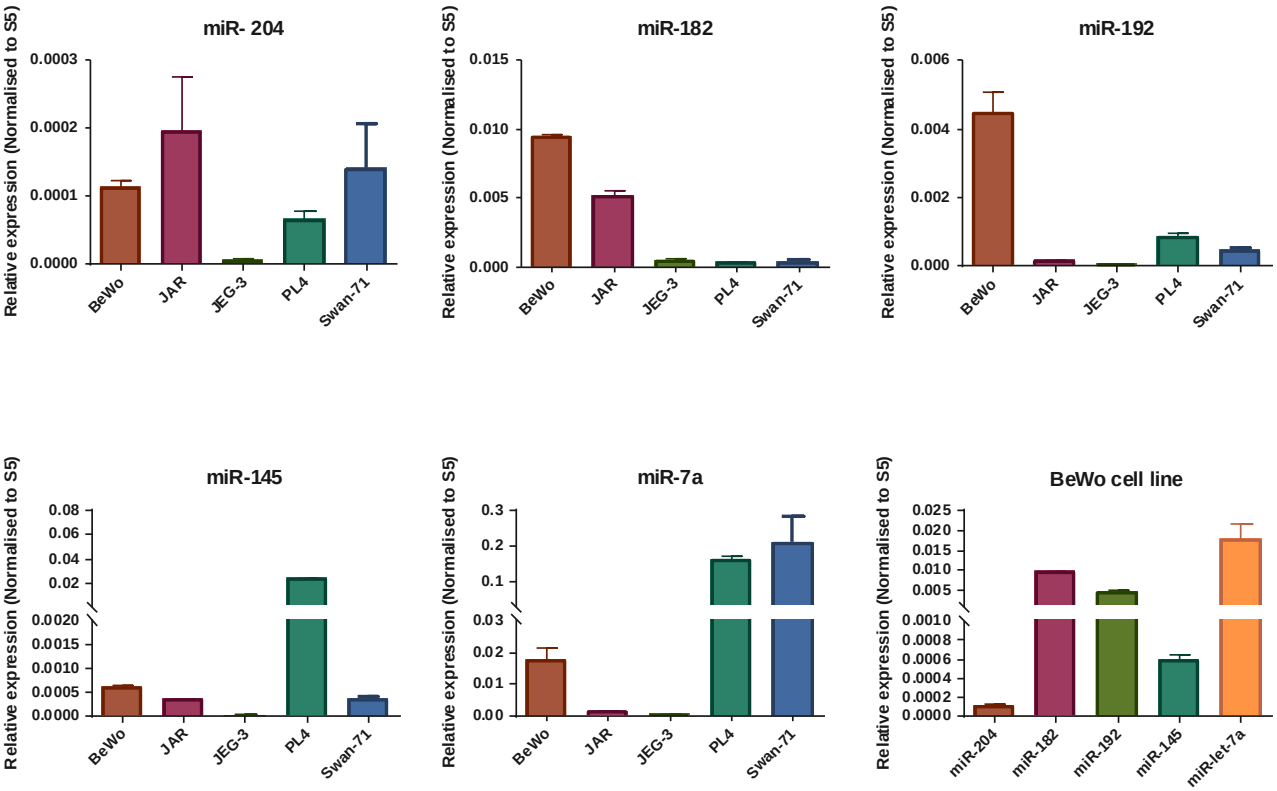

Figure 6-9 Expression levels of miR-204, miR-182, miR-192, miR-145 and miR-7a in BeWo, JAR, JEG-3, PL4 and SWAN-71 trophoblast cell lines. Expression of miR-204 was lower than the rest of miRNAs studied in BeWo cell line.

The expression levels of miR-204 were higher in the JAR villous-derived trophoblast cell line compared to all of the rest and lowest in the JEG-3 extravillous derived cell line. BeWo cells showed around half the expression levels of miR-204 in JAR cells.

On the other hand, miR-192 and miR-182 showed the highest miRNA expression in BeWo cells compared to any other cell line studied. In addition, miR-let-7a levels were the highest in placental Swan-71 cells and lowest in the JEG-3 cells (Figure 6-9).

On comparing the different expression profile of the chosen miRNAs in BeWo cells, Let-7a was the most highly expressed followed by miR-182, miR-192 and miR-145. Coming last, miR-204 had the lowest expression in BeWo cells compared to the rest of the studied miRNAs (Figure 6-9). This directed the choice for transfection with a miR-204 mimic to induce its expression in BeWo cells and explore its function in relation to the autophagy/apoptosis cascade.

6.4.3.2 Transfection efficiency and cell viability

To ensure that the transfection procedure allowed an optimum uptake of miR mimics whilst maintaining maximum cell viability, BeWo cells were transfected with 10nM, 50nM and 100nM fluorescently tagged non-targeting (NT) CY3 labelled pre-miR negative control (pre C) in addition to control and mock transfection (with the transfection reagent, Dharmafect2, without the pre-miR).

6.4.3.2.1 Fluorescence microscopy

Photomicrographs (Figure 6-10) provided visual confirmation that the miRNA mimic sequences were successfully introduced to BeWo cells with Dharmafect and quantification revealed that the transfection efficiency of the NT miRNA (Figure 6-10) at 50nM was 78.3% ± 1.3% (n=3) and 85.8% ± 3% at 100nM (n=5). Assessment of trophoblast cell viability demonstrated that the transfection procedure resulted in extremely low levels of cell toxicity (more than 86.9 ± 3.4% of cells remained viable). This was consistent with previous data that used Dharmafect to introduce siRNA into primary trophoblasts and cell lines (289) and showed that this procedure was suitable for introducing miRNAs to trophoblast cell lines.

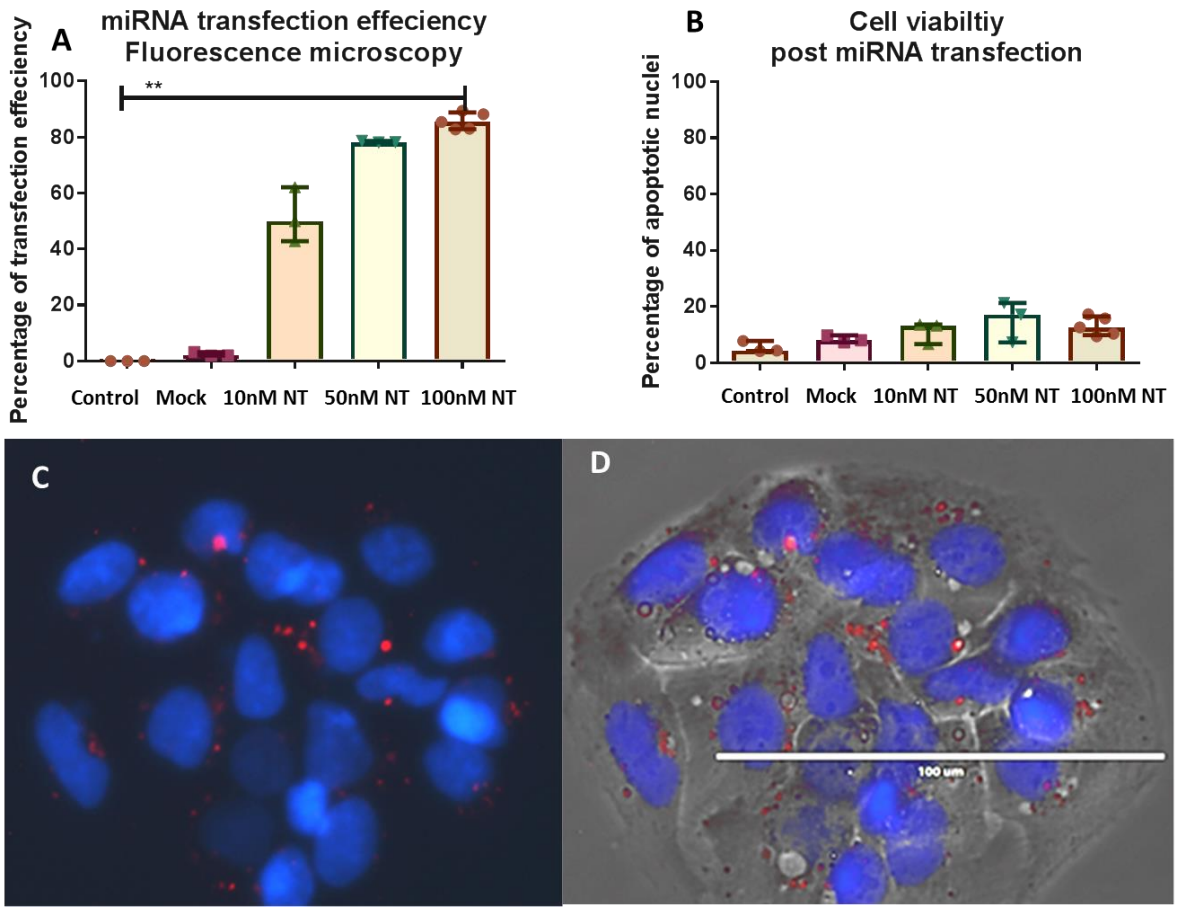

Figure 6-10 Assessment of transfection efficiency and cell viability by fluorescence microscopy. BeWo cells were visualized 24 hours after transfection and stained with Hoechst stain (blue) to demarcate cell nuclei using fluorescent microscopy. (A) BeWo cells were transfected with 10 nM, 50nM and 100nM fluorescently tagged non-targeting (NT) CY3 labelled pre-miR negative control (pre C) in addition to control and mock transfection (with the transfection reagent, Dharmafect2, without the pre-miR). Transfection efficiency was measured using fluorophore-labelled NT miRNA/nuclei counted against the total number of nuclei. (B) Cell viability was assessed from the number of apoptotic nuclei after NT miRNA transfection. (C) Fluorescently tagged NT miRNAs appear red and nuclei appearing blue. (D) A Phase image overlay of BeWo cell nuclei (stained blue) & NT-miRNA (stained red) with a transmission microscope image overlay (grey). Fluorescently tagged miRs are visible in the cytoplasm after phase overlay demonstrating successful transfection has occurred.

6.4.3.2.2 Quantification of miR-204 by qRT-PCR

Real time quantitative PCR was used to quantify the expression patterns of the miR-204 in miR-204 transfected BeWo cells at concentrations of 10, 50 and 100nM compared to control, mock transfected (Dharmafect only) and Non-Targeting (NT) miRNA transfection at 10, 50 and 100nM concentrations.

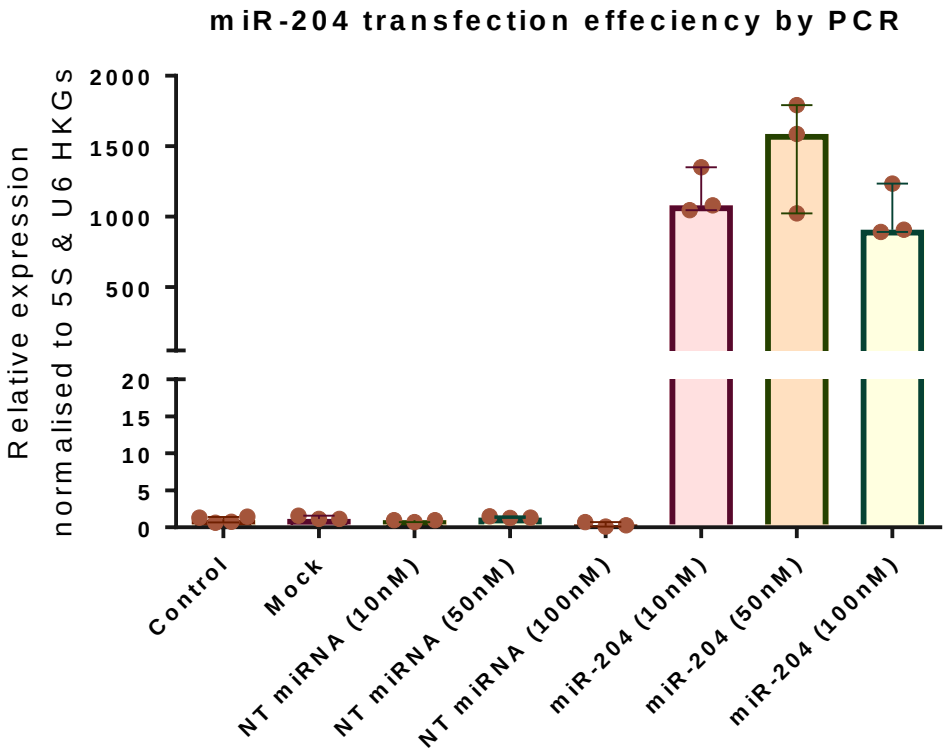

Figure 6-11 Expression levels of miR-204 using qRT-PCR in miR-204 transfected BeWo cells at concentrations of 10nM, 50nM and 100nM compared to control, Mock & Non Targeting miRNA transfected BeWo cells at concentrations of 10nM, 50nM and 100nM. miR-204 transfected BeWo at 50nM concentration displayed the highest miR-204 expression profile compared to the other transfection groups.

Results revealed that miR-204 transfected BeWo (50nM) showed the highest expression patterns (Figure 6-11) with more than 1500 transcripts quantified compared to non-miR-204 transfected BeWo cells. This data agreed with the transfection efficiency measured by fluorescence microscopy. Furthermore, these results validated the effectiveness of the BeWo cell line transfection with a miR-204 mimic and thus functional studies observed from such transfection would be valid to test our hypothesis of autophagy/apoptosis regulation by miR-204.

6.4.4 Effects of miR-204 transfection

6.4.4.1 Live cell imaging of the colony growth and numbers

The effects of miR-204 transfection on cell growth and proliferation were first studied by live-cell imaging microscopy to identify colony growth, count and size at 48 hours post transfection compared to control and NT miRNA transfection.

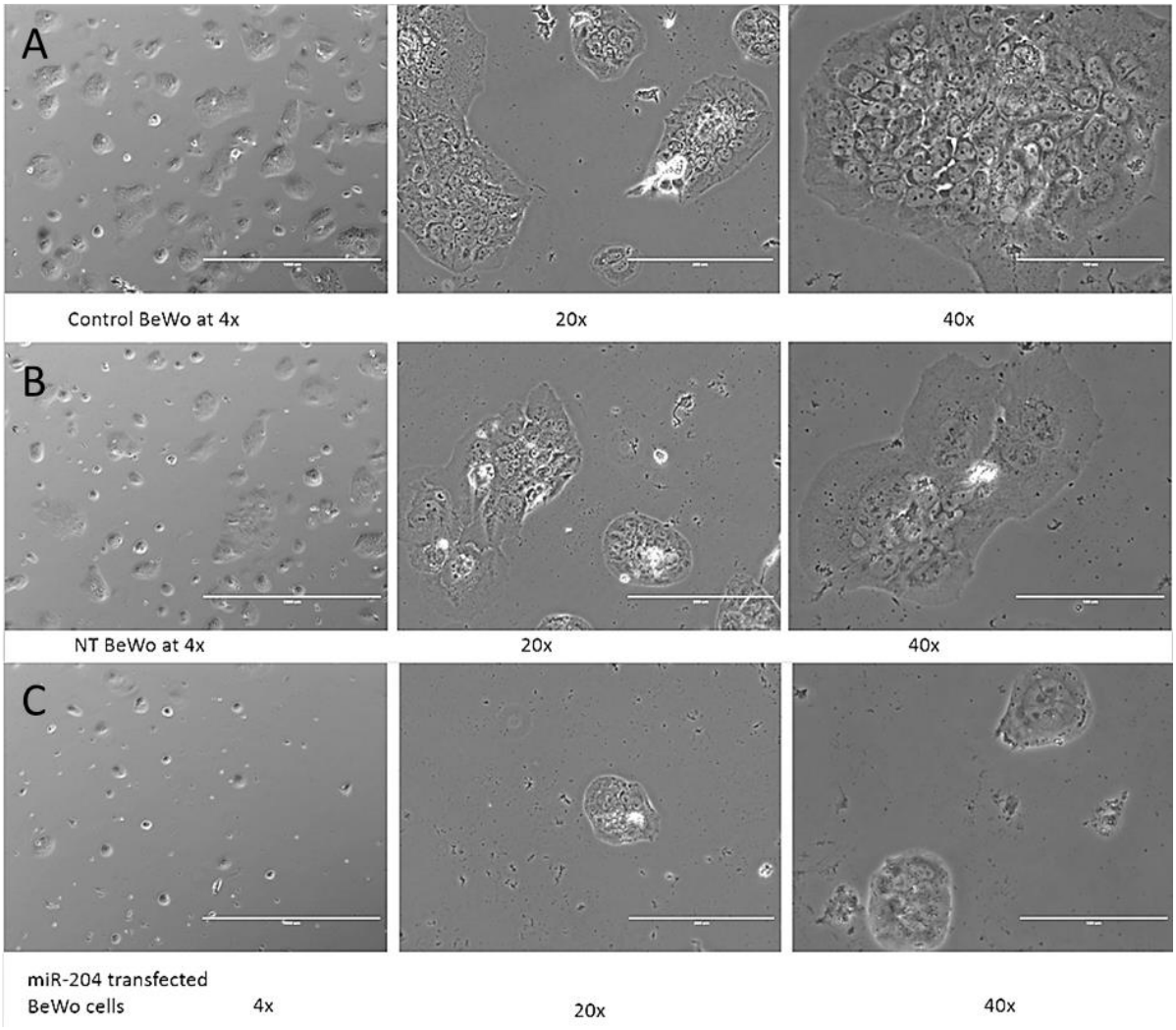

Figure 6-12 Representative images of BeWo cell colony proliferation patterns 48 hrs post-transfection in Control (A), NT miRNA transfected BeWo (B) and miR-204 transfected cells (C) visualised by EVOS® Live Cell Imaging System microscope. (A) Control BeWo cells showed typical colony growth and confluence (4x magnification) and typical colony size (20x and 40x magnification). (B) NT miRNA transfection showed similar colony number to control (4x magnification) with slightly smaller colony size (20x and 40x magnification). (C) miR-204 transfected BeWo showed markedly reduced colony numbers compared to NT transfected and Control (4x magnification) and reduced colony size as well in 20x and 40x magnifications.

Images from miR-204 transfected BeWo cells revealed evidence of reduced colony growth and proliferation indicated by the decrease in the colony numbers and size compared to NT miRNA transfected BeWo and control cells. Furthermore, miR-204 transfected cells showed more evidence of cellular debris (Figure 6-12C) around smaller colonies. This might indicate a higher propensity of cell death and slower growth in the miR-204 transfected cells.

6.4.4.2 Fluorescent microscopy

The size and the numbers of the autophagy vacuoles in miRNA transfected cells were studied using fluorescence microscopy. NT miRNA-transfected BeWo cells revealed no differences in vacuolar size or arrangements compared to control cells. They constituted multiple small sized vacuoles alongside the nucleus (Figure 6-13).

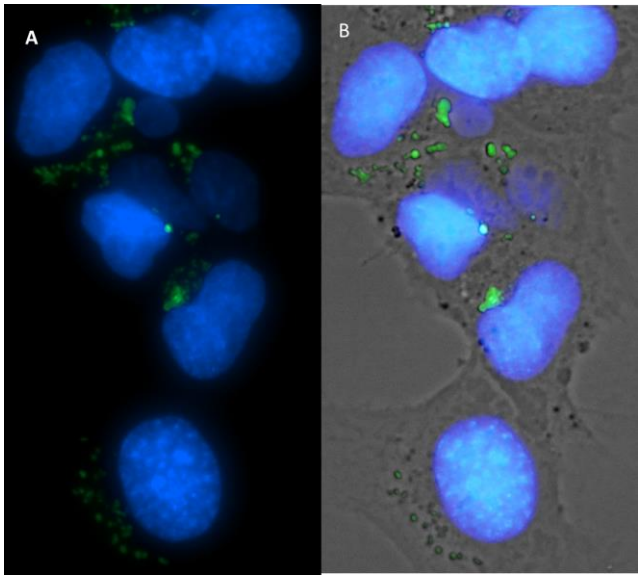

Figure 6-13 Representative images of fluorescent green autophagy vacuoles in Non-Targeting miRNA transfected BeWo. (A) with a phase overlay identifying cellular borders (B). Cells were stained with Hoechst stain (blue) to demarcate cell nuclei and autophagy vacuoles appear bright green.

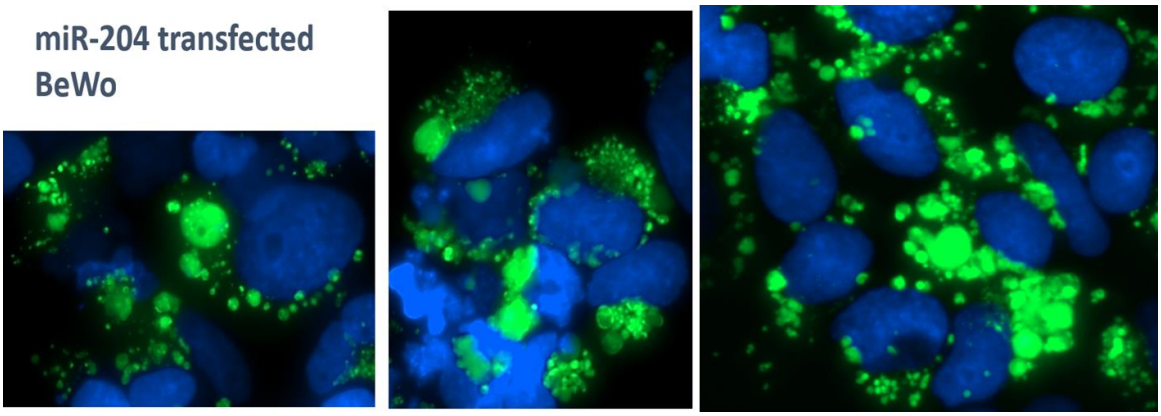

Figure 6-14 Representative images of fluorescent green vacuoles (autophagosomes) in miR-204 transfected BeWo cells. Images show an increase in the average size of each vacuole (40x magnification). Cells were stained with Hoechst stain (blue) to demarcate cell nuclei and autophagy vacuoles appear bright green.

Contrastingly, miR-204 transfected cells showed a significant increase in the accumulating number and size of the autophagy vacuoles with a propensity to form a larger coalescent vacuoles. This might be due to accumulation of cellular waste inside these autophagosomes with limited ability to recycle them and complete the autophagy flux. These enlarged autophagy vesicles were similar to those found in CLQ-treated cells (Figure 6-8). These results indicate that miR-204 is likely to play a role in the flux of the autophagy pathway (Figure 6-14).

The interlinking relationship between autophagy and apoptosis is well known in different body systems. Exploring this relationship in trophoblast cell lines is still new especially the role that miRNA have to play in such intertwined relationship. Thus, it seemed sensible to study this relationship by measuring the percentage of apoptotic/necrotic cells using flow cytometry analysis and protein expression of different autophagy and apoptotic cascade-related proteins using Western blotting.

6.4.4.3 Flow cytometry analysis

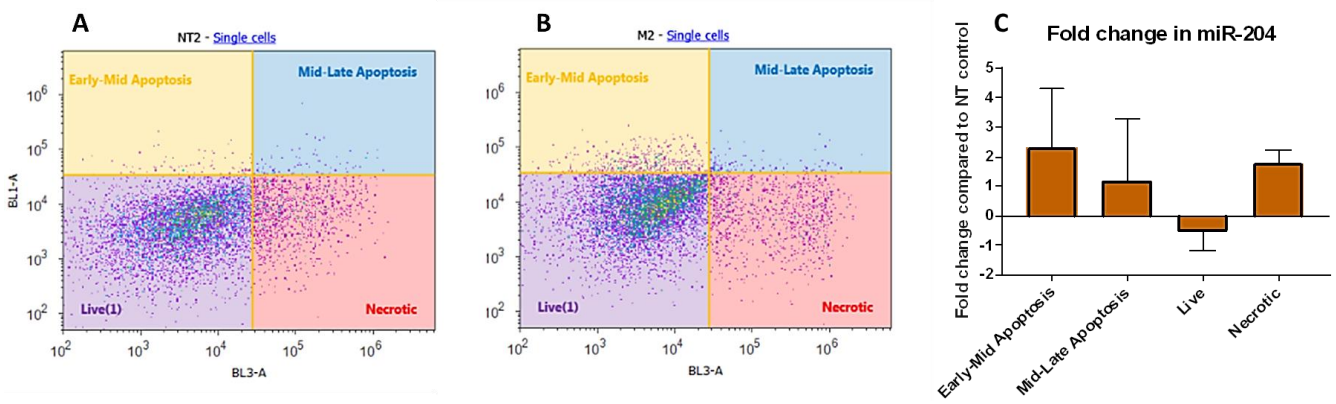

Figure 6-15 Flow cytometry analysis of (A) control NT miRNA transfected BeWo cells and (B) miR-204 transfected BeWo cells. The single cell population were segregated into four quadrants (Live, Early, Late apoptosis and Necrotic). (A) NT transfected BeWo cells showing most of its single cell population in the live quadrants with minimal early and late apoptosis sub-population. (B) miR-204 transfected BeWo showed an increase in the early apoptotic and the necrotic subpopulation with a lower live cell population (n=3). (C) Fold changes in cell populations (Early-Mid, Mid-Late apoptosis, Live and necrotic cells) of miR-204 transfected BeWo compared to Non-targeting (NT) miRNA transfected BeWo**.** miR-204 transfected BeWo cells (n=3) showed a two fold increase in early-mid apoptotic and necrotic sub-populations and a one fold increase in mid-late apoptotic sub-population with a reduction in the live cell population.

As shown in Figure 6-15, flow cytometry analysis identified the percentage of different subpopulations (Live, early, late apoptosis/necrosis) from single cell populations. miR-204 transfected BeWo cells (n=3) demonstrated a 2-fold increase in the early apoptotic subpopulation and one and half fold increase in late apoptosis/necrotic subpopulation with a reduction in the live cell population. These results were consistent with the microscopy images of the colony growth and proliferation of the miR-204 transfected BeWo that showed a slower growth patterns and increased cellular debris (Figure 6-12).

6.4.4.4 Western blotting

The expression profiles of the autophagy and the apoptotic pathway proteins in miR-204 transfected BeWo cells, compared to its control NT miRNA transfected BeWo, were assessed using western blot analysis. This enabled us to explore the relationship between trophoblast autophagy and apoptosis and how miRNAs like miR-204 might modulate such relationship.

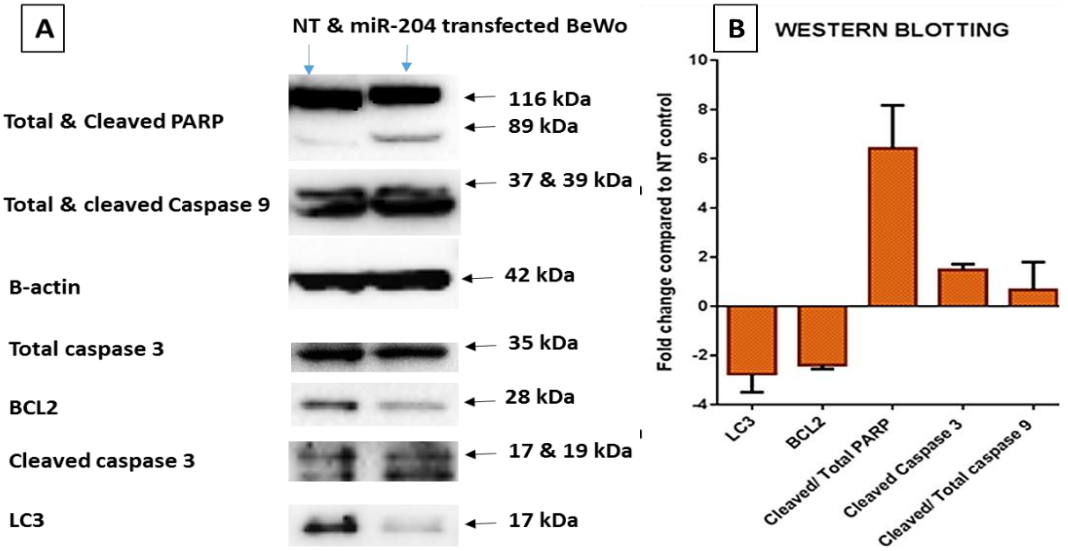

Figure 6-16 miR-204 transfection inhibits autophagosome LC3 and antiapoptotic Bcl-2 with reciprocal induction of pro-apoptotic proteins. (A) Representative western blot showing the expression of LC3, Bcl-2, cleaved & total caspase 3. Cleaved & total caspase 9, cleaved and total PARP in miR-204 transfected BeWo cells compared to NT miRNA transfected BeWo cells (n=3)**.** (B) Effects of miR-204 transfection in fold change of the LC3, Bcl-2, cleaved & total caspase 3 & 9 as well as cleaved and total PARP.

Relative protein expression bands were quantified by densitometry (OD/mm^2). Protein levels of the miR-204 transfected cells were standardised to its corresponding beta

actin as a house keeping protein, then expressed as densitometry ratio with the NT miRNA transfected control, thus represented as fold change (increase or decrease) from the control.

As a final confirmation of changes in the autophagosome LC3 protein, antiapoptotic Bcl-2, and their reciprocal relationship with the apoptotic cascade proteins, Western blot analysis revealed around a threefold reduction in the LC3 protein expression in the miR-204 transfected BeWo cells (Figure 6-16). There was also evidence of a two-fold reduction of antiapoptotic Bcl-2 protein expression. Conversely, apoptotic cascade proteins showed an upregulation compared to control. The ratio of cleaved to total caspase 3 showed just below a two-fold increase in protein expressions compared to its control. Interestingly, cleaved/total PARP, a terminal executioner apoptotic protein, was six-fold higher compared to its expression in the NT miRNA transfected control.

These data agree with the observations seen with the colony growth, size and proliferation study done using the live cell microscopy (Figure 6-12), which showed a smaller colonies, less growth confluence and higher cellular debris in the miR-204 transfected BeWo colonies compared to control and NT miRNA transfected BeWo cells. Moreover, the western blot data was consistent with the increased cell populations undergoing early and late apoptosis/necrosis using FACS in the miR-204 transfected cells.

6.5 Discussion

BeWo, a choriocarcinoma cell line, a commonly used *in vitro* model for trophoblast function was used to explore autophagy induction, regulation (291) and manipulation with drugs and miRNAs (433, 434) and its relation to the apoptotic cascade. BeWo cells proved to be a good model for autophagy induction through their response to starvation with restricting FCS, leading to an increased LC3 expression. This was consistent with another study which found that culture of BeWo cells in reduced oxygen tension and/or serum deprived settings resulted in the appearance of autophagosomes (436).

Moreover, the pre-treatment of BeWo cells with rapamycin, an autophagy inducer which inhibits mTOR kinase activity, increased LC3 expression by western blot and substantially increased the number of autophagy vacuoles by fluorescent microscopy. Rapamycin works through inactivating mammalian target of rapamycin signalling pathway, indicating that mammalian target of rapamycin regulates autophagy in BeWo cells. A similar conclusion was also suggested as well in a study carried out on cultured trophoblasts (96).

On the other hand, 3-MA, which is known to inhibit the early phase of the autophagic process (292), decreased the expression of LC3 and induced apoptosis, indicated by activation of caspase 9 & 3 and cleaved PARP using western blot analysis. These findings were validated by FACS analysis, which showed an increased percentage of apoptotic/necrotic subpopulations and a reciprocal decline in the live cell population in 3-MA treated BeWo cells. These results agree with other studies reporting a reduction in the autophagosome formation and apoptosis induction and enhanced cell death in renal tubular epithelial cells (437) as well as human breast cells (293) and human bladder cancer cells (438).

Similarly, pre-treatment of BeWo cells with Staurosporine (STP), known to induce apoptosis in many cell lines (296-298), has revealed an induced caspases and markedly elevated cleaved PARP activity (cleavage of which expedites cellular disassembly and acts as a marker of cells undergoing apoptosis) by Western blot analysis. Interestingly, this pro-apoptotic effect was associated with a marked decrease in the autophagosome marker LC3 indicating some sort of intracellular

balance between the autophagy and apoptotic cascades. This also might suggest that the pro-apoptotic effect of STP is partially through inhibiting the autophagosome recycling function. This proapoptotic effect of the protein expression data agreed with FACS analysis data revealing an increase in the apoptotic cell population and a reciprocal reduction in the live cell population.

BeWo cells were also pre-treated with chloroquine which is an anti-inflammatory drug that increases lysosomal pH, thereby inhibiting lysosomal activity and known to inhibit autophagy flux and autophagosomal function (435). It is also used in the treatment or prevention of malaria (295). Chloroquine (CLQ) treated BeWo cells, under live cell fluorescence microscopy, revealed an increase in the size of the autophagy vesicles. The chloroquine-induced increase of autophagosome size occurred in a dose-dependent manner. This data was consistent with other studies showing an increase in size of autophagy vesicles (292, 439) in CLQ-treated cells.

Moreover, this accumulating data might indicate the importance this drug could play in the regulation of autophagy in the placenta and its potential role in preventing perinatal morbidity and low birth weight. This assumption is strengthened by the findings of an epidemiological study of the effect CLQ chemoprophylaxis on perinatal morbidity and mortality in malaria-endemic regions. They prospectively studied 302 pregnant women analysing the outcome of pregnancy in relation to CLQ prophylaxis, controlling for parity and prenatal clinic attendance. The study showed that chloroquine prophylaxis was beneficial to the fetus, even in a region where endemic malaria was resistant to chloroquine with a reduced incidence of low-birth-weight infants (RR= 0.39), and perinatal death (RR=0.38) in women who took chloroquine prophylaxis (440). Nonetheless, more studies are needed to elucidate the mechanisms by which CLQ works in the placenta and the best way to regulate their function and harness their protective effects on the placenta and the fetus.

Our data consistently showed an inverse relationship between LC3 expression, an autophagic marker, and cleaved/total PARP, a terminal executory apoptosis marker, in BeWo cells under different drug treatments. This finding replicated what was found in a study carried out on cultured trophoblasts (96) suggesting there is an equilibrium between apoptosis and autophagy under standard conditions, and suggesting that

autophagy activation in trophoblasts might have a prosurvival role in an attempt to avoid late apoptotic cascade activation.

In this study, we have uncovered the presence, and started to dissect autophagy regulation in BeWo cells and demonstrated that there are intricate balance between the autophagic and apoptotic pathways which govern survival of trophoblasts. Though, the study is unlikely to mimic the placental *in vivo* milieu entirely, nonetheless, it is tempting to speculate that autophagy has an important placental housekeeping function *in vivo* by discarding damaged trophoblast organelles. Thus, providing a second chance for the placenta before progressing towards placental dysfunction.

Autophagy-related miRNAs identified from the *in silico* analysis of miRNA databases and the literature search yielded some potential miRNAs altered in placental dysfunction-related diseases that hypothetically might have a role to play in the autophagy pathway. These miRNAs were miR-204, miR-182, miR-192, miR145 and Let-7a. Their expression values in different trophoblast cell lines using qRT-PCR revealed a very low expression of the miR-204 in BeWo cells compared to the other miRNAs (Figure 6-9). Thus, miR-204 mimics was thought to be introduced into BeWo cells and upregulate their already low expression, and thus would be able to study their programmed cell death-related functions.

Visual confirmation and qRT-PCR quantification have showed that the miRNA mimic sequences were successfully introduced to BeWo cells with Dharmafect with high transfection efficiency and low level of cell toxicity. This was consistent with previous data that used Dharmafect to introduce siRNA into primary trophoblasts and cell lines (289) and showed that this procedure was successful for introducing miRNAs to trophoblast cell lines.

Our results illustrated that miR-204 transfected BeWo cells behaved differently compared to NT-miRNA transfected cells. That was evidenced by different techniques using live cell imaging, fluorescence microscopy, FACS and western blotting. Our data firstly suggested that miR-204 transfected colonies showed a slower growth potential with smaller size and reduced numbers compared to their controls. This was validated by FACS analysis that showed a higher percentage of apoptotic/necrotic cell populations with reduction of the percentages of live cells in miR-204 transfected

BeWo cells. Moreover, semi-quantitative analysis of western blotting revealed a significant reduction in the autophagosome marker LC3 and the antiapoptotic marker Bcl-2 compared to its NT control. Interestingly, this was associated with a reciprocal increase in the apoptotic markers cleaved caspase 3 and caspase 9 in addition to a marked rise in the expression of cleaved/total PARP. PARP, a 116 kDa nuclear poly (ADP-ribose) polymerase, can be cleaved *in vitro* by many Interleukin-1ß-converting enzyme (ICE)-like caspases (441) and is one of the chief cleavage targets of caspase-3 in vivo (442, 443). PARP is a marker of cells experiencing apoptosis and its cleavage is reported to expedite cellular disassembly (444).

The inverse relationship between the mature autophagosome marker LC3, antiapoptotic Bcl-2 in one side and the apoptotic caspases and PARP was also evident in BeWo cells treated with different autophagy altering drugs. This balance of autophagy with antiapoptotic markers against the apoptotic cascade proteins seems to be a hallmark of cellular integrity.

Although the pro-apoptotic role that miR-204 might play in placental dysfunction is still novel, nevertheless its role has been studied in different systems. One study showed consistent findings to ours demonstrating that miR-204 transfected human trabecular meshwork (HTM) cells had higher levels of apoptosis and decreased viability compared to control (430) suggesting that miR-204 might potentially play a central role in the regulation of apoptosis, accumulation of damaged proteins and endoplasmic stress (ER) stress response.

A possible mechanism of the pro-apoptotic effect of miR-204 is its post-transcriptional regulation by direct targeting of the 3′ UTR and thus downregulation of anti-apoptotic *BCL2* mRNA in neuroblastoma cells (445). The direct targeting of miR-204 to *BCL2* was also assessed in human colon cancer cells by transfecting an anti-miR-204 or introducing a three-point mutation into the miR-204-binding site leading to an increased *BCL2* mRNA and protein levels, while transfection with miR-204 mimic reduced their levels (446). Similarly, in gastric cancers miR-204 downregulation showed to be prognostic value and correlated with a higher Bcl-2 staining in tumour tissue (431) where miR-204 was shown to target Bcl-2 messenger RNA and increased responsiveness of gastric cancer cells to cancer chemotherapy treatment. Similarly,

miR-204 transfected cholangiocarcinoma cell lines negatively regulated Bcl-2 expression and enhanced chemotherapeutic drug-triggered apoptosis (432). Other studies have labelled miR-204 as a tumour suppressor due to its facilitated responsiveness to cancer treatment (447) in pancreatic cancer (448), head and neck cancer (449), colorectal cancer (450), neuroblastoma (451) and glioma (452).

Another possible mechanism of the pro-apoptotic effect miR-204 transfected BeWo is downregulation of autophagy, which plays a pro-survival role, as seen in our study and seen in another study done in renal cell carcinoma (RCC) through its direct targeting of the LC3B transcript (190) where overexpression of miR-204 halted tumour growth compared to a mutated seed sequence control miRNA. Interestingly, re-expression of LC3B without the 3' UTR rescued these effects on both autophagy and viability. These data were supported by a negative correlation between LC3B and miR-204 in RCC tumours (190). Another study that explored the role of miR-204 in autophagy in the context of cardiomyocytes found that ischaemia reperfusion injury (IR) induced autophagy with upregulation of LC3 protein and down regulation of miR-204 and transferring miR-204 mimic into cardiomyocytes led to the attenuation of LC3-II protein (189).

A third reason that could explain the growth inhibitory effect seen in miR-204 transfected cells, but not studied in our research, is reduction of insulin-like growth factor-binding protein 5 (IGFBP5) mRNA as seen in a study done in papillary thyroid carcinoma, where overexpression of miR-204 suppressed cell proliferation. The results of a luciferase reporter assay also showed that the 3′ untranslated region (UTR) of IGFBP5 RNA is a direct target of miR-204-5p (453).

Our study also showed that miR-204 transfected cells under fluorescent microscopy showed a significant increase in the size of the autophagy vacuoles with a propensity to form a larger coalescent vacuoles. This might be explained by a progressive accumulation of cellular waste inside these autophagosomes with a limited ability to recycle them leading to reduced autophagy flux. These enlarged autophagy vesicles were similar to those found in CLQ-treated cells, a known autophagy inhibitor that inhibits fusion of the lysosomal membranes to the autophagosomes. Therefor it is tempting to speculate that miR-204 overexpression, having a similar autophagosome

picture, might lead to a defect in the autophagosome turnover and thus reduction of the autophagy flux.

The autophagy pathway is a known source of elemental nutrients which could dispense to the maintenance of healthy growth and housekeeping of the placental villi and the fetus. A disturbance of such pathway could lead eventually to the accumulation of waste material that can result in placental dysfunction. Needless to say that more studies are needed to explore the role that miRNAs play in the intricate relationship of autophagy and apoptosis in trophoblasts, the perturbation of which might lead to placental dysfunction seen in preeclampsia and IUGR. These theories offer hypotheses to be tested for future research.

Chapter 7
General Discussion

7.1 Discussion

Placental dysfunction and its resulting pregnancy complications remains an enigmatic pathophysiological syndrome because of the lack of a well-defined characterisation (454, 455) which poses a clinical and research challenge. Despite exhaustive investigation, our current understanding of the pathophysiology of the most common consequences of placental dysfunction; preeclampsia and growth restriction is still inadequate. Because the placenta is the cornerstone to normal fetal development and pregnancy outcome, placenta-related events are believed to be central to the pathogenesis of these adverse outcomes a swell as their resolution (456).

In preeclampsia, shallow cytotrophoblast invasion of maternal endometrial spiral arteries leads to inadequate remodelling of uterine spiral arteries with placental hypoxia and/or ischemia (19, 28). Furthermore, the same pathology may commonly lead to the development of IUGR and even preterm labour without developing preeclampsia (22). This suggests that placental dysfunction triggers the release of factors, variable in quantity and function, into the maternal circulation which interacts in different ways with the mother's immune and vascular systems leading to a varied range of pregnancy complications. A challenge is that structural similarities and differences across placental dysfunction exist and that current methods of pathological placental phenotyping are inadequate, thus the need for this series of studies aiming at accurate quantification of such structural and functional differences. This will enable us to understand the pathophysiology of each entity of placental dysfunction better.

The structural characterisation of such placentas was done via stereology-based volume estimation protocols, where volumes of villous stroma, trophoblast layer, placental capillaries and SNAs were done through the technique of point counting (315). Volumes of SNAs, trophoblasts and capillaries in each placenta were then divided on its own villous volumes as percentages to neutralise differences due to discrepant villous volumes between groups.

In this study, EOPET placentas displayed a significant rise in SNA/villous volumes compared to preterm controls but showed no significant change on birth weight, placental volumes, trophoblast volumes, capillary volumes and total villous volumes and densities compared to preterm controls. In addition, EOPET/IUGR placentas showed a marked reduction in volume densities and total volumes of placental villi compared to preterm controls. These morphological findings were similar to other studies reporting a decrease in villous volumes and surface areas of placentas from preeclampsia with IUGR (320, 321). Moreover, stereological studies displayed an increased severity of the changes associated in placentas of IUGR with co-existing preeclampsia; clinically the most severe phenotype (304). Interestingly, placentas from EOPET/IUGR kept a similar pathological signature to EOIUGR placentas in SNAs, trophoblast volumes and highlighted especially in vascular volumes as compared to changes evidenced in EOPET placentas. This might suggest that the pathological signatures of growth restriction often precede those of preeclampsia and this goes in accordance with clinical studies showing that growth restriction usually comes before the development of the clinical symptoms associated with early-onset PET (309, 311).

Placentas from late-onset IUGR in this study exhibited substantial reductions in total placental and total villous volumes compared to full term controls, a result similar to another stereological study reporting a decrease in estimated total villous and placental volumes in late-onset IUGR placentas (10). In this study, placentas from idiopathic IUGR from normotensive mothers had a significantly reduction of SNA volumes by 34% compared to control. This reduction could be explained by a reduction in the trophoblast volume in IUGR placenta found in our study compared to control, leading to reduction of recruitment of cytotrophoblast nuclei to the syncytiotrophoblast and thus less formation of SNAs. Moreover, the branching pattern of the placental villi and factors controlling it, like vascularity and ischaemia, has also been linked to the altered appearance of SNAs in placental sections with increase the incidence of tangential sectioning of trophoblast layer at points of villous bending or branching (79, 80). Therefore, the reduced volumes of the SNAs in IUGR placenta may be due to the reduced branching pattern and this is supported by studies (336, 337) showing reduction in number and branching of the fetoplacental vasculature in IUGR placentas.

This study also showed that placentas from LOPET associated pregnancies had a significantly higher SNA volumes compared to gestational age matched control. Similar observations, though non-stereologically based, were reported in the literature showing PE placenta having increased syncytial knots, relative avascular terminal villi, and villous fibrosis (78, 335, 339, 340, 457, 458).

This study also demonstrated an inverse relationship seen between SNAs and vascular capillary volumes. Those with capillary ischemia had two and half times the likelihood of having high SNA than those with higher vascularity, after adjustment for the disease status. Moreover, the results from the multiple linear regression adjusting for early-late disease status showed that the lower the capillary volume, the higher the SNAs. This negative correlation found in this study might suggest that reduced capillary volumes or ischaemia in placental dysfunction might have a role in regulating the pathogenesis of SNA formation and/or shedding. This emphasised a potential role of programmed cell death (PCD) related to SNAs formation and/or shedding (75).

Apoptosis has a crucial role to play in trophoblast differentiation and syncytial fusion of villous cytotrophoblasts with the syncytium, a fusion which is known to be coupled to the early stages of the apoptotic cascade (85). Studies have reported an activation of the initiator stages of apoptosis, which is linked to the temporal and spatial regulation of cytotrophoblastic fusion to the syncytium (86), leading to phosphatidylserine (PS) flip from the inner to the outer plasma membrane of the trophoblast, and acting as a trigger for syncytial fusion (89, 90).

Apoptosis is a well characterised energy-dependent programmed cell death. Once the cascade is activated the cell is supposed to die within 24 hours but in normal pregnancy, SNAs may take around 2-3 weeks from syncytial fusion to be shed, despite activation of early apoptotic cascade needed for syncytial fusion (88). Another trophoblast discrepancy is that it is not associated with typical apoptotic morphological appearances such as nuclear blebbing or karyorrhexis and that it remains viable for several weeks (74). This indicates that the apoptosis cascade might be subject to a temporary suspension or delay. This suspension of the apoptotic cascade was partially explained by the expression of anti-apoptotic proteins like Bcl-2 (95).

Given that widespread apoptosis in villi would be detrimental to the placenta, and the developing fetus, it is tempting to speculate that the human villous trophoblasts display other mechanisms to maintain homeostasis and protect from dysregulated apoptosis. One mechanism by which cells protect themselves from stressors is autophagy (96), known to have an anti-apoptotic role in other systems, which can also orchestrate trophoblast survival in the placenta with anti-apoptotic proteins. Autophagy vacuoles has also been seen in the vicinity of SNAs and may be linked to the delay of the initiated apoptotic machinery (97).

Our results demonstrated that placentas from term IUGR as well as term and preterm preeclampsia with IUGR had a significantly higher trophoblastic apoptotic burden. This finding was supported by other semi-quantitative immuno-histochemical studies that showed a higher expression of pro-apoptotic proteins in the syncytiotrophoblast layer, in term IUGR placentas (361-364) as well as in villous cytotrophoblasts isolated from term preeclampsia and IUGR (365). Our study has also displayed a positive correlation between the autophagy marker and M30 apoptotic marker positivity in IUGR placenta (Figure 4-22G), indicating that stressful event in the IUGR placenta, even those that activated autophagy will result in more enhanced apoptotic cascade.

Our study revealed that placentas from preeclampsia and hypertensive disorders had induced autophagy expression compared to control, where EOPET/IUGR placentas had significantly higher LC3 positivity compared to preterm control (PTC) and EOPET had a trend increase compared to PTC. Similarly, placenta from term preeclampsia pregnancies showed a trend increase in LC3 positivity. This was consistent with other studies which also reported that autophagy was induced in placentas with preeclampsia (158, 375).

Our results have shown a persistently positive correlation between placental oxidative stress expressions and autophagy marker LC3 positivity either overall correlation or disease specific correlations, suggesting that autophagy plays an important role in the placental recycling mechanisms of harmful oxidised molecules. These results were consistent with several studies that proposed that oxidative stress and the discharge of oxidised macromolecules from the human placenta acted as a driver of cellular turnover in pathologies such as preeclampsia (97, 385). Moreover, failure to curb such

oxidative stress and restoring homeostasis might result in tissue turnover and activation of apoptotic and necrotic mechanisms (386, 387). Furthermore, the induction of autophagy as a result of higher oxidative stress has also been demonstrated in several tissues and cell types (388-393)

Our study using IHC image analysis have also revealed an overall inverse correlation between placental autophagy and apoptosis. Placental analysis showed the higher the placental autophagy expression, the lower the apoptotic burden expressed. Our study has showed that this inverse relationship was more pronounced in hypertensive preeclamptic placentas. This suggests that autophagy might play a prosurvival role in hypertensive placental dysfunction. In addition, our study showed that the levels of placental anti-apoptotic Bcl-2 expression were associated with higher autophagy marker positivity, suggesting a possible synergistic role in the prosurvival mechanisms exerted in the syncytiotrophoblast. This might explain the delayed "execution stages" of the apoptotic machinery activated in the syncytiotrophoblast nuclei (88).

Further analysis of the expression patterns of autophagy-related genes, using quantitative qRT-PCR, revealed that expression autophagy marker LC3 cannot be explained solely by gene expression, indicating the presence of a potential epigenetic layer of regulation. In addition, our study has conceptualised the interaction of autophagy-related genes expression in placental dysfunction. The results illustrated that the autophagy gene *MAP1LC3B* appears to in a correlation cluster with which autophagy related genes like *PARK2* and *PTPN2*, and antiapoptotic genes like *BCL11B* and *BCL2* are incorporated. Functional enrichment analysis of such network has revealed that it is potentially linked to mitochondrial dysfunctional, organisation as well as mitophagy. Other biological processes implicated include regulation of autophagy, apoptosis and negative regulation of reactive oxygen species metabolic process as well as cellular response to starvation.

Our study using focussed data mining protocol has identified potential target genes for miR-204-5p. Target genes included *MAP1LC3B* and *BCL2* in four out of the five searched databases. Interestingly, the expression levels of miR-204 by qRT-PCR in early and late onset placental dysfunction, though these did not show significant differences between groups, nevertheless showed quite a resemblance across groups

to the pattern of M30 apoptotic marker positivity by immunohistochemistry (Figure 4-3). This was assessed by regression analysis showing that higher levels of miR-204 were positively correlated with higher placental apoptotic burden. Conversely, miR-204 expression levels displayed an inverse correlation to the autophagy marker LC3 positivity and the antiapoptotic marker Bcl-2 positivity. This suggested that miR-204 in the placenta conferred a proapoptotic role in the trophoblasts, thus contributing to placental dysfunction. This is potentially through regulation of antiapoptotic protein Bcl-2 as well as inhibiting the prosurvival autophagy process. These data are consistent with another report that demonstrated that miR-204 plays a central role in the regulation of apoptosis, accumulation of damaged proteins and ER stress response (430). A possible mechanism of the enhanced apoptotic effect of miR-204 is its post-transcriptional regulation by direct targeting of the 3′ UTR and thus downregulation of anti-apoptotic *BCL2* gene expression (190, 431, 432). Another possible mechanism of the pro-apoptotic effect miR-204 transfected BeWo is downregulation of autophagy, which plays a pro-survival role, through its direct targeting of the *LC3B* transcript (189, 190).

The role that miR-204 played *in vivo* was then studied in BeWo, a choriocarcinoma cell line and a commonly used *in vitro* model for trophoblast function. BeWo was used to explore autophagy induction, regulation (291) and manipulation with drugs and miRNAs (433, 434) and its relation to the apoptotic cascade. Our study showed that BeWo cells proved to be a good model for autophagy induction through their response to starvation, treatment with drugs and manipulation by miRNAs.

Protein analysis data showed an inverse relationship between the autophagy LC3 expression and cleaved/total PARP, a terminal executory apoptosis marker, in BeWo cells under different drug treatments. This result replicates that of another study carried out in cultured trophoblasts (96), thus suggesting that there is an equilibrium between apoptosis and autophagy under standard conditions, and that autophagy activation in the trophoblasts might have a prosurvival role in an attempt to avoid late apoptotic cascade activation.

In addition, our results illustrated that miR-204 transfected BeWo cells behaved differently compared to NT-miRNA transfected cells. That was evidenced by different

techniques using live cell imaging, fluorescence microscopy, FACS and western blotting. Our data firstly suggested that miR-204 transfected colonies showed a slower growth potential with smaller size and reduced numbers compared to its control. This was validated by FACS analysis that showed a higher percentage of apoptotic/necrotic cell populations with reduction of the percentages of live cells in miR-204 transfected BeWo cells. Moreover, semi-quantitative analysis of western blotting revealed a significant reduction in the autophagosome marker LC3 and the anti-apoptotic marker Bcl-2 compared to its NT control. Interestingly, this was associated with a reciprocal increase in the apoptotic markers cleaved caspase 3 and caspase 9 in addition to a marked rise in the expression of cleaved/total PARP, the cleavage of which expedites cellular disassembly and is a marker of cells experiencing apoptosis (444).

The inverse relationship between the mature autophagosome marker LC3, anti-apoptotic Bcl-2 in one side and the apoptotic caspases and PARP summarises the balance of prosurvival versus pro-apoptosis. Such equilibrium seems to be the hallmark of cellular integrity and fate. It is tempting to speculate that the way the placenta reacts to stressful events depends on such equilibrium, the result of which is vital in determining the behaviour of placental dysfunction.

In summary, our study was able to quantify structural and molecular pathophysiological differences of placental dysfunction through a series of rigorous methodologies. A strengthening pillar of our study is that it was designed to include different entities and clinically encountered subtypes of placental dysfunction, which enabled us to identify the confounding effects of growth restriction and preeclampsia through matching groups of PET alone, IUGR alone and a combination of both compared to gestational aged-matched controls.

Furthermore, the use of a hierarchical multilevel representative random sampling technique from the placenta down to the blocks slides and finally to the fields of vision has given strength and precision to this study. Moreover, the study was able to dissect differences across interlinked clinically-phenotyped gestational diseases. A key strength of this study is its robust analysis of the expression of five autophagy related miRNAs normalised to the geomean of two HKGs and seven autophagy related genes normalised to the geomean of four HKGs in eight distinct placental dysfunction groups

with the use of real-time qRT-PCR, which is the most sensitive and specific RNA quantification method available.

This study, to the best of our knowledge, is the first to quantify objectively expression of programmed cell death and their dynamics in a full range of early and late onset placental dysfunction. This was also the first attempt to reconstruct villi, fibrin-type fibrinoid and SNAs together using histopathological slides and convert them into 3D volumes to explore the spatial relationship between them. This methodology has enabled us to see the distribution of the SNAs clustering around areas of fibrinoid degenerations which were highly abundant in the preeclamptic placenta.

Amongst the limitations of this study were the relatively small numbers of cases available for study, especially for some groups like term preeclampsia with IUGR. Another limitation is absence of placentas from pregnancies with intrauterine fetal death, the study of which would have elaborated the way PCD markers behave in such placentas.

In conclusion, our results showed that each gestational disease has a unique placental signature pattern of PCD dynamics. Further research is needed to identify the causes of these distinctive effects on the genetic and epigenetic level and whether it is correlated to differential protein levels seen in different parts of the placenta. Furthermore, the detection of trends across placental groups may help to characterize placentas and provide clinically relevant precincts for sub-phenotyping pathological placentas.

7.2 Conclusions

The principal conclusions from the present study are that:

- A virtual pathology platform incorporating 3D reconstruction, with its very high resolution, can be used to structurally characterise placental microarchitecture including spatial distributions of SNAs.

- Placentas from preeclampsia, whether early or late-onset, without clinical signs of IUGR showed divergent trophoblast and syncytial nuclear aggregates' volumes compared to placentas from IUGR-complicated pregnancies which may contribute to the maternal endothelial syndrome.

- Placental dysfunction from pregnancies with preeclampsia without any clinical signs of IUGR, preeclampsia with IUGR, and IUGR only showed a stepwise gradient increase in placental capillary vascular volumes and stepwise increase in trophoblast and SNA volumes, suggesting that capillary ischaemia might be involved in the shedding of the SNAs and thus maternal endothelial syndrome.

- Placentas from term preeclampsia, though they showed a relatively higher trophoblastic apoptosis compared to term control, displayed a relatively lower apoptotic burden and higher autophagy induction compared to placentas from late onset IUGR pregnancies, with or without PET, indicating that the higher autophagy induction, seen most specifically in preeclampsia, is partly protecting the placenta from excessive apoptotic activation.

- Differential autophagy-apoptosis dynamics depended partly on the type of placental dysfunction, where induced autophagy in term preeclampsia with or without IUGR protected from apoptosis. Conversely, it induced apoptosis in placentas from late-onset IUGR.

- Higher autophagy marker positivity was associated with areas with higher SNA volumes, suggesting a potential role in the trophoblast turnover and explaining the delay in the already initiated apoptotic pathway with syncytial fusion till shedding of SNAs.

- Our study has illustrated that the *MAP1LC3B* autophagy gene appears to in a correlation cluster with which autophagy related genes like PARK2 and PTPN2, and antiapoptotic genes like *BCL11B* and *BCL2* are incorporated.

- Expression levels of miR-204 *in vivo* were correlated to higher M30 apoptotic positivity in our placentas. Moreover, *in vitro*, using miR-204 transfected BeWo cells was associated with higher apoptotic cascade proteins and a reciprocal inhibition of the prosurvival autophagy marker as well as reduction in the anti-apoptotic Bcl-2 protein expression. This validates its pro-apoptotic role in placental dysfunction and emphasises the intricate balance that both autophagy and apoptosis play in placenta function and dysfunction.

7.3 Future Goals

- With regard to the newly developed 3D reconstruction methodology, it would be helpful to model volumes of serial immunolabelled sections with markers of programed cell death. That would enable us to visualise the spatial and temporal distribution of such markers in 3D in normal and placental dysfunction.

- Investigate further the role that the fetal/maternal placental side might have in the expression of PCD markers, which might shed light to the differential response pattern of the placenta to the stresses inflicted on it.

- Investigate further the role that activated macrophages, especially the scavenger cells, play in response to the oxidative stress in placental dysfunction.

- Investigate further the role of autophagy in syncytial shedding and in the maternal endothelial syndrome and whether the role that autophagy might play in the suspension of the apoptotic process might contribute to the failure of the expected non-inflammatory phagocytosis of the apoptotic cells.

- Further studies of the morphological and structural changes in autophagy vacuoles using placental explants from different entities of placental dysfunction i.e. preeclampsia with or without IUGR. This will validate the role that autophagy might play in the regulation of trophoblast apoptosis.

- Further validation of the autophagy related miRNAs identified by *in silico* analysis in placental cell lines.

References

1. World Health Organization International Collaborative Study of Hypertensive Disorders of Pregnancy. Geographic variation in the incidence of hypertension in pregnancy. Am J Obstet Gynecol. 1988;;158: 80–83.
2. ACOG Task Force on Hypertension in Pregnancy. Hypertension in Pregnancy, November 2013. American college of obstetricians and gynecologists. 2013.
3. Khan K. The CROWN Initiative: journal editors invite researchers to develop core outcomes in women's health. J Fam Plann Reprod Health Care. 2014;40(4):239-40.
4. von Dadelszen P, Magee LA, Roberts JM. Subclassification of preeclampsia. Hypertension in Pregnancy. 2003;22(2):143-8.
5. Redman CW, Sargent IL, Staff AC. IFPA senior award lecture: Making sense of pre-eclampsia - Two placental causes of preeclampsia? Placenta. 2014;35(SUPPL):S20-S5.
6. Arakaki T, Hasegawa J, Nakamura M, Hamada S, Muramoto M, Takita H, et al. Prediction of early- and late-onset pregnancy-induced hypertension using placental volume on three-dimensional ultrasound and uterine artery Doppler. Ultrasound in Obstetrics & Gynecology. 2015;45(5):539-43.
7. Walker JJ. Pre-eclampsia. The Lancet. 2000;356(9237):1260-5.
8. Villa PM, Kajantie E, Raikkonen K, Pesonen AK, Hamalainen E, Vainio M, et al. Aspirin in the prevention of pre-eclampsia in high-risk women: a randomised placebo-controlled PREDO Trial and a meta-analysis of randomised trials. Bjog-Int J Obstet Gy. 2013;120(1):64-74.
9. Pilalis A, Souka AP, Antsaklis P, Basayiannis K, Benardis P, Haidopoulos D, et al. Screening for pre-eclampsia and small for gestational age fetuses at the 11-14 weeks scan by uterine artery Dopplers. Acta Obstetricia Et Gynecologica Scandinavica. 2007;86(5):530-4.
10. Widdows K. Gestational related morphological abnormalities in placental villous trophoblast turnover in compromised pregnancies [PhD Thesis]. Uxbridge, UK: Brunel University, Uxbridge, UK; 2010.
11. Ghulmiyyah L, Sibai B. Maternal mortality from preeclampsia/eclampsia. Semin Perinatol. 2012;36(1):56-9.
12. Duley L. The global impact of pre-eclampsia and eclampsia. Semin Perinatol 33:130-137. 2009.
13. Khan KS, Wojdyla D, Say L, Gulmezoglu AM, Van Look PFA. WHO analysis of causes of maternal death: a systematic review. Lancet. 2006;367(9516):1066-74.
14. Ghulmiyyah L SB. Maternal mortality from preeclampsia/eclampsia. Semin Perinatol 33:130-137. 2012;36:56–59.
15. Backes CH MK, Moorehead P, Cordero L, Nankervis CA, Giannone PJ. Maternal preeclampsia and neonatal outcomes. J Pregnancy. 2011;2011:214365.
16. Carty DM DC, Dominiczak AF. . Preeclampsia and future maternal health. J Hypertens. 2010;;28:1349–1355.

17. Huppertz B. Trophoblast differentiation, fetal growth restriction and preeclampsia. Pregnancy Hypertension-an International Journal of Womens Cardiovascular Health. 2011;1(1):79-86.
18. Sibai B, Dekker, G, Kupferminc, M. Pre-eclampsia. Lancet. 2005;365: 785-799.
19. Brosens I RW, Dixon HG,. The physiological response of the vessels of the placental bed to normal pregnancy. J Pathol Bacteriol ; 93:569–579. 1967.
20. Pijnenborg R, Vercruysse L, Hanssens M. The Uterine Spiral Arteries In Human Pregnancy: Facts and Controversies. Placenta. 2006;27(9–10):939-58.
21. Trogstad L, Magnus P, Moffett A, Stoltenberg C. The effect of recurrent miscarriage and infertility on the risk of pre-eclampsia. Bjog-Int J Obstet Gy. 2009;116(1):108-13.
22. Young BC, Levine RJ, Karumanchi SA. Pathogenesis of preeclampsia. Annual review of pathology. 2010;5:173-92.
23. Haig D. Altercation of generations: Genetic conflicts of pregnancy. American Journal of Reproductive Immunology. 1996;35(3):226-32.
24. Haig D. Genetic Conflicts in Human Pregnancy. The Quarterly Review of Biology. 1993;68(4):495-532.
25. Haig D. Placental Growth Hormone-Related Proteins and Prolactin-Related Proteins. Placenta. 2008;29, Supplement:36-41.
26. Jauniaux E, Poston L, Burton GJ. Placental-related diseases of pregnancy: Involvement of oxidative stress and implications in human evolution. Hum Reprod Update. 2006;12(6):747-55.
27. Brosens JJ, Parker MG, McIndoe A, Pijnenborg R, Brosens IA. A role for menstruation in preconditioning the uterus for successful pregnancy. American Journal of Obstetrics and Gynecology. 2009;200(6).
28. Steegers EAP, von Dadelszen P, Duvekot JJ, Pijnenborg R. Pre-eclampsia. The Lancet. 2010;376(9741):631-44.
29. Battagli.Fc, Lubchenc.Lo. A Practical Classification of Newborn Infants by Weight and Gestational Age. Journal of Pediatrics. 1967;71(2):159-+.
30. Fox H. Pathology of the Placenta. Clin Obstet Gynaecol. 1986;13(3):501-19.
31. Stanek J, Biesiada J. Clustering of Maternal/Fetal Clinical Conditions and Outcomes and Placental Lesions. Placenta. 2011;32(9):A19-A.
32. Turner S, Williams M, Wood I, Gardosi J. SGA referral rates before and after implementation of the growth assessment protocol. Bjog-Int J Obstet Gy. 2016;123:13-.
33. Nicolaides KH, Bindra R, Turan OM, Chefetz I, Sammar M, Meiri H, et al. A novel approach to first-trimester screening for early pre-eclampsia combining serum PP-13 and Doppler ultrasound. Ultrasound in Obstetrics & Gynecology. 2006;27(1):13-7.
34. de Onis M, Blossner M, Villar J. Levels and patterns of intrauterine growth retardation in developing countries. Eur J Clin Nutr. 1998;52:S5-S15.
35. Wollmann HA. Intrauterine growth restriction: Definition and etiology. Horm Res. 1998;49:1-6.
36. Liu J, Wang XF, Wang Y, Wang HW, Liu Y. The Incidence Rate, High-Risk Factors, and Short-and Long-Term Adverse Outcomes of Fetal Growth Restriction A Report From Mainland China. Medicine. 2014;93(27).

37. Zeitlin J, El Ayoubi M, Jarreau PH, Draper ES, Blondel B, Kunzel W, et al. Impact of Fetal Growth Restriction on Mortality and Morbidity in a Very Preterm Birth Cohort. Journal of Pediatrics. 2010;157(5):733-U63.
38. Malloy MH. Size for gestational age at birth: impact on risk for sudden infant death and other causes of death, USA 2002. Arch Dis Child-Fetal. 2007;92(6):473-8.
39. Malin GL, Morris RK, Riley R, Teune MJ, Khan KS. When is birthweight at term abnormally low? A systematic review and meta-analysis of the association and predictive ability of current birthweight standards for neonatal outcomes. Bjog-Int J Obstet Gy. 2014;121(5):515-26.
40. Griffin IJ, Lee HC, Profit J, Tancedi DJ. The smallest of the small: short-term outcomes of profoundly growth restricted and profoundly low birth weight preterm infants. Journal of Perinatology. 2015;35(7):503-10.
41. Paz I, Seidman DS, Danon YL, Laor A, Stevenson DK, Gale R. Are Children Born Small-for-Gestational-Age at Increased Risk of Short Stature. Am J Dis Child. 1993;147(3):337-9.
42. Levine TA, Grunau RE, McAuliffe FM, Pinnamaneni R, Foran A, Alderdice FA. Early Childhood Neurodevelopment After Intrauterine Growth Restriction: A Systematic Review. Pediatrics. 2015;135(1):126-41.
43. Barker DJP. Early growth and cardiovascular disease. Arch Dis Child. 1999;80(4):305-6.
44. Carmody JB, Charlton JR. Short-Term Gestation, Long-Term Risk: Prematurity and Chronic Kidney Disease. Pediatrics. 2013;131(6):1168-79.
45. Kanasaki K, Kalluri R. The biology of preeclampsia. Kidney Int. 2009;76(8):831-7.
46. Benirschke K, Kaufmann, P., Baergen, R. . Pathology of the Human Placenta. 5th Edition ed. (5th Edition) New York.: Springer; 2006.
47. Huppertz B. Preeclampsia, aponecrosis and a dysfunctional immunological environment: Journal of Reproductive Immunology. Conference: 8th European Congress on Reproductive Immunology of the European Society for Reproductive Immunology, ESRI Munich, Bavaria Germany. Conference Start: 20101111 Conference End: 20101113. Conference Publication: (var.pagings). 86 (2) (pp 90), 2010. Date of Publication: November 2010.; 2010.
48. Okudaira Y, Matsui Y, Kanoh H. Morphological Variability of Human Trophoblasts in Normal and Neoplastic Conditions - an Ultrastructural Reappraisal. Placenta : Basic Research for Clinical Application. 1991:176-87.
49. Muhlhauser J, Crescimanno C, Kaufmann P, Hofler H, Zaccheo D, Castellucci M. Differentiation and Proliferation Patterns in Human Trophoblast Revealed by C-Erbb-2 Oncogene Product and Egf-R. Journal of Histochemistry & Cytochemistry. 1993;41(2):165-73.
50. Kaufmann P, Black S, Huppertz B. Endovascular trophoblast invasion: Implications for the pathogenesis of intrauterine growth retardation and preeclampsia. Biology of Reproduction. 2003;69(1):1-7.
51. Brosens I. How the role of the spiral arteries in the pathogenesis of preeclampsia was discovered. Hypertension in Pregnancy. 1996;15(1):143-6.
52. Ng EHY, Chan CCW, Tang OS, Yeung WSB, Ho PC. The role of endometrial and subendometrial vascularity measured by three-dimensional power Doppler ultrasound in the prediction of pregnancy during frozen-thawed embryo transfer cycles. Hum Reprod. 2006;21(6):1612-7.

53. Burton GJ, Jauniaux E, Watson AL. Maternal arterial connections to the placental intervillous space during the first trimester of human pregnancy: The Boyd Collection revisited. American Journal of Obstetrics and Gynecology. 1999;181(3):718-24.
54. Burton GJ, Jauniaux E. Placental oxidative stress: From miscarriage to preeclampsia. J Soc Gynecol Investig. 2004;11(6):342-52.
55. Burton GJ. Oxygen, the Janus gas; its effects on human placental development and function. Journal of Anatomy. 2009;215(1):27-35.
56. Mayhew TM, Simpson RA. Quantitative evidence for the spatial dispersal of trophoblast nucleic in human placental villi during gestation. Placenta. 1994;15(8):837-44.
57. Huppertz B, Borges M. Placenta trophoblast fusion. Methods in Molecular Biology2008. p. 135-47.
58. Jaameri KE, Koivuniemi, A.P., Carpen, E.O., . Occurrence of trophoblasts in the blood of toxaemic patients. Gynaecologia 160, 315–320. 1965.
59. Attwood HD, Park, W.W.,. Embolism to the lungs by trophoblast. J Obstet Gynaecol. 1961;Br. Commonw. 68, 611–617.
60. Johansen M, Redman CW, Wilkins T, Sargent IL. Trophoblast deportation in human pregnancy--its relevance for pre-eclampsia. Placenta. 1999;20(7):531-9.
61. Reddy A, Zhong XY, Rusterholz C, Hahn S, Holzgreve W, Redman CWG, et al. The Effect of Labour and Placental Separation on the Shedding of Syncytiotrophoblast Microparticles, Cell-free DNA and mRNA in Normal Pregnancy and Pre-eclampsia. Placenta. 2008;29(11):942-9.
62. Benirschke K, Kaufmann, P.,. Pathology of the Human Placenta. 1995a.
63. Desoye G, Shafrir E. Placental metabolism and its regulation in health and diabetes. Molecular aspects of medicine. 1994;15(6):505-682.
64. Schmorl G, 1893. . Pathologisch-Anatomische Untersuchungen Uber Puerperal-Eklampsie. Verlag von FC Vogel, Leipzig. 1893.
65. Douglas GW, Thomas, L., Carr, M., Cullen, N.M., Morris, R., . Trophoblast in the circulating blood during pregnancy. Am J Obstet Gynecol 78, 960–973. 1959.
66. Boyd JD, Hamilton, W.J., . The Human Placenta. London/Basingstoke.: The MacMillan Press Ltd.; 1975.
67. Covone AE, Mutton, D., Johnson, P.M., Adinolfi, M., . Trophoblast cells in peripheral blood from pregnant women. Lancet 2, 841–843. 1984.
68. Pantham P, Askelund KJ, Chamley LW. Trophoblast deportation part II: a review of the maternal consequences of trophoblast deportation. Placenta. 2011;32(10):724-31.
69. Chamley LW, Chen Q, Ding J, Stone PR, Abumaree M. Trophoblast deportation: just a waste disposal system or antigen sharing? J Reprod Immunol. 2011;88(2):99-105.
70. Fadeel B. Programmed cell clearance. Cell Mol Life Sci. 2003;60:2575–2585.
71. Huppertz B, Kingdom J, Caniggia I, Desoye G, Black S, Korr H, et al. Hypoxia favours necrotic versus apoptotic shedding of placental syncytiotrophoblast into the maternal circulation. Placenta. 2003;24(2-3):181-90.
72. Savill J, Fadok, V., . Corpse clearance defines the meaning of cell death. Nature 407, 784–788. 2000.

73. Fadok VA, Bratton, D.L., Guthrie, L., Henson, P.M., . Differential effects of apoptotic versus lysed cells on macrophage production of cytokines: role of proteases. J. Immunol. 166, 6847–6854. 2001.
74. Huppertz B, Kaufmann P, Kingdom J. Trophoblast turnover in health and disease. Fetal and Maternal Medicine Review. 2002;13(02):103-18.
75. Burton GJ, Ingram, S.C and Palmer, M.E. . The influence of mode of fixation on morphometrical data derived from terminal villi in the human placenta at term: A comparison of immersion and perfusion fixation. Placenta 8, 37-51. 1987.
76. Erwig LP, Henson PM. Immunological consequences of apoptotic cell phagocytosis. The American journal of pathology. 2007;171(1):2-8.
77. Mayhew TM. Villous trophoblast of human placenta: a coherent view of its turnover, repair and contributions to villous development and maturation. [Review] [89 refs]. Histology & Histopathology. 2001;16(4):1213-24.
78. Tenney Jr B, Parker Jr F. The placenta in toxemia of pregnancy. American Journal of Obstetrics and Gynecology. 1940;39(6):1000-5.
79. Burton GJ. Intervillous connections in the mature human placenta: Instances of syncytial fusion or section artifacts? Journal of Anatomy. 1986;VOL. 145:13-23.
80. Ali KZ, Burton GJ, Morad N, Ali ME. Does hypercapillarization influence the branching pattern of terminal villi in the human placenta at high altitude? Placenta. 1996;17(8):677-82.
81. Hirsch T, Marchetti P, Susin SA, Dallaporta B, Zamzami N, Marzo I, et al. The apoptosis-necrosis paradox. Apoptogenic proteases activated after mitochondrial permeability transition determine the mode of cell death. Oncogene. 1997;15(13):1573-81.
82. Huppertz B, Frank HG, Kaufmann P. The apoptosis cascade--morphological and immunohistochemical methods for its visualization. Anat Embryol (Berl). 1999;200(1):1-18.
83. Kroemer G, Martin SJ. Caspase-independent cell death. Nature Medicine. 2005;11(7):725-30.
84. Huppertz B, Frank HG, Reister F, Kingdom J, Korr H, Kaufmann P. Apoptosis cascade progresses during turnover of human trophoblast: analysis of villous cytotrophoblast and syncytial fragments in vitro. Lab Invest. 1999;79(12):1687-702.
85. Sakuragi N, Matsuo H, Coukos G, Furth EE, Bronner MP, VanArsdale CM, et al. Differentiation-dependent expression of the BCL-2 proto-oncogene in the human trophoblast lineage. J Soc Gynecol Investig. 1994;1(2):164-72.
86. Black S, Kadyrov M, Kaufmann P, Ugele B, Emans N, Huppertz B. Syncytial fusion of human trophoblast depends on caspase 8. Cell Death and Differentiation. 2004;11(1):90-8.
87. Baczyk D, Satkunaratnam A, Nait-Oumesmar B, Huppertz B, Cross JC, Kingdom JC. Complex patterns of GCM1 mRNA and protein in villous and extravillous trophoblast cells of the human placenta. Placenta. 2004;25(6):553-9.
88. Huppertz B, Frank HG, Kingdom JCP, Reister F, Kaufmann P. Villous cytotrophoblast regulation of the syncytial apoptotic cascade in the human placenta. Histochemistry and Cell Biology. 1998;110(5):495-508.
89. Keryer G, Alsat E, Tasken K, Evain-Brion D. Cyclic AMP-dependent protein kinases and human trophoblast cell differentiation in vitro. Journal of cell science. 1998;111 (Pt 7):995-1004.

90. Adler RR, Ng AK, Rote NS. Monoclonal antiphosphatidylserine antibody inhibits intercellular fusion of the choriocarcinoma line, JAR. Biol Reprod. 1995;53(4):905-10.
91. Steinborn A, von Gall C, Hildenbrand R, Stutte HJ, Kaufmann M. Identification of placental cytokine-producing cells in term and preterm labor. Obstet Gynecol. 1998;91(3):329-35.
92. Lea RG, Tulppala M, Critchley HO. Deficient syncytiotrophoblast tumour necrosis factor-alpha characterizes failing first trimester pregnancies in a subgroup of recurrent miscarriage patients. Hum Reprod. 1997;12(6):1313-20.
93. Ratts VS, Tao XJ, Webster CB, Swanson PE, Smith SD, Brownbill P, et al. Expression of BCL-2, BAX and BAK in the trophoblast layer of the term human placenta: a unique model of apoptosis within a syncytium. Placenta. 2000;21(4):361-6.
94. Leers MP, Kolgen W, Bjorklund V, Bergman T, Tribbick G, Persson B, et al. Immunocytochemical detection and mapping of a cytokeratin 18 neo-epitope exposed during early apoptosis. J Pathol. 1999;187(5):567-72.
95. O'Connor OA, Smith EA, Toner LE, Teruya-Feldstein J, Frankel S, Rolfe M, et al. The Combination of the Proteasome Inhibitor Bortezomib and the Bcl-2 Antisense Molecule Oblimersen Sensitizes Human B-Cell Lymphomas to Cyclophosphamide. American Association for Cancer Research. 2006;12(9):2902-11.
96. Chen B, Longtine MS, Nelson DM. Hypoxia induces autophagy in primary human trophoblasts. Endocrinology. 2012;153(10):4946-54.
97. Burton GJ, Jones CJP. Syncytial Knots, Sprouts, Apoptosis, and Trophoblast Deportation from the Human Placenta. Taiwanese Journal of Obstetrics and Gynecology. 2009;48(1):28-37.
98. C. de Duve and R.Wattiaux. “Functions of lysosomes”. Annual Review of Physiology. 1966;28(pp. 435–492,).
99. Bildirici I, Longtine MS, Chen B, Nelson DM. Survival by self-destruction: A role for autophagy in the placenta? Placenta. 2012;33(8):591-8.
100. Kanninen TT, De Andrade Ramos BR, Jaffe S, Bongiovanni AM, Linhares IM, Renzo GCD, et al. Inhibition of autophagy by sera from pregnant women. Reproductive Sciences. 2013;20(11):1327-31.
101. Rubinsztein DC, Shpilka T, Elazar Z. Mechanisms of autophagosome biogenesis. Curr Biol. 2012;22(R29e34.).
102. Klionsky DJ. Cell biology - Regulated self-cannibalism. Nature. 2004;431(7004):31-2.
103. Oh SY, Choi SJ, Kyung Hee K, Cho E, Kim JH, Roh CR. Autophagy-related proteins, LC3 and beclin-1, in placentas from pregnancies complicated by preeclampsia. Reproductive sciences. 2008;15(9):912-20.
104. Glick D, Barth S, Macleod KF. Autophagy: cellular and molecular mechanisms. J Pathol. 2010;221(3e12).
105. Chan LL-Y, Shen D, Wilkinson AR, Patton W, Lai N, Chan E, et al. A novel image-based cytometry method for autophagy detection in living cells. Autophagy. 2012;8(9):1371-82.
106. Kroemer G, Levine B. Autophagic cell death: the story of a misnomer. Nat Rev Mol Cell Biol. 2008;9(1004e10.).
107. Del Roso A VS, Cavallini G, Donati A, Gori Z, Masini M, et al. . Ageingrelated changes in the in vivo function of rat liver macroautophagy and proteolysis. Exp Gerontol. 2003;38(519e27).

108. Cavallini G DA, Gori Z, Bergamini E. . Towards an understanding of the anti-aging mechanism of caloric restriction. Curr Aging Sci. 2008;1(4e9).
109. Levine B, Klionsky DJ. Development by self-digestion: Molecular mechanisms and biological functions of autophagy. Developmental Cell. 2004;6(4):463-77.
110. Mizushima N, Levine B, Cuervo AM, Klionsky DJ. Autophagy fights disease through cellular self-digestion. Nature. 2008;451(7182):1069-75.
111. Levine B, Kroemer G. Autophagy in the Pathogenesis of Disease. Cell. 2008;132(1):27-42.
112. Nicklin P, Bergman P, Zhang B, Triantafellow E, Wang H, Nyfeler B. Bidirectional transport of amino acids regulates mTOR and autophagy. Cell. 2009;136(521e34).
113. Lum JJ, Bauer DE, Kong M, Harris MH, Li C, Lindsten T, et al. Growth factor regulation of autophagy and cell survival in the absence of apoptosis. Cell. 2005;120(2):237-48.
114. Stokoe D, Stephens LR, Copeland T, Gaffney PR, Reese CB, Painter GF, et al. Dual role of phosphatidylinositol-3,4,5-trisphosphate in the activation of protein kinase B. Science. 1997;277(5325):567-70.
115. Alessi DR, James SR, Downes CP, Holmes AB, Gaffney PR, Reese CB, et al. Characterization of a 3-phosphoinositide-dependent protein kinase which phosphorylates and activates protein kinase Balpha. Curr Biol. 1997;7(4):261-9.
116. Huang J, Manning BD. The TSC1-TSC2 complex: a molecular switchboard controlling cell growth. Biochem J. 2008;412(179e90).
117. Inoki K, Zhu T, Guan KL. TSC2 mediates cellular energy response to control cell growth and survival. Cell. 2003;115(577e90).
118. Liang J, Shao SH, Xu ZX, Hennessy B, Ding Z, Larrea M. The energy sensing LKB1-AMPK pathway regulates p27(kip1)hosphorylation mediating the decision to enter autophagy or apoptosis. Nat Cell Biol. 2007;9(218e24).
119. Lorin S, Pattingre S, Meijer AJ, Codogno P. Chapter 14 - Regulation of Macroautophagy by Nutrients and Metabolites A2 - Dardevet, Dominique. The Molecular Nutrition of Amino Acids and Proteins. Boston: Academic Press; 2016. p. 181-203.
120. DeYoung MP, Horak P, Sofer A, Sgroi D, Ellisen LW. Hypoxia regulates TSC1/2-mTOR signaling and tumor suppression through REDD1-mediated 14-3-3 shuttling. Genes Dev. 2008;22(239e51).
121. Kiffin R, Bandyopadhyay U, Cuervo AM. Oxidative stress and autophagy. Antioxid Redox Signal. 2006;8(152e62).
122. Narendra D, Tanaka A, Suen DF, Youle RJ. Parkin is recruited selectively to impaired mitochondria and promotes their autophagy. J Cell Biol. 2008;183(795e803).
123. Rodriguez-Hernandez A, Cordero MD, Salviati L, Artuch R, Pineda M, Briones P. Coenzyme Q deficiency triggers mitochondria degradation by mitophagy. Autophagy. 2009;5(19e32).
124. Spalinger MR, Rogler G, Scharl M. Crohn's disease: Loss of tolerance or a disorder of autophagy? Digestive Diseases. 2014;32(4):370-7.
125. Scharl M, Rogler G. The role for protein tyrosine phosphatase nonreceptor type 2 in regulating autophagosome formation. Annals of the New York Academy of Sciences2012. p. 93-102.

126. Dalby KN, Tekedereli I, Lopez-Berestein G, Ozpolat B. Targeting the prodeath and prosurvival functions of autophagy as novel therapeutic strategies in cancer. Autophagy. 2010;6(3):322-9.
127. Eisenberg-Lerner A, Bialik S, Simon HU, Kimchi A. Life and death partners: apoptosis, autophagy and the cross-talk between them. Cell Death and Differentiation. 2009;16(7):966-75.
128. Yu L, Wan FY, Dutta S, Welsh S, Liu ZH, Freundt E, et al. Autophagic programmed cell death by selective catalase degradation. P Natl Acad Sci USA. 2006;103(13):4952-7.
129. Mathew R, Karantza-Wadsworth V, White E. Role of autophagy in cancer. Nat Rev Cancer. 2007;7(12):961-7.
130. Ravikumar B, Vacher C, Berger Z, Davies JE, Luo SQ, Oroz LG, et al. Inhibition of mTOR induces autophagy and reduces toxicity of polyglutamine expansions in fly and mouse models of Huntington disease. Nat Genet. 2004;36(6):585-95.
131. White E, DiPaola RS. The Double-Edged Sword of Autophagy Modulation in Cancer. Clin Cancer Res. 2009;15(17):5308-16.
132. Gump JM, Thorburn A. Autophagy and apoptosis: what is the connection? Trends Cell Biol. 2011;21(7):387-92.
133. Gump JM, Thorburn A. Autophagy and apoptosis- what's the connection? Trends Cell Biol. 2011;21(7):387-92.
134. Lartigue L, Kushnareva Y, Seong Y, Lin H, Faustin B, Newmeyer DD. Caspase-independent Mitochondrial Cell Death Results from Loss of Respiration, Not Cytotoxic Protein Release. Mol Biol Cell. 2009;20(23):4871-84.
135. Thorburn A. Apoptosis and autophagy: regulatory connections between two supposedly different processes. Apoptosis : an international journal on programmed cell death. 2008;13(1):1-9.
136. Chipuk JE, Moldoveanu T, Llambi F, Parsons MJ, Green DR. The BCL-2 Family Reunion. Mol Cell. 2010;37(3):299-310.
137. Djavaheri-Mergny M, Maiuri MC, Kroemer G. Cross talk between apoptosis and autophagy by caspase-mediated cleavage of Beclin 1. Oncogene. 2010;29(12):1717-9.
138. Wei Y, Pattingre S, Sinha S, Bassik M, Levine B. JNK1-mediated phosphorylation of Bcl-2 regulates starvation-induced autophagy. Mol Cell. 2008;30(6):678-88.
139. Pattingre S, Tassa A, Qu X, Garuti R, Liang XH, Mizushima N, et al. Bcl-2 antiapoptotic proteins inhibit Beclin 1-dependent autophagy. Cell. 2005;122(6):927-39.
140. Youle RJ, Narendra DP. Mechanisms of mitophagy. Nat Rev Mol Cell Bio. 2011;12(1):9-14.
141. Hung TH, Hsieh TT, Chen SF, Li MJ, Yeh YL. Autophagy in the human placenta throughout gestation. PLoS ONE. 2013;8(12).
142. Adhikari D, Zheng W, Shen Y, Gorre N, Hämäläinen T, Cooney AJ, et al. Tsc/mTORC1 signaling in oocytes governs the quiescence and activation of primordial follicles. Human Molecular Genetics. 2010;19(3):397-410.
143. Reddy P, Liu L, Adhikari D, Jagarlamudi K, Rajareddy S, Shen Y, et al. Oocyte-specific deletion of Pten causes premature activation of the primordial follicle pool. Science. 2008;319(5863):611-3.

144. Bolanos JMG, Moran AM, da Silva CMB, Rodriguez AM, Davila MP, Aparicio IM, et al. Autophagy and Apoptosis Have a Role in the Survival or Death of Stallion Spermatozoa during Conservation in Refrigeration. Plos One. 2012;7(1).
145. Bustamante-Marin X, Quiroga C, Lavandero S, Reyes JG, Moreno RD. Apoptosis, necrosis and autophagy are influenced by metabolic energy sources in cultured rat spermatocytes. Apoptosis : an international journal on programmed cell death. 2012;17(6):539-50.
146. Sato M, Sato K. Dynamic Regulation of Autophagy and Endocytosis for Cell Remodeling During Early Development. Traffic. 2013;14(5):479-86.
147. Sato M, Sato K. Degradation of Paternal Mitochondria by Fertilization-Triggered Autophagy in C. elegans Embryos. Science. 2011;334(6059):1141-4.
148. Yue ZY, Jin SK, Yang CW, Levine AJ, Heintz N. Beclin 1, an autophagy gene essential for early embryonic development, is a haploinsufficient tumor suppressor. P Natl Acad Sci USA. 2003;100(25):15077-82.
149. Egli D, Rosains J, Birkhoff G, Eggan K. Developmental reprogramming after chromosome transfer into mitotic mouse zygotes. Nature. 2007;447(7145):679-U8.
150. Tsukamoto S, Kuma A, Murakami M, Kishi C, Yamamoto A, Mizushima N. Autophagy is essential for preimplantation development of mouse embryos. Science. 2008;321(5885):117-20.
151. Qu XP, Zou ZJ, Sun QH, Luby-Phelps K, Cheng PF, Hogan RN, et al. Autophagy gene-dependent clearance of apoptotic cells during embryonic development. Cell. 2007;128(5):931-46.
152. Wada Y, Sun-Wada GH, Kawamura N. Microautophagy in the visceral endoderm is essential for mouse early development. Autophagy. 2013;9(2):252-4.
153. Lee JE, Oh HA, Song H, Jun JH, Roh CR, Xie H, et al. Autophagy Regulates Embryonic Survival During Delayed Implantation. Endocrinology. 2011;152(5):2067-75.
154. Lee J-E, Oh H-A, Song H, Jun JH, Roh C-R, Xie H, et al. Autophagy Regulates Embryonic Survival During Delayed Implantation. Endocrinology. 2011;152(5):2067-75.
155. Mintern JD, Villadangos JA. Autophagy and mechanisms of effective immunity. Front Immunol. 2012;3:60.
156. Abumaree MH, Chamley LW, Badri M, El-Muzaini MF. Trophoblast debris modulates the expression of immune proteins in macrophages: A key to maternal tolerance of the fetal allograft? Journal of Reproductive Immunology. 2012;94(2):131-41.
157. Saito S, Nakashima A. Review: The role of autophagy in extravillous trophoblast function under hypoxia. Placenta. 2013;34(SUPPL):S79-S84.
158. Signorelli P, Avagliano L, Virgili E, Gagliostro V, Doi P, Braidotti P, et al. Autophagy in term normal human placentas. Placenta. 2011;32(6):482-5.
159. Curtis S, Jones CJP, Garrod A, Hulme CH, Heazell AEP. Identification of autophagic vacuoles and regulators of autophagy in villous trophoblast from normal term pregnancies and in fetal growth restriction. Journal of Maternal-Fetal & Neonatal Medicine. 2013;26(4):339-46.
160. Shen ZY, Li EM, Lu SQ, Shen J, Cai YM, Wu YE, et al. Autophagic and Apoptotic Cell Death in Amniotic Epithelial Cells. Placenta. 2008;29(11):956-61.

161. Saito S, Nakashima A. A review of the mechanism for poor placentation in early-onset preeclampsia: The role of autophagy in trophoblast invasion and vascular remodeling. Journal of Reproductive Immunology. 2014;101-102(1):80-8.
162. Nakashima A, Yamanaka-Tatematsu M, Fujita N, Koizumi K, Shima T, Yoshida T, et al. Impaired autophagy by soluble endoglin, under physiological hypoxia in early pregnant period, is involved in poor placentation in preeclampsia. Autophagy. 2013;9(3):303-16.
163. Gamerdinger M, Kaya AM, Wolfrum U, Clement AM, Behl C. BAG3 mediates chaperone-based aggresome-targeting and selective autophagy of misfolded proteins. Embo Rep. 2011;12(2):149-56.
164. Kon M, Cuervo AM. Autophagy: An Alternative Degradation Mechanism for Misfolded Proteins. Protein Misfolding Diseases: Current and Emerging Principles and Therapies2010. p. 113-29.
165. Metcalf DJ, García-Arencibia M, Hochfeld WE, Rubinsztein DC. Autophagy and misfolded proteins in neurodegeneration. Experimental Neurology. 2012;238(1):22-8.
166. Olzmann JA, Chin LS. Parkin-mediated K63-linked polyubiquitination: A signal for targeting misfolded proteins to the aggresome-autophagy pathway. Autophagy. 2008;4(1):85-7.
167. Frid P, Anisimov SV, Popovic N. Congo red and protein aggregation in neurodegenerative diseases. Brain Research Reviews. 2007;53(1):135-60.
168. Buhimschi IA, Nayeri UA, Zhao G, Shook LL, Pensalfini A, Funai EF, et al. Protein misfolding, congophilia, oligomerization, and defective amyloid processing in Preeclampsia. Science Translational Medicine. 2014;6(245).
169. Halimi M, Dayan-Amouyal Y, Kariv-Inbal Z, Friedman-Levi Y, Mayer-Sonnenfeld T, Gabizon R. Prion urine comprises a glycosaminoglycan-light chain IgG complex that can be stained by Congo red. Journal of Virological Methods. 2006;133(2):205-10.
170. Linke RP. Highly sensitive diagnosis of amyloid and various amyloid syndromes using Congo red fluorescence. Virchows Archiv. 2000;436(5):439-48.
171. Schroeder BM. ACOG practice bulletin on diagnosing and managing preeclampsia and eclampsia. Am Fam Physician. 2002;66(2):330-1.
172. R. Guidotti, D. Jobson. Detecting Preeclampsia: A Practical Guide. World Health Organization, Geneva; 2005.
173. Buhimschi CS, Norwitz ER, Funai E, Richman S, Guller S, Lockwood CJ, et al. Urinary angiogenic factors cluster hypertensive disorders and identify women with severe preeclampsia. Am J Obstet Gynecol. 2005;192(3):734-41.
174. Buhimschi IA, Zhao G, Funai EF, Harris N, Sasson IE, Bernstein IM, et al. Proteomic profiling of urine identifies specific fragments of SERPINA1 and albumin as biomarkers of preeclampsia. Am J Obstet Gynecol. 2008;199(5):551 e1-16.
175. Tanzi RE, Moir RD, Wagner SL. Clearance of Alzheimer's Aβ peptide: The many roads to perdition. Neuron. 2004;43(5):605-8.
176. Carrell RW, Lomas DA. Conformational disease. Lancet. 1997;350(9071):134-8.
177. Hayden MR, Tyagi SC, Kerklo MM, Nicolls MR. Type 2 diabetes mellitus as a conformational disease. Journal of the Pancreas. 2005;6(4):287-302.
178. Plantinga TS, Joosten LAB, Netea MG. ATG16L1 polymorphisms are associated with NOD2-induced hyperinflammation. Autophagy. 2011;7(9):1074-5.

179. Doulaveris G, Orfanelli T, Benn K, Zervoudakis I, Skupski D, Witkin S. Association between a polymorphism in an autophagy-related gene, ATG16L1, and time to delivery in women who require induction of labor. American Journal of Obstetrics and Gynecology. 2013;208(1):S140-S.
180. Bartel DP. MicroRNAs: target recognition and regulatory functions. Cell. 2009;136:215–33.
181. Wiemer EA. The role of microRNAs in cancer: no small matter. Eur J Cancer. 2007;43(10):1529-44.
182. Bartel DP. MicroRNAs: Genomics, Biogenesis, Mechanism, and Function. Cell. 2004;116(2):281-97.
183. Morales Prieto DM, Markert UR. MicroRNAs in pregnancy. Journal of Reproductive Immunology. 2011;88(2):106-11.
184. Macfarlane LA, Murphy PR. MicroRNA: Biogenesis, Function and Role in Cancer. Curr Genomics. 2010;11(7):537-61.
185. Cecconi F. Autophagy regulation by miRNAs: when cleaning goes out of service. Embo J. 2011;30(22):4517-9.
186. Di Leva G, Croce CM. Roles of small RNAs in tumor formation. Trends in Molecular Medicine. 2010;16:257–67.
187. Fu LL, Wen X, Bao JK, Liu B. MicroRNA-modulated autophagic signaling networks in cancer. International Journal of Biochemistry and Cell Biology. 2012;44(5):733-6.
188. Frankel LB, Lund AH. MicroRNA regulation of autophagy. Carcinogenesis. 2012;33(11):2018-25.
189. Xiao J, Zhu X, He B, Zhang Y, Kang B, Wang Z, et al. MiR-204 regulates cardiomyocyte autophagy induced by ischemia-reperfusion through LC3-II. Journal of Biomedical Science. 2011;18(1).
190. Mikhaylova O, Stratton Y, Hall D, Kellner E, Ehmer B, Drew A, et al. VHL-Regulated MiR-204 Suppresses Tumor Growth through Inhibition of LC3B-Mediated Autophagy in Renal Clear Cell Carcinoma. Cancer cell. 2012;21(4):532-46.
191. Korkmaz G, Le Sage C, Tekirdag KA, Agami R, Gozuacik D. miR-376b controls starvation and mTOR inhibition-related autophagy by targeting ATG4C and BECN1. Autophagy. 2012;8(2).
192. Frankel LB, Wen J, Lees M, Hoyer-Hansen M, Farkas T, Krogh A, et al. microRNA-101 is a potent inhibitor of autophagy. Embo J. 2011;30(22):4628-41.
193. Fujita N, Hayashi-Nishino M, Fukumoto H, Omori H, Yamamoto A, Noda T, et al. An Atg4B mutant hampers the lipidation of LC3 paralogues and causes defects in autophagosome closure. Mol Biol Cell. 2008;19(11):4651-9.
194. Kaminskyy V, Zhivotovsky B. Proteases in autophagy. Biochim Biophys Acta. 2012;1824(1):44-50.
195. Jegga AG, Schneider L, Ouyang X, Zhang J. Systems biology of the autophagy-lysosomal pathway. Autophagy. 2011;7(5):477-89.
196. Fader CM, Sanchez DG, Mestre MB, Colombo MI. TI-VAMP/VAMP7 and VAMP3/cellubrevin: two v-SNARE proteins involved in specific steps of the autophagy/multivesicular body pathways. Biochim Biophys Acta. 2009;1793(12):1901-16.
197. Yang Y. and Liang C. MicroRNAs: an emerging player in autophagy. ScienceOpen Research. 2015;(DOI: 10.14293/S2199-1006.1.SOR-LIFE.A181CU.v1).

198. Chang Y, Yan W, He X, Zhang L, Li C, Huang H, et al. miR-375 inhibits autophagy and reduces viability of hepatocellular carcinoma cells under hypoxic conditions. Gastroenterology. 2012;143(1):177-87.e8.
199. Brest P, Lapaquette P, Souidi M, Lebrigand K, Cesaro A, Vouret-Craviari V, et al. A synonymous variant in IRGM alters a binding site for miR-196 and causes deregulation of IRGM-dependent xenophagy in Crohn's disease. Nat Genet. 2011;43(3):242-5.
200. Bauckman KA, Owusu-Boaitey N, Mysorekar IU. Selective autophagy: xenophagy. Methods. 2015;75:120-7.
201. Gibbings D, Mostowy S, Jay F, Schwab Y, Cossart P, Voinnet O. Selective autophagy degrades DICER and AGO2 and regulates miRNA activity. Nat Cell Biol. 2012;14(12):1314-21.
202. Yang BF, Lu YJ, Wang ZG. MicroRNAs and apoptosis: implications in the molecular therapy of human disease. Clinical and experimental pharmacology & physiology. 2009;36(10):951-60.
203. Lee RC, Feinbaum RL, Ambros V. The C. elegans heterochronic gene lin-4 encodes small RNAs with antisense complementarity to lin-14. Cell. 1993;75(843-854).
204. Bentwich I AA, Karov Y, Aharonov R, Gilad S, Barad O, Barzilai A, Einat P, Einav U, Meiri E, Sharon E, Spector Y, et al. Identification of hundreds of conserved and nonconserved human microRNAs. Nat Genet. 2005;37(766-770).
205. Nelissen EC, van Montfoort AP, Dumoulin JC, Evers JL. Epigenetics and the placenta. Hum Reprod Update. 2011;17(3):397-417.
206. Henriksen T, Clausen T. The fetal origins hypothesis: Placental insufficiency and inheritance versus maternal malnutrition in well-nourished populations. Acta Obstetricia et Gynecologica Scandinavica. 2002;81(2):112-4.
207. Barker DJP. Fetal and infant origins of adult disease. Monatsschrift fur Kinderheilkunde. 2001;149(SUPPL. 1):S2-S6.
208. Enquobahrie DA, Abetew DF, Sorensen TK, Willoughby D, Chidambaram K, Williams MA. Placental microRNA expression in pregnancies complicated by preeclampsia. American Journal of Obstetrics and Gynecology. 2011;204(2):178.e12-.e21.
209. Choudhury M, Friedman JE. Epigenetics and microRNAs in preeclampsia. Clinical and Experimental Hypertension. 2012;34(5):334-41.
210. Denli AM TB, Plasterk RH, Ketting RF, Hannon GJ. Processing of primary microRNAs by the Microprocessor complex. Nature. 2004;432(231-235).
211. Lund E, Güttinger S, Calado A, Dahlberg JE, Kutay U. Nuclear Export of MicroRNA Precursors. Science. 2004;303(5654):95-8.
212. Tomari Y, Zamore PD. Perspective: machines for RNAi. Genes Dev. 2005;19:517-29.
213. Meister G, Tuschl T. mechanisms of gene silencing double stranded RNA. Nature. 2004;431:343-9.
214. Li H, Dakour J, Kaufman S, Guilbert LJ, Winkler-Lowen B, Morrish DW. Adrenomedullin is decreased in preeclampsia because of failed response to epidermal growth factor and impaired syncytialization. Hypertension. 2003;42(5):895-900.
215. Iruloh CG, D'Souza SW, Fergusson WD, Baker PN, Sibley CP, Glazier JD. Amino acid transport systems beta and A in fetal T lymphocytes in intrauterine growth

restriction and with tumor necrosis factor-alpha treatment. Pediatr Res. 2009;65(1):51-6.
216. Zhang B, Pan X, Cobb GP, TA A. microRNAs as oncogenes and tumor suppressors. Dev Biol. 2007;302:1-12.
217. Lu J, Getz G, Miska EA, Alvarez-Saavedra E, Lamb J, Peck D. MicroRNA expression profiles classify human cancers. Nature. 2005;435:834-8.
218. Liang Y RD, Wong L, Chen C. Characterization of microRNA expression profiles in normal human tissues. BMC Genomics. 2007;8(166).
219. Mouillet JF, Chu T, Sadovsky Y. Expression patterns of placental microRNAs. Birth Defects Research Part A - Clinical and Molecular Teratology. 2011;91(8):737-43.
220. Luo SS, Ishibashi O, Ishikawa G, Ishikawa T, Katayama A, Mishima T, et al. Human villous trophoblasts express and secrete placenta-specific microRNAs into maternal circulation via exosomes. Biology of Reproduction. 2009;81(4):717-29.
221. Barad O, Meiri E, Avniel A, Aharonov R, Barzilai A, Bentwich I, et al. MicroRNA expression detected by oligonucleotide microarrays: System establishment and expression profiling in human tissues. Genome Research. 2004;14(12):2486-94.
222. Luo SS IO, Ishikawa G, Ishikawa T, Katayama A, Mishima T, Takizawa T, Shigihara T, Goto T, Izumi A, Ohkuchi A, Matsubara S, et al. Human villous trophoblasts express and secrete placenta-specific microRNAs into maternal circulation via exosomes. Biol Reprod. 2009;81(717-729).
223. Tsai KW, Kao HW, Chen HC, Chen SJ, Lin WC. Epigenetic control of the expression of a primate-specific microRNA cluster in human cancer cells. Epigenetics. 2009;4(8):587-92.
224. Bortolin-Cavaille ML, Dance M, Weber M, Cavaille J. C19MC microRNAs are processed from introns of large Pol-II, non-protein-coding transcripts. Nucleic Acids Research. 2009;37(10):3464-73.
225. Hromadnikova I, Kotlabova K, Ondrackova M, Kestlerova A, Novotna V, Hympanova L, et al. Circulating C19MC MicroRNAs in preeclampsia, gestational hypertension, and fetal growth restriction. Mediators of Inflammation. 2013;2013.
226. Cheloufi S, Dos Santos CO, Chong MMW, Hannon GJ. A dicer-independent miRNA biogenesis pathway that requires Ago catalysis. Nature. 2010;465(7298):584-9.
227. Chen DB, Wang W. Human placental microRNAs and preeclampsia. Biology of Reproduction. 2013;88(5).
228. Noack F, Ribbat-Idel J, Thorns C, Chiriac A, Axt-Fliedner R, Diedrich K, et al. miRNA Expression profiling in formalin-fixed and paraffin-embedded placental tissue samples from pregnancies with severe preeclampsia. Journal of Perinatal Medicine. 2011;39(3):267-71.
229. Choi SY, Yun J, Lee OJ, Han HS, Yeo MK, Lee MA, et al. MicroRNA expression profiles in placenta with severe preeclampsia using a PNA-based microarray. Placenta. 2013;34(9):799-804.
230. Hu Y, Li P, Hao S, Liu L, Zhao J, Hou Y. Differential expression of microRNAs in the placentae of Chinese patients with severe pre-eclampsia. Clinical Chemistry and Laboratory Medicine. 2009;47(8):923-9.
231. Zhu Xm, Han T, Sargent IL, Yin Gw, Yao Yq. Differential expression profile of microRNAs in human placentas from preeclamptic pregnancies vs normal

pregnancies. American Journal of Obstetrics and Gynecology. 2009;200(6):661.e1-.e7.
232. Mayor-Lynn K, Toloubeydokhti T, Cruz AC, Chegini N. Expression profile of microRNAs and mRNAs in human placentas from pregnancies complicated by preeclampsia and preterm labor. Reproductive Sciences. 2011;18(1):46-56.
233. Takizawa T, Ishibashi O, Ohkuchi A, Moksed Ali M, Kurashina R, Luo SS, et al. Hydroxysteroid (17-β) dehydrogenase 1 is dysregulated by miR-210 and miR-518c that are aberrantly expressed in preeclamptic placentas: A novel marker for predicting preeclampsia. Hypertension. 2012;59(2):265-73.
234. Hoefig KP, Thorns C, Roehle A, Kaehler C, Wesche KO, Repsilber D. Unlocking pathology archives for microRNA-profiling. Anticancer Res. 2008;28(1A):119-23.
235. Verghese ET, Hanby AM, Speirs V, Hughes TA. Small is beautiful: microRNAs and breast cancer-where are we now? J Pathol. 2008;215(3):214-21.
236. Pineles BL, Romero R, Montenegro D, Tarca AL, Han YM, Kim YM, et al. Distinct subsets of microRNAs are expressed differentially in the human placentas of patients with preeclampsia. American Journal of Obstetrics and Gynecology. 2007;196(3):261.e1-.e6.
237. Yang Q, Lu J, Wang S, Li H, Ge Q, Lu Z. Application of next-generation sequencing technology to profile the circulating microRNAs in the serum of preeclampsia versus normal pregnant women. Clinica Chimica Acta. 2011;412(23-24):2167-73.
238. Xu P, Zhao Y, Liu M, Wang Y, Wang H, Li Y-x, et al. Variations of MicroRNAs in Human Placentas and Plasma From Preeclamptic Pregnancy. Hypertension. 2014.
239. Levy R, Smith SD, Chandler K, Sadovsky Y, Nelson DM. Apoptosis in human cultured trophoblasts is enhanced by hypoxia and diminished by epidermal growth factor. American Journal of Physiology - Cell Physiology. 2000;278(5):C982-8.
240. Pardi G, Marconi AM, Cetin I. Placental-fetal interrelationship in IUGR fetuses - A review. Placenta. 2002;23(SUPPL. 1):S136-S41.
241. Baschat AA, Hecher K. Fetal Growth Restriction due to Placental Disease. Seminars in Perinatology. 2004;28(1):67-80.
242. Wang K, Jiang Yz, Chen Db, Zheng J. Hypoxia Enhances FGF2- and VEGF-Stimulated Human Placental Artery Endothelial Cell Proliferation: Roles of MEK1/2/ERK1/2 and PI3K/AKT1 Pathways. Placenta. 2009;30(12):1045-51.
243. Gunel T, Zeybek YG, Akçakaya P, Kalelioğlu I, Benian A, Ermis H, et al. Serum microRNA expression in pregnancies with preeclampsia. Genetics and molecular research : GMR. 2011;10(4):4034-40.
244. Zhang Y, Fei M, Xue G, Zhou Q, Jia Y, Li L, et al. Elevated levels of hypoxia-inducible microRNA-210 in pre-eclampsia: New insights into molecular mechanisms for the disease. Journal of Cellular and Molecular Medicine. 2012;16(2):249-59.
245. Miura K, Miura S, Yamasaki K, Higashijima A, Kinoshita A, Yoshiura KI. Identification of pregnancy-associated microRNAs in maternal plasma. Clin Chem. 2010.
246. Fu G, Ye G, Nadeem L, Ji L, Manchanda T, Wang Y, et al. MicroRNA-376c impairs transforming growth factor-β and nodal signaling to promote trophoblast cell proliferation and invasion. Hypertension. 2013;61(4):864-72.

247. Zhao Z, Moley KH, Gronowski AM. Diagnostic potential for miRNAs as biomarkers for pregnancy-specific diseases. Clinical Biochemistry. 2013;46(10-11):953-60.
248. Conde-Agudelo A, Villar J, Lindheimer M. World Health Organization systematic review of screening tests for preeclampsia. Obstet Gynecol. 2004(104):1367-91.
249. Wittmann J, Ja¨ck HM. Serum microRNAs as a powerful cancer biomarkers. Biochim Biophys Acta. 2010;1806:200-7.
250. Zernecke A, Bidzhekov K, Noels H. Delivery of microRNA- 126 by apoptotic bodies induces CXCL12-dependent vascular protection. Sci Signal. 2009;2:ra81.
251. Valadi H, Ekstro¨m K, Bossios A. Exosome-mediated transfer of mRNAs and microRNAs is a novel mechanism of genetic exchange between cells. Nat Cell Biol. 2007(9):654-9.
252. Chen X, Ba Y, Ma L, Cai X, Yin Y, Wang K, et al. Characterization of microRNAs in serum: A novel class of biomarkers for diagnosis of cancer and other diseases. Cell Research. 2008;18(10):997-1006.
253. Mitchell PS, Parkin RK, Kroh EM, Fritz BR, Wyman SK, Pogosova-Agadjanyan EL, et al. Circulating microRNAs as stable blood-based markers for cancer detection. P Natl Acad Sci USA. 2008;105(30):10513-8.
254. Chim SSC, Shing TKF, Hung ECW, Leung TY, Lau TK, Chiu RWK, et al. Detection and characterization of placental microRNAs in maternal plasma. Clinical Chemistry. 2008;54(3):482-90.
255. Hromadnikova I, Kotlabova K, Doucha J, Dlouha K, Krofta L. Absolute and relative quantification of placenta-specific microRNAs in maternal circulation with placental insufficiency - Related complications. Journal of Molecular Diagnostics. 2012;14(2):160-7.
256. Weedon-Fekjær MS, Sheng Y, Sugulle M, Johnsen GM, Herse F, Redman CW, et al. Placental miR-1301 is dysregulated in early-onset preeclampsia and inversely correlated with maternal circulating leptin. Placenta. 2014;35(9):709-17.
257. Wilcox MA JI, Maynard PV, Smith SJ & Chilvers CE The individualised birthweight ratio: a more logical outcome measure of pregnancy than birthweight alone. Br J Obstet Gynaecol,. 1993;100, 342–347.
258. ACOG practice bulletin. Diagnosis and management of preeclampsia and eclampsia.Number 33, January 2002. American College of Obstetricians and Gynecologists.. Int J Gynaecol Obstet. 2002;;77:67–75.
259. Clausen HV, Larsen LG, Gundersen HJG. Simple and efficient stereological quantitation of some placental structures: A review. Placenta. 1998;19, Supplement 2(0):41-56.
260. Treanor D, Jordan-Owers N, Hodrien J, Wood J, Quirke P, Ruddle RA. Virtual reality Powerwall versus conventional microscope for viewing pathology slides: An experimental comparison. Histopathology. 2009;55(3):294-300.
261. Treanor D, Lim CH, Magee D, Bulpitt A, Quirke P. Tracking with virtual slides: A tool to study diagnostic error in histopathology. Histopathology. 2009;55(1):37-45.
262. Roberts N, Magee D, Song Y, Brabazon K, Shires M, Crellin D, et al. Toward routine use of 3D histopathology as a research tool. American Journal of Pathology. 2012;180(5):1835-42.
263. Mayhew TM. Stereology and the Placenta: Where's the Point? – A Review. Placenta. 2006;27, Supplement(0):17-25.

264. Mayhew TM. Stereology and the Placenta: Where's the Point? - A Review. Placenta. 2006;27(SUPPL.):17-25.
265. Gundersen HJ BP, Bendtsen TF, Evans SM, Korbo L, Marcussen N, Møller A, Nielsen K, Nyengaard JR, Pakkenberg B,. The new stereological tools: disector, fractionator, nucleator and point sampled intercepts and their use in pathological research and diagnosis. APMIS. 1988 Oct.;96(10):857-81.
266. Mayhew TM. Stereology and the placenta - Where's the point? Placenta. 2005;26(8-9):A2-A.
267. Mayhew TM. A stereological perspective on placental morphology in normal and complicated pregnancies. Journal of Anatomy. 2009;215(1):77-90.
268. Mayhew TM, Gundersen HJG. 'If you assume, you can make an ass out of u and me': A decade of the disector for stereological counting of particles in 3D space. Journal of Anatomy. 1996;188:1-15.
269. Mayhew TM, and Gundersen, H.J.G. . ‘‘If you assume, you can make an ass out of u and me’’: A decade of the disector for stereological counting of particles in 3D space. J Anat. 1995;188:1–15.
270. Cruz-Orive LM. Weibel ER. Recent stereological methods for cell biology: a brief survey. Am J Physiol. 1990;258:L148e56.
271. Stuart A. Basic ideas of scientific sampling. 2nd ed. London & High Wycombe: Charles Griffin and Company Ltd;. 1976.
272. Gundersen HJG. Jensen EB. The efficiency of systematic sampling in stereology and its prediction. J Microsc. 1987;147:229e63.
273. Mayhew TM. The new stereological methods for interpreting functional morphology from slices of cells and organs. Exp Physiol. 1991;76:639e65.
274. Slomianka L, West, M.J.,. Estimators of the precision of stereological estimates: an example based on the CA1 pyramidal cell layer of rats. Neuroscience. 2005;136(3):757-67.
275. Gundersen HJG, Bendtsen TF, Korbo L, Marcussen N, Moller A, Nielsen K, et al. Some New, Simple and Efficient Stereological Methods and Their Use in Pathological Research and Diagnosis - Review Article. Apmis. 1988;96(5):379-94.
276. Mouton P. Principles and Practices of Unbiased Stereology, An Introduction for Bioscientists. 1st edn, The John Hopkins University Press, USA.2002.
277. Wikstrom Shemer E, Thorsell M, Ostlund E, Blomgren B, Marschall HU. Stereological assessment of placental morphology in intrahepatic cholestasis of pregnancy: Placenta. 33 (11) (pp 914-918), 2012. Date of Publication: November 2012.; 2012.
278. Mayhew TM, Huppertz, B., Kaufmann, P., Kingdom, J.C.,. The 'reference trap' revisited:examles of the dangers in using ratios to describe fetoplacental angiogenesis and trophoblastic turnover. Placenta. 2003;24(1-7).
279. Schmitz C, Hof PR. Design-based stereology in neuroscience. Neuroscience. 2005;130(4):813-31.
280. Laga E, Driscoll, SG., Munro, HN., . Quantitative studies of human placenta. I. Morphometry Biol Neonate. 1973;23:231e59.
281. Haeussner E, Buehlmeyer A, Schmitz C, von Koch FE, Frank H-G. Novel 3D Microscopic Analysis of Human Placental Villous Trees Reveals Unexpected Significance of Branching Angles. Scientific Reports. 2014;4:6192.

282. Tang Y, Nyengaard JR, Andersen JB, Baandrup U, Gundersen HJG. The Application of Stereological Methods for Estimating Structural Parameters in the Human Heart. Anat Rec. 2009;292(10):1630-47.
283. Gundersen HJG. Jensen EB. Kieu K. Nielsen J. The efficiency of systematic sampling in stereology reconsidered. J Microsc. 1999;193:199e211.
284. Wright AI, Grabsch, H. I., Treanor, D. E. . RandomSpot: a web-based tool for systematic random sampling of virtual slides. J Pathol Inform (In press). 2015.
285. Magee D TD, Quirke P. A New Image Registration algorithm with application to 3D Histopathology. Microscopic Image Analysis with Applications in Biology (MICCAI Workshop);. 2008.
286. Sharma M, Kumar R, Bhatla N, Dhingra R. A Comparative Study of Apoptosis in Placentas of Normal and Preeclamptic Indian Pregnant Women by TUNEL Assay and M30 Immunostaining. Journal of Clinical Laboratory Analysis. 2012;26(6):459-66.
287. Kadyrov M, Kaufmann P, Huppertz B. Expression of a cytokeratin 18 neo-epitope is a specific marker for trophoblast apoptosis in human placenta. Placenta. 2001;22(1):44-8.
288. Cantaloni C, Tonini R E, Eccher C, Morelli L, Leonardi E, Bragantini E, et al. Diagnostic value of automated Her2 evaluation in breast cancer: A study on 272 equivocal (score 2+) Her2 immunoreactive cases using an FDA approved system. Applied Immunohistochemistry and Molecular Morphology. 2011;19(4):306-12.
289. Forbes K, Desforges M, Garside R, Aplin JD, Westwood M. Methods for siRNA-mediated Reduction of mRNA and Protein Expression in Human Placental Explants, Isolated Primary Cells and Cell Lines. Placenta. 2009;30(2):124-9.
290. Tekirdag KA, Korkmaz G, Ozturk DG, Agami R, Gozuacik D. MIR181A regulates starvation-and rapamycininduced autophagy through targeting of ATG5. Autophagy. 2013;9(3):374-85.
291. He B, Zhang N, Zhao R. Dexamethasone Downregulates SLC7A5 Expression and Promotes Cell Cycle Arrest, Autophagy and Apoptosis in BeWo Cells. Journal of Cellular Physiology. 2016;231(1):233-42.
292. Lwai-Kanai E, Yuan H, Huang C, Sayen MR, Perry-Garza CN, Kim L, et al. A method to measure cardiac autophagic flux in vivo. Autophagy. 2008;4(3):322-9.
293. Choi C-H, Jung Y-K, Oh S-H. Autophagy Induction by Capsaicin in Malignant Human Breast Cells Is Modulated by p38 and Extracellular Signal-Regulated Mitogen-Activated Protein Kinases and Retards Cell Death by Suppressing Endoplasmic Reticulum Stress-Mediated Apoptosis. Molecular Pharmacology. 2010;78(1):114-25.
294. Yamamoto A, Tagawa Y, Yoshimori T, Moriyama Y, Masaki R, Tashiro Y. Bafilomycin A1 prevents maturation of autophagic vacuoles by inhibiting fusion between autophagosomes and lysosomes in rat hepatoma cell line, H-4-II-E cells. Cell Structure and Function. 1998;23(1):33-42.
295. O'Neill PM, Bray PG, Hawley SR, Ward SA, Park BK. 4-aminoquinolines - Past, present, and future: A chemical perspective. Pharmacol Therapeut. 1998;77(1):29-58.
296. Johansson AC, Steen H, Ollinger K, Roberg K. Cathepsin D mediates cytochrome c release and caspase activation in human fibroblast apoptosis induced by staurosporine. Cell Death Differ. 2003;10(11):1253-9.
297. Omura S, Iwai Y, Hirano A, Nakagawa A, Awaya J, Tsuchya H, et al. A new alkaloid AM-2282 OF Streptomyces origin. Taxonomy, fermentation, isolation and preliminary characterization. J Antibiot (Tokyo). 1977;30(4):275-82.

298. Zhang XD, Gillespie SK, Hersey P. Staurosporine induces apoptosis of melanoma by both caspase-dependent and -independent apoptotic pathways. Mol Cancer Ther. 2004;3(2):187-97.
299. Lall S, Grun D, Krek A, Chen K, Wang YL, Dewey CN, et al. A genome-wide map of conserved microRNA targets in C. elegans. Curr Biol. 2006;16(5):460-71.
300. Vandesompele J, De Preter K, Pattyn F, Poppe B, Van Roy N, De Paepe A, et al. Accurate normalization of real-time quantitative RT-PCR data by geometric averaging of multiple internal control genes. Genome Biology. 2002;3(7):research0034.1-research.11.
301. Penna A, Cahalan M. Western Blotting using the Invitrogen NuPage Novex Bis Tris minigels. J Vis Exp. 2007(7):264.
302. Aplin J. Maternal influences on placental development. Semin Cell Dev Biol. 2000;11(2):115-25.
303. Mayhew TM, Wijesekara J, Baker PN, Ong SS. Morphometric evidence that villous development and fetoplacental angiogenesis are compromised by intrauterine growth restriction but not by pre-eclampsia. Placenta. 2004;25(10):829-33.
304. Mayhew TM, Ohadike C, Baker PN, Crocker IP, Mitchell C, Ong SS. Stereological Investigation of Placental Morphology in Pregnancies Complicated by Pre-eclampsia with and without Intrauterine Growth Restriction. Placenta. 2003;24(2–3):219-26.
305. Heazell AEP, Warrander LK, Greenwood SL, Jones RL, Sibley CP. Placental size is reduced and placental infarction and syncytial knots are increased in pregnancies complicated by decreased fetal movements: Placenta. Conference: International Federation of Placenta Associations Meeting 2010 Santiago Chile. Conference Start: 20101019 Conference End: 20101022. Conference Publication: (var.pagings). 31 (9) (pp A103), 2010. Date of Publication: September 2010.; 2010.
306. Kaufmann P, Huppertz B. Tenney-Parker changes and apoptotic versus necrotic shedding of trophoblast in normal pregnancy and pre-eclampsia. Pre-Eclampsia: Etiology and Clinical Practice. 2007:152-63.
307. Jones CJ, Fox H. Syncytial knots and intervillous bridges in the human placenta: an ultrastructural study. Journal of Anatomy. 1977;124(Pt 2):275-86.
308. Kweider N, Huppertz B, Rath W, Lambertz J, Caspers R, ElMoursi M, et al. The effects of Nrf2 deletion on placental morphology and exchange capacity in the mouse. J Matern Fetal Neonatal Med. 2016:1-17.
309. Rasmussen S, Irgens LM. Fetal growth and body proportion in preeclampsia. Obstet Gynecol. 2003;101(3):575-83.
310. Ghidini A, Salafia CM, Pezzullo JC. Placental vascular lesions and likelihood of diagnosis of preeclampsia. Obstet Gynecol. 1997;90(4):542-5.
311. Long PA, Abell DA, Beischer NA. Fetal Growth-Retardation and Pre-Eclampsia. British journal of obstetrics and gynaecology. 1980;87(1):13-8.
312. Odegard RA, Vatten LJ, Nilsen ST, Salvesen KA, Austgulen R. Preeclampsia and fetal growth. Obstet Gynecol. 2000;96(6):950-5.
313. Moore MP, Redman CWG. Case-Control Study of Severe Pre-Eclampsia of Early Onset. Brit Med J. 1983;287(6392):580-3.
314. Huppertz B. Placental pathology in pregnancy complications. Thrombosis Research. 2011;127 Suppl 3:S96-9.

315. Howard CV. Reed MG. Estimation of component volume and volume fraction. Unbiased stereology Three-dimensional measurement in microscopy 2nd ed. Abingdon: Garland Science/Bios Scientific;2005.
316. Mayhew TM, Burton GJ. Methodological problems in placental morphometry: Apologia for the use of stereology based on sound sampling practice. Placenta. 1988;9(6):565-81.
317. Xiong X, Demianczuk NN, Buekens P, Saunders LD. Association of preeclampsia with high birth weight for gestational age. American Journal of Obstetrics and Gynecology. 2000;183(1):148-55.
318. Egbor M, Ansari T, Morris N, Green CJ, Sibbons PD. Morphometric placental villous and vascular abnormalities in early- and late-onset pre-eclampsia with and without fetal growth restriction. BJOG: An International Journal of Obstetrics and Gynaecology. 2006;113(5):580-9.
319. Egbor M, Ansari T, Morris N, Green CJ, Sibbons PD. Pre-eclampsia and Fetal Growth Restriction: How Morphometrically Different is the Placenta? Placenta. 2006;27(6–7):727-34.
320. Teasdale F. Histomorphometry of the human placenta in pre-eclampsia associated with severe intrauterine growth retardation. Placenta. 1987;8(2):119-28.
321. Teasdale F. Idiopathic intrauterine growth retardation: histomorphometry of the human placenta. Placenta. 1984;5(1):83-92.
322. Mayhew TM. Changes in Fetal Capillaries During Preplacental Hypoxia: Growth, Shape Remodelling and Villous Capillarization in Placentae from High-Altitude Pregnancies. Placenta. 2003;24(2–3):191-8.
323. Kaufmann P, Mayhew TM, Charnock-Jones DS. Aspects of Human Fetoplacental Vasculogenesis and Angiogenesis. II. Changes During Normal Pregnancy. Placenta. 2004;25(2–3):114-26.
324. Burton GJ, Jauniaux E. Sonographic, stereological and Doppler flow velocimetric assessments of placental maturity. British journal of obstetrics and gynaecology. 1995;102(10):818-25.
325. Ong SS, Tyler DJ, Moore RJ, Gowland PA, Baker PN, Johnson IR, et al. Functional magnetic resonance imaging (magnetization transfer) and stereological analysis of human placentae in normal pregnancy and in pre-eclampsia and intrauterine growth restriction. Placenta. 2004;25(5):408-12.
326. Peeters LL, Sheldon RE, Jones MD, Jr., Makowski EL, Meschia G. Blood flow to fetal organs as a function of arterial oxygen content. Am J Obstet Gynecol. 1979;135(5):637-46.
327. Stanek J, Biesiada J. Clustering of maternal-fetal clinical conditions and outcomes and placental lesions. American Journal of Obstetrics and Gynecology. 2012;206(6).
328. Stanek J. Chorangiosis of chorionic villi: what does it really mean? Accepted for publication in Arch Pathol Lab Med. 2016.
329. Bacon BJ, Gilbert RD, Kaufmann P, Smith AD, Trevino FT, Longo LD. Placental anatomy and diffusing capacity in guinea pigs following long-term maternal hypoxia. Placenta. 1984;5(6):475-87.
330. Scheffen I KP, Phillipens L, Leiser R, Geisen C, Mottaghy K.,. Alteration of the fetal capillary bed in the guinea pig placenta following long-term hypoxia. In: Piiper J GT, Mayer D.,, editor. Oxygen transfer of tissue. New York: XII. Plenum Press.

331. Fox H. Placental pathology. In: Kingdom J BP, editor. Intrauterine growth restriction: aetiology and management. London: Springer:; 2000. p. p991-8.
332. Ingram E, Morris D, Naish J, Myers J, Johnstone AD. Arterial spin labelling MRI measures increased placental perfusion with gestation. Royal college of Obstetrics and Gynaecolgoy Annual academic meeting; London2016.
333. Zadrozna M, Nowak B, Marcinek A, Duc J. Villous trophoblast cell turnover in placentas from preterm pregnancy and pregnancy complicated by intrauterine growth restriction (IUGR). Folia Biologica. 2010;58(1-2):79-83.
334. Tomas SZ, Roje D, Prusac IK, Tadin I, Capkun V. Morphological characteristics of placentas associated with idiopathic intrauterine growth retardation: a clinicopathologic study. Eur J Obstet Gynecol Reprod Biol. 2010;152(1):39-43.
335. Calvert SJ, Jones CJP, Sibley CP, Aplin JD, Heazell AEP. Analysis of syncytial nuclear aggregates in preeclampsia shows increased sectioning artefacts and decreased inter-villous bridges compared to healthy placentas. Placenta. 2013;34(12):1251-4.
336. Krebs C, Macara LM, Leiser R, Bowman AW, Greer IA, Kingdom JCP. Intrauterine growth restriction with absent end-diastolic flow velocity in the umbilical artery is associated with maldevelopment of the placental terminal villous tree. American Journal of Obstetrics and Gynecology. 1996;175(6):1534-42.
337. Chen C-P, Bajoria R, Aplin JD. Decreased vascularization and cell proliferation in placentas of intrauterine growth–restricted fetuses with abnormal umbilical artery flow velocity waveforms. American Journal of Obstetrics and Gynecology. 2002;187(3):764-9.
338. Kurtoglu E, Altunkaynak BZ, Aydin I, Ozdemir AZ, Altun G, Kokcu A, et al. Role of vascular endothelial growth factor and placental growth factor expression on placenta structure in pre-eclamptic pregnancy. Journal of Obstetrics and Gynaecology Research. 2015;41(10):1533-40.
339. Nafees H, Jain S, Khare S, Khare A, Kansal R. Histopathological study of placental villi in pre-eclampsia-a quantitative study. Journal of the Anatomical Society of India. 2012;61(2):159-62.
340. Devisme L, Merlot B, Ego A, Houfflin-Debarge V, Deruelle P, Subtil D. A case-control study of placental lesions associated with pre-eclampsia. International Journal of Gynaecology & Obstetrics. 2013;120(2):165-8.
341. Benirschke K, Kaufmann, P. Pathology of the Human Placenta. New York.: Springer; 2000.
342. Heazell AE, Moll SJ, Jones CJ, Baker PN, Crocker IP. Formation of syncytial knots is increased by hyperoxia, hypoxia and reactive oxygen species.[Erratum appears in Placenta. 2007 Aug-Sep;28(8-9):973]. Placenta. 2007;28(40).
343. Fox H. The Significance of Villous Syncytial Knots in the Human Placenta. Journal of Obstetrics & Gynaecology of the British Commonwealth. 1965;72:347-55.
344. Longtine MS, Chen B, Odibo AO, Zhong Y, Nelson DM. Villous trophoblast apoptosis is elevated and restricted to cytotrophoblasts in pregnancies complicated by preeclampsia, IUGR, or preeclampsia with IUGR. Placenta. 2012;33(5):352-9.
345. Engelberg-Kulka H, Amitai S, Kolodkin-Gal I, Hazan R. Bacterial Programmed Cell Death and Multicellular Behavior in Bacteria. PLOS Genetics. 2006;2(10):e135.
346. Lockshin RA, Williams CM. Programmed cell death—II. Endocrine potentiation of the breakdown of the intersegmental muscles of silkmoths. Journal of Insect Physiology. 1964;10(4):643-9.

347. Deter RL, Baudhuin P, Deduve C. Participation of Lysosomes in Cellular Autophagy Induced in Rat Liver by Glucagon. Journal of Cell Biology. 1967;35(2p1):C11-&.
348. Jones CJP, Fox H. An ultrahistochemical study of the distribution of acid and alkaline phosphatases in placentae from normal and complicated pregnancies. Journal of Pathology. 1976;118(3):143-51.
349. Levine B, Mizushima N, Virgin HW. Autophagy in immunity and inflammation. Nature. 2011;469(7330):323-35.
350. De Almodóvar CR, Ruiz-Ruiz C, Muñoz-Pinedo C, Robledo G, López-Rivas A. The differential sensitivity of Bcl-2-overexpressing human breast tumor cells to TRAIL or doxorubicin-induced apoptosis is dependent on Bc1-2 protein levels. Oncogene. 2001;20(48):7128-33.
351. Rahman T, Hosen I, Islam MT, Shekhar HU. Oxidative stress and human health. Advances in Bioscience and Biotechnology. 2012;3(7A):997.
352. Etzerodt A, Moestrup SK. CD163 and inflammation: Biological, diagnostic, and therapeutic aspects. Antioxidants and Redox Signaling. 2013;18(17):2352-63.
353. Lubbock ALR, Katz, E., Harrison, D. J. & Overton, I. M. TMA Navigator: network inference, patient stratification and survival analysis with tissue microarray data. Nucl Acids Res. 2013;41:W562–W8.
354. Rexhepaj E, Brennan DJ, Holloway P, Kay EW, McCann AH, Landberg G, et al. Novel image analysis approach for quantifying expression of nuclear proteins assessed by immunohistochemistry: application to measurement of oestrogen and progesterone receptor levels in breast cancer. Breast Cancer Res. 2008;10(5):R89.
355. Polcz ME, Adamson LA, Lu X, Chang MN, Fowler LJ, Hobbs JA. Increased IL-6 detection in adult and pediatric lymphoid tissue harboring Parvovirus B19. Journal of Clinical Virology. 2013;57(3):233-8.
356. Kridel R, Xerri L, Gelas-Dore B, Tan K, Feugier P, Vawda A, et al. The Prognostic Impact of CD163-Positive Macrophages in Follicular Lymphoma: A Study from the BC Cancer Agency and the Lymphoma Study Association. Clin Cancer Res. 2015;21(15):3428-35.
357. Gertych A, Mohan S, Maclary S, Mohanty S, Wawrowsky K, Mirocha J, et al. Effects of tissue decalcification on the quantification of breast cancer biomarkers by digital image analysis. Diagn Pathol. 2014;9:213.
358. Kalra J, Dragowska WH, Bally MB. Using Pharmacokinetic Profiles and Digital Quantification of Stained Tissue Microarrays as a Medium-Throughput, Quantitative Method for Measuring the Kinetics of Early Signaling Changes Following Integrin-Linked Kinase Inhibition in an In Vivo Model of Cancer. J Histochem Cytochem. 2015;63(9):691-709.
359. Laurinaviciene A, Dasevicius D, Ostapenko V, Jarmalaite S, Lazutka J, Laurinavicius A. Membrane connectivity estimated by digital image analysis of HER2 immunohistochemistry is concordant with visual scoring and fluorescence in situ hybridization results: algorithm evaluation on breast cancer tissue microarrays. Diagn Pathol. 2011;6:87.
360. Garcia-Rojo M, Sanchez J, de la Santa E, Duran E, Ruiz JL, Silva A, et al. Automated image analysis in the study of lymphocyte subpopulation in eosinophilic oesophagitis. Diagn Pathol. 2014;9 Suppl 1:S7.

361. Smith SC, Baker PN, Symonds EM. Increased placental apoptosis in intrauterine growth restriction. American Journal of Obstetrics and Gynecology. 1997;177(6):1395-401.
362. Ishihara N, Matsuo H, Murakoshi H, Laoag-Fernandez JB, Samoto T, Maruo T. Increased apoptosis in the syncytiotrophoblast in human term placentas complicated by either preeclampsia or intrauterine growth retardation. American Journal of Obstetrics and Gynecology. 2002;186(1):158-66.
363. Levy R, Smith SD, Yusuf K, Huettner PC, Kraus FT, Sadovsky Y, et al. Trophoblast apoptosis from pregnancies complicated by fetal growth restriction is associated with enhanced p53 expression. American Journal of Obstetrics & Gynecology. 2002;186(5):1056-61.
364. Endo H, Okamoto A, Yamada K, Nikaido T, Tanaka T. Frequent apoptosis in placental villi from pregnancies complicated with intrauterine growth restriction and without maternal symptoms. International Journal of Molecular Medicine. 2005;16(1):79-84.
365. Crocker IP, Cooper S, Ong SC, Baker PN. Differences in apoptotic susceptibility of cytotrophoblasts and syncytiotrophoblasts in normal pregnancy to those complicated with preeclampsia and intrauterine growth restriction. American Journal of Pathology. 2003;162(2):637-43.
366. Jones HN, Powell TL, Jansson T. Regulation of placental nutrient transport - A review. Placenta. 2007;28(8-9):763-74.
367. Rote NS, Lyden TW, Vogt E, Adler RR, Chang J, Katsuragawa H, et al. Expression of Phosphatidylserine Epitopes during Trophoblast Membrane-Fusion - an Alternative Hypothesis for Antiphospholipid Antibody Associated Pregnancy Disorders. Serono Sym. 1993;97:281-4.
368. Katsuragawa H, Kanzaki H, Inoue T, Hirano T, Mori T, Rote NS. Monoclonal antibody against phosphatidylserine inhibits in vitro human trophoblastic hormone production and invasion. Biology of Reproduction. 1997;56(1):50-8.
369. Longtine MS, Chen B, Odibo AO, Zhong Y, Nelson DM. Caspase-mediated apoptosis of trophoblasts in term human placental villi is restricted to cytotrophoblasts and absent from the multinucleated syncytiotrophoblast. Reproduction. 2012;143(1):107-21.
370. Kerr JFR, Gobe GC, Winterford CM, Harmon BV. Anatomical Methods in Cell-Death. Method Cell Biol. 1995;46:1-27.
371. Yang T, Kozopas KM, Craig RW. The Intracellular-Distribution and Pattern of Expression of Mcl-1 Overlap with, but Are Not Identical to, Those of Bcl-2. Journal of Cell Biology. 1995;128(6):1173-84.
372. Tomas SZ, Prusac IK, Roje D, Tadin I. Trophoblast apoptosis in placentas from pregnancies complicated by preeclampsia. Gynecologic & Obstetric Investigation. 2011;71(4):250-5.
373. Whitehead CL, Walker SP, Lappas M, Tong S. Circulating RNA coding genes regulating apoptosis in maternal blood in severe early onset fetal growth restriction and pre-eclampsia. Journal of Perinatology. 2013;33(8):600-4.
374. A.M. Choi SWR, and B. Levine, . Autophagy in human health and disease. The New England Journal of Medicine. 2013;vol. 368(no. 7):pp. 651–62.
375. Chifenti B, Locci MT, Lazzeri G, Guagnozzi M, Dinucci D, Chiellini F, et al. Autophagy-related protein LC3 and Beclin-1 in the first trimester of pregnancy. Clinical and Experimental Reproductive Medicine. 2013;40(1):33-7.

376. Chen GQ, Zhang H, Qi HB, Yao ZW, Gao L, Qiu CL. Effects and mechanisms of autophagy of trophoblast cells in severe preeclampsia. Xi bao yu fen zi mian yi xue za zhi = Chinese journal of cellular and molecular immunology. 2012;28(3):294-6.
377. Akaishi R, Yamada T, Nakabayashi K, Nishihara H, Furuta I, Kojima T, et al. Autophagy in the placenta of women with hypertensive disorders in pregnancy. Placenta. 2014;35(12):974-80.
378. Karaman E, Arslan H, Çetin O, Şahin HG, Bora A, Yavuz A, et al. Comparison of placental elasticity in normal and pre-eclamptic pregnant women by acoustic radiation force impulse elastosonography. Journal of Obstetrics and Gynaecology Research. 2016:n/a-n/a.
379. Nishizawa H, Suzuki M, Pryor-Koishi K, Sekiya T, Tada S, Kurahashi H, et al. Impact of indoleamine 2,3-dioxygenase on the antioxidant system in the placentas of severely pre-eclamptic patients. Systems Biology in Reproductive Medicine. 2011;57(4):174-8.
380. Kimura C, Watanabe K, Iwasaki A, Mori T, Matsushita H, Shinohara K, et al. The severity of hypoxic changes and oxidative DNA damage in the placenta of early-onset preeclamptic women and fetal growth restriction. Journal of Maternal-Fetal and Neonatal Medicine. 2013;26(5):491-6.
381. Takagi Y, Nikaido T, Toki T, Kita N, Kanai M, Ashida T, et al. Levels of oxidative stress and redox-related molecules in the placenta in preeclampsia and fetal growth restriction. Virchows Archiv. 2004;444(1):49-55.
382. Moestrup SK, Moller HJ. CD163: A regulated hemoglobin scavenger receptor with a role in the anti-inflammatory response. Annals of Medicine. 2004;36(5):347-54.
383. Schonkeren D, Van Der Hoorn ML, Khedoe P, Swings G, Van Beelen E, Claas F, et al. Differential distribution and phenotype of decidual macrophages in preeclamptic versus control pregnancies. American Journal of Pathology. 2011;178(2):709-17.
384. Kronborg CS, Knudsen UB, Moestrup SK, Allen J, Vittinghus E, Møller HJ. Serum markers of macrophage activation in pre-eclampsia: No predictive value of soluble CD163 and neopterin. Acta Obstetricia et Gynecologica Scandinavica. 2007;86(9):1041-6.
385. Patil SB, Kodliwadmath MV, Kodliwadrnathl SM. Role of lipid peroxidation and enzymatic antioxidants in pregnancy-induced hypertension. Clin Exp Obstet Gyn. 2007;34(4):239-41.
386. Halliwell B, Gutteridge J. Free radicals in biology and medicine. 4th ed ed. Oxford University: Press; 2007.
387. Burton GJ, Yung HW. Endoplasmic reticulum stress in the pathogenesis of early-onset pre-eclampsia. Pregnancy hypertension. 2011;1(1-2):72-8.
388. Essick EE, Sam F. Oxidative stress and autophagy in cardiac disease, neurological disorders, aging and cancer. Oxidative Medicine and Cellular Longevity. 2010;3(3):168-77.
389. Essick EE, Wilson RM, Pimentel DR, Shimano M, Baid S, Ouchi N, et al. Adiponectin Modulates Oxidative Stress-Induced Autophagy in Cardiomyocytes. PLoS ONE. 2013;8(7).
390. Lin WJ, Kuang HY. Oxidative stress induces autophagy in response to multiple noxious stimuli in retinal ganglion cells. Autophagy. 2014;10(10):1692-701.
391. Malaviya R, Laskin JD, Laskin DL. Oxidative stress-induced autophagy: Role in pulmonary toxicity. Toxicology and Applied Pharmacology. 2014;275(2):145-51.

392. Sureshbabu A, Ryter SW, Choi ME. Oxidative stress and autophagy: Crucial modulators of kidney injury. Redox Biol. 2015;4:208-14.
393. West RJH, Sweeney ST. Oxidative stress and autophagy: Mediators of synapse growth? Autophagy. 2012;8(2).
394. Maiuri MC, Criollo A, Tasdemir E, Vicencio JM, Tajeddine N, Hickman JA, et al. BH3-only proteins and BH3 mimetics induce autophagy by competitively disrupting the interaction between Beclin 1 and Bcl-2/Bcl-X(L). Autophagy. 2007;3(4):374-6.
395. Shen S, Kepp O, Kroemer G. The end of autophagic cell death? Autophagy. 2012;8(1):1-3.
396. Shen S, Kepp O, Michaud M, Martins I, Minoux H, Metivier D, et al. Association and dissociation of autophagy, apoptosis and necrosis by systematic chemical study. Oncogene. 2011;30(45):4544-56.
397. Boya P, Gonzalez-Polo RA, Casares N, Perfettini JL, Dessen P, Larochette N, et al. Inhibition of macroautophagy triggers apoptosis. Molecular and cellular biology. 2005;25(3):1025-40.
398. Gonzalez-Polo RA, Boya P, Pauleau AL, Jalil A, Larochette N, Souquere S, et al. The apoptosis/autophagy paradox: autophagic vacuolization before apoptotic death. Journal of cell science. 2005;118(Pt 14):3091-102.
399. Li Q, Pan Z, Wang X, Gao Z, Ren C, Yang W. MiR-125b-1-3p inhibits trophoblast cell invasion by targeting sphingosine-1-phosphate receptor 1 in preeclampsia. Biochemical and Biophysical Research Communications. 2014;453(1):57-63.
400. Fu G, Brkić J, Hayder H, Peng C. MicroRNAs in human placental development and pregnancy complications. International Journal of Molecular Sciences. 2013;14(3):5519-44.
401. Li H, Ge Q, Guo L, Lu Z. Maternal plasma miRNAs expression in preeclamptic pregnancies. BioMed Research International. 2013;2013.
402. Wong N, Wang X. miRDB: an online resource for microRNA target prediction and functional annotations. Nucleic Acids Res. 2015;43(Database issue):D146-52.
403. Kertesz M, Iovino N, Unnerstall U, Gaul U, Segal E. The role of site accessibility in microRNA target recognition. Nat Genet. 2007;39(10):1278-84.
404. Garcia DM, Baek D, Shin C, Bell GW, Grimson A, Bartel DP. Weak seed-pairing stability and high target-site abundance decrease the proficiency of lsy-6 and other microRNAs. Nat Struct Mol Biol. 2011;18(10):1139-46.
405. Nishizawa H, Pryor-Koishi K, Suzuki M, Kato T, Kogo H, Sekiya T, et al. Increased levels of pregnancy-associated plasma protein-A2 in the serum of pre-eclamptic patients. Molecular Human Reproduction. 2008;14(10):595-602.
406. Narendra D, Tanaka A, Suen DF, Youle RJ. Parkin is recruited selectively to impaired mitochondria and promotes their autophagy. Journal of Cell Biology. 2008;183(5):795-803.
407. Cai Q, Zakaria HM, Sheng ZH. Long time-lapse imaging reveals unique features of PARK2/Parkin-mediated mitophagy in mature cortical neurons. Autophagy. 2012;8(6):976-8.
408. Lim KL, Chua DSK, Palau XG, Yao TP. PARK2 Induces Autophagy Removal of Impaired Mitochondria via Ubiquitination. Autophagy: Cancer, Other Pathologies, Inflammation, Immunity, Infection, and Aging. 42014. p. 175-88.
409. Drewlo S, Levytska K, Kingdom J. Revisiting the housekeeping genes of human placental development and insufficiency syndromes. Placenta. 2012;33(11):952-4.

410. Meller M, Vadachkoira S, Luthy DA, Williams MA. Evaluation of housekeeping genes in placental comparative expression studies. Placenta. 2005;26(8-9):601-7.
411. Murthi P, Fitzpatrick E, Borg AJ, Donath S, Brennecke SP, Kalionis B. GAPDH, 18S rRNA and YWHAZ are suitable endogenous reference genes for relative gene expression studies in placental tissues from human idiopathic fetal growth restriction. Placenta. 2008;29(9):798-801.
412. Szklarczyk D, Franceschini A, Wyder S, Forslund K, Heller D, Huerta-Cepas J, et al. STRING v10: protein-protein interaction networks, integrated over the tree of life. Nucleic Acids Res. 2015;43(Database issue):D447-52.
413. Chao DT, Korsmeyer SJ. BCL-2 FAMILY: Regulators of Cell Death. Annual Review of Immunology. 1998;16(1):395-419.
414. Heath-Engel HM, Chang NC, Shore GC. The endoplasmic reticulum in apoptosis and autophagy: role of the BCL-2 protein family. Oncogene. 2008;27(50):6419-33.
415. Ray JE, Garcia J, Jurisicova A, Caniggia I. Mtd/Bok takes a swing: proapoptotic Mtd/Bok regulates trophoblast cell proliferation during human placental development and in preeclampsia. Cell Death & Differentiation. 2010;17(5):846-59.
416. Kalkat M, Garcia J, Ebrahimi J, Melland-Smith M, Todros T, Post M, et al. Placental autophagy regulation by the BOK-MCL1 rheostat. Autophagy. 2013;9(12):2140-53.
417. Bruey JM, Bruey-Sedano N, Luciano F, Zhai D, Balpai R, Xu C, et al. Bcl-2 and Bcl-XL regulate proinflammatory caspase-1 activation by interaction with NALP1. Cell. 2007;129(1):45-56.
418. Farrokhnia F, Aplin JD, Westwood M, Forbes K. MicroRNA regulation of mitogenic signaling networks in the human placenta. Journal of Biological Chemistry. 2014;289(44):30404-16.
419. Liu YM, Xia Y, Dai W, Han HY, Dong YX, Cai J, et al. Cholesterol-conjugated let-7a mimics: Antitumor efficacy on hepatocellular carcinoma in vitro and in a preclinical orthotopic xenograft model of systemic therapy. BMC Cancer. 2014;14(1).
420. Chen GQ, Wang CH, Liu LH, Wang Z, Zhu XS. Effect of autophagy regulated by let-7a on cell proliferation of hypoxic ovarian cancer HO-8910 cells. Chinese Journal of Cancer Prevention and Treatment. 2015;22(22):1741-6.
421. Higashi K, Yamada Y, Minatoguchi S, Baba S, Iwasa M, Kanamori H, et al. MicroRNA-145 repairs infarcted myocardium by accelerating cardiomyocyte autophagy. American Journal of Physiology - Heart and Circulatory Physiology. 2015;309(11):H1813-H26.
422. Wang W, Feng L, Zhang H, Hachy S, Satohisa S, Laurent LC, et al. Preeclampsia up-regulates angiogenesis-associated microRNA (i.e., miR-17, -20a, and -20b) that target ephrin-B2 and EPHB4 in human placenta. Journal of Clinical Endocrinology and Metabolism. 2012;97(6):E1051-E9.
423. Jin Y, Lu J, Wen J, Shen Y, Wen X. Regulation of growth of human bladder cancer by miR-192. Tumor Biology. 2015;36(5):3791-7.
424. Georges SA, Biery MC, Kim SY, Schelter JM, Guo J, Chang AN, et al. Coordinated regulation of cell cycle transcripts by p53-inducible microRNAs, miR-192 and miR-215. Cancer Research. 2008;68(24):10105-12.
425. Li R, Yan G, Li Q, Sun H, Hu Y, Sun J, et al. MicroRNA-145 Protects Cardiomyocytes against Hydrogen Peroxide (H2O2)-Induced Apoptosis through Targeting the Mitochondria Apoptotic Pathway. PLoS ONE. 2012;7(9).

426. Yeon MK, Romero R, Seo YO, Chong JK, Kilburn BA, Armant DR, et al. Toll-like receptor 4: A potential link between "danger signals," the innate immune system, and preeclampsia? American Journal of Obstetrics and Gynecology. 2005;193(3 SUPPL.):921.e1-.e8.
427. Yan D, da Dong X, Chen X, Yao S, Wang L, Wang J, et al. Role of microRNA-182 in posterior uveal melanoma: Regulation of tumor development through MITF, BCL2 and cyclin D2. PLoS ONE. 2012;7(7).
428. Kouri FM, Hurley LA, Daniel WL, Day ES, Hua Y, Hao L, et al. MiR-182 integrates apoptosis, growth, and differentiation programs in glioblastoma. Genes and Development. 2015;29(7):732-45.
429. Peng X, Li W, Yuan L, Mehta RG, Kopelovich L, McCormick DL. Inhibition of Proliferation and Induction of Autophagy by Atorvastatin in PC3 Prostate Cancer Cells Correlate with Downregulation of Bcl2 and Upregulation of miR-182 and p21. PLoS ONE. 2013;8(8).
430. Li G, Luna C, Qiu J, Epstein DL, Gonzalez P. Role of miR-204 in the regulation of apoptosis, endoplasmic reticulum stress response, and inflammation in human trabecular meshwork cells. Investigative Ophthalmology and Visual Science. 2011;52(6):2999-3007.
431. Sacconi A, Biagioni F, Canu V, Mori F, Di Benedetto A, Lorenzon L, et al. miR-204 targets Bcl-2 expression and enhances responsiveness of gastric cancer. Cell Death Dis. 2012;3:e423.
432. Chen L, Yan HX, Yang W, Hu L, Yu LX, Liu Q, et al. The role of microRNA expression pattern in human intrahepatic cholangiocarcinoma. Journal of Hepatology. 2009;50(2):358-69.
433. Kurashina R, Kikuchi K, Iwaki J, Yoshitake H, Takeshita T, Takizawa T. Placenta-specific miRNA (miR-512-3p) targets PPP3R1 encoding the calcineurin B regulatory subunit in BeWo cells. Journal of Obstetrics and Gynaecology Research. 2014;40(3):650-60.
434. Li P, Guo W, Du L, Zhao J, Wang Y, Liu L, et al. MicroRNA-29b contributes to pre-eclampsia through its effects on apoptosis, invasion and angiogenesis of trophoblast cells. Clin Sci (Lond). 2013;124(1):27-40.
435. Egger ME, Huang JS, Yin W, McMasters KM, McNally LR. Inhibition of autophagy with chloroquine is effective in melanoma. Journal of Surgical Research. 2013;184(1):274-81.
436. Curtis S, Jones CJ, Garrod A, Hulme CH, Heazell AE. Identification of autophagic vacuoles and regulators of autophagy in villous trophoblast from normal term pregnancies and in fetal growth restriction. J Matern Fetal Neonatal Med. 2013;26(4):339-46.
437. Yang C, Kaushal V, Shah SV, Kaushal GP. Autophagy is associated with apoptosis in cisplatin injury to renal tubular epithelial cells. Am J Physiol-Renal. 2008;294(4):F777-F87.
438. Lihuan D, Jingcun Z, Ning J, Guozeng W, Yiwei C, Wei L, et al. Photodynamic therapy with the novel photosensitizer chlorophyllin f induces apoptosis and autophagy in human bladder cancer cells. Lasers in Surgery and Medicine. 2014;46(4):319-24.
439. Oeste CL, Seco E, Patton WF, Boya P, Pérez-Sala D. Interactions between autophagic and endo-lysosomal markers in endothelial cells. Histochemistry and Cell Biology. 2012:1-12.

440. Nyirjesy P, Kavasya T, Axelrod P, Fischer PR. Malaria During Pregnancy: Neonatal Morbidity and Mortality and the Efficacy of Chloroquine Chemoprophylaxis. Clinical Infectious Diseases. 1993;16(1):127-32.
441. Lazebnik YA, Kaufmann SH, Desnoyers S, Poirier GG, Earnshaw WC. Cleavage of poly(ADP-ribose) polymerase by a proteinase with properties like ICE. Nature. 1994;371(6495):346-7.
442. Nicholson DW, Ali A, Thornberry NA, Vaillancourt JP, Ding CK, Gallant M, et al. Identification and inhibition of the ICE/CED-3 protease necessary for mammalian apoptosis. Nature. 1995;376(6535):37-43.
443. Tewari M, Quan LT, O'Rourke K, Desnoyers S, Zeng Z, Beidler DR, et al. Yama/CPP32 beta, a mammalian homolog of CED-3, is a CrmA-inhibitable protease that cleaves the death substrate poly(ADP-ribose) polymerase. Cell. 1995;81(5):801-9.
444. Oliver FJ, de la Rubia G, Rolli V, Ruiz-Ruiz MC, de Murcia G, Murcia JM. Importance of poly(ADP-ribose) polymerase and its cleavage in apoptosis. Lesson from an uncleavable mutant. J Biol Chem. 1998;273(50):33533-9.
445. Ryan J, Tivnan A, Fay J, Bryan K, Meehan M, Creevey L, et al. MicroRNA-204 increases sensitivity of neuroblastoma cells to cisplatin and is associated with a favourable clinical outcome. British Journal of Cancer. 2012;107(6):967-76.
446. Kuwano Y, Nishida K, Kajita K, Satake Y, Akaike Y, Fujita K, et al. Transformer 2β and miR-204 regulate apoptosis through competitive binding to 3′ UTR of BCL2 mRNA. Cell Death and Differentiation. 2014.
447. Imam JS, Plyler JR, Bansal H, Prajapati S, Bansal S, Rebeles J, et al. Genomic loss of tumor suppressor miRNA-204 promotes cancer cell migration and invasion by activating AKT/mTOR/Rac1 signaling and actin reorganization. PLoS One. 2012;7(12):e52397.
448. Ohuchida K, Mizumoto K, Kayashima T, Fujita H, Moriyama T, Ohtsuka T, et al. MicroRNA expression as a predictive marker for gemcitabine response after surgical resection of pancreatic cancer. Ann Surg Oncol. 2011;18(8):2381-7.
449. Lee Y, Yang X, Huang Y, Fan H, Zhang Q, Wu Y, et al. Network modeling identifies molecular functions targeted by miR-204 to suppress head and neck tumor metastasis. PLoS Comput Biol. 2010;6(4):e1000730.
450. Sümbül AT, Göğebakan B, Ergün S, Yengil E, Batmacı CY, Tonyalı, et al. miR-204-5p expression in colorectal cancer: an autophagy-associated gene. Tumor Biology. 2014;35(12):12713-9.
451. Ryan J, Tivnan A, Fay J, Bryan K, Meehan M, Creevey L, et al. MicroRNA-204 increases sensitivity of neuroblastoma cells to cisplatin and is associated with a favourable clinical outcome. Br J Cancer. 2012;107(6):967-76.
452. Ying Z, Li Y, Wu J, Zhu X, Yang Y, Tian H, et al. Loss of miR-204 expression enhances glioma migration and stem cell-like phenotype. Cancer Res. 2013;73(2):990-9.
453. Liu L, Wang J, Li X, Ma J, Shi C, Zhu H, et al. MiR-204-5p suppresses cell proliferation by inhibiting IGFBP5 in papillary thyroid carcinoma. Biochemical and Biophysical Research Communications. 2015;457(4):621-6.
454. Podjarny E, Losonczy G, Baylis C. Animal Models of Preeclampsia. Seminars in nephrology. 2004;24(6):596-606.
455. Elmoursi M, Simpson NAB. Placental dysfunction and pre-eclampsia. Hospital Healthcare Europe. June 2014.

456. Sankaralingam S, Arenas IA, Lalu MM, Davidge ST. Preeclampsia: current understanding of the molecular basis of vascular dysfunction. Expert reviews in molecular medicine. 2006;8(3):1-20.
457. Benirschke K, Spinosa JC, McGinniss MJ, Marchevsky A, Sanchez J. Partial molar transformation of the placenta of presumably monozygotic twins. Pediatric and Developmental Pathology. 2000;3(1):95-100.
458. Heazell AEP, Moll SJ, Jones CJP, Baker PN, Crocker IP. Formation of Syncytial Knots is Increased by Hyperoxia, Hypoxia and Reactive Oxygen Species. Placenta. 2007;28(SUPPL.):S33-S40.

Appendix

Consent form

The Leeds Teaching Hospitals NHS

NHS Trust

Centre Number:

Study Number:

Patient Identification Number for this trial:

CONSENT FORM

Title of Project: **Placenta Origins of Adverse Pregnancy Outcome**

Name of Researcher:

Please initial all boxes

1. I confirm that I have read and understand the information sheet (version [2.0]) for the above study. I have had the opportunity to consider the information, ask questions and have had these answered satisfactorily. ☐
2. I understand that my participation is voluntary and that I am free to withdraw at any time without giving any reason, without my medical care or legal rights being affected. ☐
3. I understand that relevant sections of my medical notes and data collected during the study may be looked at by individuals from the research team, from regulatory authorities or from the NHS Trust, where it is relevant to my taking part in this research. I give permission for these individuals to have access to my records. ☐
4. I understand that a blood, urine and placental sample will be taken from me for this study. ☐
5. I agree to take part in the above study. ☐

Name of Participant	Date	Signature
Name of Person	Date	Signature

Ethical Approval document

Health Research Authority
NRES Committee Yorkshire & The Humber - Bradford Leeds
North East REC Centre
Room 002
TEDCO Business Centre
Viking Industrial Park
Rolling Mill Road
Jarrow
NE32 3DT

Telephone: 0191 4283545

01 November 2013

Mohamed Elmoursi
University of Leeds
Clinical Sciences Building, Room 8.3,
St James' University Hospital
LS9 7TF

Dear Mohamed

Study title:	**Understanding the placental structure, function and pathophysiology underlying the development of adverse pregnancy outcomes such as pre-eclampsia, intrauterine growth restriction, gestational diabetes, and preterm birth**
REC reference:	**13/YH/0344**
IRAS project ID:	**130157**

Thank you for your letter of 30 October 2013, responding to the Committee's request for further information on the above research and submitting revised documentation.

The further information has been considered on behalf of the Committee by the Chair.

We plan to publish your research summary wording for the above study on the NRES website, together with your contact details, unless you expressly withhold permission to do so. Publication will be no earlier than three months from the date of this favourable opinion letter. Should you wish to provide a substitute contact point, require further information, or wish to withhold permission to publish, please contact the REC Manager Hayley Jeffries, nrescommittee.yorkandhumber-leedsbradford@nhs.net

Confirmation of ethical opinion
On behalf of the Committee, I am pleased to confirm a favourable ethical opinion for the above research on the basis described in the application form, protocol and supporting documentation as revised, subject to the conditions specified below.

List of Publications

Published articles

1. **Elmoursi M** and Simpson NAB, *Placental dysfunction and pre-eclampsia.* Hospital Healthcare Europe, 2014. June 2014.
2. Kweider N, Huppertz B, Rath W, Lambertz J, Caspers R, **ElMoursi M**, et al. The effects of Nrf2 deletion on placental morphology and exchange capacity in the mouse. J Matern Fetal Neonatal Med. 2016:1-17.

Published oral presentations at international conferences

1. **Elmoursi M**, Stahlshmidt J, Treanor D, Simpson N. Novel insights from using Stereology in virtual slides to quantify placental vasculature in intrauterine growth restriction. Virchows Archiv; Aug2014. p. S31-S.
2. **Elmoursi M**, Treanor D, Simpson N. A novel approach towards three dimensional reconstruction of placental micro-architecture. Virchows Archiv. 2014;465:S30-S1.

Published poster presentations

1. **Elmoursi M**, Treanor D, Simpson NAB. Novel insights from using Stereology based volume estimation of Syncytial nuclear aggregates in Diabetic placenta. **Arch Dis Child Fetal Neonatal Ed**. 2014;99(Suppl 1 A158 doi:10.1136/archdischild-2014-306576.465).
2. **ElMoursi M**, Stahlschmidt J, Treanor D, Simpson N. SYNCYTIAL NUCLEAR AGGREGATES AND VILLOUS CAPILLARY VOLUME IN IUGR PLACENTAS: A STEREOLOGY-BASED STUDY ON VIRTUAL SLIDES. **Placenta**. 2014;35(9):A11-A.
3. **Elmoursi MSE**, Speirs V, Stahlschmidt J, Treanor D, Simpson NAB. Digital Pathology Analysis Reveals an Increased Trophoblast Apoptotic Burden in Normotensive and Hypertensive Fetal Growth Restriction. **Reproductive Sciences**. 2015;22:187a-a.

4. **ElMoursi MSE**, Simpson NAB, Stahlschmidt J, Treanor D, Speirs V. Differential Autophagy Expression in Placental Dysfunction. **Reproductive Sciences**. 2015;22:187a-a.
5. **ElMoursi M**, Simpson NAB, Stahlschmidt J, Treanor D, Speirs V. Digital pathology analysis reveals enhanced autophagy expression in pre-eclamptic placenta. **Bjog-Int J Obstet Gy**. 2015;122(12):E2-E.
6. **ElMoursi M**, Treanor D, Simpson N. A novel approach towards three dimensional reconstruction of placenta micro-architecture. **Placenta**. 2014;35(9):A11.
7. **ElMoursi M**, Speirs V, Stahlschmidt J, Treanor D, Simpson NAB. Trophoblast apoptotic burden in fetal growth restriction (FGR) placenta: an image analysis study. **Bjog-Int J Obstet Gy**. 2015;122(12):E1-E2.